CONFOUNDING VARIABLES IN TRANSGENIC MOUSE MODELS OF TAUOPATHY

A THESIS SUBMITTED TO THE FACULTY OF THE UNIVERSITY OF MINNESOTA BY

JULIA ELISE GAMACHE

IN PARTIAL FULFILLMENT OF THE REQUIREMENTS FOR THE DEGREE OF DOCTOR OF PHILOSOPHY

DR. KAREN H. ASHE
DR. MICHAEL D. KOOB

JULY 2019

Acknowledgements

This work could not have been accomplished without the help and support of many people. I would first like to acknowledge my advisors, Karen Ashe and Michael Koob, who allowed me to be a part of a unique collaboration that yielded a very interesting and important project that taught me the valuable skill of responding to unexpected results. The guidance and mentorship of these experts in their respective fields of mouse modeling and genetic engineering provided a training environment of the highest quality and has allowed me to become the scientist I am today. I am also grateful for the guidance provided by other members of my thesis committee, including Harry Orr, Marija Cvetanovic, and David Largaespada. Bringing in their expertise and perspectives helped ensure that my project was rigorous and complete. In addition, I am truly blessed to have had the love and support of my friends and family throughout graduate school. I especially would like to acknowledge my soon-to-be husband, Matthew Green, who always reminded me of the importance of work-life balance and, having just gotten a Ph.D. in neuroscience himself, was a phenomenal sounding board for scientific ideas and research in general. I'd also like to extend a special thank-you to my parents, Terri and Dan, who have always encouraged and supported me in everything I've done.

Next, I want to acknowledge past and present members of the Ashe and Koob labs that trained me and also performed some of the experiments included in this work. Lisa Kemper oversaw our large mouse colony, which was also maintained by Kailee Leinonen, Elizabeth Steuer, Chris Hlynialuk, and Eric Huang. Lisa was always helpful in designing breeding schemes for my experiments and was flexible in shifting the schedule around to fit my needs. Lisa, Kailee, and Beth also conducted many of the behavioral experiments included in this work, and Beth performed some of the immunohistology with remarkable speed. Chris contributed his expertise in R programming language to help with more complicated statistical analyses. I am also very grateful for the technical training and assistance provided by Kathleen Zahs and Samantha Shapiro. Kathy worked with me on the tau ELISAs and Sam trained me in many techniques when I first joined the lab, most notably in western blotting, which I did very frequently. Others in the Ashe lab including Benjamin Smith, Peng Liu, Michelle Gastecki, and Xiaohui Zhao were always available for technical assistance, feedback,

and help with experimental design. Ashe lab administrative staff members including Vandana Murthy and Patty Carlson were also very helpful in answering my various program-related questions and in placing orders. In the Koob lab, Kellie Benzow and Kul Karanjeet were also always available for technical assistance, especially with cloning experiments, which I struggled with in the beginning. Kellie deserves a special mention for her tremendous work in generating the ES cell clones used to make the targeted transgenic lines used throughout this work. Kyle O'Connor previously worked in the UMN Mouse Genetics Laboratory and did the blastocyst injections to make the chimeric mice for us.

I am fortunate to have conducted this work at the University of Minnesota, which has a uniquely collaborative atmosphere. I'd like to acknowledge Eva Furrow in the Veterinary Clinical Sciences department for helping us decipher the complicated whole-genome sequencing results for the Tg4510 mouse. Keith Vossel was also instrumental in overseeing the mitochondria experiments, and his lab members Jessica Choquette and Samuel Peters provided technical assistance in conducting those studies. Jessica in particular made the primary hippocampal cultures used for those experiments. The University of MN also houses a number of core facilities that provide many special services and equipment. Colleen Forster in the Clinical and Translational Science Institute Histology lab performed some of the immunohistology for this work, and was very accommodating of my particular experimental needs and special requests. Leanne Oseth in the Cytogenomics center performed FISH to help us identify the transgene insertion site in Tg4510. In the Genomics Center, Daryl Gohl, Elyse Cooper, and Aaron Becker all played a part in helping us design the whole-genome sequencing experiments and in communicating our results to us. I am grateful for the training and guidance provided by Yung Kim and Mark Sanders in the University Imaging Center for the live cell imaging experiments. A few other people have contributed invaluable advice including Jim Cleary (Grossman Center) for statistical analyses, Kevin Silverstein (Minnesota Supercomputing Institute) for whole-genome sequencing analysis, and Pascal Verdier-Pinard (Centre de Recherche en Cancérologie de Marseille) for microtubule isolation methodology.

I am so fortunate to have joined the Graduate Program in Neuroscience at the University of MN. I really enjoyed getting to know my class of 2014 including Elias Boroda, Zoe Christenson-Wick, Michelle Corkrum, Justin Lines, Morgan Newhoff,

Balvindar Singh, Brian Sweis, and Zachary Zeidler. I couldn't have asked for a more fabulous and goofy group of people to get my Ph.D. with. I look forward to seeing them at SfN in future years for reunions and hope to have the opportunity to collaborate with some of them as colleagues. I am grateful for the guidance provided by the past and present GPN directors of graduate studies Jim Ashe, David Redish, and Linda McLoon. I would like to thank the wonderful GPN administrative staff including John Paton, Elaine McCauley, Kathleen Beterams, and Rebecca Hervonen for their help in resolving the various issues that came up throughout graduate school and for answering all of my program-related questions. Lastly, this work could not have been accomplished without the following funding sources: my NRSA F31 (AG057104-01), the Alzheimer's Association Zenith Award (453589), and the NIH/NINDS R01 (NS079374-02).

Abstract

Tau is the main axonal microtubule-associated protein in the mammalian central nervous system (CNS) and functions primarily in microtubule assembly and axonal transport. However, tau also has diverse other functions ranging from postsynaptic receptor scaffolding to chromatin protection and organization. Tauopathies are a family of over 20 neurodegenerative diseases characterized by tau pathology in the brain, which is an indication of tau dysfunction and dysregulation. Importantly, tauopathies include Alzheimer's disease and frontotemporal dementia, which are among the leading causes of early-onset dementia and are growing in prevalence due to an increasingly older population. To date, no disease-modifying therapies exist for tauopathies in part because the complex and multifunctional nature of tau biology makes it difficult to understand its role in disease pathogenesis.

Mouse modeling is an invaluable research tool frequently employed to test hypotheses about the role of tau in tauopathies, but has unfortunately yielded inconsistent results and extreme phenotypic variability. 'Conventional' techniques have historically been used to generate such mouse models, involving random insertion of synthetic mini-gene constructs into the mouse genome. In the current work, we have employed new 'targeted' genome engineering techniques to precisely insert a human tau (hTau) transgene into a predetermined, non-disruptive locus. We hypothesized that a targeted model harboring the pathogenic P301L hTau mutation would develop a disease-like phenotype and thus could be used as a positive control in comparison to genetically matched mice with different hTau modifications.

Unlike the widely used conventionally-made tauopathy model rTg4510, which harbors a P301L hTau transgene, our targeted equivalent (rT2/T2) did not quickly develop a robust tauopathy-like phenotype. We found this discrepancy could be explained by a large transgene insertion-deletion (TgINDEL) mutation that disrupts and dysregulates *Fgf14*, a gene important for neuronal function. A tet-transactivator (tTA) transgene, required to activate hTau expression, also caused a TgINDEL that disrupts another five genes in this mouse line, four of which have prominent forebrain expression. Comparing this model to rT2/T2 mice revealed that the two TgINDELs allow for acceleration of the rTg4510 phenotype, including neurodegeneration and tau

histopathology. In addition, we found that extreme overexpression of hTau, or ‘hyperexpression,’ is necessary to drive the severe phenotype.

We also generated a targeted transgenic mouse overexpressing non-mutant (NM) hTau, with the intention of using it as a genetically-matched negative control in comparison to the P301L line. Surprisingly, NM hTau was associated with a developmental phenotype, characterized by reduced clearance and hyperphosphorylation of hTau. We found that disrupted mitochondrial dynamics and elevated oxidative stress were involved in NM hTau pathogenicity, underlying abnormal brain development and cognitive deficits. Interestingly, these phenotypes were lost with the P301L mutation, suggesting it conferred a beneficial loss of function during development. We speculate the molecular and behavioral differences between the NM and P301L hTau lines are driven by hTau-microtubule binding, which was found to be reduced in the P301L line.

Together, this work identifies and characterizes confounding variables in mouse models of tauopathy including genomic disruption, transgene hyperexpression, and overexpression of transgenes during early postnatal development. We take initial steps to improve mouse transgenesis approaches and find genetic matching to be advantageous for probing molecular phenotypes of different forms of tau. We assert that it is important to eliminate confounding variables and use proper controls where possible to ensure phenotypes are relevant to the disease of interest. These findings are an example of a broader problem affecting neurodegenerative disease research, which can be avoided in future studies with more rigorous genomic characterization of mouse models as well as careful consideration of the timing and level of transgene expression as appropriate for the hypothesis in question.

Table of Contents

List of Figures

List of Tables

List of Abbreviations

3'-UTR	3' untranslated region
8OHdG	8-hydroxy-2'-deoxyguanosine
Aβ	amyloid β
AAV	Adeno-associated virus
AIS	Axon initial segment
ALS	Amyotrophic lateral sclerosis
AMPA	α-amino-3-hydroxy-5-methyl-4-isoxazolepropionic acid
AMPAR	AMPA receptor
ANOVA	Analysis of variance
APOE	Apolipoprotein E
App	Amyloid precursor protein
Biels	Bielschowsky stain
C9ORF72	chromosome 9 open reading frame 72
CaMKIIα	Calcium/calmodulin-dependent protein kinase II
cAMP	Cyclic adenosine monophosphate
cDNA	Complementary DNA
CKTTA	CaMKIIα-tTA
CNS	Central nervous system
Col1A1	Collagen type 1 alpha 1
Ctx	Cortex
DG	Dentate gyrus
DNA	Deoxyribonucleic acid
DOX	Doxycycline
Drp1	Dynamin related protein 1
ER	Endoplasmic reticulum
EGFP	Enhanced green fluorescent protein
ELISA	Enzyme-linked immunosorbent assay
Esyt2	Extended synaptotagmin 2
ES cells	Embryonic stem cells
EWS	Ewing's sarcoma
FDA	Food and Drug Administration

Fgf14	Fibroblast growth factor 14
FISH	Fluorescence in situ hybridization
FTDP-17	Frontotemporal dementia and parkinsonism linked to chromosome 17
FTLD	Frontotemporal lobar degeneration
FUS	Fused in sarcoma
G-E	GAPDH-enriched
GRN	Progranulin
GSK-3	Glycogen synthase kinase 3
hIPSC	Human-derived induced pluripotent stem cell
HMW	High-molecular weight
Hprt	hypoxanthine guanine phosphoribosyl transferase
hTau	Human tau
Ilf3	Interleukin enhancer binding factor 3
INDEL	Insertion-deletion mutation
IRE1	inositol-requiring enzyme 1
LTD	Long-term depression
LTP	Long-term potentiation
MAP	Microtubule-associated protein
MAPT	Microtubule-associated protein tau
MCI	Mild cognitive impairment
MLR	Multiple linear regression
mRNA	Messenger RNA
MT	Microtubule
Ncapg2	Non-SMC Condensin II Complex Subunit G2
NCBI	National Center for Biotechnology Information
NFT	Neurofibrillary tangle
NGF	Nerve growth factor
NM	Non-mutant
NMDA	N-methyl-D-aspartate
NMDAR	NMDA receptor
NT	Non-transgenic
P-E	PSD-95-enriched
PCR	Polymerase chain reaction

PET	Positron emission tomography
Prnp	Prion protein
pSer	Phosphorylated serine
pTau	Phosphorylated tau
Ptprn2	Protein tyrosine phosphatase receptor type N2
qRT-PCR	Quantitative real time PCR
RFP	Red fluorescent protein
RNA	Ribonulceic acid
ROI	Region of interest
ROS	Reactive oxygen species
S-E	Synaptophysin-enriched
SDS-PAGE	Sodium dodecyl sulfate polyacrylamide gel electrophoresis
SLR	Simple linear regression
SNP	Single nucleotide polymorphism
TAF-15	TATA-Box Binding Protein Associated Factor 15
TDP-43	TAR DNA-binding protein 43
TgINDEL	Transgene INDEL
TRE	Tetracycline response element
TREM2	Triggering receptor expressed on myeloid cells 2
tTA	Tetracycline transactivator
UPR	Unfolded protein response
Vipr2	Vasoactive Intestinal Peptide Receptor 2
Wdr60	WD repeat-containing protein 60
WT	Wild-type
XBP1	X-Box Binding Protein 1

Chapter One:
Introduction

I. Outline and rationale for current work

Mouse modeling is an invaluable research tool commonly used to test hypotheses about neurodegenerative diseases. Because mice do not naturally develop these aging-dependent diseases, artificial human transgenes are introduced in the hopes of mimicking human disease phenotypes. Tauopathies are a large family of neurodegenerative diseases, such as Alzheimer's disease and frontotemporal dementia, characterized by dysfunction and dysregulation of tau. Perhaps due to the complex biology underlying these diseases, it has been difficult to determine the role of tau in the pathogenesis of tauopathies. Unfortunately, no disease-modifying treatments yet exist for tauopathies in part due to a problem of translatability from mouse models to human clinical trials. It seems as the impetus for developing therapies becomes more urgent as the aging population increases, new discoveries about the biological functions of tau are made, making its role in neurodegeneration increasingly complex.

When this work began, my goal was to use novel transgenic mice expressing human tau (hTau) to answer one of the major questions in the tauopathy field: which post-translational modifications create toxic species of tau, and are there pathways that can be targeted to reverse or slow that toxicity? To accomplish this, the Ashe and Koob labs formed a collaboration to generate genetically matched 'Targeted' transgenic lines harboring different hTau modifications, termed the T-series. As a positive control, the P301L mutation was introduced into one of these lines (rT2) to replicate the strong tauopathy-like phenotype of a widely accepted yet genetically uncharacterized mouse model called rTg4510, generated by the Ashe lab in the early 2000s. My early pilot studies revealed that rT2 mice did not develop robust tau histopathology like rTg4510, but we hypothesized this was due to the lower level of hTau expression. Making the mice homozygous for the transgene (rT2/T2) greatly increased hTau expression to a level even higher than that of rTg4510, but surprisingly the histopathology and neurodegenerative phenotypes were still not as robust as expected.

Therefore, it quickly became a priority to determine why the rTg4510 phenotype could not be replicated in a targeted model. While the post-translational modification question remains of vital importance, it will become clear in the following chapters that this work evolved into an investigation of confounding variables that contribute to phenotypes of mouse models of tauopathy, in both the 'conventional' rTg4510 model as well as our new T-series models. My findings provide a few examples of a much broader

problem affecting neurodegenerative research, and suggest that the design of mouse models needs to be improved in order to truly understand tau pathogenicity in the mammalian brain. I have found that not only is detailed genetic characterization of transgenic mice of utmost importance to understanding phenotypes, but also the level of transgene expression as well as the stage in life during which such transgenes are activated. My work highlights confounding aspects of these artificial systems, and takes initial steps toward eliminating them. The implications of this work extend to all cases in which mouse modeling is used, and do not apply to tauopathy models alone.

In the following sections, I will show that tau's biological function is diverse and therefore its role in disease is complex and incompletely understood. There are many layers of complexity to tau's function that have been uncovered over the years that partially explain why it has been so difficult to develop disease-modifying therapies. On the other hand, the failure of therapies found to be successful in mouse models to translate to humans suggests there are problems with the mouse models themselves. In Chapters Two and Three I will discuss the two projects I conducted that revealed major confounding variables in transgenic mouse models of tauopathy that may contribute to this problem of translatability.

II. Tauopathies and Alzheimer's Disease

A. Historical perspective

Alois Alzheimer first described the disease that now bears his name in 1907. His patient, Auguste Deter, was 51 years old and suffered from paranoia, disorientation, memory problems, and language impairments (1). What was striking about this case was the young age at which the patient was exhibiting symptoms of senility. Upon examining her brain after death, Alzheimer observed not only general cortical atrophy, but also argyrophilic "neurofibrils" first described in senile dementia two years prior (2) and also by his contemporary Oskar Fischer (3). Today this pathological hallmark is known as neurofibrillary tangles (NFTs). Around the same time, Arnold Pick was beginning his investigations of a distinct disease clinically similar to Alzheimer's, but with atrophy localized specifically to frontal and temporal lobes (4,5). In what became known as Pick's disease, spherical argyrophilic intraneuronal inclusions found in neuronal cytoplasms (now 'Pick bodies') were histopathologically distinct from the tangles of Alzheimer's disease (6).

Many years later, research unrelated to neurodegenerative disease led to the identification and isolation of the protein tau (tubulin-associated unit, or τ), which was discovered to be the exchangeable factor responsible for the assembly of microtubules (7). Further investigations into its properties revealed that tau could become phosphorylated (8), and that this phosphorylation reduced microtubule assembly (9). It was not until anti-tau antibodies were generated, and were found to produce a pattern of immunohistochemical staining identical to the inclusions of Alzheimer's and Pick's disease, that a connection was finally made between tau and the pathology of these diseases (10,11). Advancements in electron microscopy enabled the observation that the NFTs of Alzheimer's disease were composed of filaments (12). Biochemical analysis revealed that tau indeed formed the core of the filaments (13). Confirming the identity of the core element of neurofibrillary tangles launched decades of research on the complex protein, tau.

B. Classification of tauopathies

Since the discovery of tau inclusions in Alzheimer's disease and Pick's disease, tau pathology of various shapes and sizes has been observed in a number of other neurodegenerative disorders. This collection of over 20 disorders associated with tau pathology is known as tauopathies. The classification of tauopathies has evolved over time as our understanding of disease etiology has improved. Broadly, tauopathies are divided into primary and secondary tauopathies. In primary tauopathies tau pathology is the only or the predominant neuropathology, but in secondary tauopathies, comorbidities are found such as amyloid-β (Aβ) plaques, α-synuclein Lewy bodies, and transactive response DNA-binding protein 43 (TDP-43) inclusions.

Secondary tauopathies include Alzheimer's disease, Down's syndrome, Lewy body disorders, prion disease, and chronic traumatic encephalopathy, among ten other disorders (14). Other well-known neurodegenerative diseases such as Parkinson's (15) and Huntington's (16) disease have also been proposed to be identified as secondary tauopathies based on accumulating evidence of tau pathology in the brains of these patients. Comparisons between the progression of primary and secondary tauopathies suggests that the presence of comorbid pathologies exacerbates the severity of disease due to synergistic effects (17), but more research in this area is warranted.

Primary tauopathies are grouped into a class of diseases called frontotemporal lobar degeneration with tau-immunopositive inclusions (FTLD-Tau), and are named according to the affected brain regions. Frontotemporal lobar degeneration (FTLD) is a pathological description of what presents clinically as frontotemporal dementia, and FTLD-Tau makes up 40% of these diseases (18). The other 60% are characterized by inclusions of TDP-43, fused in sarcoma (FUS), Ewing's sarcoma (EWS), TATA-binding protein-associated factor 15 (TAF15), and ubiquitin proteasome system markers (18). Frontotemporal dementia is one of the most common causes of early-onset dementia, behind Alzheimer's disease and vascular dementia (19), and thus it is critical that we continue to better our understanding of disease mechanisms to develop new therapeutic strategies.

The molecular subtypes of primary tauopathies are differentiated post mortem based on the morphology of the tau inclusions. Primary tauopathies include Pick's disease, progressive supranuclear palsy, corticobasal degeneration, globular glial tauopathy, argyrophilic grain disease, multiple system tauopathy with dementia, and neurofibrillary tangle dementia. These subtypes differ in the predominant tau isoforms comprising the inclusions, the cell types containing inclusions, the degree of tau phosphorylation, and morphology of the inclusions themselves (18). For instance, Pick bodies are composed primarily of tau isoforms containing 3 instead of 4 microtubule-binding domains (see discussion of isoforms in part III), and tau inclusions of a glob-like morphology are found primarily in oligodendrocytes and astrocytes in globular glial tauopathy (18). As our understanding of pathogenic mechanisms of tauopathies becomes more complete, this classification system will undoubtedly continue to evolve.

The clinical presentation of primary tauopathies is quite heterogeneous and can range from pure cognitive to pure motor syndromes. While secondary tauopathies like Alzheimer's are distinct clinicopathological entities and have validated criteria for diagnosis, diagnosis of primary tauopathies presents a clinical challenge because they are so diverse. Furthermore, only 40% of clinical frontotemporal dementia has underlying tauopathy, so clinical assessment alone is insufficient to diagnose these diseases. However, increasingly finely-tuned cognitive testing and imaging of brain structural changes (20) may allow for more conclusive diagnosis of FLTD-Tau subtypes. In addition, tau positron emission tomography (PET) tracers have recently been developed but have yet to be used in the clinic (21). The involvement of tau in such a

large number of diverse neurodegenerative diseases underlines the importance of 'untangling' its pathogenic properties.

C. Treatments and outlook for public health

The prevalence of tauopathies has been increasing as the population ages, and Alzheimer's alone contributes to 5.7 million Americans, costing the nation $277 billion just in 2018 (22). It is projected that by 2050, the number of people with Alzheimer's will increase to almost 14 million, costing the nation as much as $1.1 trillion (22). Soon, the United States will not be able to afford to care for these patients, causing some to call this a public health crisis. No disease-modifying treatments, or those that slow or halt the progression of disease, yet exist for any tauopathies. Symptomatic treatments for Alzheimer's focus on clinical features of the disease and include acetylcholinesterase inhibitors, N-methyl-D-aspartate (NMDA) antagonists (memantine), antidepressants, and atypical antipsychotics (23). Disease-modifying therapies have been largely focused on amyloid-β, but none have been FDA-approved.

More recently, the field is shifting its focus to tau-directed therapies. As of January 2018, there were ten tau-directed therapies in clinical trials, one in phase III and nine in phase II, split between inhibitors of aggregation and immunotherapies (24). While these studies are showing promising results, it is still hotly debated whether tau aggregates are toxic or a protective response, so it may be premature to assume prevention of tau aggregation will be beneficial. Regarding immunotherapies, because tau is primarily intracellular, the size and charge of antibodies should be carefully considered to increase neuronal uptake, and species-specificity presents further constraints when moving from preclinical rodent studies to humans (25). Other tau therapeutic avenues being investigated include altering post-translational modifications, stabilization of microtubules, and gene therapy to reduce tau levels (26). The pipeline for Alzheimer's treatments consisted of 112 agents as of January 2018 (24). The number of participants and amount of funding needed to conduct well-designed studies are prohibitively large. With pharmaceutical industries terminating Alzheimer's research due to repetitive failures, academic researchers may need to take initiative in drug development to overcome this enormous hurdle.

III. The tau gene and mutations in tauopathies

The tau gene, *Microtubule-Associated Protein Tau* (*MAPT*), is located on the long arm of chromosome 17 (region 17q21.31) and has eight currently known splice variants expressed from a total of sixteen exons (Figure 1). Two of these splice forms, referred to as “big tau”, are expressed in the peripheral nervous system and limited areas of the central nervous system (CNS) (27,28), whereas the rest are expressed only in the CNS (29). Usage of an alternative polyadenylation site encodes an additional ubiquitous form of tau that localizes to neuronal nuclei (30). The splice variants specific to the CNS differ in inclusion of two N-terminal exons and exon 10, which encodes a fourth microtubule-binding repeat domain of the protein (Figure 1).

An important function of tau is the stabilization and assembly of microtubules, and therefore exon 10 splicing is of great interest in the tauopathy field. Splice variants lacking exon 10 are referred to as three-repeat, 3R, isoforms whereas inclusion of exon 10 results in 4-repeat, 4R, isoforms. The CNS *MAPT* variants undergo precise regulation in the developing and adult brain. In both humans and mice, 3R isoforms predominate in the developing brain (31,32) but adult mice express exclusively 4R tau (33) whereas adult humans express equal amounts of 3R and 4R tau (34). This developmental switch is thought to play an important role in dynamic developmental processes such as neuronal maturation due to differences in microtubule binding capacity. The functions of MAPT protein isoforms will be discussed in more detail in subsequent sections.

MAPT displays a pattern of linkage disequilibrium resulting in two haplotypes, H1 and H2. These haplotypes diverged nearly 3 million years ago due to a 900 kilobase-pair inversion of several genes including the entire *MAPT* sequence (35). The H1 haplotype (non-inverted) recombines and is more common worldwide, but less so in those of European descent, whereas the H2 haplotype (inverted) has shown limited diversity (35). In general, H1 is considered to be a risk factor for neurodegenerative diseases because it is over-represented in individuals with progressive supranuclear palsy and corticobasal degeneration (36), as well as in those with sporadic Parkinson’s disease (37). The proposed pathogenic mechanisms of H1 include increased inclusion of exon 10 (38) perhaps due to an additional 238 base pairs in intron 9 (39), and enhanced promoter activity driving higher tau expression levels (37).

In contrast, H2 is thought to be protective for neurodegenerative diseases by

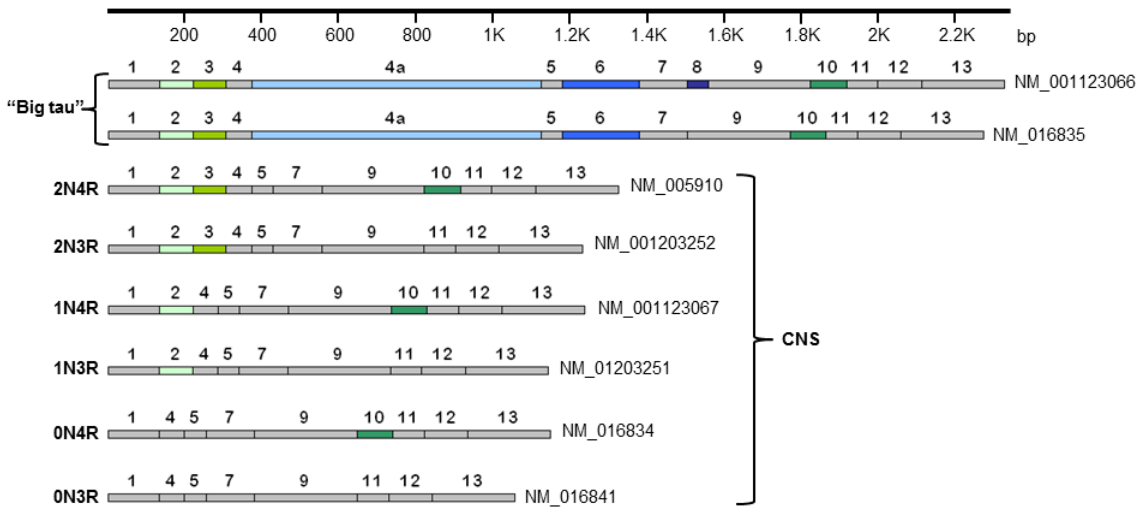

Figure 1. The eight known human *MAPT* transcript splice variants. Alternatively spliced exons in the periphery include exons 4a, 6, and 8, and alternatively spliced exons in the central nervous system (CNS) include exons 2, 3, and 10. Short-hand names of the splice variants are based on inclusion of 1 or 2 'N'-terminal exons and the presence of 3 or 4 microtubule-binding 'r'epeat domains in the protein isoforms, and are indicated to the left of each. Length in base pairs, or 'bp', is indicated at the top, and the National Center for Biotechnology Information (NCBI) RefSeq accession numbers for each variant are indicated to the right of each. Two additional exons encoding the 5' and 3' untranslated regions are not shown.

increasing inclusion of exon 3 (40). The inversion polymorphism does affect expression of other genes in the region (41), but it is assumed that the linkage to neurodegenerative disease depends on *MAPT* specifically due to its high expression level in the brain. The situation is further complicated by the existence of multiple sub-haplotypes due to single-nucleotide polymorphisms (42), some of which cause H1 to be protective and H2 to be a risk factor. Interestingly, the H2 haplotype may predispose individuals to a microdeletion syndrome characterized by mental retardation (43). Overall, the complexity of the *MAPT* genomic region can drive differences in tau expression levels and ratios of splice variants, which modify susceptibility to disease.

While *MAPT* haplotypes can serve as risk factors, there are particular autosomal dominant genetic mutations within the *MAPT* gene that are known to cause neurodegenerative disease. Diseases caused by mutations are familial, or heritable, and are typically rare and associated with an earlier age of onset (44). In contrast, sporadic forms of disease have unknown causes and are much more common. Alzheimer's and FTLD can occur in either a familial or sporadic form, and it is currently unknown whether these forms share common mechanisms. Mutations in *MAPT* account for 5-20% of FTLD-Tau cases depending on geographic distribution, making them the second or third most common cause of familial FTLD behind *C9ORF72* and possibly *progranulin* (*GRN*) mutations (45). A recent study of a large cohort found that 9% of FTLD-Tau patients had *MAPT* mutations whereas 62% had sporadic disease, and the other 25% had some family history (46). Although *MAPT* mutations are rare, they provide a convenient tool to study tau pathogenicity, and may ultimately give insights into mechanisms of both familial and sporadic disease.

A tauopathy called frontotemporal degeneration and parkinsonism linked to chromosome 17 (FTDP-17) has typically been considered separate from the rest of FTLD-Tau because it can also be caused by mutations in *GRN* also on chromosome 17, resulting in FTLD associated with TDP-43-immunopositive inclusions (FTLD-TDP) (47,48). However, because FTDP-17 is associated with similar neuropathological phenotypes to sporadic FTLD-Tau, some argue that it should be classified together with FTLD-Tau or that the term FTDP-17 should be done away with altogether (44). Regardless, FTDP-17 is an autosomal dominant neurodegenerative disease recognized to have a genetic cause by a series of important studies that progressively narrowed down the genomic locus to *MAPT* (49-52). It was this realization that established tau

itself as a disease-causing agent, and sparked renewed interest into the complex protein.

MAPT mutations not only cause FTDP-17, but can also be associated with Pick's disease, progressive supranuclear palsy, corticobasal degeneration, and globular glial tauopathy. There is generally poor correlation between mutations and disease phenotype (53), and there can even be diverse symptoms between family members with the same mutation (54). Because of this phenotypic diversity frontotemporal dementia disorders are typically referred to as a spectrum (55), but they can broadly be divided into dementia-dominant and parkinsonism-dominant. Anecdotal evidence suggests that mutations affecting exon 10 splicing are more often of the parkinsonism-type whereas mutations with other pathogenic effects cause the dementia-type (56). Because, particular mutations are not associated with specific phenotypes, other genetic or perhaps epigenetic mechanisms may be responsible for clinical manifestation. In addition, *MAPT* mutation carriers may have a broad range of age-of-onset from the second to the eighth decade (57), however, disease onset is before 50 years of age in about 50% of cases (58). Interestingly, this is on average earlier than for mutations in other genes underlying FTLD, including *GRN* and *C9ORF72*, suggesting that tau pathogenicity may be particularly potent.

A recent study found that of the 87 *MAPT* mutations that have been identified, 22 of these have confirmed pathogenicity based on strict criteria including segregation of the mutation with the phenotype within families, existence of multiple independent cases, existence of other mutations at the same residue, and supportive functional studies (14). Complementary to this study as well as the alzforum.org database, I have made an updated table summarizing the characteristics of the known *MAPT* mutations in FTDP-17, which now total to 96 (Table 1). Using next generation sequencing technology, a recent report suggests that more mutations may need to be added to this list (59). Importantly, mutations in 21 genes besides *MAPT* can be associated with tau pathology, suggesting that tau may be a pathogenic agent in some diseases, but tangles can develop in other diseases in the absence of mutation-driven tau toxicity per se (60).

To add to the complexity of the *MAPT* gene, pathogenic mutations do not have consistent effects on tau biology. Generally, they can affect microtubule (MT) assembly, propensity of tau aggregation, and the 4R to 3R isoform ratio (Table 1). Amino acid

Table 1. Known *MAPT* mutations in FTDP-17 and postulated pathogenic effects. Confirmed pathogenic mutations are in bolded font. Note that amino acid numbering is based on the 2N4R isoform except for mutations in exons 4a, 6, 8. This list was updated in March 2019.

Type of mutation	Mutation	Location	Pathogenic effects	References
Missense (71)	P4T	Exon 1	Unknown	(61)
	R5L	Exon 1	↑ MT assembly ↑ soluble tau ↑ aggregation	(62,63)
	R5H	Exon 1	↑ aggregation ↓ MT assembly	(64)
	R5C	Exon 1	Unknown	(65)
	A41T	Exon 1	Unknown	(65)
	L48V	Exon 2	Unknown	(66)
	G55R	Exon 2	↑ MT assembly	(67)
	V75A	Exon 3	Unknown	(68)
	A90V	Exon 3	Unknown	(61)
	Q124E	Exon 4	Unknown	(69)
	D177V	Exon 4a	Unknown	(70,71)
	G213R	Exon 4a	Unknown	(72,73)
	V224G	Exon 4a	Unknown	(61,72)
	Q230R	Exon 4a	Unknown	(72)
	A297V	Exon 4a	Unknown	(72)
	S318L	Exon 4a	Unknown	(72)
	L410F	Exon 6	Unknown	(74)
	A152T	Exon 7	↑ aggregation ↑ proteolysis ↓ MT assembly	(72,75)
	A178T	Exon 7	Unknown	(76,77)
	S427F	Exon 8	Unknown	(65,78)
	P512H	Exon 8	Unknown	(74)
	P513A	Exon 8	Unknown	(71)

	G201S	Exon 9	Unknown	(78)
	R221Q	Exon 9	Unknown	(79)
	A239T	Exon 9	Unknown	(78,80,81)
	K257T	Exon 9	↑ aggregation ↑ proteolysis ↓ MT assembly	(80,82)
	I260V	Exon 9	↑ aggregation ↓ MT assembly	(83)
	T263P	Exon 9	Unknown	(84)
	L266V	Exon 9	↑ aggregation ↑ 4R:3R ↓ MT assembly	(85,86)
	G272V	Exon 9	↑ aggregation	(87)
	G273R	Exon 9	Unknown	(88)
	N279K	Exon 10	↑ 4R:3R	(89,90)
	L284R	Exon 10	Unknown	(91)
	S285R	Exon 10	↑ 4R:3R	(92)
	V287I	Exon 10	Unknown	(72)
	C291R	Exon 10	↑ 4R:3R	(93)
	N296D	Exon 10	Unknown	(94)
	N296H	Exon 10	↑ aggregation ↑ 4R:3R ↓ MT assembly	(95-97)
	K298E	Exon 10	↓ MT assembly ↑ 4R:3R	(98)
	H299Y	Exon 10	Unknown	(99)
	P301T	Exon 10	↑ aggregation	(100,101)
	P301S	Exon 10	↑ aggregation ↓ MT assembly ↓ axonal transport ↓ synapses	(102-104)

	P301L	Exon 10	↑ aggregation ↓ MT assembly	(63,105,106)
	G303V	Exon 10	↑ 4R:3R	(107)
	G304S	Exon 10	Unknown	(108)
	S305N	Exon 10	↑ 4R:3R	(54,109,110)
	S305I	Exon 10	↑ 4R:3R	(111)
	L315R	Exon 11	↓ MT assembly	(112)
	K317M	Exon 11	Unknown	(113)
	K317N	Exon 11	↑ aggregation for 4R ↓ aggregation for 3R ↑ 4R:3R	(114)
	S320F	Exon 11	↓ MT assembly	(115)
	P332S	Exon 11	↓ MT assembly	(116)
	G335S	Exon 12	↓ MT assembly	(117)
	G335V	Exon 12	↑ aggregation ↓ MT assembly	(118)
	Q336R	Exon 12	↑ aggregation ↑ MT assembly	(119,120)
	Q336H	Exon 12	↑ aggregation ↑ MT assembly	(120)
	V337M	Exon 12	↑ aggregation ↓ MT assembly	(50,121)
	E342V	Exon 12	↑ 4R:3R	(122)
	S352L	Exon 12	↑ aggregation ↓ MT assembly	(123,124)
	S356T	Exon 12	Unknown	(125)
	I360V	Exon 12	Unknown	(65)
	V363I	Exon 12	↑ MT assembly	(126,127)
	P364S	Exon 12	↓ MT assembly	(128,129)

			↑ chromosome instability	
	G366R	Exon 12	↓ MT assembly ↑ chromosome instability	(128,129)
	K369I	Exon 12	↓ MT assembly	(130)
	E372G	Exon 13	↑ aggregation ↓ MT assembly	(131)
	G389R	Exon 13	↓ MT assembly ↑ proteolysis	(132-136)
	R406W	Exon 13	↓ MT assembly	(34,105,137)
	N410H	Exon 13	↓ MT assembly ↑ aggregation ↑ 4R:3R	(138)
	D418N	Exon 13	↑ chromosome instability	(129)
	T427M	Exon 13	Unknown	(139)
Silent (22)	T39T	Exon 1	Unknown	(76)
	P176P	Exon 7	Unknown	(106)
	g(+33)a	Intron 9	Unknown	(106)
	t(-15)c	Intron 9	↓ 4R:3R	(140)
	g(-10)t	Intron 9	↑ 4R:3R	(141)
	L284L	Exon 10	↑ 4R:3R	(142,143)
	N286N	Exon 10	Unknown	(144)
	N296N	Exon 10	↑ 4R:3R	(96,145)
	P301P	Exon 10	Unknown	(146)
	S305S	Exon 10	↑ 4R:3R	(147-149)
	g(+3)a	Intron 10	↑ 4R:3R	(51,150,151)
	a(+4)c	Intron 10	↓ 4R:3R	(140)
	t(+11)c	Intron 10	↑ 4R:3R	(152)
	c(+12)t	Intron 10	↑ 4R:3R	(153)

	a(+13)g	Intron 10	↑ 4R:3R	(80)
	c(+14)t	Intron 10	↑ 4R:3R	(105,154-156)
	a(+15)c	Intron 10	↑ 4R:3R	(157)
	c(+16)t	Intron 10	↑ 4R:3R	(105,158)
	c(+19)g	Intron 10	↓ 4R:3R	(144,159)
	c(+25)t	Intron 10	Unknown	(160)
	g(+29)a	Intron 10	↓ 4R:3R	(142,159,160)
	a(+34)g	Intron 11	Unknown	(161)
Deletion (43)	ΔK280	Exon 10	↑ aggregation ↓ 4R:3R ↓ MT assembly	(106,162-164)
	ΔN296	Exon 10	↑ aggregation ↓ MT assembly	(96,165)
Nonsense (1)	R448*	Exon 8	Unknown	(65)

substitutions caused by missense mutations in the MT-binding domains may cause conformational changes or changes in electrical charge that influence the ability of tau to bind and assemble MTs (34). This can lead to abnormalities in neuronal cytoskeletal structure as well as disruption of axonal transport (166), which each have the potential to affect a broad range of cellular functions. Other missense mutations can change the propensity for domains on tau to form β-structures that enhance fibrillization into pathological aggregates. Finally, silent mutations in splicing enhancer or silencer sites, or those in the stem-loop structure in the 5' region of intron 10 of tau RNA have the ability to influence inclusion of exon 10 in the mature messenger RNA (mRNA) (167). Other silent mutations in exons may be pathogenic via changes in tRNA utilization (168). While the majority of mutations with known effects seem to reduce MT assembly (e.g. A152T, L266V, P301L, V337M), others can *increase* MT polymerization (e.g. R5L, Q336H). Similarly, most mutations increase tau aggregation (e.g. G272V, P301L, G335V) and the 4R to 3R ratio (e.g. N279K, G303V, Intron 10 g(+3)a), but others have the opposite effect (e.g. K317N for aggregation; ΔK280 for 4R:3R) (Table 1). Frustratingly, this prevents generalization of any of these pathogenic effects as being causative of disease. These paradoxes indicate that either the effects of *MAPT* mutations need to be studied beyond these parameters, or simply that tau dysregulation in general is pathogenic.

The most common *MAPT* mutation is the P301L mutation, identified in 32 families worldwide (AD & FTD mutation database)(169). This mutation is confirmed to be pathogenic and, as it is located in exon 10 which encodes one of the MT-binding domains, it has been shown to reduce MT binding (34) and consequently the ability of tau to facilitate MT assembly (106). The P301L mutation is also known to make tau a more favorable substrate for phosphorylation by kinases (170) and to enhance tau aggregation (63,171,172). Finally, P301L tau has a unique ability to infiltrate dendritic spines, where it may interfere with synaptic transmission through dislocation of glutamatergic receptors from the cell membrane (173). The prevalence of the P301L *MAPT* mutation has caused it to become the most well-studied of all the tau mutations, and has motivated the generation of eight different animal models harboring the mutation to elucidate its effects in the mammalian brain (Alzforum research model database). Despite these efforts and although much has been learned about mutant tau from this work, the mechanisms of P301L-induced toxicity remain unclear.

IV. The tau protein and its diverse functions

A. Typical functions

As the main microtubule-associated protein in neuronal axons, the 'typical' or canonical functions of tau are directly related to its ability to bind microtubules (MTs) in this cellular region. In the healthy adult brain, the main function of tau is to facilitate MT polymerization in axons (7) in a way that reduces dynamic instability (174). Tau decorates the MT bundles that extend throughout neuronal axons, and is therefore important for providing support to this elongated structure. The tau protein itself has little secondary structure, and is divided into four sub-regions: the N-terminal projection domain, proline-rich region, MT-binding repeat domain, and C-terminal domain. The MT-binding repeat domain facilitates tau-MT interactions and MT assembly (175) while the C-terminal domain negatively regulates MT polymerization (176). The proline-rich domain can also bind MTs (177) but is also involved in cell signaling through a variety of binding partners (14). The negatively-charged projection domain is repelled away from MTs (178) and therefore determines spacing between MTs (179) – splicing of exons 2 and 3 at the N-terminus lengthens that distance. Various imaging techniques suggest that tau binds laterally to the inner surface of protofilament sheets while the proline-rich region curves around the side (180), or that the entire tau molecule binds longitudinally to protofilaments (181). At any given time, up to 98% of tau in cells is MT-bound (182), however, the dwell time on microtubules lasts only 40ms (183), freeing tau up to interact with other proteins and perform other functions.

Transient binding of tau to MTs through this "kiss and hop" mechanism (183) is sufficient for tau to facilitate axonal transport of cargo such as mitochondria and neurotransmitter-containing vesicles along MTs through interactions with molecular motors kinesin and dynein (184). Within the axon tau levels exhibit a gradient, with the highest concentration at the axon terminal (185). This gradient of tau, combined with its ability to cause detachment of kinesin from MTs (184) facilitates release of cargo at the axon terminal. Tau's inhibition of kinesin depends on both the tau isoform and the nucleotide-binding state of the microtubules (186), making this interaction and consequently tau's role in axonal transport inherently complex. Nonetheless, by aiding the delivery of newly synthesized neurotransmitter to the axon terminal, tau has a role in synaptic transmission at the presynaptic side.

In the adult brain, tau is primarily localized to neuronal axons perhaps due to selective stabilization of tau protein in this region or to selective degradation of tau in other subcellular compartments (187). In addition, tau mRNA contains an axon localization signal in its 3' untranslated region (3'UTR) (188). RNA-binding proteins such as interleukin enhancer binding factor 3 (Ilf3) can bind this signal and act as chaperones to escort tau mRNA (189) to the axon where it can be locally translated (188). Tau is prevented from leaving axons through several mechanisms. Interactions with membrane proteins such as Annexin A2 keep tau in this region (190). In addition, it has been suggested that a molecular barrier exists at the axon initial segment (AIS) that prevents tau from leaving the axon (191).

In the developing brain, before neurons have axons or dendrites, tau is involved in neuronal morphogenesis and differentiation, as well as neurite outgrowth and elongation through its interactions with MTs (192). In support of this, loss of tau prevents proper neuronal maturation *in vitro* (193). While neurites form normally, neurite polarity, or differentiation of dendrites vs. axon, fails to be established and these tau-deficient neurons fail to form an axon (194). Initial observations that tau is concentrated at the growth cone of maturing neurites (185) suggested it had functions other than stabilization of MTs per se. More recent work has revealed that tau directly interacts with and regulates localization of the core MT plus-end tracking proteins required for neurite elongation during differentiation (195).

As stated previously, 3R tau isoforms are more prominently expressed in the brain than 4R isoforms during development and at young ages (31). The nature of tau interactions with MTs depends on the number of repeat domains, and this has important functional implications. 4R tau has a three-fold higher MT-binding capacity than 3R tau (196), and therefore is better at facilitating MT polymerization (197). 4R tau is also a more potent inhibitor of MT dynamics (198,199), suggesting that the more transient binding of 3R tau to MTs is necessary for dynamic developmental processes to occur. Indeed, the period of 3R tau predominance coincides with the ages at which neurogenesis peaks and axon and dendrite densities are on the rise (200). The favored view is that 3R tau enables MTs to be in a dynamic state, whereas 4R tau maintains MT stability needed in adult neurons (201). This is supported by the fact that 3R tau expression in the adult brain is restricted to the subgranular zone of the dentate gyrus,

where adult neurogenesis takes place (33). Overall, canonical functions of tau differ at different times in the lifespan, mediated by changes splicing.

B. Atypical functions

A smaller pool of tau exists in the brain that performs functions unrelated to its ability to bind axonal MTs. These 'atypical' functions occur in neuronal somata, nuclei, and dendrites, and also outside of neurons altogether. Despite the mechanisms designed to compartmentalize tau to neuronal axons, specific isoforms are found at lower levels in other regions of the cell. In a transgenic mouse with the full human *MAPT* sequence, 3R tau was found to be more prominent in the cell body during development whereas 4R staining was "synaptic-like" in adult brains suggesting its presence in dendrites (33). In addition to exon 10, N-terminal exons 2 and 3 are alternatively spliced resulting in 0N, 1N, and 2N isoforms. 0N isoforms are prominent in both neuronal somata and axons, 1N isoforms are overrepresented in nuclei, and 2N isoforms are prominent in neuronal somata and dendrites (202). Some isoforms such as 2N4R tau more readily leak past the AIS barrier (discussed in the previous section) into the somatodendritic compartment (203), providing a mechanistic explanation for isoform-dependent sorting of tau. These isoforms perform specific atypical functions within each of those subcellular compartments.

Tau isoforms present in dendrites, likely 2N isoforms (202), participate in synaptic plasticity, which consists of both structural and electrophysiological changes. In terms of structure, tau is postulated to play a role in growth and retraction of synapses through its interactions with filamentous actin (F-actin) in dendritic spines (204,205). Plasticity also occurs on an electrophysiological level in the form of long-term potentiation (LTP) and long-term depression (LTD). Following neuronal activation, tau has been observed to move from dendritic shafts into spines (206). Not only could this translocation of tau be important for plasticity, but also local translation of tau in dendrites, which has also been observed to be driven by neuronal activity (207).

Within dendritic spines, tau interacts with post-synaptic proteins such as PSD-95 (208) and Src-family tyrosine kinases such as Fyn (209) to facilitate the scaffolding of excitatory NMDA receptors (210,211). Site-specific phosphorylation of tau following NMDA receptor activation weakens its relationship with Fyn and PSD-95, thus reducing receptor anchoring and preventing overexcitation (208). Site-specific phosphorylation of

tau also facilitates LTD through internalization of excitatory α-amino-3-hydroxy-5-methyl-4-isoxazolepropionic acid (AMPA) receptors (212). In support of tau's functions in dendrites, studies done *in vivo* have shown that loss of tau can result in deficits in LTP underlying cognitive impairments (213), as well as deficits in adult neurogenesis following environmental enrichment (214).

Tau isoforms enriched in neuronal nuclei, likely 1N isoforms (202), have an established role in DNA protection. A recent study confirmed nuclear localization of tau using several methods, including biochemical isolation of nuclei from mouse brain tissue (215). Tau can bind to both single- and double- stranded DNA, through part of its proline-rich domain and the second microtubule-binding repeat domain (216). Studies have shown that tau-DNA binding increases during oxidative stress (217-219), suggesting that this interaction is a protective response. This is a reversible process that depends on the availability of tau, suggesting tau protection of DNA occurs on demand, and stops once the brain is no longer under stress (220). Tau binds DNA even in the absence of stress to maintain chromosome stability and prevent chromosomal aberrations such as breakages or translocations (221,222). A recent genomics study indicated that tau likely plays a role in genome spatial organization, and may also influence transcription of genes involved in neurological processes (218).

Although tau is expressed primarily in neurons, it is expressed at lower levels in glial cells including astrocytes (223) and oligodendrocytes (224,225). Little is known about tau functions in healthy astrocytes, but the accumulation of hyperphosphorylated tau in astrocytes of diseased brains has been well-characterized (226). In contrast, tau has a defined biological role in oligodendrocytes, particularly in myelination. Through its interactions with MTs, tau sorts into oligodendrocyte processes to control myelin formation and thickness, possibly by aiding in the transport of myelin basic protein (225). Indeed, downregulation of tau or the mislocalization of tau to the soma results in a thinner myelin sheath and can cause movement disorders (227,228). Interestingly, tau isoform regulation is different in neurons and oligodendrocytes, indicating cell-type specific mechanisms controlling tau splicing over the course of development. While in neurons there is a developmental switch from 3R to 4R tau isoforms (31,33,34), both 3R and 4R tau are expressed in developing and adult oligodendrocytes (229,230). It is thought that the persistence of 3R tau expression in adult oligodendrocytes helps

maintain a “young” and plastic physiological state, capable of active adaptation to ever-changing myelination needs (231).

More limited evidence suggests that tau may have a number of other functions, which warrant further research. Although tau’s function in neurite outgrowth is believed to be dependent on its interactions with MTs, tau can also function as a signaling protein to facilitate the downstream effects of nerve growth factor (NGF) stimulation, independent of MT binding (232). Tau’s interactions with neuronal plasma membranes (233) and cellular organelles such as the endoplasmic reticulum (234), Golgi apparatus (235), vacuoles, and mitochondria (236), suggest it may have other diverse functions such as in protein production and regulation.

C. Post-translational modifications of tau

Post-translational modifications modulate tau function. Tau can be phosphorylated, acetylated, ubiquitinated, *O*-GlcNAcylated, sumoylated, oxidated, nitrated, and more (237). Such a diversity of post-translational modifications that can be applied to the tau protein adds an additional level of complexity to its regulation and function in the brain. Phosphorylation is the most well-studied of tau modifications. A basal level of phosphorylation is required for endogenous tau function. Serine, threonine, and tyrosine residues are targeted by both proline- and non-proline- directed kinases. Among the proline-directed kinases, glycogen synthase kinase 3 (GSK-3) and cyclin-dependent kinase 5 have been shown to be involved in endogenous tau function (238,239). Non-proline directed kinases that target tau include cAMP-dependent protein kinase (240) and Ca^{2+}/calmodulin-dependent protein kinase 2 (CaMKII) (241).

Phosphorylation occurs mainly in the proline-rich domain on tau (242) and modulates essentially every aspect of tau function in a site-specific manner including MT binding (191), neurite elongation (243), tau sorting (191,219), DNA interactions (216), interactions with the plasma membrane (244), and plasticity (212). Consistent with tau’s role in neurite elongation, a phosphorylation gradient exists in growing axons to allow distal MTs to be dynamic (245). Intriguingly, in hibernating animals such as squirrels, tau phosphorylation is dramatically upregulated during periods of torpor, or drops in metabolic rate (246,247). This effect is reversible and appears to be a mechanism for controlled down-regulation of synaptic transmission (248). Tau phosphorylation and activation of tau-targeting kinases are also precisely regulated during development. A

high level of phosphorylation is maintained early in postnatal development, likely to facilitate dynamic interactions with MTs, but phosphorylation declines with age, likely to maintain MT stability (249,250).

It should be noted that many of the studies of tau's function have been performed in rodents, and differential portions of sequence in primate-specific tau may impact its function, particularly in relation to its binding partners (251). The involvement of tau in such diverse functions essential for neuronal survival raise the possibility that tauopathies are caused by tau loss-of-function. However, much research indicates that tauopathies can also be caused by toxic gain-of-function.

V. Tau dysfunction in tauopathies

A. Formation and spread of pathological tau

Due to the complex and multifunctional role of tau in the brain, tau dysfunction in neurodegenerative diseases is also inherently complex and incompletely understood. The prevailing hypothesis for tau's role in disease pathogenesis is that it becomes hyperphosphorylated, is unable to bind MTs, missorts to somatodendritic regions of neurons, and causes cellular dysfunctions through numerous molecular pathways. Although a certain level of phosphorylation is required for normal tau function, this becomes exaggerated in disease (252). Rather than a single phosphorylation site driving tau pathogenicity, multiple phosphorylation sites work in concert to generate a pathological form of tau (253,254). This hyperphosphorylation, perhaps caused by an imbalance in kinase and phosphatase activity, can prevent MT binding by modifying electrical affinity of tau for MTs (255) and/or inducing conformational changes in tau (256). Tau that is dissociated from MTs can take on conformations such as a "paperclip-like" conformation (257), which may increase the propensity for motifs in the MT-binding domain to form β-sheets (258), which are structural components linked to tau toxicity (259). Hyperphosphorylated, dissociated tau is then freed up to mislocalize to somatodendritic regions of neurons where it aggregates. Consequently, MTs are observed to become destabilized (260), leading to impairments in axonal transport (261) and other problems.

The process of tau aggregation is thought to involve a sequential evolution of different tau species (262). Once a tau monomer takes on a pathological conformation, formation of tau dimers/trimers and oligomers proceeds spontaneously because it is

energetically favorable (263). Dimers, trimers, and small soluble oligomers are composed of antiparallel tau monomers linked by disulfide bridging (264). From these species or from monomers alone, granular oligomers can form, which are densely packed aggregates of about 40 tau monomers and are insoluble, meaning they cannot be broken up or dissolved (265). Tau filaments can be formed either from oligomers or smaller dimers and trimers when motifs in tau's MT-binding domain change from random coil structure to β-sheets (266). Filaments can take on a variety of shapes in tauopathies (267), however paired helical filaments are commonly observed and consist of two straight filaments wound around each other (268). Finally, filaments cluster together to form neurofibrillary tangles (269).

There is much debate in the field about which of the tau species on the soluble-insoluble spectrum are to blame for toxicity. On one hand, the presence and regional localization of tangles correlate well with disease progression (270,271), and cerebrospinal fluid biomarkers for tau pathology including high levels of total tau and phospho-tau are associated with rapid progression from mild cognitive impairment to Alzheimer's disease (272). However, tangles can also be found in cognitively healthy individuals (273), can form in mouse models without causing neurodegeneration (274), and can remain in surviving neurons for long periods (275). Therefore, tangles are hypothesized by some to be a protective response to sequester harmful soluble tau species.

Oligomers are increasingly thought to be involved in disease pathogenesis. Growing evidence indicates that hyperphosphorylated, soluble oligomers cause synapse loss (276) while granular oligomers cause neurons loss (277). This supports the idea that tau toxicity can occur regardless of the presence of insoluble tau. Others are investigating the hypothesis that truncated forms of tau are the primary toxic entities in neurodegenerative diseases. In non-apoptotic pathways, caspases can cleave tau (278), and caspase-3 cleavage of tau at aspartate 421 seems to be more strongly associated with cognitive impairments in Alzheimer's disease than tangles themselves (279). In addition, caspase-2 generates a tau fragment that causes synaptic and cognitive deficits despite resisting fibrillation in a mouse model of tauopathy (280). Soluble forms of tau including oligomers and fragments may act in concert to exert toxic effects in neurons, while tangles form as a consequence or perhaps a protective response.

The patterns of tau spreading throughout the brain are heterogenous among tauopathies (281,282), but the stereotypical spread through interconnected regions in Alzheimer's has led researchers to propose a neuron-to-neuron propagation mechanism (283). There are several ways this could occur. Based on findings indicating that application of exogenous pathological tau can stimulate tau aggregation *in vivo* (284), and that tau can be found in the extracellular space (285), a "prion-like" mechanism has been proposed whereby pathological tau 'seeds' are released from an infected neuron and taken up by neighboring neurons where they seed the formation of more insoluble aggregates (286). Indeed, cells are able to internalize tau aggregates via endocytosis mediated by surface heparan sulfate proteoglycans (287). As neuronal activity is associated with increased release of tau and exacerbation of tau pathology (288), another postulated mechanism for neuron-to-neuron tau spread is via synaptic transfer. Tau spreading may also occur through a microglia-dependent membrane-based mechanism (289). In this scenario microglia engulf tau-containing dying neurons and/or synapses, and release pathological tau via exosomes. Indeed, exosomes isolated from Alzheimer's disease patients contain pathological tau (290).

B. Mechanisms of tau toxicity

Once pathological tau forms in a neuron or is internalized, how does it go on to disrupt cellular processes? As stated above, the favored hypothesis is that hyperphosphorylation of tau triggers a cascade of pathological events associated with missorting, or mislocalization, of tau. Phosphorylation (191) and acetylation (291) at specific sites, disease-linked mutations (173), as well as truncation (280) of tau allow it to cross the barrier at the AIS and infiltrate somatodendritic regions of neurons. Tau that mislocalizes to dendritic spines is observed to reduce synaptic transmission via internalization of AMPA receptors (AMPARs), underlying cognitive impairments in a transgenic mouse model (173,280). This may occur through activation of calcineurin (protein phosphatase 2B), which dephosphorylates AMPARs to cause their internalization (292). Similarly, acetylated tau in dendritic spines interferes with AMPAR recruitment, thus disrupting long-term potentiation and memory (293). Excitotoxicity driven by NMDA receptor (NMDAR) overactivation has also been implicated in tauopathies, mediated by tau that has been phosphorylated by Fyn (294). Not only could imbalance of AMPARs and NMDARs be involved, but also total loss of synapses due to

tau mislocalization (295). These studies show that tau mislocalization to the synapse can have a variety of toxic effects, from electrophysiological to structural.

Tau dysfunction is also tied to oxidative stress and mitochondrial abnormalities. Mitochondria are dynamic organelles that undergo constant fission and fusion, and produce ATP to meet the high energy demands of neurons. As part of this process, mitochondria normally produce low levels of reactive oxygen species (ROS) as a byproduct of oxygen metabolism. Oxidative stress refers to an imbalance of ROS and the antioxidants that keep them in check. In tauopathies such as Alzheimer's disease, increased ROS production and reduced antioxidants are observed (296,297), even in earlier mild cognitive impairment (MCI) stages (298,299). Therefore, oxidative stress seems to be an early event in tauopathies, and has been shown to cause tau hyperphosphorylation (300) via upregulation of kinases such as GSK-3 (301) and downregulation of phosphatases such as protein phosphatase 2A (302).

Tau hyperphosphorylation resulting from oxidative stress leads to numerous problems with mitochondria, creating a vicious cycle. Tau-induced disassembly of MTs is associated with impairments in mitochondrial transport along axonal MTs (303) leading to mislocalization and perinuclear accumulation of mitochondria (304). Hyperphosphorylated tau also disrupts the delicate balance between mitochondrial fission and fusion (305), leading to aberrant fragmentation (306) or elongation (307) of mitochondria, possibly through interactions with Dynamin-related protein 1 (Drp1) (308). Deficits in mitochondrial bioenergetics are also observed in tauopathies including altered levels of mitochondrial enzymes (309), which have the potential to impact ATP production, electron transport, and respiratory activity. Not only is tau hyperphosphorylation implicated in these toxic mechanisms, but also truncation (310) as well as disease-linked *MAPT* mutations like P301L (311-313). Finally, oxidative stress and mitochondrial abnormalities are also linked to autophagic dysfunction, leading to reduction of tau clearance (314). Overall, vicious cycles on multiple levels of the relationship between pathological tau, mitochondrial dynamics, and oxidative stress may contribute to progressive worsening of cell health and eventual cognitive decline in tauopathies.

Tau's nuclear function can also go awry in disease, leading to problems like chromosome instability, aneuploidy, and cell cycle reentry. Several studies suggest that pathological tau causes chromatin instability and disorganization (129,315). In tauopathy

models and in human neurodegenerative disease, tau dysfunction is associated with loss of heterochromatin, tightly packed DNA that is unavailable for transcription (316). This 'relaxation' of heterochromatin causes aberrant expression of genes normally silenced (316). Tau-induced mislocalization of nuclear transcription factors to the cytoplasm is another way tau can affect global gene transcription (317). Mature neurons are non-dividing because they have exited the cell cycle. However, cell cycle proteins have been observed to become aberrantly activated in a fly model (318), mouse model (319), and in human tauopathy (320), leading to incomplete 'de-differentiation' and cell death (321). Tau's association with the mitotic spindle has been shown to be necessary for normal chromosome segregation, and its dysfunction is implicated in aneuploidy, or abnormal chromosome number (222). While aneuploidy increases with normal aging (322), this is exaggerated in Alzheimer's disease and is linked to cell death (323,324). Nuclear abnormalities in tauopathies provide an example of how tau as a multifunctional protein can cause diverse dysfunctions in disease.

Neuroinflammatory markers have persistently been found to be upregulated in tauopathies (325) and have been considered a downstream response to other pathological mechanisms. However, recent studies support the idea that neuroinflammation, involving both microglia and astrocytes, is a driver of neurodegeneration or at least plays an active role in worsening tau pathology. A favored hypothesis is that microglia become activated in response to pathological tau (such as oligomers) released from affected neurons (326). The microglia release inflammatory chemokines and cytokines that activate astrocytes (327), which in turn release more proinflammatory molecules. These secreted factors have direct impacts on neurons to further exacerbate tau pathology (328-330). This activates a chronic inflammatory process composed of a vicious cycle between tau pathology and microglia/astrocyte activation that contributes to synaptic and neuronal dysfunction (329,331). Several differences between Alzheimer's and primary tauopathies suggest that different inflammatory mechanisms are involved. For example, genetic risk factors like variants of immune proteins Triggering receptor expressed on myeloid cells 2 (TREM2) and apolipoprotein E (APOE), as well as Aβ may contribute to Alzheimer's pathogenesis but not primary tauopathies (332,333). Many other important questions remain regarding the role of neuroinflammation in tauopathies, warranting further investigation.

There are several other cellular dysfunctions in tauopathies in which the role of tau is gaining increasing attention. The idea that divergence from protein homeostasis has negative impacts on cellular functions is not novel. Either increases or decreases in tau beyond normal levels can result in abnormalities (37,334). However, mechanisms controlling tau homeostasis are currently being investigated, and have so far revealed that tau acetylation competes for ubiquitination of lysines to slow tau clearance, resulting in increases in tau levels (335). Slowing tau turnover was associated with promotion of tau accumulation, exacerbation of neurodegeneration, and behavioral deficits in a tauopathy mouse model (335). Recently, somatodendritic mislocalization of tau was found to promote a natural stress response in neurons – the formation of complexes composed of RNA-binding proteins and mRNA termed 'stress granules,' which ensure proper translation of proteins involved in the stress response. This area of research suggests that in tauopathies, stress granules become overactive and large, and that tau and RNA-binding proteins act synergistically to promote pathological tau aggregation, exacerbating cellular dysfunction (336-338). This is supported by the idea that tau harboring disease-linked *MAPT* mutations also promotes pathological stress granule formation (90).

A burgeoning body of literature also suggests that the formation of pathological tau aggregates has a negative impact on metabolic and neuroendocrine processes. Specifically, tau is involved in the dysregulation of glucose metabolism in the brain and hypothalamic control of food intake via insulin signaling (339). Insulin resistance has been frequently observed in Alzheimer's disease (340), and has been shown to contribute to imbalance of tau kinases and phosphatases to cause tau hyperphosphorylation. Conversely, pathological tau can also influence insulin signaling via neuroinflammatory pathways or intraneuronal sequestration of insulin (341), resulting in a vicious cycle. Finally, roles for tau in suppression of adult neurogenesis (342,343) and in blood vessel abnormalities (344) have also been described.

C. Remaining questions and final comments

Aside from the research described above for which the pathogenic mechanisms of tau remain unclear, a number of general questions remain concerning the role of tau in neurodegenerative diseases. For instance, are the mechanisms of tau pathogenicity the same between sporadic and familial diseases? Phrased differently, do mutant tau

and non-mutant tau disrupt cellular functions in the same way in the aging brain? While there are obvious differences in the clinical and neuropathological manifestation of sporadic and familial diseases, it is possible that tau mechanisms are similar but more severe and earlier onset in familial diseases due to the presence of *MAPT* mutations. Mutations, while they do not have consistent effects on tau biology, exhibit general trends in that the majority of mutations increase 4R:3R tau isoform ratios, increase aggregation, and reduce MT assembly (Table 1). These phenotypes can be observed in sporadic disease as well.

In sporadic disease, the presence of other pathologies such as Aβ in Alzheimer's, α-synuclein in Lewy body disorders, and TDP-43 in FTLD, amyotrophic lateral sclerosis (ALS), and other diseases may have synergistic effects with tau that result in a range of different phenotypes. Deciphering the role of tau in Alzheimer's disease is of particular importance because of growing prevalence of this disease coupled to lack of disease-modifying therapies. This is a controversial topic because the amyloid-cascade hypothesis is at odds with repeated failures of amyloid-targeting drugs in clinical trials, leading researchers to favor tau-targeting therapeutic strategies more recently (345). However, hypotheses favoring Aβ vs. tau are not necessarily mutually exclusive. Multiple lines of evidence suggest that Alzheimer's disease is an Aβ-assisted tauopathy (346), meaning Aβ pathology is permissive for tau toxicity, which ultimately drives progression of disease.

The information covered in this chapter reveals many layers of complexity that contribute to tau function and dysfunction in the brain: 1) *MAPT* mutations have contrasting effects, 2) there are many possible toxic species of tau on the soluble-insoluble spectrum, 3) post-translational modifications modulate virtually all aspects of tau biology, 4) tau's function depends on isoform, cell type, and subcellular compartment, and 5) tau's function changes over the lifespan. The subsequent work in this thesis identifies and characterizes confounding variables in transgenic mouse models of tauopathy, which, together with the inherent complexity of tau's role in neurodegeneration, have contributed to the failure of therapies to translate from pre-clinical studies to human clinical trials. The studies presented in the following chapters advocate for improvement in the design and use of mouse models in order to enhance our understanding of tau pathogenicity and ultimately develop disease-modifying therapies for tauopathies.

Chapter Two:
Factors other than hTau overexpression that contribute to tauopathy-like phenotype in rTg4510 mice

Julia Gamache, Kellie Benzow, Colleen Forster, Lisa Kemper, Chris Hlynialuk, Eva Furrow, Karen H. Ashe, and Michael D. Koob

Content adapted from published article: Gamache, J., Benzow, K., Forster, C., Kemper, L., Hlynialuk, C., Furrow, E., Ashe, K. H., and Koob, M. D. (2019) Factors other than hTau overexpression that contribute to tauopathy-like phenotype in rTg4510 mice. *Nat Commun* **10**, 2479

Contributions: M.K. and K.A. directed the study and made intellectual contributions to experimental design and discussion. K.B. and M.K developed the T2 mouse line, J.G. bred and performed all of the characterization of the rT2/T2 and control lines discussed, other than tau histopathology, which was conducted primarily by C.F. Behavior experiments were performed by L.K. C.H. assisted with statistical analyses of tau histopathology. Genomic sequence analysis was performed by M.K. with assistance from E.F., and the manuscript was written primarily by M.K. and J.G. with input from K.A.

I. Introduction

The widely used rTg4510 mouse model of tauopathy recapitulates key features of these human diseases, including progressive age-related neurofibrillary tangles (NFTs), memory impairment and a dramatic loss of neurons in young mice (274,347). The rapid onset and severity of neuron loss in this model was particularly surprising when first reported given that earlier mouse models incorporating similar human *Microtubule-Associated Protein Tau* (*MAPT*) transgenes with the pathogenic P301L mutation do not develop overt atrophy (348,349). Unlike these other tau_{P301L} overexpression models, however, rTg4510 uses a responder-driver system to activate transgene expression specifically in forebrain neurons. Responder Tg4510 mice are crossed to a driver line (350) that harbors a tetracycline transactivator (tTA) transgene to generate bi-transgenic rTg4510 ("r" refers to regulatable) progeny. The particularly high level of tau_{P301L} overexpression specifically in the forebrain of these mice has generally been accepted as the direct cause of the premature gross forebrain atrophy and other tauopathy-like phenotypes in this line, a hypothesis supported by the fact that suppression of tau_{P301L} expression by doxycycline (DOX) halted neuronal loss and improved memory function (274). Mice from a control line in which wild-type (WT) human tau is expressed at levels roughly equivalent to tau_{P301L} in rTg4510 mice do not develop either progressive memory deficits or overt atrophy, supporting the idea that the tau_{P301L} mutant form of tau in particular was the direct cause of these phenotypes in rTg4510 (173).

Our overall goal when we began the project described here was to determine the precise molecular features of the tau_{P301L} protein that cause the rapid neurodegeneration phenotype characteristic of rTg4510, but we realized that this line was an inadequate starting point for this work. Although the transgene construct used to generate Tg4510 could be systematically altered and used to make new lines by pronuclear injection, the random integration process through which Tg4510 was established could never be precisely repeated, and any transgenic lines generated from these modified constructs would not adequately match the original Tg4510 line. We therefore first sought to establish a targeted-insertion equivalent to Tg4510 to which subsequent targeted-insertion lines expressing specific human tau variants could be precisely matched (an overview of the mouse lines generated and used is shown in Figure 20).

Preliminary observations of tau_{P301L} histopathology and brain mass in this targeted-insertion line (designated rT2/T2) suggested its phenotype was not as early or as robust as rTg4510, despite overexpressing even more tau_{P301L} protein than rTg4510. To determine if genetic differences contribute to the rTg4510 phenotype, we used whole-genome sequence analyses, which revealed a transgene insertion/deletion (TgINDEL) mutation in rTg4510 consisting of a multimer array of approximately 70 copies of the tau transgene, which inserted in a ~250 kilobase deletion of the first exons and promoter regions of *Fibroblast growth factor 14* (*Fgf14*). Furthermore, we found that a tTA Tg-INDEL allele, which drives tau_{P301L} expression in both lines and is known to be sufficient to cause a more limited but progressive neuron loss, consists of an approximately 7-copy tTA-transgene insertion in a ~500kb deletion that disrupts another five annotated genes (*Vipr2* - *Ptprn2*). Finally, we found that, in the absence of the *Fgf14* tau-TgINDEL, matching the high level of transgene overexpression in rTg4510 appears to be necessary to cause premature ($\leq$7 months) tau histopathology, late-stage (>12 months) overt atrophy, and behavior abnormalities. In the following sections, we present our genomic findings before phenotypic characterization in order to discuss differences between rT2/T2 and rTg4510 in the context of both Tg-INDELs.

II. Materials and Methods

Animals

We generated ES cells with a Col1A1 “Flp-in” integration cassette by electroporating 25ug of purified Col1a-frt-hygro-pA Plasmid (Addgene) into V6.5 Mouse Embryonic stem cells (C57BL/6 X 129/sv) (Novus Biologicals NBP1-41162 passage 22). After G418 selection, Clone 15 was found to have integrated properly and had a perfect karyotype. All further FRT mediated targeting is to this ES modified cell line (V6.5Col1a#15). A construct was generated that was essentially identical to the construct used to generate Tg4510, but incorporated a Flp-In promoter cassette (PGK promoter-ATG-FRT), and 6ug this construct and 0.5ug pCAGGS-FlpE (Gene Bridges cat# A201) was transfected into the V6.5Col1a#15 ES cell line. Hygromycin selection at 140ug/mL was added day 2 through day 6, and Hygro resistant ES clones were picked on day 7. DNA was analyzed for 5’ (5ArmCol1A assay primer + TRE start Rev) and 3’ (AMP R Reverse + Hygro Connection) junctions, internal Tau (TAU assay F and R), and multiple integration assay (AMP R Reverse + TRE start R) by PCR. Southern blot was done for multiple integration confirmation using EcoRI digested genomic DNA and a 470bp probe generated from the AmpR gene (Amp F + Amp R). Clone 6 was positive for all assays and the P301L mutation was verified by the Tau Assay below, and this clone was expanded and karyotyped, and mice were generated by injection into blastocysts. These mice were back-crossed five times to FVB prior to generating the T2/T2 lines.

<u>ES Cell Assay Primer sequences:</u>

5ArmCol1A pcr assay	5’-CAGGTGCACAGCATTGCGGACATG-3’
TRE Start Rev	5’-ATTGCTCCAGGCGATCTGAC-3’
Amp R Reverse	5’-GGAATAAGGGCGACACGGAA-3’
Hygro Connecton	5’-ATCCACGCCCTCCTACATCGAA-3’
Tau Assay F	5’-GTTCGAAGTGATGGAAGATCACG-3’
Tau Assay R	5’-TTGGGTGGAGTACGGACCA-3’

<u>PCR Probe Primers:</u>

Amp F	5’-CCTCCATCCAGTCTATTAATT-3’
Amp R	5’-TCCTTGAGAGTTTTCGCCCCG-3’

Generation of rTg4510 mice, which utilizes an activator and responder system for transgene expression, has previously been described (274). Briefly, a pTRE-prnp-tau plasmid was used to generate Tg4510 responders, which harbor a 0N4R human tau cDNA transgene regulated by a tetracycline response element (TRE). Tau expression is activated in bigenic rTg4510 progeny of an activator-responder cross. Activator mice harbor a tetracycline transactivator (tTA) transgene under the control of the CaMKIIα promoter (CKTTA transgene) to drive expression specifically in forebrain excitatory neurons (350). To generate tau-homozygous rT2/T2 mice from tau-hemizygous T2 mice, transgene-activated hemizygous males ($CKTTA^{+/-}Tau^{+/-}$) were bred to non-activated hemizygous females ($CKTTA^{-/-}Tau^{+/-}$), resulting in tau homozygous progeny ($Tau^{+/+}$). To maintain the rT2/T2 line, transgene-activated homozygous males ($CKTTA^{+/-}Tau^{+/+}$) were bred to non-activated homozygous females ($CKTTA^{-/-}Tau^{+/+}$). For the rTg4510 line, responder Tg4510 were maintained on a FVB/N background while activator mice were maintained on a 129S6 background. To match the genetic background to that of rT2/T2 mice, we increased the amount of FVB/N and used these mice to compare expression levels in rTg4510 and rT2/T2 mice. To generate these mice, responder Tg4510 mice were maintained on a FVB/N background while activator mice were maintained on a mixed 129S6 and FVB/N background. Non-tau-expressing transgenic littermates were used as controls. Both male and female mice were used, and were combined in statistical analyses after demonstrating the absence of significant gender effects ($P > 0.05$). All experiments with animals described in this study were approved by and conducted in full accordance with the American Association for the Accreditation of Laboratory Animal Care and the Institutional Animal Care and Use Committee at the University of Minnesota.

qRT-PCR

mRNA expression levels of each Fgf14 variant were quantified relative to a reference gene, hypoxanthine-guanine phosphoribosyltransferase (*Hprt*). All Fgf14 primers (Table 5) were designed to span at least partially unique regions of each variant. Total cellular RNA was extracted from homogenized forebrain tissue using RNeasy Lipid Tissue Kit (Qiagen) according to the manufacturer's instructions. RNA samples were treated with DNaseI (New England Biolabs) to digest contaminating DNA, and subjected to cDNA synthesis using the iScript cDNA synthesis kit (Invitrogen) according to the

manufacturer's instructions. PCR reactions were set up in a 20-µl volume in 96-well plates, with 2 to 3 replicates per sample. Roche SYBR Green PCR master mix was used and reactions were run in the Roche LightCycler® 480 instrument. A final melting curve confirmed that single amplicons were present for each variant and reference reactions, and a basic relative quantification was performed using the $\Delta\Delta C_T$-Method (LightCycler® 480 Software release 1.5.0 SP3). All data were normalized to a positive calibrator sample used in each experiment.

Protein extraction and phosphatase treatment

Total protein was extracted from mouse forebrain hemisphere tissue in RIPA buffer (50 mM Tris-HCl, 150 mM NaCl, 1 mM EDTA, 0.5% Triton X-100, 1% sodium deoxycholate, 0.3% SDS, 0.1 mM phenylmethyl sulfonyl fluoride, 0.2 mM 1,10-Phenoanthroline Monohydrate, Phosphatase Inhibitor Cocktail A (Sigma), Protease Inhibitor Cocktail (Sigma), Phosphatase Inhibitor Cocktail 2 (Sigma)). Homogenates were nutated and centrifuged at 15,700 x*g* for 90 minutes at 4°C and the supernatant was collected.

To obtain RIPA-insoluble, sarkosyl-insoluble fractions, a modified version of a previously published method was used (351). RIPA-insoluble pellets were homogenized in 1% sarkosyl and incubated at room temperature for 30 minutes with constant shaking. Samples were centrifuged for 1 hour at 100,000 x*g* at 20°C, and the supernatant and pellet were separated and diluted in O+ buffer (62.5 mM Tris-HCl, pH 6.8; 10% glycerol; 5% 2-mercaptoethanol; 2.3% SDS; 1 mM EGTA; 1 mM EDTA; 1 mM PMSF; 1 mM Na3VO4; 1 mM NaF; 10 µl/ml of protease inhibitor cocktail P8340; Sigma-Aldrich). Samples were boiled for 3 minutes and stored at -20°C.

For treatment with calf intestinal alkaline phosphatase (CIP, New England Biolabs), samples were resuspended in 10 µl CIP buffer (100 mM NaCl, 50 mM Tris-HCl, 10 mM MgCl2, 1 mM dithiothreitol, EDTA-free protease inhibitor cocktail, pH 7.9) per 1 µg protein. One unit CIP per µg protein was added to the samples prior to incubation at 37°C for 30 minutes. Samples were then concentrated using Amicon Ultra centrifugal filters (Millipore).

Western blot and analysis

For sarkosyl-insoluble fractions, total protein concentration was normalized according to pellet weights. Total protein concentrations for all other samples were determined by Pierce™ Bicinchoninic Acid protein assay (Thermo Scientific). Equal amounts of protein for each sample were loaded and separated using SDS-PAGE on 10%, 10.5-14%, or 10-20% Tris-HCl gels (Bio Rad). Protein was transferred to nitrocellulose membranes (Bio Rad), which were blocked with 5% Bovine Serum Albumin (Sigma) in 1X TBST buffer (10 mM Tris-Base (Sigma), 0.2 M NaCl (Macron Chemicals), 0.1% Tween-20 (Sigma) pH 7.4). Protein was immunoblotted with Tau46 (Cell Signaling Technology #4019, dilution 1:10,000), Tau13 (BioLegend #MMS-520R, dilution 1:60,000), GAPDH (14C10) (Cell Signaling Technology #2118, dilution 1:4,000), GAPDH (GA1R) (Thermo Scientific #MA5-15738, dilution 1:5,000), AT8 (Thermo Scientific #MN1020, dilution 1:1,000), anti- human tau (Abcam # ab74391, dilution 1:10,000), and βIII-tubulin (ProSci #79-720, dilution 1:10,000) antibodies. Additional antibodies from Peter Davies for phospho-epitopes on tau included MC1 (dilution 1:800), CP13 (dilution 1:1,000), and PHF1 (dilution 1:1,500). To visualize antibody immunoreactivity using a LiCor imaging system and Image Studio software, IRDye-linked goat anti-mouse 800CW and goat anti-rabbit 680LT secondary antibodies were used (LI-COR Biosciences, dilution 1:100,000). Following LiCor image acquisition using Image Studio software (Odyssey), Amido black staining solution (Sigma-Aldrich) was used for total protein quantification according to manufacturer's instructions. Immunoreactivity and Amido black staining were quantified by densitometry using OptiQuant version 3 software, following guidelines for total protein quantification (352).

Total Tau Measurements by Enzyme-linked Sandwich Immunoassay (Simoa)

Mouse hemi-forebrains of rT2, rT2/T2, and rTg4510 mice were dissected and transferred to 1 mL of ice-cold RIPA buffer (50 mM Tris-HCl, 150 mM NaCl, 1 mM EDTA, 0.5% Triton X-100, 1% sodium deoxycholate, 0.3% SDS, 0.1 mM phenylmethyl sulfonyl fluoride, 0.2 mM 1,10-Phenoanthroline Monohydrate, Phosphatase Inhibitor Cocktail A (Sigma), Protease Inhibitor Cocktail (Sigma), Phosphatase Inhibitor Cocktail 2 (Sigma)). Homogenates were nutated and centrifuged at 15,700 x*g* for 90 minutes at 4°C and the supernatant was collected. Samples were then diluted 1:100,000 in ice cold PBS (0.01 M phosphate buffer, 0.0027 M potassium chloride, 0.137 M sodium chloride pH 7.4; Sigma). Samples were analyzed using Quanterix™ ultra-sensitive, single

molecule array (Simoa) technology with the HD-1 analyzer (Quanterix, Lexington, MA). Total tau (T-tau) was measured using Tau 2.0 kits (Quanterix™). All measurements were performed on the same day in the same run using the same reagents. Background signal generated from tTA-only samples was averaged and subtracted from all other data.

Immunohistochemistry and analysis

Mouse brain hemispheres were immersion-fixed in 10% formalin for 48 hours before processing. Unstained sagittal TMA sections (4 µm) were de-paraffinized and rehydrated using standard methods. Bielschowsky silver staining was performed using standard techniques. For antigen retrieval, slides were incubated in 6.0 pH buffer (Reveal Decloaking reagent, Biocare Medical, Concord, CA) in a steamer for 30 min at 95-98°C, followed by a 20 min cool down period. Subsequent steps were automated using an immunohistochemical staining platform (Nemesis, Biocare). Endogenous peroxidase activity was quenched by slide immersion in 3% hydrogen peroxide solution (Peroxidazed, Biocare) for 10 min followed by TBST rinse. A serum-free blocking solution (Rodent Block M, Biocare Medical, Concord, CA) was placed on sections for 20 min. Blocking solution was removed and slides were incubated in primary antibody diluted in 10% blocking solution/90% TBST. Mouse monoclonal antibodies from Peter Davies were applied at the following dilutions: CP13 1:1,000, MC-1 1:800 and PHF1 1:1,500, mouse monoclonal PHF-Tau: clone AT8 (Thermo Scientific #MN1020) 1:1,000. Sections were incubated in primary antibody for 60 min at room temperature followed by TBST rinse and detection with biotinylated anti-mouse secondary (Vector Laboratories #BP-9200, dilution 1:200) for 30 minutes followed by a TBST rinse. After the rinse, SA-HRP (Biolegend #405210, RTU) was applied for 30 minutes. All slides then proceeded with TBST rinse and detection with diaminobenzidine (Covance, Dedham, MA). Slides were incubated for 5 min followed by TBS rinse then counterstained with CAT Hematoxylin (Biocare, Concord, CA) for 5 minutes. Slides were then dehydrated and coverslipped. Images were gathered using an Axioskop microscope (Zeiss, Germany) at 40X magnification and a PixeLINK microscope camera (PL-A623C) with PixeLINK Capture SE software version 2.2 (Firewire camera release 4, Copyright © 2000-2006). Adobe Photoshop CS2 version 9.0 was used to match the color of different images of the same histological stain. Semi-quantitative analysis of images was conducted using a

‘+’ system (347). A blinded observer gave scores for three sections per sample indicating severity of pathology using ‘-’ for no positive labeling, ‘+’ for occasional positive labeling, ‘++’ for moderate positive labeling, ‘+++’ for prominent positive labeling. To summarize these results, the number of ‘+’ signs was counted for each animal and region, and multiple linear regression analyses were conducted using R statistical programming language to test for differences between rTg4510, rT2/T2, and rT2.

Whole-genome sequencing and sequence analyses

Genomic DNA was extracted from a non-activated Tg4510 mouse harboring the 0N4R human tau transgene using the DNeasy Blood & Tissue kit (Qiagen) according to the manufacturer’s instructions. Genomic DNA was analyzed by nanodrop and agarose gel to verify the quality (O.D. 260/280 ratio > 1.8) and quantity (300 ng for library construction).

Sequencing was performed on Illumina HiSeq 2500 High-Output system using rapid SBS chemistry at the University of Minnesota Genomics Center, Minneapolis, MN. Following quality control, a TruSeq Nano DNA library was prepared from the genomic DNA sample and was sequenced on a single Illumina lane to generate 2x125 bp paired-end reads. The average insert length in the library was 350 bp.

All sequence analyses were conducted using the University of Minnesota’s installation of the Galaxy web-based suite of software (353). We isolated individual sequence reads that spanned the end of the transgene using the BLAT alignment tool (354) and mapped paired sequence reads to the transgene sequence using Bowtie2 (355). We screened these data sets and identified unmapped reads in which the paired read mapped to the transgene sequence and then further analyzed these screened sets, in part using the Integrative Genomic Viewer (IGV) (356), to find the genomic insertion points and a single 5’ -5’ transgene fragment junction. Bowtie2 mapping of the sequence data to the *Fgf14* genomic or *Vipr2-Ptprn2* data (as appropriate) indicated that roughly half as many reads mapped to the unique sequences between the insertion points as mapped outside of this region, indicating that the Tg4510 mice have only a single copy of this portion of the *Fgf14* genomic sequence. To estimate transgene copy number, we used sets of closely linked SNPs to distinguish between the *PrnP* sequence in the transgene and that in the FVB genome (357), and found that the dataset contains more than 35-fold more reads generated from transgene *PrnP* sequences than from the

diploid mouse *PrnP* sequence on chromosome 2, indicating that more than 70 copies of transgene sequence are inserted at the *Fgf14* locus in the Tg4510 mice. Similar analyses were performed using polymorphisms in the CamKII genomic data to determine the copy number in the tTA transgene array. Sequences mapped to the reference Tg sequence were assemble into a consensus transgene sequence using SPADES (358).

PCR and Sequencing

Selected regions of Tg4510 and rT2/T2 genomic DNA were amplified by polymerase chain reaction (PCR) using Herculase II Fusion DNA polymerase (Agilent Technologies). For Tau transgene junctions in Tg4510 DNA, PCR and nested PCR reactions were run (Tables 2, 3 and 4). CaMKIIα-tTA transgene junctions were confirmed using rT2/T2 DNA (Tables 7 and 8). Gel bands were isolated from a low melting point agarose gel (NuSieve GTG, Lonza) and DNA was purified following digestion with β-agarase (New England Biolabs). Gel-purified PCR products were sequenced with classical Sanger sequencing at the University of Minnesota Genomics Center, Minneapolis, MN.

Mouse cell culture and metaphase slide preparation

Spleen from a Tg4510 mouse (28th generation backcross onto FVB genetic background) was minced into a single cell suspension and cultured for 24-28 hours with 5ug/ml Concavalin A (mouse T-cell mitogen). Cultures were exposed to colcemid (Irvine Scientific) for 15 hrs overnight followed by harvest using standard cytogenetic protocols. Metaphase spread slides were prepared from methanol-acetic acid fixed cell pellets and FISH was performed the following day.

Fluorescent in situ hybridization (FISH)

DNA probes derived from the tau transgene sequence were labeled by nick translation reaction (Nick Translation Kit - Abbott Molecular) using Orange 552 dUTP (Enzo Life Science), ethanol precipitated and resuspended in hybridization buffer. The probe/hybridization buffer mix and slide were denatured, probe was applied to the metaphase slide, and slide was hybridized for 24 hours at 37°C in a humidified chamber. After hybridization, the FISH slides were washed in a 2xSSC solution and

counterstained with DAPI stain to enable chromosome identification by G-band patterning. Fluorescent signals were visualized on an Olympus BX61 microscope workstation (Applied Spectral Imaging, Vista, CA) with DAPI and Texas Red filter sets. FISH images were captured using an interferometer-based CCD cooled camera (ASI) and FISHView ASI software.

Behavioral Experiments

For nesting experiments, animals were not disturbed for at least 24 hours prior to testing. Each animal was placed in its own clean cage with a new nestlet placed in the center of the cage in the morning. Nests were photographed and scored 2 hours, 6 hours and 24 hours after the start of the test. Scores of 0-7 were given as follows (75): 0- nestlet untouched, 1- <10% of nestlet was shredded, 2- 10-50% of nestlet shredded but no shape to nest (flat), 3- 10-50% of nestlet shredded and there is shape to nest, 4- 50-90% of nestlet shredded but no shape to nest (flat), 5- 50-90% of nestlet shredded and there is shape to nest, 6- >90% of nestlet shredded but no shape to nest (flat), 7- >90% of nestlet shredded and nest had walls that were at least as tall as the mouse on 50% of the sides. Reported scores are the average of two individual blinded scorers.

Open field testing was done two days after the conclusion of nesting experiments. Animals were not disturbed for at least 24 hours prior to testing and were placed in the testing room for 30 minutes prior to testing. The Open field setup was a plastic tub with opaque white walls, measuring 15 inches wide by 18.5 inches long by 12 inches high. The arena floor was covered with new, pre-scented cage bedding. Each mouse was released in the center of the arena and allowed to freely explore for 10 minutes. All trials were monitored using a computerized tracking system (Noldus Ethovision XT 10.0; Noldus Information Technology). All animals were tested in the morning to avoid activity differences from time of day.

Statistical Analysis

Analyses were conducted using GraphPad Prism version 6.00 software (GraphPad Software) and R statistical programming language. Gender differences were detected only in nest-building behavioral assays and analyses were conducted accordingly. In all cases, $p<0.05$ was considered to be statistically significant.

III. Results

TAU_{P301L} overexpression

We used Flp/Frt recombination to target a single copy of the same tau_{P301L} transgene used to generate Tg4510 into mouse embryonic stem cells at an intergenic site downstream of *Collagen type I alpha I (Col1A1)*, a site previously demonstrated to promote transgene expression without dysregulating endogenous genes (359). Mice with this single targeted *MAPT* cDNA transgene insertion are designated T2. In order to match the expression pattern in rTg4510 mice, these new T2 mice are crossed to the same tTA-driver line (350) used to generate rTg4510 mice, resulting in rT2 mice. The rT2 mice are again crossed to T2 mice to generate mice homozygous for the tau_{P301L} transgene (i.e., rT2/T2, as shown in Figure 20).

We find that rT2/T2 mice express two to three times as much human tau_{P301L} mRNA and protein in the forebrain as hemizygous rT2 (Figure 2A-C). Despite expressing similar levels of tau_{P301L} mRNA (0N4R isoform only) as rTg4510 (Figure 2A), rT2/T2 overexpress even higher levels of protein than rTg4510, however this trend was not statistically significant (Fig. 2B-C).

TAU_{P301L}-TgINDEL in Tg4510 disrupts Fgf14

Preliminary results showed that tau_{P301L} histopathology in rT2/T2 brains was not as robust as in rTg4510 at 5 months of age. To determine if an insertion mutation caused by the tau_{P301L} transgene in Tg4510 could explain this phenotypic difference, we performed whole-genome sequencing on DNA from a Tg4510 responder mouse using the Illumina HiSeq2500 High-Output system. Assembly and analyses of these reads revealed that approximately 70 head-to-tail copies of the tau transgene form an array that replaces a 243,608bp region of *Fibroblast growth factor 14* (*Fgf14*), the most telomeric gene on the long arm of chromosome 14 (Figure 3B). Within the insertion array the transgene orientation switches from a 3'→5' orientation to a 5'→3' orientation, however we are unable to determine precisely at which point in the array this switch occurs due to repetitive sequences in the reads (Figure 3B). We confirmed the transgene insertions sites by PCR amplifying and resequencing key junctions and by performing Fluorescence In Situ Hybridization (FISH) on Tg4510 genomic DNA (Figure 4, Tables 2-4). The compiled tau transgene monomer sequence and all junction sequences have been submitted to GenBank.

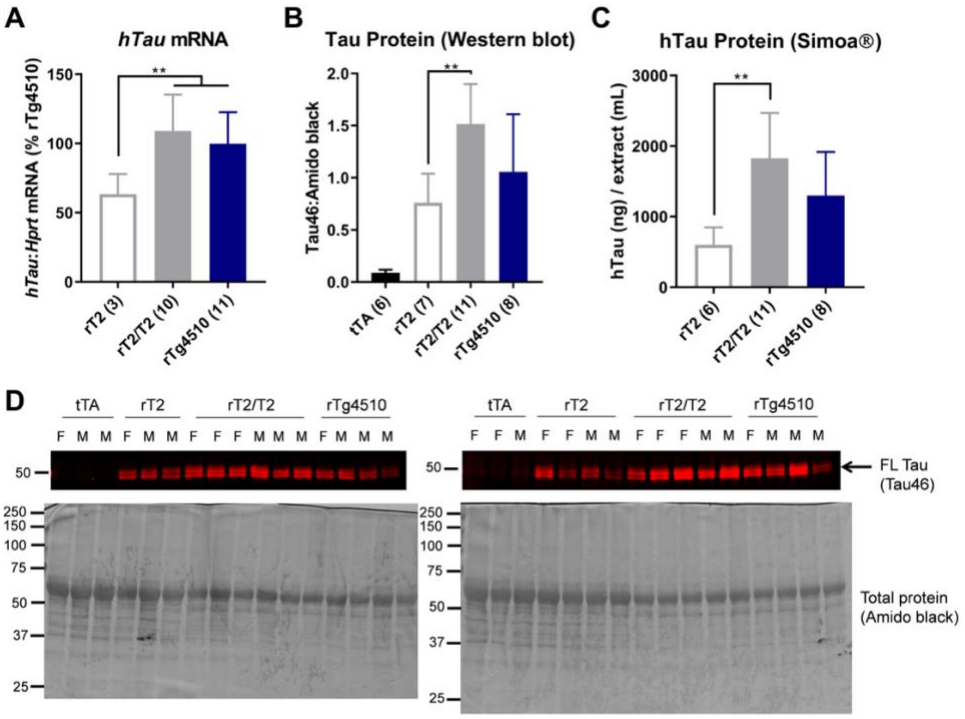

Figure 2. Human tau expression in transgenic lines. (A) *hTau* mRNA was measured in 8-week old mouse forebrains by RT-qPCR relative to housekeeping gene *Hprt*. A One-way ANOVA with Holm-Sidak's multiple comparisons test showed significantly lower levels in rT2 compared to rT2/T2 and rTg4510 ($F(2, 17) = 7.98$, $p = .0019$). Of note, rT2 *hTau* expression was 58% and rTg4510 was 92% that of rT2/T2. (B) hTau protein overexpression relative to endogenous mouse tau in the tTA line was measured in 8-week old mouse forebrains by western blot. A One-way ANOVA with Holm-Sidak's multiple comparisons test showed significantly lower levels in rT2 than rT2/T2 ($F(2, 23) = 7.38$, $p = .0033$). rT2 expression levels were 50% and rTg4510 were 70% that of rT2/T2. Overexpression of human relative to endogenous mouse tau was 8.5x in rT2, 17x in rT2/T2, and 11.8x in rTg4510. (C) A Simoa® ELISA system was used to confirm protein expression levels of samples in panel *B*, and showed by One-way ANOVA and Holm-Sidak's multiple comparisons test that, again, rT2 levels were significantly lower than rT2/T2 ($F(2, 22) = 9.073$, $p = .0013$). Samples were diluted one thousand-fold to be within range of detection for the assay and tTA controls were used to measure background signal. Data was adjusted to account for background and dilution. rT2 levels were 33% and rTg4510 were 71% of rT2/T2 by this method. (D) Western blots quantified by densitometry in panel *B*. Samples were treated with a phosphatase before being run through SDS-PAGE. Tau46 antibody, which recognizes human and mouse tau, was used to measure full-length (FL) tau levels. Amido black stain was used to normalize to total protein. Molecular weights for each blot in kDa are shown on the left, with sex of each mouse indicated above. Graphs show group means + SD with *n*'s in parentheses. **p<0.01.

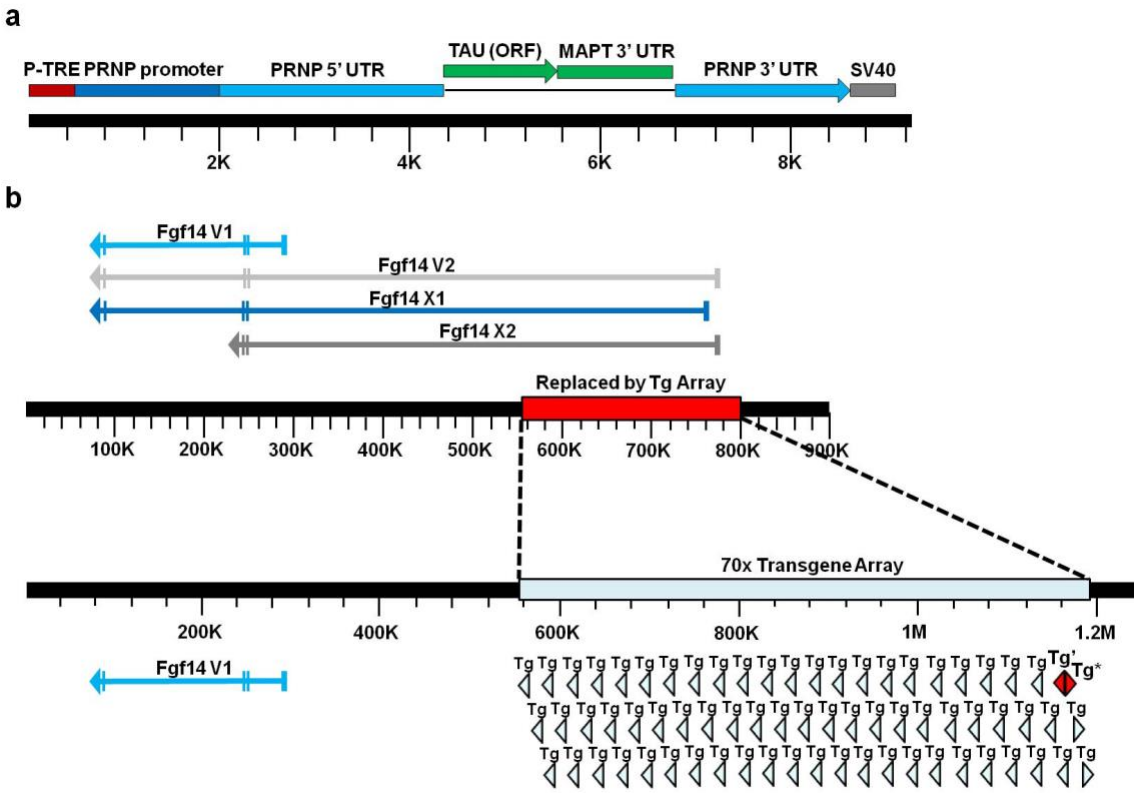

Figure 3. *Fgf14* is disrupted by a tau transgene array in Tg4510 mice. (a) Structure of the tau transgene monomer including the TRE promoter, prion protein (*Prnp*) sequences, tau cDNA ORF, *Mapt* 3' UTR, and SV40 signal (see text for details). (b) Diagram of *Fgf14* mRNA splice variants and disruption by the transgene array. Tg', final transgene copy in the 3'→5' orientation. Tg*, first transgene copy in the 5'→3' orientation.

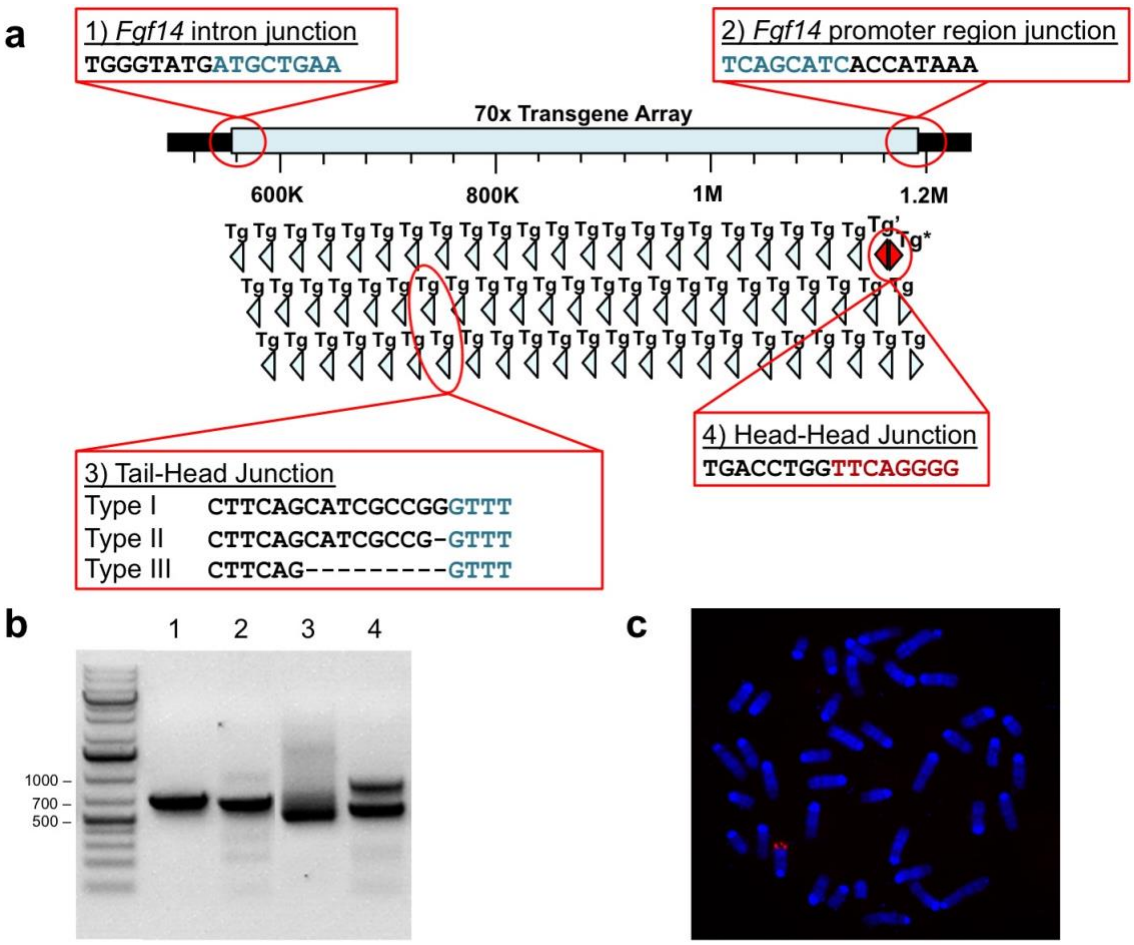

Figure 4. Confirmation of transgene insertion sites and array junctions in the Tg4510 genome. (a) Diagram of the following key junctions: 1) the junction between the transgene array and the *Fgf14* intron, 2) the junction between the transgene array and the *Fgf14* promoter region, 3) Tail-Head junctions between adjacent transgene copies (which occurred in three Types), and 4) the Head-Head junction at the point in the array in which the transgene flips orientation. Note that the transgene copies at the *Fgf14* intron, *Fgf14* promoter region, and Head-Head junctions are truncated and therefore do not have aligned sequences. (b) Gel electrophoresis of PCR products shown in part *a*. The *Fgf14* intron junction amplicon is 811 bp, the Tail-Head junction amplicon is 685 bp, the Head-Head junction amplicon is 626 bp, and the *Fgf14* promoter region junction amplicon is 767 bp. (c) Metaphase chromosomes from a Tg4510 mouse were subjected to FISH, using DNA probes derived from the tau transgene sequence tagged with an Orange 552 fluorescent label. Fluorescent signal is detected near the telomere on the long arm of chromosome 14, identified by its unique G-band patterning.

Table 2. Primer sequences used to amplify hTau transgene-*Fgf14* junctions.

Junction Product	**Primers**		**Nested primers**	
	Forward	**Reverse**	**Forward**	**Reverse**
5’	5’-CAGCATCAAGCCCCAGAGAA -3’	5’-ACGCTATCTGTGCAAGGTCC -3’	5’-GCTCTGGATTTCTGTGAGCCT -3’	5’-GTAACCGGCCTCTTCATCGG -3’
3’	5’-TCTGGAACTCACCAGGTAATC -3’	5’-AACAAGGGTGGTTTTCAAGAG -3’	N/A	N/A
Tail-Head	5’-TCTGGAACTCACCAGGTAATC -3’	5’-CATGGGTAGGCTCACACAGT -3’	5’-ACCACGCTATCTGTGCAAG -3’	5’-GGATGACTGCATCTGTCAAG -3’
Head-Head	5’-GAGCGAGGAAGCCATCGTT -3’	5’-CAGATAGCGTGGTCCGGC -3’	N/A	N/A

Table 3. PCR cycling conditions used for non-nested PCR reactions for hTau transgene-*Fgf14* junctions.

5'			**3'**			**Tail-Head**			**Head-Head**		
#	°C	Time	#	°C	Time	#	°C	Time	#	°C	Time
1	94	08:00	1	95	02:00	1	94	08:00	1	95	02:00
33	94	01:15	35	95	00:20	33	95	00:20	35	95	00:20
	55	00:30		53.6	00:20		56	00:20		54	00:20
	72	01:00		72	00:30		72	00:36		72	00:30
1	72	03:00	1	72	03:00	1	72	03:00	1	72	03:00

(#) number of cycles, (°C) temperature, Time (minutes:seconds)

Table 4. PCR cycling conditions used for nested PCR reactions for hTau transgene-*Fgf14* junctions.

5' Nested			**Tail-Head Nested**		
#	°C	Time	#	°C	Time
1	94	08:00	1	94	08:00
33	94	01:15	35	95	00:20
	55	00:30		57.2	00:20
	72	01:00		72	00:30
1	72	03:00	1	72	03:00
1	4	∞	1	4	∞

(#) number of cycles, (°C) temperature, Time (minutes:seconds)

Fgf14 *expression is dysregulated in rTg4510 mice*

Although transcription of *FGF14* has been reported to initiate at over unique 100 start sites (360), at the time we began our analyses four representative splice variants of *Fgf14* were present in GenBank, and we restricted our analyses to these variants: V1 (NM_010201.4, encodes isoform 1a), V2 (NM_207667.3, encodes isoform 1b), X1 (XM_011244952.1), and X2 (XM_006518549.2). The deletion in Tg4510 removes the first 219kb of V2 and terminates 266kb upstream of the transcription start site for V1. Overall, this removes the promoters and first exons of variants V2, X1, and X2, leaving the coding region of only variant V1 intact (Figure 3B). Available antibodies to Fgf14 protein do not distinguish between the products of these splice variants, and as a result Western blot analyses of Fgf14 differences between these lines was uninformative with respect to altered ratios of Fgf14 isoforms (not shown). We performed quantitative real-time PCR (qRT-PCR) of splice variants using RNA extracted from forebrain tissue of rTg4510, Tg4510, and non-transgenic (NT) mice and found that rTg4510 mice express 5.6-fold higher mRNA levels of variant V1 than NT mice and 2.8-fold higher levels of V1 than Tg4510 mice in their forebrains (Figure 5A, Tables 5-6). Both rTg4510 and Tg4510 mice exhibit decreased expression of *Fgf14* variants V2, X1, and X2, presumably due to haploinsufficiency (Figure 5B-D, Tables 5-6). This reflects a dramatic imbalance of the ratios of these variants in relation to one another in rTg4510 compared to NT mice (Figure 5E). We attribute the slight upregulation of *Fgf14* V1 in responder Tg4510 brains to altered chromatin structure and/or effects of the non-coding *Prnp* sequences in the tau_{P301L} transgene array (Figure 3A).

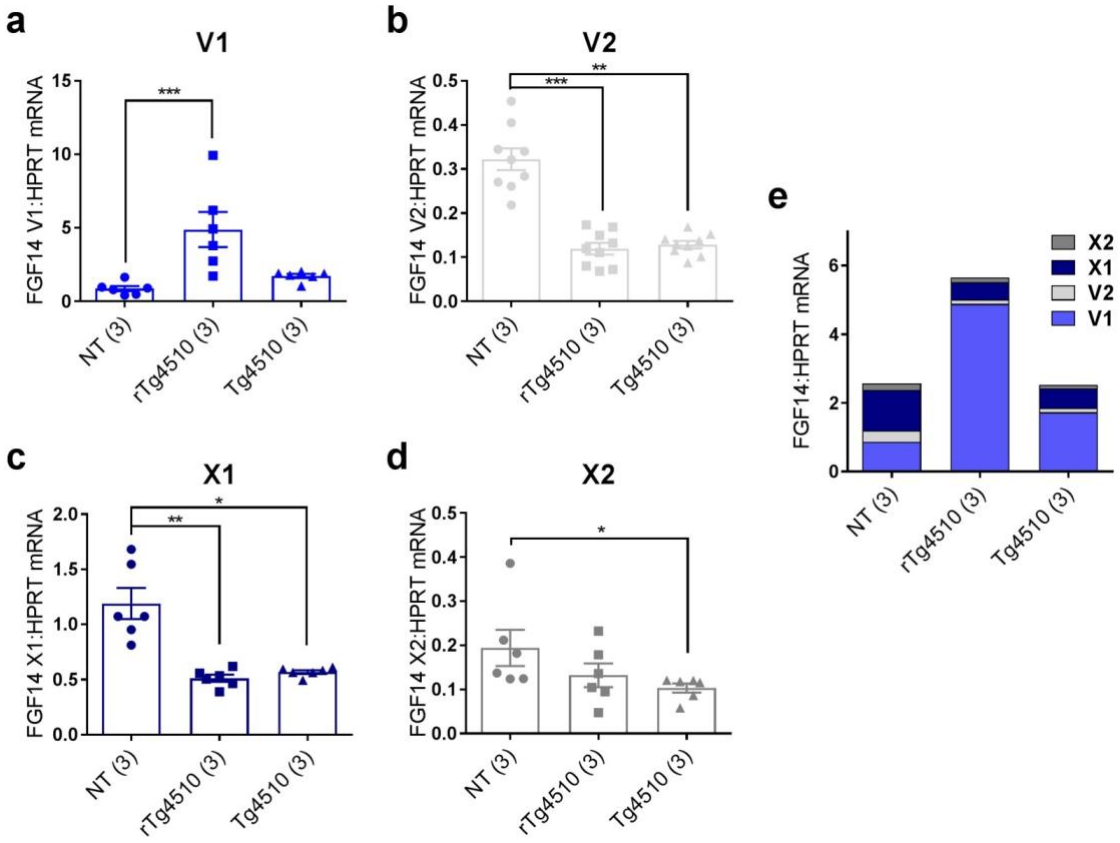

Figure 5. Dysregulation of *Fgf14* mRNA splice variants in rTg4510 and Tg4510 mice. Expression levels in the rostral one-third of dissected forebrain hemispheres of *Fgf14* variants V1 (a), V2 (b), X1 (c), and X2 (d) in non-transgenic (NT), rTg4510, and Tg4510 mice (*n* for each group in parentheses). Data points represent duplicates of qPCR. Expression levels of each variant were determined by qRT-PCR relative to housekeeping gene *Hprt*. All samples were run in duplicate. Kruskal-Wallis tests were performed for V1 ($H=13.2$, $df=2$, $p<0.0001$), V2 ($H=17.5$, $df=2$, $p<0.0002$), X1 ($H=12.3$, $df=2$, $p=0.0001$), and X2 ($H=6.9$, $df=2$, $p=0.026$) groups, followed by Dunn's multiple comparisons tests. All data were normalized to a positive calibrator, and are expressed as the group mean ± SEM. (e) Compiled group mean data for all variants. *p ≤0.05, **p≤0.01, ***p≤0.001

Table 5. Primer sequences used to measure *hTau* and *Fgf14* mRNA relative to *Hprt* in RT-qPCR experiments.

Target	**Primers**	
	Forward	Reverse
hTau	5'- CTACACCATGCACCAAGACC -3'	5'- TGCTTTTACTGACCATGCGA -3'
Fgf14 variant V1	5'- CATCTTCGGCCTCAAGAAGC -3'	5'- TCAGAACACCTGAGGATCTGGC -3'
Fgf14 variant V2	5'- GGCCTCTTCTTTCTCAGGGT -3'	5'- CATGCAAGGATGGTTCTCGG -3'
Fgf14 variant X1	5'- TGCTAGGCTGAGCAATGTAG -3'	5'- CCTTGGATCTTCGATAGGGC -3'
Fgf14 variant X2	5'- ATGCTGCAGTGTCTTTGTGG -3'	5'- TCACAGGGGATGCTCAGAAG -3'
Hprt	5'- GCTGGTGAAAAGGACCTCT -3'	5'- CCACAGGACTAGAACACCTGCTA -3'

Table 6. PCR cycling conditions using for relative RT-qPCR to measure *hTau* and *Fgf14* expression.

hTau			***Fgf14 variant V1***			***Fgf14 variant V2***			***Fgf14 variant X1***			***Fgf14 variant X2***		
#	°C	Time	#	°C	Time	#	°C	Time	#	°C	Time	#	°C	Time
1	95	10:00	1	95	10:00	1	95	10:00	1	95	10:00	1	95	10:00
32	95	00:10	45	95	00:10	40	95	00:10	40	95	00:10	45	95	00:10
	55	00:10		56	00:15		52	00:15		57	00:15		56	00:15
	72	00:10		72	00:25		72	00:28		72	00:12		72	00:16

(#) number of cycles, (°C) temperature, Time (minutes:seconds)

tTA-TgINDEL in rTg4510 and rT2/T2 disrupts five more genes

We also performed whole-genome sequencing on DNA from an rT2/T2 mouse. We confirmed the expected configuration of the targeted tau_{P301L} transgene insertion in this line and also defined the hemizygous tTA-TgINDEL mutation used to drive expression both in this line and in rTg4510. We found that approximately 7 head-to-tail copies of the tTA transgene form an array that replaces 508,119bp in a gene-rich region of mouse chromosome 12 near the immunoglobulin heavy chain complex (Figure 6). Similar to the configuration within the *Fgf14* tau-TgINDEL allele, the transgene orientation within the tTA insertion array switches from a 3'→5' orientation to a 5'→3' orientation, although in this instance a cloning vector DNA fragment is also incorporated at this inversion point. The massive genomic deletion in the tTA-TgINDEL removes the 3' portion of *Vasoactive intestinal peptide receptor 2* (*Vipr2*), the 5' portion of *Protein tyrosine phosphatase, receptor type, N polypeptide 2* (*Ptprn2*), and encompasses all of the annotated genes *WD repeat domain 60* (*Wdr60*), *Extended synaptotagmin-like protein 2* (*Esyt2*), and *Non-SMC condensin II complex, subunit G2* (*Ncapg2*), as well as several predicted but uncharacterized genes (e.g. Gm20658). We confirmed the transgene insertions sites by PCR amplifying and resequencing key junctions (Figure 7, Tables 7-8). All junction sequences and the compiled tTA transgene monomer sequence, which includes a Ca^{2+}-calmodulin kinase II (CaMKII) promoter fragment, have been submitted to GenBank.

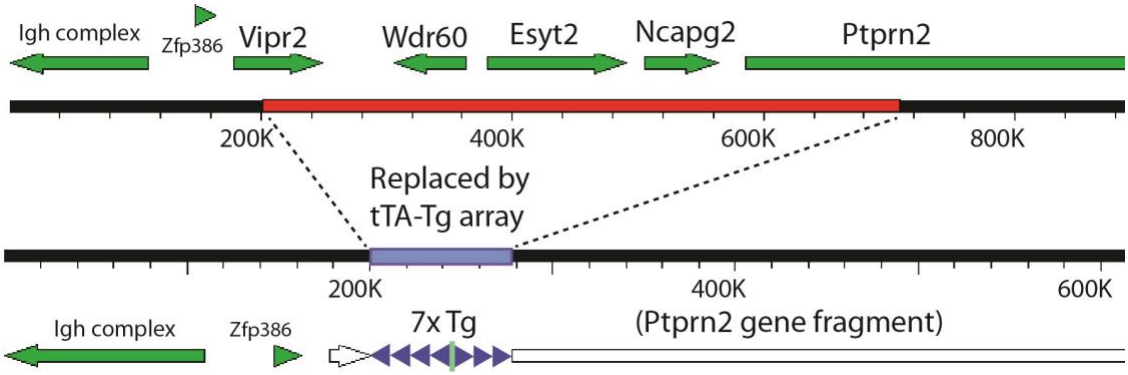

Figure 6. The tTA transgene array in rTg4510 and rT2/T2 mice disrupts genes on chromosome 12. Diagram of the uninterrupted chromosomal region and its disruption by the tTA-TgINDEL mutation. Tg, transgenes are blue triangles, cloning vector in inversion point of Tg array is a green line, uninterrupted genes are filled arrows, and partially deleted gene fragments are white arrows.

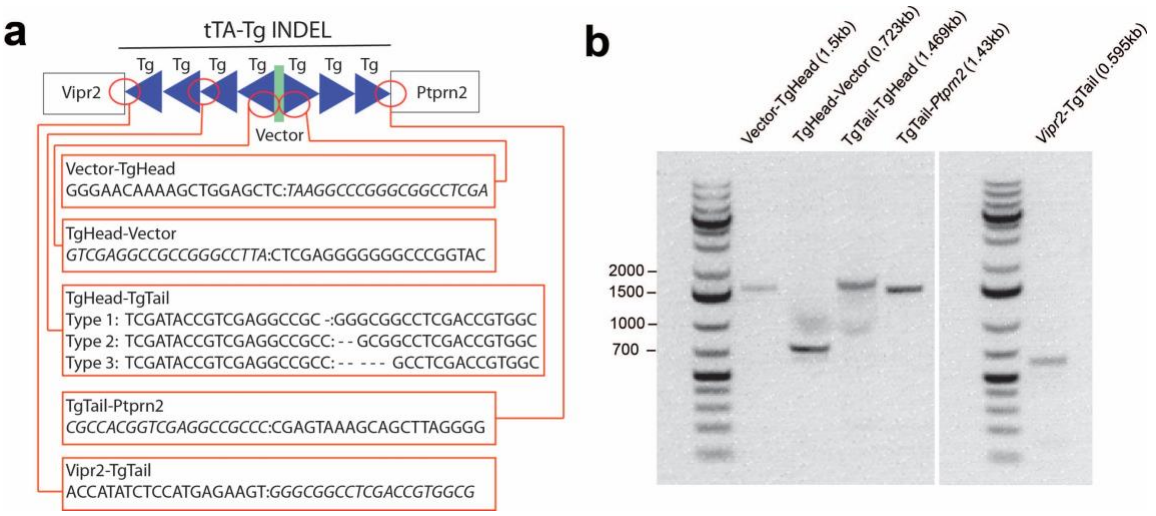

Figure 7. Confirmation of the junctions in the tTA-TgINDEL allele. (a) Diagram of the following key junctions: 1) the junction between the transgene array and *Vipr2*, 2) the junction between the transgene array and *Ptprn2*, 3) Tail-Head junctions between adjacent transgene copies (which occurred in three Types), 4) TgHead-Vector, and 5) vector-TgHead. (b) Gel electrophoresis of PCR products shown in panel *a*.

Table 7. Primer sequences used to amplify CaMKIIα-tTA transgene-genome junctions.

Junction	Forward	Reverse
Vector-TgHead	5' – AAGCCCTCCCGTATCGTAGTTAT – 3'	5' – GATGAAGACTTGACCTTGCCTC – 3'
TgHead-Vector	5' – TCCACTAGGCTCCCAAGTCAT – 3'	5' – AAGGCGATTAAGTTGGGTAACG – 3'
TgTail-TgHead	5' – AGGAACCTTACTTCTGTGGTGTG – 3'	5' – TCCACTAGGCTCCCAAGTCAT – 3'
TgTail-*Ptprn2*	5' – AGGAACCTTACTTCTGTGGTGTG – 3'	5' – CCCATTTACAGGGAAAATAAAGCC – 3'
Vipr2-TgTail	5' – CTCAGTGGGACAAGCTACCAAA – 3'	5' – AAATAGCTTCTGCCGAGAGTCC – 3'

Table 8. PCR cycling conditions used for CaMKIIα-tTA transgene-genome junctions.

Vector-TgHead			**TgHead-Vector**			**TgTail-TgHead**			**TgTail-*Ptprn2***			***Vipr2*-TgTail**		
#	°C	Time	#	°C	Time	#	°C	Time	#	°C	Time	#	°C	Time
1	95	02:00	1	95	02:00	1	95	02:00	1	95	02:00	1	95	02:00
30	95	00:20	30	95	00:20	30	95	00:20	30	95	00:20	30	95	00:20
	52	00:30		52	00:20		52	00:20		52	00:20		52	00:20
	72	00:45		72	00:30		72	00:50		72	00:43		72	00:30
1	72	03:00	1	72	03:00	1	72	03:00	1	72	03:00	1	72	03:00

(#) number of cycles, (°C) temperature, Time (minutes:seconds)

Transgene expression and Fgf14-*TgINDEL accelerate pathology*

We evaluated human tau histopathology in somatomotor cortex and hippocampus of 2-, 5-, and 7-month old male and female rTg4510, rT2/T2, and rT2 mice using MC1, AT8, CP13, and PHF1 antibodies as well as a Bielschowsky (Biels.) silver stain. Semi-quantitative analyses of stained sections (Figures 8-12) revealed similar pathological forms of tau in the first two of these three lines, although these accumulated at earlier ages and to a greater extent in rTg4510 than in rT2/T2 (Figure 13). Western blot densitometry of phosphorylated tau (pTau) showed higher signal in transgene-positive than transgene-negative control mice, but not between rTg4510 and rT2/T2, possibly due to variability in the data (Figures 14-15). However, analyses of insoluble high-molecular-weight (HMW) tau was more consistent with the histopathology data (Figure 16). When we examined tissue samples from the rT2 line with less extreme tau_{P301L} overexpression (8.5x endogenous mouse tau level in rT2 vs. 17x in rT2/T2, see Figure 2) we found only limited instances of pathological-associated forms of human tau protein in a few tissue samples from 7-month old mice (Figure 13).

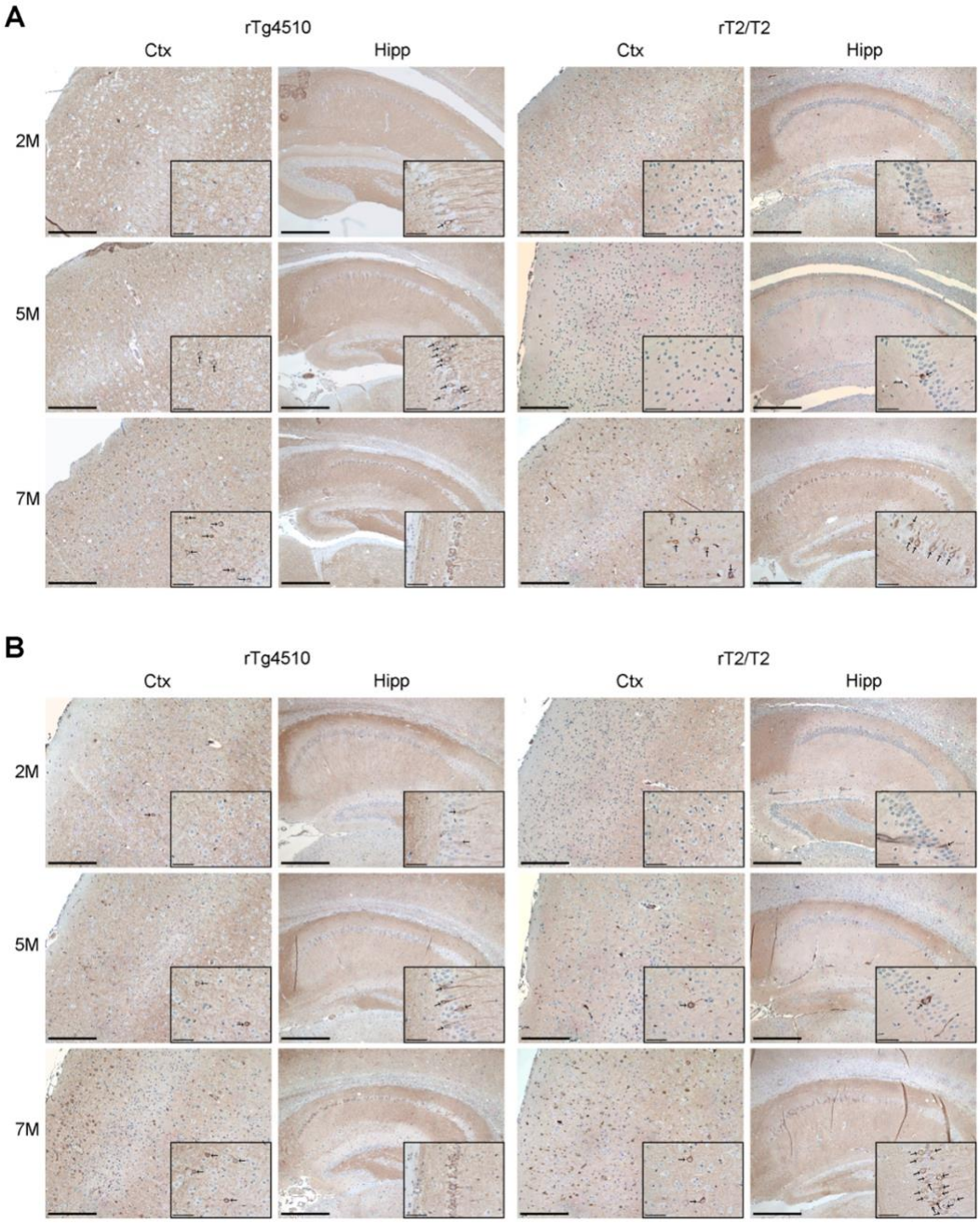

Figure 8. Accumulation of MC1-positive neurons progresses more slowly in rT2/T2 than in rTg4510 brains. MC1 (Tau aa 7-9 and 326-330) antibody was used to detect an early-stage pathological change in tau conformation in the hippocampus (Hipp) and somatomotor areas of cortex (Ctx) of 2-month, 5-month, and 7-month old female (A) and male (B) rTg4510 and rT2/T2 mice. Insets of hippocampal images show the CA1 region. MC1-positive tau deposits in rTg4510 brains appear smaller than in rT2/T2 brains due to neuronal shrinkage. Scale bars in low magnification images represent 250 µm in hippocampus and 200 µm in cortex. Scale bars in high magnification insets represent 50 µm.

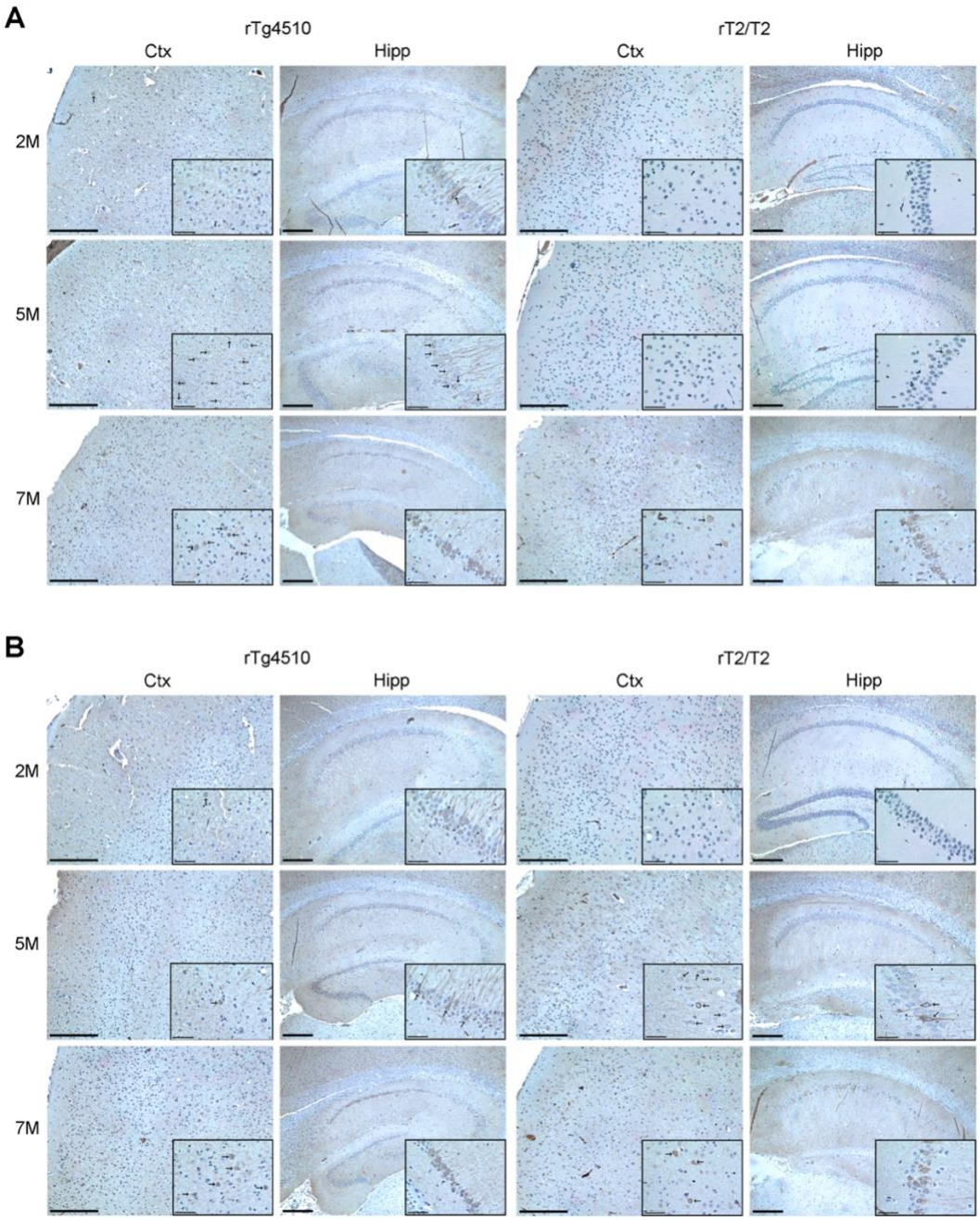

Figure 9. Accumulation of CP13-positive neurons progresses more slowly in rT2/T2 than rTg4510 brains. CP13 (Tau pSer^{202}) antibody was used to detect an early-stage pathological phosphoepitope on tau in the hippocampus (Hipp) and somatomotor areas of cortex (Ctx) of 2-month, 5-month, and 7-month old female (A) and male (B) rTg4510 and rT2/T2 mice. Insets of hippocampal images show the CA1 region. CP13-positive tau deposits in rTg4510 brains appear smaller than in rT2/T2 brains due to neuronal shrinkage. Scale bars in low magnification images represent 250 µm in hippocampus and 200 µm in cortex. Scale bars in high magnification insets represent 50 µm.

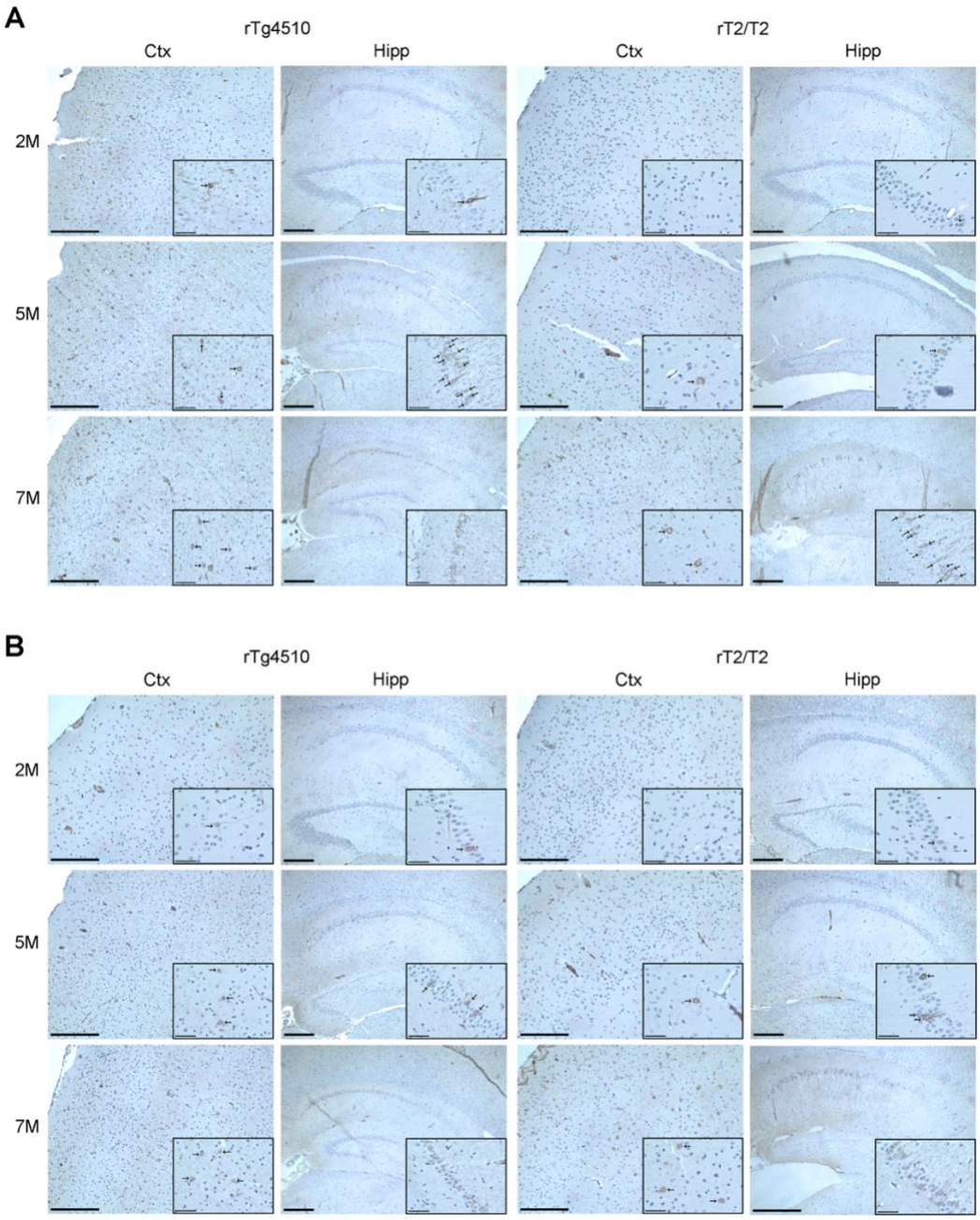

Figure 10. Accumulation of AT8-positive neurons progresses more slowly in rT2/T2 than rTg4510 brains. AT8 (Tau pSer^{202}/pThr^{205}) antibody was used to detect a pathological pre-tangle phosphoepitope on tau in the hippocampus (Hipp) and somatomotor areas of cortex (Ctx) of 2-month, 5-month, and 7-month old female (A) and male (B) rTg4510 and rT2/T2 mice. Insets of hippocampal images show the CA1 region. AT8-positive tau deposits in rTg4510 brains appear smaller than in rT2/T2 brains due to neuronal shrinkage. Scale bars in low magnification images represent 250 µm in hippocampus and 200 µm in cortex. Scale bars in high magnification insets represent 50 µm.

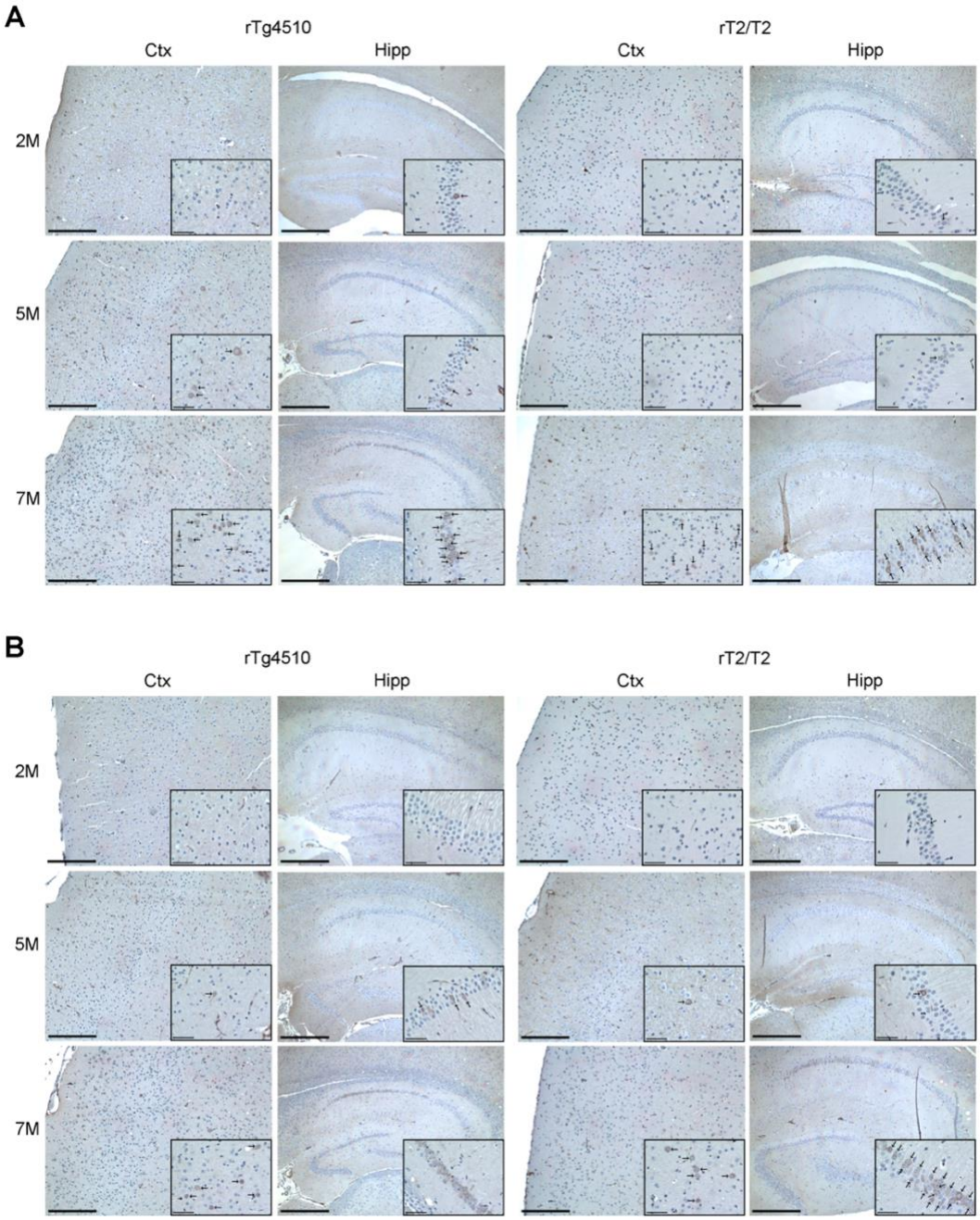

Figure 11. Accumulation of PHF1-positive neurons progresses more slowly in rT2/T2 than rTg4510 brains. PHF1 (Tau pSer^{396}/pSer^{404}) antibody was used to detect a late-stage pathological phosphoepitope on tau in the hippocampus (Hipp) and somatomotor areas of cortex (Ctx) of 2-month, 5-month, and 7-month old female (A) and male (B) rTg4510 and rT2/T2 mice. Insets of hippocampal images show the CA1 region. PHF1-positive tau deposits in rTg4510 brains appear smaller than in rT2/T2 brains due to neuronal shrinkage. Scale bars in low magnification images represent 250 µm in hippocampus and 200 µm in cortex. Scale bars in high magnification insets represent 50 µm.

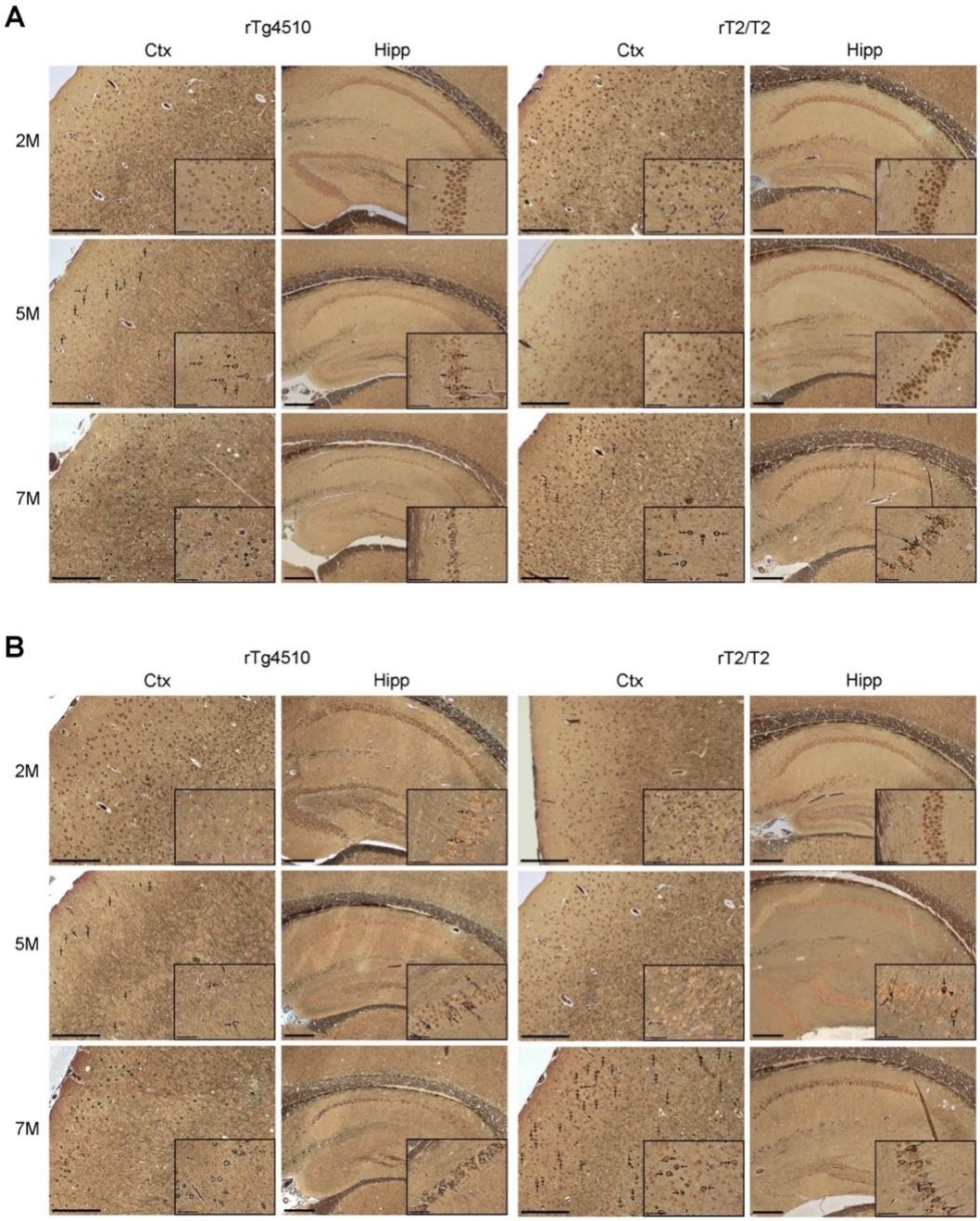

Figure 12. Accumulation of neurofibrillary tangle-positive neurons progresses more slowly in rT2/T2 than rTg4510 brains. Bielschowsky silver stain was used to detect mature neurofibrillary tangles in the hippocampus (Hipp) and somatomotor areas of cortex (Ctx) of 2-month, 5-month, and 7-month old female (A) and male (B) rTg4510 and rT2/T2 mice. Insets of hippocampal images show the CA1 region. Deposits in rTg4510 brains appear smaller than in rT2/T2 brains due to neuronal shrinkage. Scale bars in low magnification images represent 250 µm in hippocampus and 200 µm in cortex. Scale bars in high magnification insets represent 50 µm.

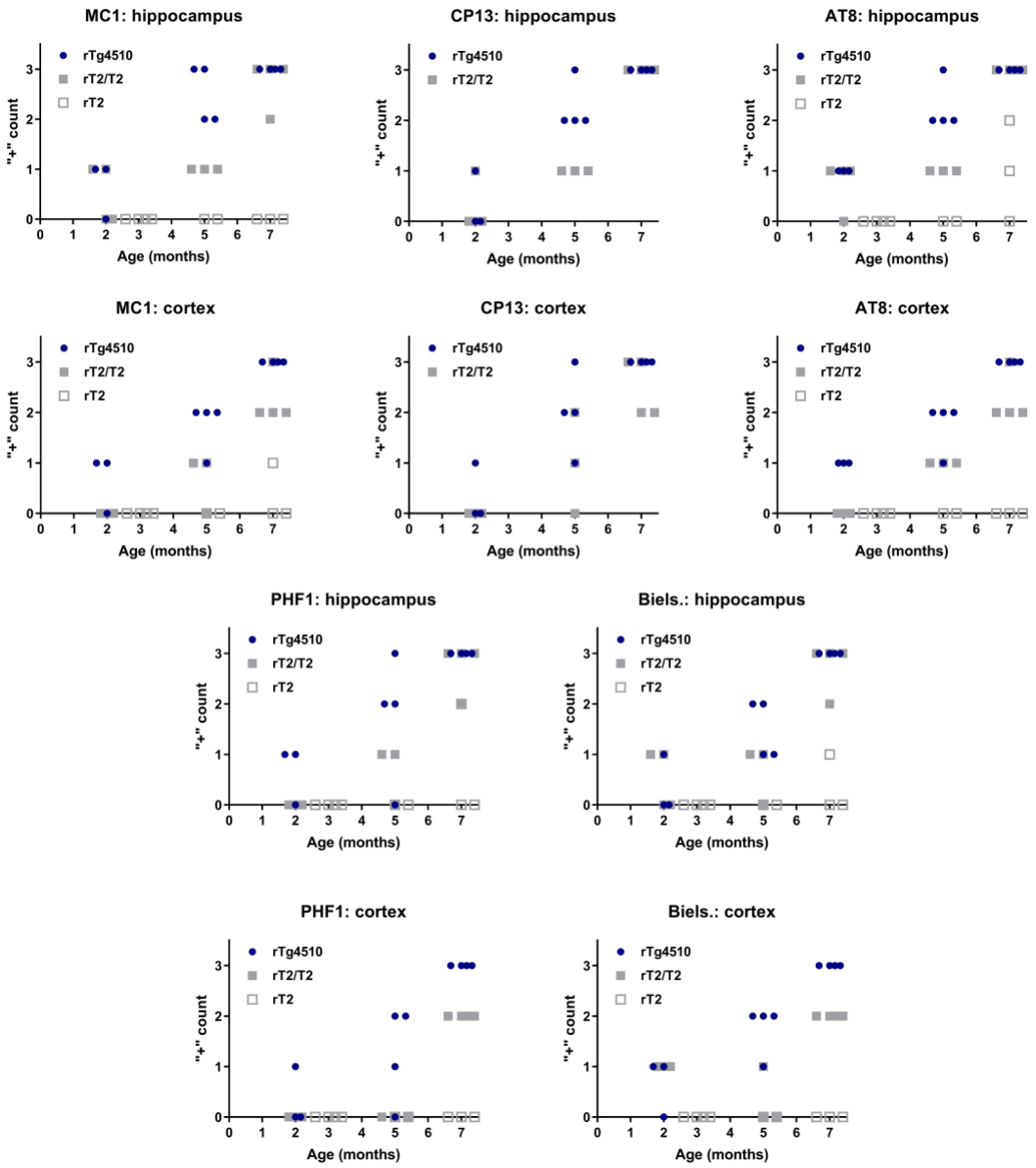

Figure 13. Slower progression of histopathology in rT2/T2 than rTg4510, and correlation of hTau expression level with severity. Summary of semi-quantitative analysis of tau histopathology progression in rTg4510 (*n* = 3 2M, 4 5M, 4 7M), rT2/T2 (*n* = 4 2M, 3 5M, 4 7M), and rT2 (*n* = 4 2M, 2 5M, 3 7M) mice. Severity of histopathology was measured on a semi-quantitative scale ('-' for no, '+' for occasional, '++' for moderate, and '+++' for prominent positive labeling). For each stain in each region, '+' signs were counted for each animal. Multiple linear regression analyses were conducted to test for differences between groups. A significant difference between rTg4510 and rT2/T2 y-intercepts was found for AT8 in the cortex (p=0.017) and between rTg4510 and rT2/T2 progression of pathology (slope) was for Biels. in the cortex

(p=0.024). A significant difference between rT2/T2 and rT2 y-intercepts was found for AT8 in the cortex (p=0.014) and between rT2/T2 and rT2 progression of pathology in MC1 in the hippocampus (p=0.0006), MC1 in the cortex (p=0.002), AT8 in the cortex (p<0.001), PHF1 in the hippocampus (p=0.03), PHF1 in the cortex (p=0.009), and Biels. in the hippocampus (p=0.02). A significant difference between rTg4510 and rT2 progression of pathology was found for MC1 in the hippocampus (p=0.0004), MC1 in the cortex (p=0.001), AT8 in the cortex (p<0.0001), PHF1 in the cortex (p=0.0007), Biels. in the hippocampus (p=0.004), and Biels. in the cortex (p=0.0006).

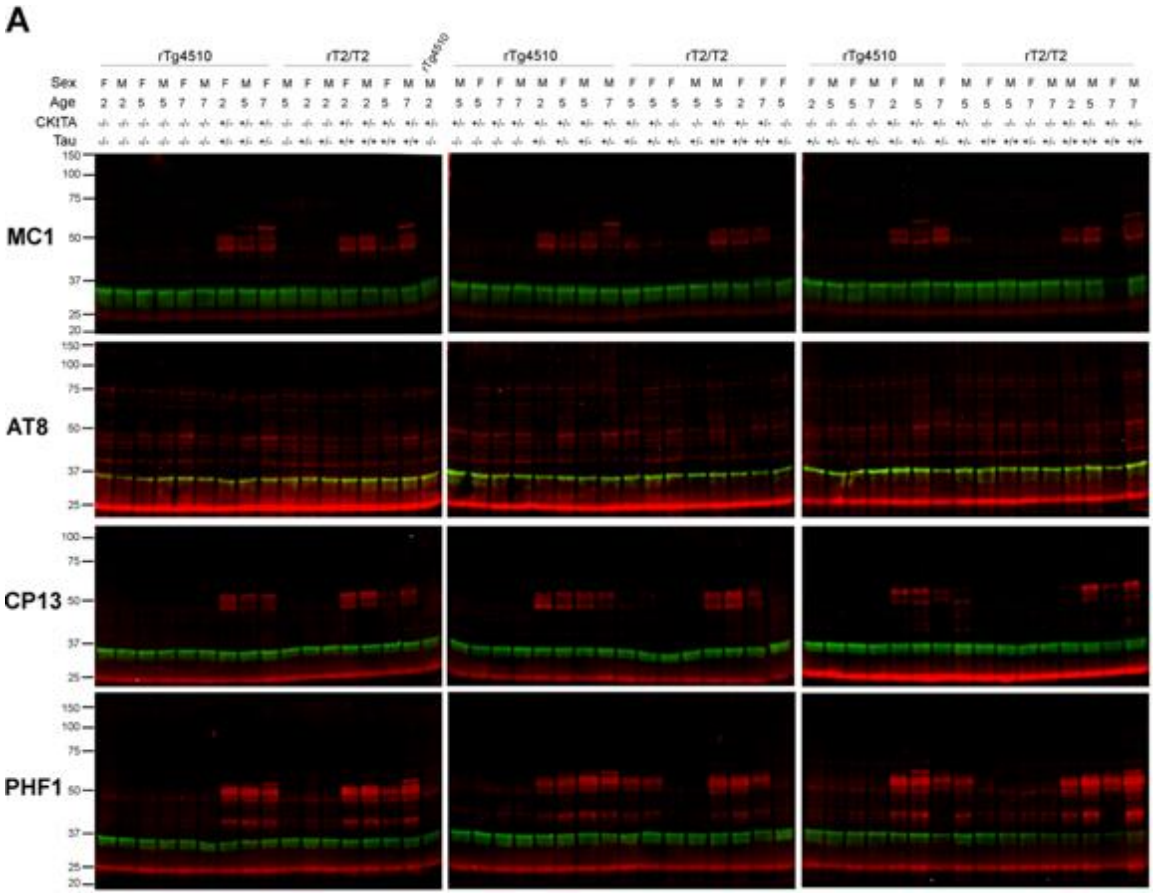
A
rTg4510
rT2/T2
rTg4510
rTg4510
rT2/T2
rTg4510
rT2/T2
Sex
Age
CK!TA
Tau
MC1
AT8
CP13
PHF1

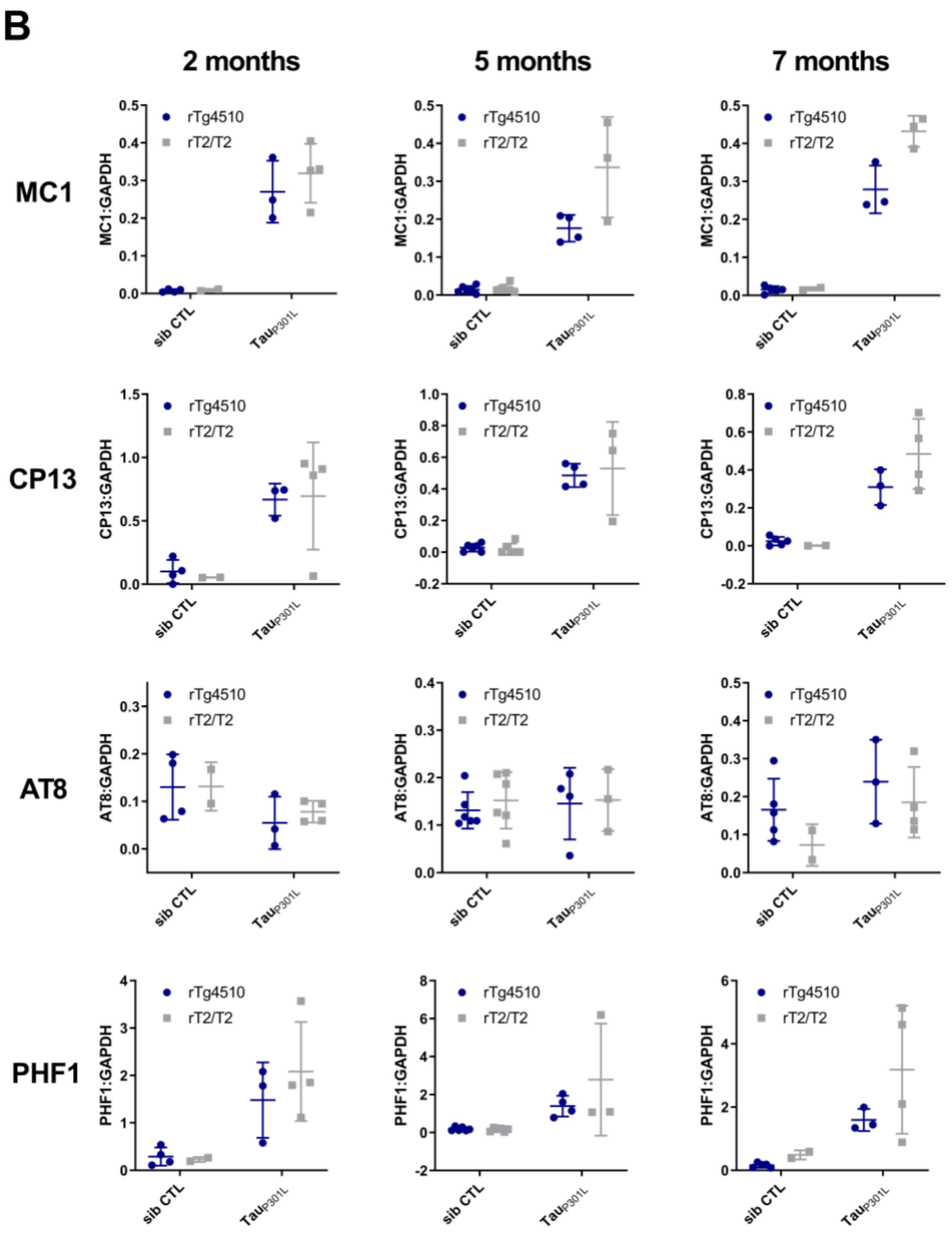

Figure 14. Quantification of pathological tau in rTg4510 and rT2/T2 forebrains relative to GAPDH. Western blots (a) and densitometric quantification (b) of pathological Tau relative to GAPDH (14C10) levels in rTg4510 (*n* = 3 2M, 4 5M, 4 7M), rT2/T2 (*n* = 4 2M, 3 5M, 4 7M), and sibling controls (rTg4510 *n* = 4 2M, 6 5M, 5 7M; rT2/T2 *n* = 2 2M, 6 5M, 2 7M). (a) Antibodies for pathological Tau included MC1 (Tau aa 7-9 and 326-330), AT8 (Tau pSer^{202}/pThr^{205}), CP13 (Tau pSer^{202}), and PHF1(Tau pSer^{396}/pSer^{404}). Sibling controls showed little to no positive labeling, and the AT8 antibody gave a weak signal. Tau-hemizygous rT2/T2 samples were excluded from all analyses. (b) Mann-Whitney tests were conducted to compare Tau$_{P301L}$–expressing rTg4510 to rT2/T2 and revealed no significant differences for any age or any immunolabeling.

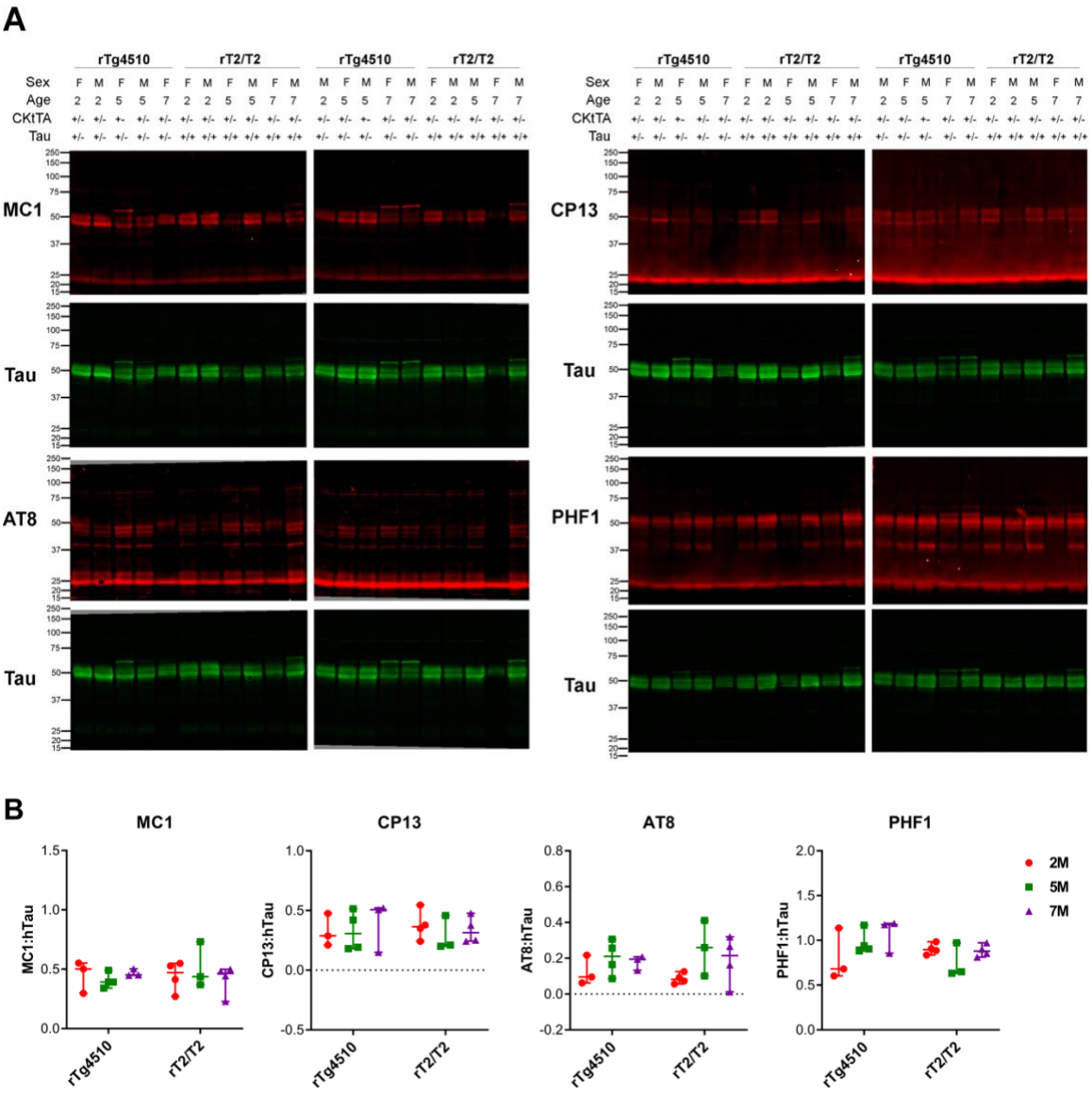

Figure 15. Quantification of pathological Tau in rTg4510 and rT2/T2 forebrains relative to human tau. Western blots (a) and densitometric quantification (b) of pathological Tau relative to human Tau (ab74391) levels in rTg4510 (*n* = 3 2M, 4 5M, 4 7M) and rT2/T2 (*n* = 4 2M, 3 5M, 4 7M) mice. (a) Antibodies for pathological Tau included MC1 (Tau aa 7-9 and 326-330), AT8 (Tau pSer^{202}/pThr^{205}), CP13 (Tau pSer^{202}), and PHF1(Tau pSer^{396}/pSer^{404}). Tau (ab74391, Abcam) immunoblots used for normalization are shown below the appropriate pathological Tau immunoblot. The AT8 antibody gave a weak signal. (b) Two-Way ANOVAs were conducted on MC1:Tau, AT8:Tau, CP13:Tau, and PHF1:Tau signal at 2, 5, and 7 months of age, and revealed no main effects of Age or Transgene for any measure. Graphs display group medians ± 95% confidence intervals.

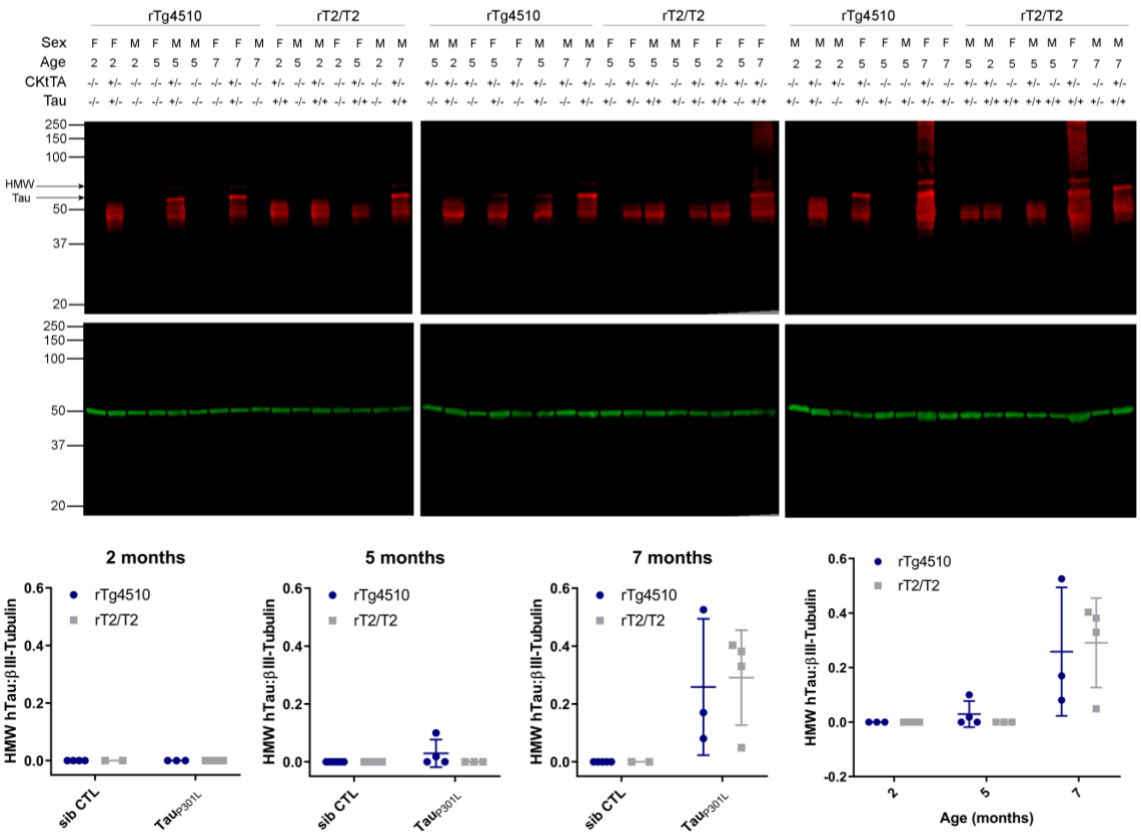

Figure 16. High-molecular-weight (HMW) human tau in RIPA-insoluble, sarkosyl-insoluble fraction increases with age in both rTg4510 and rT2/T2. Protein from rTg4510 (*n* = 3 2M, 4 5M, 4 7M), rT2/T2 (*n* = 4 2M, 3 5M, 4 7M), and sibling control mouse brains was extracted in RIPA buffer. RIPA-insoluble protein was solubilized in 1% sarkosyl, and the remaining pellet was kept as the RIPA-insoluble, sarkosyl-insoluble fraction. Top: Western blots showing tau (Tau13, BioLegend) and βIII-tubulin in the RIPA-insoluble, sarkosyl-insoluble fraction. High-molecular-weight (HMW) tau consists of one bands above 50 kDa. Genotypes, age, and sex are shown for each sample. Bottom: The HMW tau band was quantified relative to βIII-tubulin by densitometry for sibling controls (sib CTL) and Tau_{P301L} –expressing mice. Hemizygous rT2 samples were excluded from all analyses. Mann-Whitney tests comparing rTg4510 to rT2/T2 showed no significant differences at any age.

Transgene expression and Fgf14-*TgINDEL modulate severity of brain atrophy*

rT2/T2 mice do not exhibit the dramatic premature loss of brain mass shown by rTg4510, which lose ~20% of their forebrain mass by 7 months of age (Figure 17A, B). Gross forebrain atrophy, evident in rTg4510, is also absent in rT2/T2 at 7 months of age (Figure 17C).

Our experimental design for the work described here included evaluating forebrain mass loss through 7 months, at which point rTg4510 mice exhibit severe forebrain mass loss and obvious gross forebrain atrophy (Figure 17). Although the rT2/T2 mice do not share these phenotypes by 7 months, we had sufficient animal numbers to continue these evaluations at 9 months, and then with fewer animals per time point at 10, 13, and 15 months (Figure 18). The few rT2/T2 animals examined at 13 and 15 months in this pilot experiment each had severe forebrain mass loss and obvious gross forebrain atrophy that matched that of the few remaining background strain-matched rTg4510 examined at similar ages. We used rT2 mice as controls that incorporated the effects of the tTA TgINDEL but with more moderate overexpression of tau_{P301L}. We did not find severe forebrain mass loss or obvious gross forebrain atrophy by even 18 months in the rT2 mice, although brain mass may be trending lower in the oldest rT2 mice evaluated. Expected rTg4510 brain mass values based on accumulated data from the Ashe lab are shown for comparison (Figure 18B).

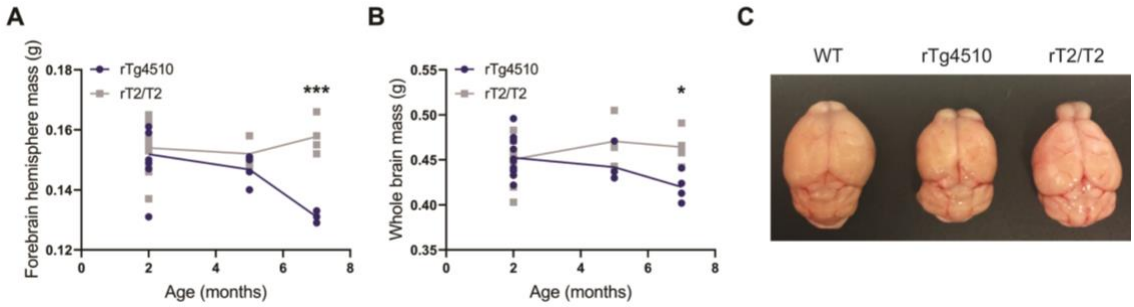

Figure 17. rT2/T2 do not exhibit gross forebrain atrophy by 7 months of age. (A) Forebrain-hemispheres were dissected from 2-month (rTg4510 *n*=9, SD= 0.010; rT2/T2 *n*=10, SD=0.009), 5-month (rTg4510 *n*=4, SD=0.005; rT2/T2 *n*=3, SD=0.005), and 7-month (rTg4510 *n*=3, SD=0.002; rT2/T2 *n*=4, SD=0.006) old mice and weighed. A one-way ANOVA was conducted ($F(5, 27)=5.034$, $p=0.0022$) with Bonferroni's multiple comparisons test for 2-month ($p>0.99$, $t=0.31$, $df=27$, 95% CI [-0.008, 0.010]), 5-month ($p>0.99$, $t=0.87$, $df=27$, 95% CI [-0.010, 0.021]), and 7-month ($p=0.0004$, $t=4.42$, $df=27$, 95% CI [0.011, 0.0422]) groups. (B) Whole brains were dissected from 2-month (rTg4510 *n*=10, SD=0.022; rT2/T2 *n*=11, SD=0.023), 5-month (rTg4510 *n*= 4, SD=0.020; rT2/T2 *n*=3, SD=0.032), and 7-month (rTg4510 *n*=4, SD=0.017; rT2/T2 *n*=4, SD=0.020) old mice and weighed. Bonferroni-corrected unpaired two-tailed t-tests were conducted for 2-month ($p=2.56$, $t=0.1894$, $df=19$, 95% CI [-0.02, 0.02]), 5-month ($p=0.58$, $t=1.497$, $df=5$, 95% CI [-0.08, 0.02]), and 7-month ($p=0.046$, $t=3.359$, $df=6$, 95% CI [-0.08, -0.01]) groups. (C) Frozen brains from a 7-month female wild-type (WT) (left), rTg4510 (middle) and rT2/T2 (right) mouse were thawed and immersion-fixed in 10% formalin. Data in (A) and (B) are represented as connected means. *$p \leq 0.05$, ***$p \leq 0.001$

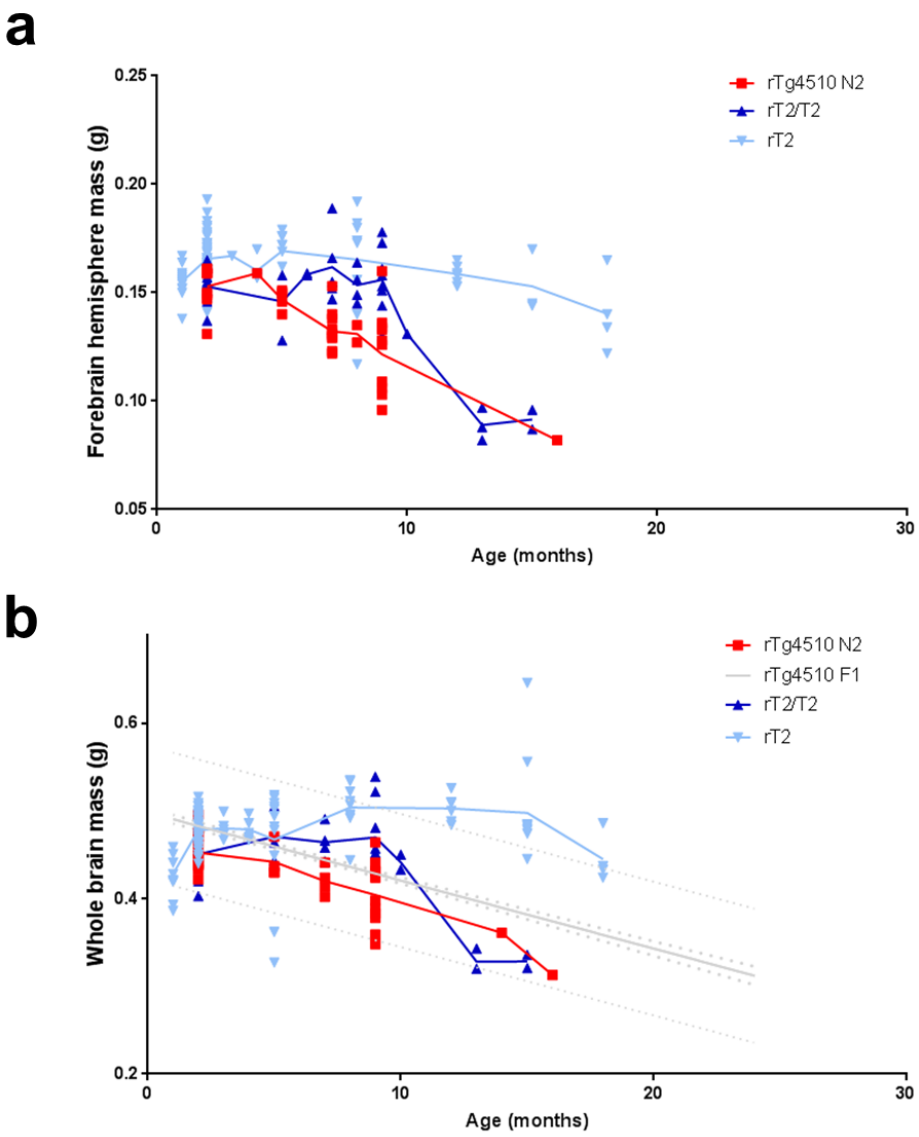

Figure 18. The *Fgf14* Tau-TgINDEL accelerates and tau expression level correlates with severity of brain mass loss. Forebrain-hemisphere (a) and whole brain (b) mass were measured for rT2/T2 (n=32), rT2 (n=120), rTg4510 F1 (FVB/129S6) (n=554), and rTg4510 N2 (FVB x FVB/129S6) (n=32) mice at varying ages. Note that the genetic background of rTg4510 N2 is matched to rT2/T2 and that of rTg4510 F1 is matched to rT2. Comparing rT2/T2 to rTg4510 N2, a delay in the drop in brain mass is observed for both forebrain-hemisphere and whole brain measurements. A comparison between rT2 and rT2/T2 reveals that a higher level of human tau expression results in a more severe loss in brain mass. Finally, these data suggest that a higher amount of FVB genetic background exacerbates brain mass loss when comparing rTg4510 N2 to rTg4510 F1 (b). Lines represent connected means. Thick dotted lines for rTg4510 F1 data represent 95% confidence bands while thin dotted lines represent 95% prediction bands.

Age-related behavior changes in rT2/T2 not seen in rTg4510

The Morris Water Maze has been regularly used to detect memory impairment in rTg4510 mice (274,347), but we were unable to evaluate mice from the rT2/T2 line using this test because these mice develop an age-related high intensity flight response phenotype at ~7M, not present in either the rTg4510 or rT2 lines, that make them unable to perform this task. This flight response appears to become more similar to that of non-domesticated mice as the rT2/T2 mice age. Nest building activity, which is a natural behavior in mice that has been used as a measure of behavior dysfunction in other mouse models of tauopathy (75), was severely impaired in the rT2/T2 mice by 8.5 months whereas the rT2 mice exhibited normal nest building activity (Figure 19A, B). Additional evaluation of the behavior phenotype in 8.5-month old rT2/T2 mice using open field analysis suggest that these mice are hyperactive as indicated by distance traveled (Figure 19C), but do not spend more time moving (Figure 19D) and do not exhibit a higher level of anxiety (Figure 19E). As these mice age (12.5 months), distance traveled is reduced, but apparently primarily due to significant reductions in time moving (Figure 19C, D). We did not examine nest building activity or open field behavior in age-matched rTg4510 mice.

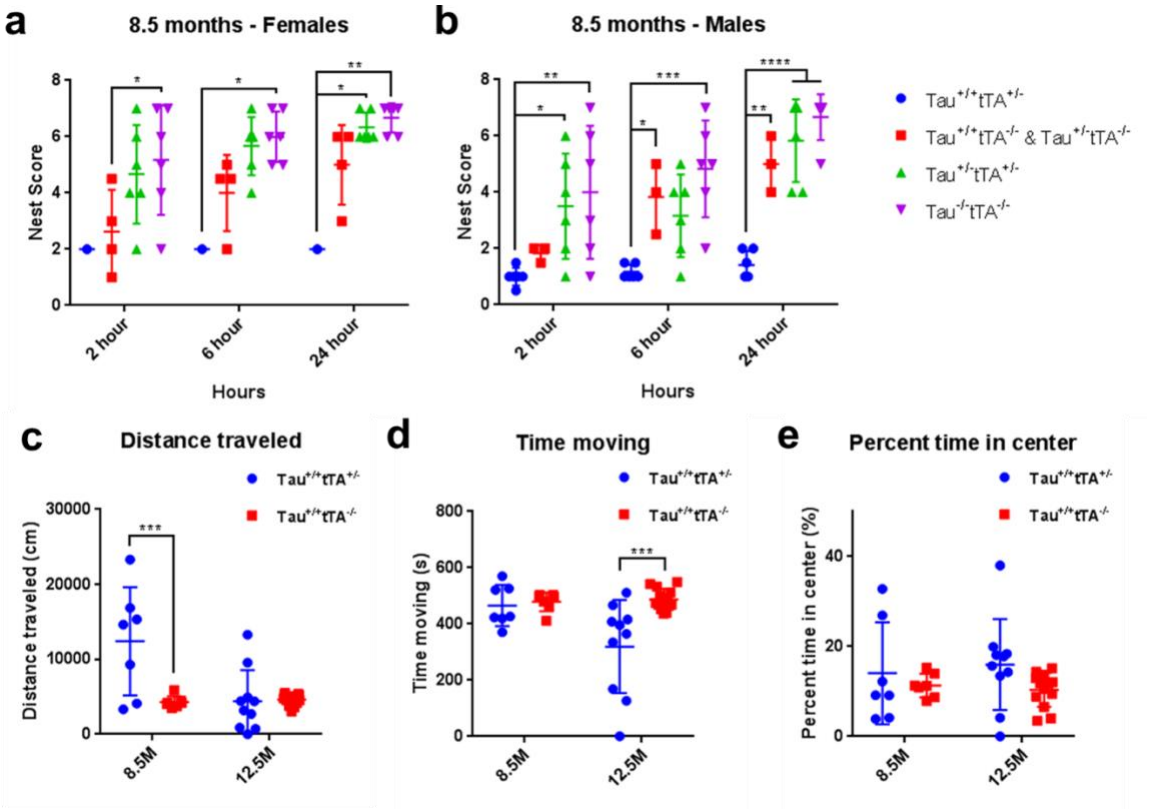

Figure 19. Nesting and open field behavior in rT2/T2 mice. (155) At 8.5 months of age, rT2/T2 (n=7), rT2 (n=12), and control littermates ($Tau^{+/+}tTA^{-/-}$ n=7, $Tau^{-/-}tTA^{-/-}$ n=12) were tested for their natural ability to construct a well-structured nest, which was scored 2, 6, and 24 hours after presenting the mice with a fresh nestlet. An overall sex effect was detected indicating that females tended to build better nests than males. Therefore, each sex was analyzed separately. An impairment in nesting was observed in both male and female rT2/T2 mice, with rT2 mice sometimes performing significantly better than rT2/T2 mice. For females (a), a Two-way Repeated Measures ANOVA revealed a significant main effect of genotype ($F(3, 13) = 6.5$, $p=0.006$). For males (b), a Two-way Repeated Measures ANOVA also revealed a significant main effect of genotype ($F(3, 17) = 14.3$, $p<0.0001$). Tukey's multiple comparisons test were run to compare genotypes within time points. (c-e) rT2/T2 and control littermates were tested in the open field at 8.5 months of age (n=7 per group) and at 12.5 months of age ($Tau^{+/+}tTA^{+/-}$ n=10, $Tau^{-/-}tTA^{-/-}$ n=13). Two-way ANOVAs showed that rT2/T2 mice exhibit signs of hyperactivity in that they travel significantly farther in the open field than controls at 8.5 months ($F(1, 33) = 9.395$, main effect of genotype $p=0.0043$), however, this declines to normal distance by 12.5 months (c). This shorter distance traveled at 12.5 months is reflected in less time spent moving ($F(1, 33) = 7.748$, main effect of genotype, $p=0.0088$) (d). rT2/T2 mice do not exhibit signs of anxiety, as they spend about the same amount of time in the center of the field as controls (e). Data represent mean ± standard deviation.

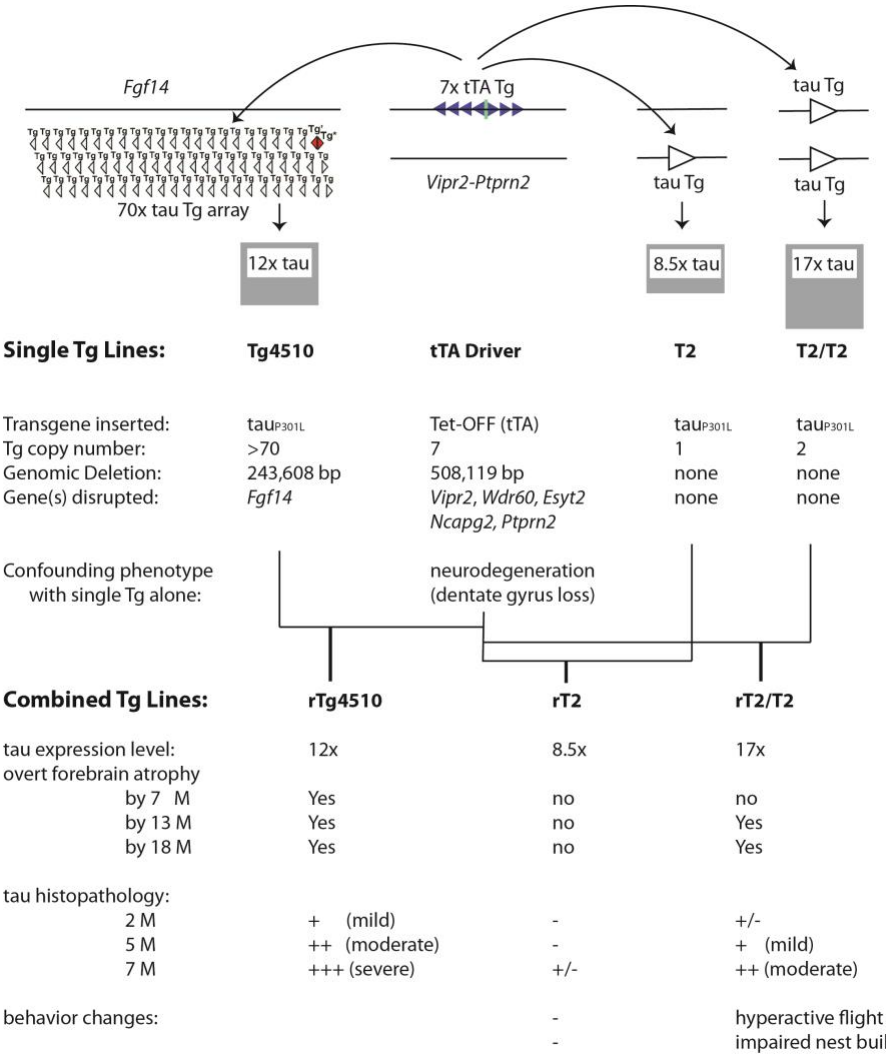

Figure 20. Overview of mouse lines and key phenotypic differences. The tau$_{P301L}$ transgene array in Tg4510 and the tTA (Tet-Off) transgene array in the expression driver line, both of which replace large segments of the mouse genome, can only be maintained as hemizygous alleles, as depicted. The single-copy targeted insertion of the same tau$_{P301L}$ transgene generated for the work described here does not disrupt any endogenous genes and was used as either a hemigyous (T2) or homozygous (T2/T2) allele, as shown. Expression from the tau$_{P301L}$ transgene requires the tTA transcription activator protein from the driver transgene, and bi-transgenic lines that carry both the driver and responder transgenes are designated as rTg4510, rT2 or rT2/T2 ("r" = regulatable). Our work demonstrates that the *Fgf14* tau-TgINDEL mutation is necessary to cause the rapidly progressive tauopathy phenocopy in rTg4510 (rTg4510 vs rT2/T2), and that key hallmarks of this phenocopy do not develop without extremely high levels of tau$_{P301L}$ overexpression (rT2 vs rT2/T2). The *Vipr2-Ptprn2* tTA-TgINDEL allele alone without the tau$_{P301L}$ transgene is sufficient to cause significant neurodegeneration, and contributions from this allele must be controlled for in any line using this allele.

IV. Discussion

Of more than 300 therapeutic agents that had been reported by 2011 to effectively treat deficits in transgenic mouse models of Alzheimer's disease, none had shown significant clinical benefit in human clinical trials (361). An expert advisory panel of academic, industry, and government scientists convened to address this failure recommended in its 'best practices' report "choosing models for preclinical studies that exhibit significant and well-characterized pathology relevant to the disease process of interest (that is, amyloid plaques, tau pathology, neuronal loss, oxidative stress/inflammatory changes, and so on)" (361). Perhaps due in part to this recommendation, the rTg4510 mouse model of tauopathy, which exhibits profound premature neurodegeneration and neurofibrillary tangles, has become widely used for both basic and preclinical studies. Among models of tauopathy, rTg4510 mice display the most dramatic loss of neurons, and this loss progresses rapidly in young animals (2-7 months) (Figure 17). However, we have now found that overexpression of the pathogenic tau variant in these mice is not sufficient to cause this premature and robust age-related loss of forebrain mass and gross forebrain atrophy, as originally and currently thought.

Two distinct mutant alleles are combined in rTg4510 mice: 1) the tau_{P301L}-TgINDEL, and 2) the tTA-TgINDEL needed to drive expression from the tau_{P301L} transgene allele. Both of these mutations were generated by pronuclear injection of synthetic mini-gene constructs into mouse single-cell embryos and were selected from among the many random integration events that occurred by screening for alleles that conferred the desired phenotype. In neither case, however, were the selected mutations themselves mapped or characterized. Our work presented here together with growing evidence from other groups indicates that the attractive rTg4510 tauopathy phenocopy found by screening for pathology similar to those found in human tauopathies arises from unintended dysfunctions conferred by the tau_{P301L} and tTA TgINDEL mutations.

Precisely defining the effects of the *Vipr2-Ptprn2* tTA-TgINDEL allele on the tauopathy phenocopy of rTg4510 is complex and in some ways problematic. The pronuclear injection experiment used to make this tTA allele, which is nominally expressed from a *CamKII* promoter fragment, generated lines with a wide array of expression patterns (350) and the primary phenotype originally used to select this particular tTA-TgINDEL allele was functional tTA-driven overexpression selectively in

mouse forebrain neurons (350). Since genomic regulators retained in flanking sequences at each insertion site dictate the unique temporal and spatial expression pattern of tTA from each mutant allele, we were not surprised to find that four of the five annotated genes disrupted by this particular recombination event (*Vipr2*, *Ptprn2*, *Wdr60*, and *Esyt2*, Figure 6) have prominent forebrain expression patterns (https://www.ncbi.nlm.nih.gov/gene/) (362). We note that loss of both copies of the fifth annotated gene, encoding the chromosome condensin Ncapg2, results in embryonic lethality (363). If nothing else, the unique tTA expression pattern generated from the combination of the *CamKII* promoter fragment within the context of the *Vipr2-Ptprn2* tTA-TgINDEL mutation defines the tau_{P301L} expression pattern in rTg4510, and likely defines the tissue specificity of the tauopathy phenocopy as well. Because we did not generate an alternative targeted insertion of a tTA transgene for our current work, we cannot determine if the loss of the genes disrupted by the *Vipr2-Ptprn2* tTA-TgINDEL directly affect the tauopathy phenocopy of rTg4510.

Because the tau transgene is expressed from a synthetic tTA-responsive promoter, tTA activity and tau expression are intrinsically linked, and as a result conclusively extricating the impacts of tau_{P301L} from those of tTA activity on phenotypes in rTg4510 may not be possible. The *Vipr2-Ptprn2* tTA-TgINDEL allele alone has been shown to be sufficient to cause a progressive neuron loss that leads to obvious degeneration of the dentate gyrus (364). Suppression of tTA activity during the first six weeks of postnatal development with doxycycline (Dox) has been shown to eliminate this observed neuron loss (364), presumably by eliminating tTA binding and subsequent unintended activation of non-target gene expression at undefined loci in the genome. We note that the 490+ cognate tTA binding sites within the *Fgf14* tau-TgINDEL would also be expected to modify binding of excess tTA to and transcription activation at noncognate genomic sites, potentially complicating the interpretation of direct comparisons between rTg4510 mice and tTA-only littermates. For example, neuron loss in rTg4510 mice is less obvious in the dentate gyrus than in other regions of the hippocampus and cortex (347), suggesting that the course of the documented tTA-driven neuronal toxicity is significantly altered in rTg4510 mice and may not contribute significantly to neuron loss. The design of the rTg4510 model precludes testing the alternative but not mutually exclusive hypotheses that overexpression of tau_{P301L} or tTA in this early developmental window is necessary to cause neuron loss. Administering

Dox to rTg4510 mice from conception to 6 weeks, followed by removal of Dox resulted in robust tau histopathology by 54 weeks of age; neuron loss was reported to be absent, but data for neuron loss was not shown (365). In addition, Dox suppression during development has been shown to result in a lower level of transgene overexpression in a model in which the *Vipr2-Ptprn2* tTA-TgINDEL allele drives expression of a CamKII target transgene (366). If this is also true for expression from the *Fgf14* tau-TgINDEL, then the post-suppression level of transgene overexpression following Dox suppression during development (365) may not be sufficient to drive neuron loss.

The fact that the *Vipr2-Ptprn2* tTA-TgINDEL allele is not genetically linked to the *Fgf14* tau-TgINDEL in rTg4510 has allowed us to use this same allele to drive expression in our new targeted-insertion rT2/T2 mice, and thereby matching the pattern of transgene expression and incorporating *Vipr2-Ptprn2* tTA-TgINDEL-linked confounding effects essentially identical to those found in rTg4510. Our new targeted-insertion rT2/T2 mice overexpress tau_{P301L} at levels even higher than in rTg4510 mice (Figure 2B, C) from the same basic transgene construct (Figure 3A), but only the rTg4510 mice exhibit robust age-related loss of forebrain mass and gross forebrain atrophy prior to one year of age (Figure 17). This result clearly demonstrates that a functional contribution from the *Fgf14* tau-TgINDEL mutation other than tau_{P301L} overexpression is a necessary cause of this premature overt atrophy. By comparing tau_{P301L} histopathology in tissue samples from rT2/T2 and rTg4510 mice (Figures 8-16), we are also able to conclude that confounding contributions from the *Fgf14* tau_{P301L}-TgINDEL mutation accelerate the rate at which and the extent to which tau_{P301L} histopathology develops in rTg4510. Finally, we found that mice from the rT2/T2 line develop an age-related high intensity flight response phenotype that make them unable to perform the Morris Water Maze, the task that has been used to measure memory impairment in rTg4510 mice (274,347).

We found that the random recombination event that integrated the tau_{P301L} transgene array into the mouse genome in Tg4510 deleted 244kb of the *Fgf14* gene (Figure 3B, Figure 4), and that this disruption results in the dysregulation of the ratios of *Fgf14* splice variants in mice that carry this mutation (Figure 5). Unfortunately for anyone attempting to determine molecular mechanisms of tau-related dysfunctions using rTg4510, confounding dysfunctions in Fgf14 have the potential to impact almost every aspect of neurobiology including synaptic transmission, plasticity and neurogenesis

(367). The splice variants of the internal growth factor *Fgf14* differ in their N-terminal amino acid sequences, which contribute to their subcellular localization and their ability to regulate the voltage-gated sodium channels with which they interact (367-375). The fact that unbiased transcriptome analyses of the extent of alternative promoter usage in adult human brains identified *FGF14* as one of the few outlier genes with more than 100 transcription start sites strongly suggests that differential regulation of this gene is critical for establishing and maintaining normal brain function (360). The deletion of 244kb of this gene in the *Fgf14* tau_{P301L}-TgINDEL mutation would severely compromise the differential regulation of these functionally distinct *Fgf14* isoforms by removing a large percentage of these transcription start sites and alternative N-terminal coding sequences (Figures 3 and 5). A translocation within a region of the human *FGF14* gene that is nearly identical to the syntenic segment of *Fgf14* disrupted by the tau transgene in rTg4510 has been reported to be linked to phenotypes ranging from ataxia (mother) to microcephaly and severe mental retardation (proband) (376), suggesting that these types of *FGF14* disruptions may increase susceptibility to significant loss of brain mass and function.

Comparisons between homozygous rT2/T2 and hemizygous rT2, which overexpress tau_{P301L} at 50% that of rT2/T2 (Figure 2), has allowed us to determine that high transgene overexpression is a third critically important contributor to the tauopathy phenocopy in rTg4510 mice. By comparing tau_{P301L} histopathology in tissue samples from rT2 to those from rT2/T2 mice (Figure 13) we are able to conclude that pushing the level of tau_{P301L} overexpression to match or exceed that found in rTg4510 dramatically accelerates the rate and extent to which tau histopathology develops. The obvious age-related high intensity flight response phenotype observed in rT2/T2 but not rT2 mice is also a phenotype that appears to be linked to the hyperexpression level of tau overexpression in these models. Open field analysis (Figure 19C-E) revealed that the rT2/T2 mice traveled a greater distance than controls, but did not move more often, indicating that the true difference was the speed at which these mice moved. A similar increase in distance traveled in open field analysis was also seen in a mouse tauopathy model in which tau_{P301L} was overexpressed from an adeno-associated virus (AAV) vector, although in that model the increase in distance traveled paralleled a similar increase in time moving (377). Similar to our findings with rT2/T2, the AAV1-tau_{P301L} overexpression model exhibited widespread accumulation of tau histopathology by 6

months without overt loss of neurons (377). The overt atrophy that we did observe in limited numbers of aged rT2/T2 mice (>12 months), also appears to be a phenotype linked to hyperexpression of transgene, since we did not observe signs of overt atrophy in aged rT2 mice (Figure 18). We note that the overt atrophy that appears to develop in aged rT2/T2 mice is similar to the ages at which neuron loss is seen in another tauopathy mouse model (319). Further studies with additional control lines (e.g., rT1 without the P301L mutation in the tau transgene) will be needed to conclude whether these impacts of transgene hyperexpression on phenotype in rT2/T2 are due specifically to extremely high levels of tau_{P301L} in particular, or to less specific cellular stresses caused by extreme overexpression of an exogenous gene in general. Our finding that high levels of tau_{P301L} overexpression directly leads to measureable dysfunctions in this protein product parallel findings in which overexpression of amyloid precursor protein causes additional phenotypes not found in models based on endogenous *App* expression levels (378,379). Although massive overexpression of a transgene has been used as a means of inducing dysfunctions in many mouse models and is rationalized as accelerating dysfunctions that also might develop more slowly at physiological levels of expression, we need to remain cognizant of the fact that the mechanisms underlying these hyperexpression-induced dysfunctions may be unrelated to those that cause disease in patients.

Our work highlights the critical importance of identifying and using proper control lines in any experiments involving transgenic animal models. The classic controls for confounding contributions from the genomic position effects of randomly integrated transgenes has been to characterize populations of experimental lines (e.g., transgene with a mutation) and of control lines (e.g., transgene without a mutation), and then either continue to work with small populations of these lines ($\geq$3 lines) with phenotypes that are representative of the average phenotypes of these characterized lines, or in most cases, with only single representative lines from each population. In almost every instance, lines with outlier phenotypes will have confounding contributions from their unique TgINDEL mutation. Although it may eventually be possible to reproduce the full range of premature tauopathy-like phenotypes found in rTg4510 by using targeted genomic modifications to generate control lines that more precisely and reproducibly generate the confounding contributions from the *Fgf14*-TgINDEL mutation (e.g., similar *Fgf14* dysregulation), this would be a new experimental system, and key findings from rTg4510

would need to be reproduced in this new system. Given the high cost in time and resources involved in making such a replacement, the onus of pursuing that work would have to fall on any group proposing to continue to use rTg4510 in their research. At this point, the targeted insertion mouse models we are developing offers a system in which the *Fgf14*-TgINDEL mutation and the potential confounding contributions from this mutation are eliminated. If crossed to mice that carry the *Vipr2-Ptprn2* tTA-TgINDEL, as described here, these mice will still have confounding contributions from this activator allele, but this artificial environment would be matched in all mice in the series, with the only difference between lines being the particular tau variant specifically introduced into the targeted tau transgene. Nonetheless, mechanistic studies using our transgenic models would still need to account for possible contributions from the *Vipr2-Ptprn2* tTA-TgINDEL and from non-physiological levels of transgene overexpression.

For more than a decade rTg4510 mice have been widely used as a model of human tauopathy but without recognizing the necessary confounding contributions from the *Fgf14* tau_{P301L}-TgINDEL, and with only recent and inconsistent attempts to control for the contributions from the previously undefined *Vipr2-Ptprn2* tTA-TgINDEL allele (364). We are explicitly not asserting that any hypotheses regarding tau pathophysiology generated from these studies using the rTg4510 model are incorrect. However, we believe that in all of these studies it is critical to account for possible contributions from the confounding effects that we have now defined. In particular, we caution against the use of rTg4510 for testing potential disease therapies, as we now know that a therapeutic agent could significantly improve or even eliminate tauopathy-like phenotypes in rTg4510 by incidentally correcting effects such as the contributions from the *Fgf14* tau_{P301L}-TgINDEL mutation (i.e., as in rT2/T2) without modifying the intended drug target.

Although we have restricted our work to characterizing rTg4510, we believe that our findings are indicative of a much broader and deeper problem. Classic pronuclear injection technology generates mice in which a transgene construct is typically arrayed as multimers in unpredictable and irreproducible configurations (see Figure 3B and Figure 6) inserted in random locations into the mouse genome. Genomic position effects on transgene expression patterns as well as gene disruption and dysregulation caused by these random insert events invariably result in dramatic phenotypic variation between the mouse lines generated by this technology. All too often the mouse line selected for

detailed characterization from among these many lines has been the line that exhibits the most “significant… pathology relevant to the disease process of interest” (361), as was the case with rTg4510. Although such mouse lines are widely and routinely used, many of the TgINDEL mutations in these lines remain only marginally characterized at the genetic level. As we have shown here, advances in genomic DNA sequencing technology now allow us to fully define the TgINDEL mutations in these lines, enabling us to more accurately identify the confounding effects caused by these mutations and to account for their possible impacts on our work.

Chapter Three:
Developmental pathogenicity of 4-repeat human tau is lost with the P301L mutation in genetically matched tau-transgenic mice

Julia E. Gamache, Lisa Kemper, Elizabeth Steuer, Kailee Leinonen-Wright, Jessica M. Choquette, Chris Hlynialuk, Kellie Benzow, Keith A. Vossel, Weiming Xia, Michael D. Koob, and Karen H. Ashe

Content adapted from a manuscript submitted for publication, 2019.

Contributions: K.A. directed the study and both K.A. and M.K. made intellectual contributions to experimental design. K.B. and M.K developed the T1 and T2 mouse lines. J.G. bred and performed all of the characterization of the rT1, rT2, and control lines discussed, performed all statistical analyses except for half-life study, and wrote the manuscript with input from K.A. and M.K. Behavior experiments in non-suppressed mice were performed by L.K., E.S., and K.L. E.S. did all fluorescent immunohistochemistry. K.V. directed mitochondrial transport assays and J.C. made neuronal cultures for those experiments. For the half-life study. W.X. ran the ELISAs and C.H. assisted with statistical analyses.

I. Introduction

Tau is the main axonal microtubule-associated protein of the mammalian central nervous system. Though tau is principally found in neuronal axons where it aids in microtubule assembly (7) and regulates cargo transport along microtubules (184), it has other 'atypical' functions in different regions in an isoform-dependent manner (202) such as growth factor signaling (232), receptor anchoring (211), and DNA protection (218). Perhaps because of the complex and multifunctional role of tau in neuron biology, tau dysfunction in a family of neurodegenerative diseases called tauopathies can result in a wide spectrum of clinical and neuropathological phenotypes.

The mechanisms underlying tau pathogenicity remain unclear, in part due to extreme variability in phenotypes of tauopathy mouse models. The P301L mutation is frequently used to model human disease because it is the most common *MAPT* mutation (AD & FTD mutation database). Although *in vitro* studies indicate that this mutation confers pathogenic properties to the tau protein such as reduced microtubule binding (34), this idea is inconsistently replicated in mouse models. Transgenic mice harboring the P301L mutation exhibit diverse phenotypes such as severe early neuropathology (274), late-onset tauopathy (380), progressive motor impairments (348), mild or absent phenotypes (277,381), or even *improvements* in cognition (382). Mouse models expressing non-mutant (NM) human tau should be used as controls for P301L models, however, NM tau mouse models also have a range of phenotypes including mild phenotypes (383,384), developmental neuropathology (385,386), progressive synaptic and cognitive impairments (387), neurodegeneration (319), progressive tauopathy (388-390), glial pathology (391,392), and axonopathy associated with motor deficits (385,393,394).

Variability in tauopathy mouse models can be attributed to differential tau isoforms, expression levels, promoters, and disruption of endogenous genes (395). We recently found that in a popular tauopathy mouse model, rTg4510, two transgene insertion-deletion (INDEL) mutations disrupt genes important for brain function, calling into question the precise role of tau in that phenotype (396). If confounding variables such as those associated with random genome disruption are not specifically accounted for, it is difficult to draw conclusions about the biological role of tau in tauopathies.

In this study, our goal was to characterize phenotypes associated with the P301L mutation by systematically comparing a novel P301L mouse model to a genetically

matched non-mutant (NM) mouse line with the same human tau (hTau) isoform, expression pattern, and transgene insertion sites in the genome. These lines harbor a single copy of a 'responder' human tau transgene in the same non-disruptive genomic locus. To activate hTau expression, they are crossed to the same 'activator' tTA line used in our previous publication, which has a transgene INDEL mutation that disrupts several forebrain genes and causes dentate gyrus degeneration (364,396). Unfortunately, these studies began before we were aware of the genomic disruption in the tTA line, however, we control for this confound because the lines are genetically identical except for the P301L mutation.

Unexpectedly, we found that the NM mouse line we intended to use as a control exhibited a robust and early phenotype, which was absent in the P301L line. Our findings indicate that overexpression of the 0N4R isoform of NM hTau is pathogenic during postnatal development, in a manner distinct from classical aging-related tauopathy. We show that developmental toxicity of NM hTau is associated with strong microtubule binding, which we hypothesize is a pathological trigger that leads to a disruption of cellular processes and eventual cognitive dysfunction.

II. Materials and Methods

Animals

An ES cell line generated in the Koob lab was used for this work (396). A construct was generated that was essentially identical to the construct used to generate Tg4510, but incorporated a Flp-In promoter cassette (PGK promoter-ATG-FRT), and 6 µg this construct and 0.5 ug pCAGGS-FlpE (Gene Bridges cat# A201) were transfected into the V6.5Col1a#15 ES cell line. Hygromycin selection at 140ug/mL was added day 2 through day 6, and Hygro resistant ES clones were picked on day 7. DNA was analyzed for 5' (5ArmCol1A assay primer + TRE start Rev) and 3' (AMP R Reverse + Hygro Connection) junctions, internal Tau (TAU assay F and R), and multiple integration assay (AMP R Reverse + TRE start R) by PCR. Clones that passed all assays were expanded and karyotyped, and T1 (non-mutant) and T2 (P301L) responder mice were generated by injection into blastocysts. These mice were back-crossed five times to FVB prior to generating the rT1 and rT2 lines.

ES Cell Assay Primer sequences:

5ArmCol1A pcr assay 5'-CAGGTGCACAGCATTGCGGACATG-3'
TRE Start Rev 5'-ATTGCTCCAGGCGATCTGAC-3'
Amp R Reverse 5'-GGAATAAGGGCGACACGGAA-3'
Hygro Connecton 5'-ATCCACGCCCTCCTACATCGAA-3'
Tau Assay F 5'-GTTCGAAGTGATGGAAGATCACG-3'
Tau Assay R 5'-TTGGGTGGAGTACGGACCA-3'

PCR Probe Primers:

Amp F 5'-CCTCCATCCAGTCTATTAATT-3'
Amp R 5'-TCCTTGAGAGTTTTCGCCCCG-3'

A human tau plasmid was used to generate T1 and T2 responders, which harbor a 0N4R human tau cDNA transgene flanked by non-coding regions of the murine *Prion protein* gene and regulated by a tetracycline response element (TRE). Activator mice harbor a tetracycline transactivator (tTA) transgene under the control of the CaMKIIα-tTA (tTA) promoter to drive expression specifically in forebrain excitatory neurons (350). Human tau expression is activated in bigenic $hTau^{+/-}tTA^{+/-}$ rT1 and rT2 progeny of an

activator-responder cross. Responder T1 and T2 mice were maintained on an FVB/N background while activator mice were maintained on a 129S6 background. Littermates $hTau^{+/-}tTA^{-/-}$, $hTau^{-/-}tTA^{+/-}$, and $hTau^{-/-}tTA^{-/-}$ genotypes were used as controls. Both male and female mice were used, and were combined in statistical analyses after demonstrating the absence of significant gender effects ($P > 0.05$). All animal breeding was conducted conservatively assuming 8 pups per litter based on accumulated data from the Ashe lab colony. All experiments with animals described in this study were conducted in full accordance with the American Association for the Accreditation of Laboratory Animal Care and the Institutional Animal Care and Use Committee at the University of Minnesota.

qRT-PCR

mRNA expression levels of hTau were quantified relative to a reference gene, *Hprt* (Table 2). Total cellular RNA was extracted from homogenized forebrain tissue using RNeasy Lipid Tissue Kit (Qiagen) according to the manufacturer's instructions. RNA samples were treated with DNaseI (New England Biolabs) to digest contaminating DNA, and subjected to cDNA synthesis using the iScript cDNA synthesis kit (Invitrogen) according to the manufacturer's instructions. PCR reactions were set up in a 20-µl volume in 96-well plates, with 3 replicates per sample. Roche SYBR Green PCR master mix was used and reactions were run in the Roche LightCycler® 480 instrument (Table 3). A final melting curve confirmed that single amplicons were present for each variant and reference reactions, and a basic relative quantification was performed using the $\Delta\Delta C_T$-Method (LightCycler® 480 Software release 1.5.0 SP3). All data were normalized to a positive calibrator sample used in each experiment.

Protein extraction from brain tissue in RIPA buffer

Soluble and insoluble protein was extracted from mouse forebrain hemisphere tissue in RIPA buffer (50 mM Tris-HCl, 150 mM NaCl, 1 mM EDTA, 0.5% Triton X-100, 1% sodium deoxycholate, 0.3% SDS, 0.1 mM phenylmethyl sulfonyl fluoride, 0.2 mM 1,10-Phenoanthroline Monohydrate, Phosphatase Inhibitor Cocktail A (Sigma), Protease Inhibitor Cocktail (Sigma), Phosphatase Inhibitor Cocktail 2 (Sigma)) by drawing up and expulsing tissue through 1 mL Monoject™ syringes (Covidien) first without and then with

20G BD PrecisionGlide™ needles. Homogenates were nutated for 1 hour at 4°C then centrifuged at 13,000 rpm for 90 minutes at 4°C, and the supernatant was collected.

Protein extraction from brain tissue in TBS buffer

Soluble protein was extracted from mouse left forebrain hemispheres in TBS buffer (25 mM Tris-HCl, pH 7.4, 140 mM NaCl, 3 mM KCl) using a Dounce Homogenizer (PolyScience) at setting 10 for 25 strokes. A series of protease inhibitors were added to buffer within 1 hour of use at the following final concentrations: 0.1 mM phenylmethyl sulfonyl fluoride, 0.2 mM 1,10-Phenoanthroline Monohydrate, Phosphatase Inhibitor Cocktail A (Sigma), Protease Inhibitor Cocktail (Sigma), Phosphatase Inhibitor Cocktail 2 (Sigma). After homogenization, samples were centrifuged at 15.6 x *g* for 90 minutes at 4°C. Supernatants were collected and diluted appropriately for ELISA.

Subcellular fractionation of brain tissue

Mouse right forebrain hemispheres were biochemically fractionated into cytosolic and light membrane (GAPDH-enriched, G-E), presynaptic (Synaptophysin-enriched, S-E), and postsynaptic (PSD-95-enriched, P-E) fractions using a modified version of a previously published protocol (397). Briefly, to obtain the G-E fraction, tissue was gently homogenized in sucrose buffer (0.32 M sucrose, 25 mM HEPES, pH 7.4) using a Dounce Homogenizer (PolyScience) at setting 1 for 12 strokes. Homogenates were centrifuged at 3,000 x *g* for 5 minutes at 4°C. The supernatant was then centrifuged at 10,000 x *g* for 12 minutes at 4°C, and the resulting supernatant was collected. To obtain the S-E fraction, pellets were washed in sucrose buffer and then resuspended in HBS (25 mM HEPES, 150 mM NaCl, pH 7.4). 80% Triton X-100 (Sigma) was added to the suspension for a final concentration of 2%. Samples were then incubated on ice for 30 minutes, centrifuged at 10,000 x *g* for 20 minutes at 4°C, and the resulting supernatant was collected. To obtain the P-E fraction, pellets were resuspended in PBS (0.01 M phosphate buffer, 0.0027 M KCl, 0.137 M NaCl, pH 7.4). A series of protease inhibitors were added to all buffers within 1 hour of use at the following final concentrations: 0.1 mM phenylmethyl sulfonyl fluoride, 0.2 mM 1,10-Phenoanthroline Monohydrate, Phosphatase Inhibitor Cocktail A (Sigma), Protease Inhibitor Cocktail (Sigma), Phosphatase Inhibitor Cocktail 2 (Sigma).

Phosphatase treatment of brain extracts

RIPA extracts (see above) were treated with calf intestinal alkaline phosphatase (CIP, New England Biolabs), and samples were resuspended in 10 µl CIP buffer (100 mM NaCl, 50 mM Tris-HCl, 10 mM MgCl2, 1 mM dithiothreitol, EDTA-free protease inhibitor cocktail, pH 7.9) per 1 µg protein. One unit CIP per µg protein was added to the samples prior to incubation at 37°C for 30 minutes. Samples were then concentrated using 0.5mL 10K Amicon Ultra centrifugal filters (Millipore, UFC501096).

Isolation of microtubules and associated proteins

Microtubules (MTs) and microtubule-associated proteins were isolated using a previously published protocol (398), which was modified from two original publications (399,400). Mouse forebrains were flash frozen in liquid nitrogen and crushed into a powder using a mortar and pestle. The powder was resuspended in 1.5X volume of MES/glutamate buffer (0.1M pH6.8 2-(N-morpholino)ethanesulfonic acid, 0.5mM $MgCl_2$, 1mM EGTA, 1M glutamate) containing 1mM DTT. The suspensions were sonicated 5 times for 10 seconds with 30-second rest intervals on ice (sonicator amplitude 20%, 1 short burst per second done manually in Continuous mode) (Fisher Scientific 150E Digital Sonic Dismembrator, with model 4C15 cell disruptor). Samples were ultracentrifuged at 30,000 x *g* at 4°C for 15 minutes, and then supernatants were ultracentrifuged at 120,000 x *g* at 4°C for 1 hour (Beckman Coulter Optima™ L-80 XP Ultracentrifuge with Type 70.1 Ti Fixed-Angle Titanium rotor and 4mL thick-walled polycarbonate tubes). 20µM Taxol (Paclitaxel, ApexBio #A4393) and 1mM GTP were added to the clarified supernatants, which were then incubated at 37°C for 30 minutes. Samples were gently layered onto a sucrose cushion (MES/glutamate buffer containing 20% sucrose) and ultracentrifuged at 30,000 x *g* at 37°C for 30 minutes. The supernatants were then collected as the cytosolic fraction while MT/MAP pellets were resuspended in 50ul MES/glutamate buffer containing 20µM taxol and stored at -80°C.

Sarkosyl extraction

To obtain sarkosyl-insoluble fractions, a modified version of a previously published method was used (351). Briefly, RIPA-insoluble pellets were homogenized in 1% sarkosyl and incubated at room temperature for 30 minutes with constant shaking. Samples were centrifuged for 1 hour at 100,000 x*g* at 20°C, and the supernatant and

pellet were separated and diluted in O+ buffer (62.5 mM Tris-HCl, pH 6.8; 10% glycerol; 5% 2-mercaptoethanol; 2.3% SDS; 1 mM EGTA; 1 mM EDTA; 1 mM PMSF; 1 mM Na3VO4; 1 mM NaF; 10 µl/ml of protease inhibitor cocktail P8340; Sigma-Aldrich). Samples were boiled for 3 minutes and stored at -20°C.

Western blot and analysis

Total protein concentrations for each sample were determined by Pierce™ Bicinchoninic Acid protein assay (Thermo Scientific). Equal amounts of protein for each sample were loaded and separated using SDS-PAGE on 10%, 10-20% or 10.5-14% Criterion™ pre-cast Tris-HCl gels (Bio Rad). Protein was transferred to nitrocellulose membranes (Bio Rad), which were blocked with 5% Bovine Serum Albumin (Sigma) in 1X TBST buffer (10 mM Tris-Base (Sigma), 0.2 M NaCl (Macron Chemicals), 0.1% Tween-20 (Sigma) pH 7.4). Protein was immunoblotted with Tau13 (1:60,000, BioLegend), GAPDH (14C10, Cell Signaling Technology, 1:4,000), Tau46 (4019T, Cell Signaling Technology, 1:10,000), β-III tubulin (79-720, ProSci, 1:10,000), Synaptophysin (SY38 ab8049, Abcam, 1:10,000), PSD-95 (2507S, Cell Signaling Technology, 1:10,000), CP13 (pSer202, Peter Davies, 1:1,000) , PHF1 (pSer396/404, Peter Davies, 1:1,500), rabbit anti-human tau (ab74391, Abcam, 1:10,000), α-tubulin (ThermoFisher, DM1A 62204, 1:10,000), MAPK (05-481, Millipore, 1:250) and JNK/SAPK1 (06-748, Millipore, 1:5,000) antibodies. For total protein analysis, Li-Cor REVERT™ total protein stain kit (product #926-11010) was used to obtain normalized phospho-tau to total tau ratios on separate western blots, after ab74391 was discontinued. To visualize immunoreactivity using a LiCor imaging system, IRDye-linked goat anti-mouse 800CW and goat anti-rabbit 680LT secondary antibodies were used (LI-COR Biosciences,1:100,000). Immunoreactivity was quantified by densitometry using OptiQuant version 3 software.

ELISA

Samples were run in duplicate in the Human Total Tau V-Plex™ ELISA kit (Meso Scale Discovery) according to the manufacturer's instructions. To be within the range of detection for this assay, extracts were diluted in Diluent 35 at the following ratios: TBS 1:10,000, G-E 1:5,000, S-E 1:2,000, and P-E 1:150.

Half-life measurements

Doxycycline chow (DOX) (Diet 7013, 200mg/kg) was administered to 8-week old rT1 and rT2 mice 3 times per week for 0, 1, 3, 6, 11, 16, and 21 days resulting in suppression of *hTau mRNA* expression for 0, 2, 5, 10, 15, and 20 days, because it takes 24 hours to suppress hTau suppression in these mouse lines (data not shown). hTau protein levels measured by ELISA (ng hTau / mg brain mass) were Log transformed and plotted over days on DOX chow. Simple linear regressions were used to determine the slopes (k') of rT1 and rT2 lines and the half-life ($t_{1/2}$) was determined based on the integrated rate law of first-order chemical reactions: $k = 2.303 * k'$; and $t_{1/2} = 0.693 / k$ (401).

Morris Water Maze

The investigators were blinded to the group allocation and mice were randomized to control for potential age, gender and litter effects. Sample sizes were estimated based on our unpublished data. Spatial reference memory was measured by using a modified Morris water maze with a protocol tailored for rapid learning in the 129/FVB F1 mice (402). Mice were prehandled for 5 sessions during the week preceding testing to gradually introduce the animals to handler manipulations and exposure to the transportation devices (beaker and scoop). In addition, there was a gradual increase in the time that mice were in home cages without micro-isolator lids and then outside of their cage in an open field and under brighter light conditions without exposure to water. Mice received visible-platform training for 5 d, with three trials per day, followed by hidden-platform training for 8 d, with two trials per day. The path lengths to the hidden platform were averaged over two-day periods (two trials per day, four trials total) for statistical analysis. There was a 3-d rest period between the visible- and hidden-platform training sessions. Three probe trials of 30 s duration each, during which the platform was removed from the pool, were performed 72 h after the 8th, 12th and 16th trials of hidden-platform training, after days 4, 6, and 8 of hidden training, respectively. Hidden training continued immediately after the first and second probe trials. Accordingly, there was 72-h interval between hidden trials 8 and 9 (days 4 and 5) and between trials 12 and 13 (days 6 and 7). The quadrant occupancy scores of the three probe trial scores were averaged for statistical analysis. For developmental suppression experiments, DOX chow (40 mg/kg, Envigo) was administered 3 times per week to either pregnant T1 and

T2 dams (Diet 5015) upon separation from sires or to weaned litters (Diet 7013). This dosage of DOX was chosen because higher doses cause placental abnormalities and fetal loss (403). rT1 and rT2 $hTau^{+/-}tTA^{+/-}$ mice in addition to $hTau^{-/-}tTA^{-/-}$ and $hTau^{-/-}tTA^{+/-}$ littermates included in this study all received the DOX chow diet. Upon switching diets between DOX and regular chow, clean cages were used. All trials were monitored, and performance measures were extracted using a computerized tracking system (Noldus EthoVision XT 10; Noldus Information Technology). $hTau^{-/-}tTA^{-/-}$ and $hTau^{+/-}tTA^{+/-}$ mice of the same line underwent water maze training at the same time to control for batch effects.

Mitochondrial length and transport measurements

Mitochondria were examined using methods validated previously (404). Primary hippocampal cultures were established using postnatal day 0 pups. The hippocampus was dissected in cold Earle's balanced salt solution (Gibco) and digested with 10 U/ml papain (Worthington Biochemical Corporation) in Earle's balanced salt solution at 37°C for 15 min. Low ovomucoid solution containing 0.15% BSA (Sigma-Aldrich), 0.15% trypsin inhibitor (Sigma-Aldrich) in Dulbecco's phosphate-buffered saline (DPBS) with calcium and magnesium (Gibco), and 66.6 U/ml deoxyribonuclease I (Sigma-Aldrich) was added to stop the digestion reaction. After 5 min, cells were suspended in fresh low ovomucoid solution. Debris was removed with a BD 70-μm nylon strainer, and the cells were spun at 341x *g* for 7 min. Cell pellets were then resuspended in warm Neurobasal A medium (Gibco) containing 2% B27 (Gibco), 0.5 mM GlutaMAX (Gibco), and 100 U/ml penicillin/streptomycin (Gibco).

Hippocampal primary neurons were plated on glass-bottom microwell dishes (MatTek Corporation) that had been coated overnight with 0.5 mg/ml poly-L-lysine (Sigma-Aldrich) in borate buffer and for 1-2 h with 0.005 mg/ml laminin in neurobasal A. Hippocampal cells were plated at a density of 350,000 cells per 10-mm microwell dish. After 24 h, 5-fluoro-2'-deoxyuridine (Sigma-Aldrich) was added at a final concentration of 7.15 μg/ml to inhibit glial growth. Half-medium changes were performed every 7 d to maintain culture health.

Transfections of hippocampal cultures were performed on DIV 8-11. Plasmids used (provided by K. Vossel, University of MN) included an FUGW EGFP construct (405) and mito-RFP, which was constructed by fusing the mitochondrial-targeting

sequence of human isovaleryl coenzyme A dehydrogenase to the N terminus of RFP within the pDsRed1-N1 vector backbone containing a CMV promoter (Takara Bio Inc.) (406). After removal of conditioned medium, cells were washed once with warm DPBS without calcium or magnesium (Gibco) and immediately placed into 500 μl warm transfection medium consisting of Neurobasal A (Gibco) with 0.5 mM GlutaMAX (Gibco), 1 mM kynurenic acid (Sigma-Aldrich) and 10 mM magnesium chloride (Sigma-Aldrich). To prepare transfection complexes, Lipofectamine 2000 (Invitrogen) was added to OptiMEM reduced serum medium with GlutaMAX (Gibco) at a ratio of 1.35 μl Lipofectamine per 25 μl OptiMEM. In separate tubes, plasmid DNA was combined in amounts that were equimolar to 1 μg FUGW per 25 ml OptiMEM. After incubating separately 5 min, the Lipofectamine-OptiMEM and DNA-OptiMEM solutions were combined and incubated at room temperature while covered for 25 min. Then, 50 ml of combined transfection solution was added to each microwell dish. Neuronal cultures were then incubated for 30 min at 37°C. Finally, cells were washed twice with warm DPBS and immediately placed in ¾ conditioned medium and ¼ fresh medium.

Live imaging of axonal mitochondria was conducted on DIV 10-13 with a Nikon inverted TiE deconvolution microscope system with Ibidi live cell environmental chamber, PFS Perfect Focus III focus lock technology, LED Light engine, motorized stage, Zyla 5.5MP sCMOS camera, and Nikon NIS-Elements Viewer imaging software version 5.10. Objective lenses were 10x (PlanFluor, NA 0.25), 20x (PlanFluor, NA 0.25 ELWD), and 40x (Plan Apo, NA 0.95). EGFP and RFP were illuminated at wavelengths of 470 nm and 555 nm, respectively.

At the beginning of each section, positions of neurons with easily identifiable axons were recorded at 10x magnification, using FUGW (EGFP) as a morphology marker. Cells exhibiting axonal beading were excluded from imaging sessions. Axons were distinguished as the longest neurite (≥3 times longer than other neurites), validated previously (404). Imaging of axonal mitochondria using mito-RFP was performed for each axon with a 40x objective. Images were acquired every 1 s for 150 s, with an exposure time of 100 ms per frame.

Images were processed in Fiji using the Multiple Kymograph and tsp050706 plugins. Moving mitochondria were defined as showing displacement of at least 2 μm, which was the average length of mitochondria observed previously (404). Velocity was measured for each moving mitochondrion by averaging its total velocity, including brief

pauses, while in the image frame. Lengths of mitochondria were measured on the kymographs. Pixels were converted to μm based on the calibration of the objective.

Fluorescent immunohistochemistry, imaging, and analysis

At two months of age mice were transcardially perfused with 50ml phosphate-buffered saline followed by 50ml 4% paraformaldehyde. Brains were removed, post-fixed overnight in 4% paraformaldehyde, and cryoprotected for 48hr in 30% sucrose. Brains were coronally cryo-sectioned at 40 microns, and all subsequent incubations and washes were performed free-floating in 24-well plates.

Following three washes of PBS+ .1% TritonX-100, sections were placed in 1% NaBH for 20 min at room temperature. Sections were washed 5x15minutes in PBS+ .1% TritonX-100. Sections were incubated in an antigen retrieval sodium citrate buffer (Reveal Decloaker, Pacheco, CA) for 30 minutes at 80° and allowed to cool for 30 minutes. Sections were washed 3x15min in PBS+ .1% TritonX-100 and transferred to blocking buffer of PBS + .5% triton X-100, 5% Normal goat serum. Sections were incubated for 48hr at 4° in primary antibody solution of PBS + .3% triton X-100, 3% Normal goat serum, at a 1:1,000 dilution (DNA/RNA Oxidative Damage Oh8dG, QED Bioscience Inc. San Diego, CA).

Following three washes of PBS+ .1% TritonX-100, sections were incubated for 1hr at room temperature in secondary antibody solution of PBS + .3% triton X-100, 3% Normal goat serum, at a 1:1,000 dilution (Goat Anti-Mouse IgG H&L Alexa Fluor594, Abcam, Cambridge, United Kingdom). Sections were washed 3x15min in PBS and placed onto Superfrost slides. Sections were treated for 30 seconds with TrueBlack® Lipofuscin Autofluorescence Quencher and washed 3x15min with PBS. Slides were coverslipped with Vectashield mounting media containing DAPI (Vector Laboratories, Burlingame, CA). Note that RNase treatment did not affect signal intensity in pilot experiments, and thus was not used for experimental tissue.

After blinding the investigator, samples were imaged on a Nikon NiE C2 Upright Confocal microscope and 10x images were taken of the dentate gyrus of the hippocampus, CA1 region of the hippocampus, and the cortex. Analysis of the Alexa Fluor594 signal intensity was performed in Fiji/ImageJ. The pyramidal layer of the CA1 region of the hippocampus, the granular cell layer of the dentate gyrus, and all cortical layers were outlined as the region of interest (ROI) using the polygon tool. The

integrated density (area x mean intensity) of the ROI was measured to account for differences in area between samples.

Experimental Design and Statistical Analysis

Power analyses on preliminary data were performed for pTau quantification, hTau ELISA, and Morris Water Maze. For pTau detection by western blot, it was determined that an *n* of 6 mice would be sufficient to have an 84% chance of detecting a 39% difference in means at a significance level of 0.05. For ELISA experiments, it was determined that an *n* of 4 mice per line would be sufficient to have a 91% chance of detecting a 21% difference in means. Therefore, a group size of 6 was chosen for tau quantification experiments by western blot and ELISA. For behavioral experiments, it was determined that a sample size of 12 would be sufficient for a 64% chance of detecting a 41% difference in group means.

For half-life experiments, R programming language was used to conduct multiple linear regressions for detecting differences between linear regression slopes. Statistical analyses for all other data were conducted using GraphPad Prism version 7.00 software (GraphPad Software). Unpaired two-tailed t-tests were used to detect differences between rT1 and rT2 *hTau* mRNA, protein (by western blot and ELISA), phosphorylated hTau at 8 weeks of age, and NM vs. P301L hTau levels in microtubule-binding experiments. Two-way ANOVAs with Sidak's multiple comparisons test were used for comparing human and mouse tau levels in rT1 and rT2 mice, as well as hTau levels and phosphorylation with or without DOX suppression. Simple linear regression was used to calculate slopes, y-intercepts, and R^2 values for NM and P301L hTau half-life data. Bonferroni-corrected unpaired two-tailed t-tests were used to compare phosphorylation levels of hTau in rT1 and rT2 at 3, 5, and 7 weeks of age. Two-way ANOVAs with Tukey's multiple comparisons test were used to detect differences in hTau levels and phosphorylation with 4 or 12 weeks of DOX suppression in rT1 and rT2.

Two-way repeated measures ANOVAs with Sidak's multiple comparisons tests were used for Morris Water Maze visible and hidden trial data to determine if rT1, rT2, and non-transgenic littermate path lengths changed over time. Two-Way repeated measures ANOVAs with Tukey's multiple comparisons tests were used for Water Maze visible and hidden data to determine if rT1 and rT2 path lengths differed from 4-week and 12-week DOX suppression groups. One-way ANOVAs followed by Holm-Sidak's

multiple comparisons tests with target (T) as the control column were to assess search bias in Water Maze probe trial data to separately determine if each group spent more time in the target than the other 3 quadrants (407). One-way ANOVAs followed by Holm-Sidak's multiple comparisons tests were also used to compare 0-, 4-, and 12- week suppression groups and to compare $hTau^{-/-}tTA^{-/-}$, $hTau^{-/-}tTA^{+/-}$, and $hTau^{+/-}tTA^{+/-}$ genotypes in time spent only in the target quadrant. Two-tailed Mann Whitney tests were used to directly compare the percent time spent only in the target quadrant between rT1 or rT2 and non-transgenic littermates. A Kruskal-Wallis test with Dunn's multiple comparisons test was used to analyze mitochondrial length data. Two-way ANOVAs with Sidak's multiple comparisons tests were used to determine whether there were differences in oxidative stress between rT1 and rT2 and between each of the genotypes in each brain region. Two-way ANOVAs with Sidak's multiple comparisons test were used to test if postnatal brain mass differed between genotypes, if rT1 brain mass differed from rT2, and to test if DOX suppression affected rT1 and rT2 brain mass. In all cases, $p<0.05$ was considered to be statistically significant.

III. Results

Elevated steady-state levels of 4R NM compared to P301L hTau

Responder T1 and T2 mice were generated using site-specific targeting of a human tau (hTau) transgene downstream of the *Col1A1* 3' untranslated region in modified embryonic stem cells. Correct single-copy integration was confirmed using PCR assays and whole-genome sequencing (396). The transgene consists of the cDNA sequence for the 0N4R isoform of hTau, flanked by non-coding regions of the murine *Prion protein* gene to enhance brain expression (274), and regulated by a tetracycline response element (TRE) promoter. T1 mice harbor a non-mutant hTau transgene while T2 harbor a P301L mutant hTau transgene. Responder T1 and T2 mice are crossed to the CaMKIIα-tTA line (350) to generate Tet-OFF bigenic rT1 and rT2 (r = regulatable) progeny that express 0N4R hTau selectively in forebrain neurons, except in the presence of doxycycline.

hTau transgene expression was not 'leaky' in the absence of the activator transgene in T1 and T2 responder lines (Figure 21A, Table 10). Despite expressing similar levels of *hTau* mRNA in the forebrain (Figure 21A, Table 10), rT1 mice had elevated steady-state levels of hTau protein at 8 weeks of age ($t(21) = 4.60$, $p = .0002$, 95% CI [-1.10 , -.42]) (Figure 21B). A difference in electrophoretic mobility also suggested a difference in post-translational modifications (Figure 21C). A human tau ELISA (Meso Scale Discovery) confirmed the difference in hTau steady-state levels ($t(10) = 5.06$, $p = .0005$, 95% CI [-112.3 , -43.66]) (Figure 21D). To quantify fold-overexpression of hTau relative to endogenous mouse tau, phosphatase-treated extracts from rT1 and rT2 were compared to activator-only (tTA) brains using a pan-tau antibody, which revealed 12.6-fold overexpression in rT1 and 6.2-fold in rT2 (tTA vs. hTau $F(1, 20) = 73.71$, $p < .0001$; rT1 vs. rT2 $F(1, 20) = 12.01$, $p = .0024$) (Figure 21E,F). rT1 hTau overexpression was significantly higher than that of rT2 ($p = .0002$).

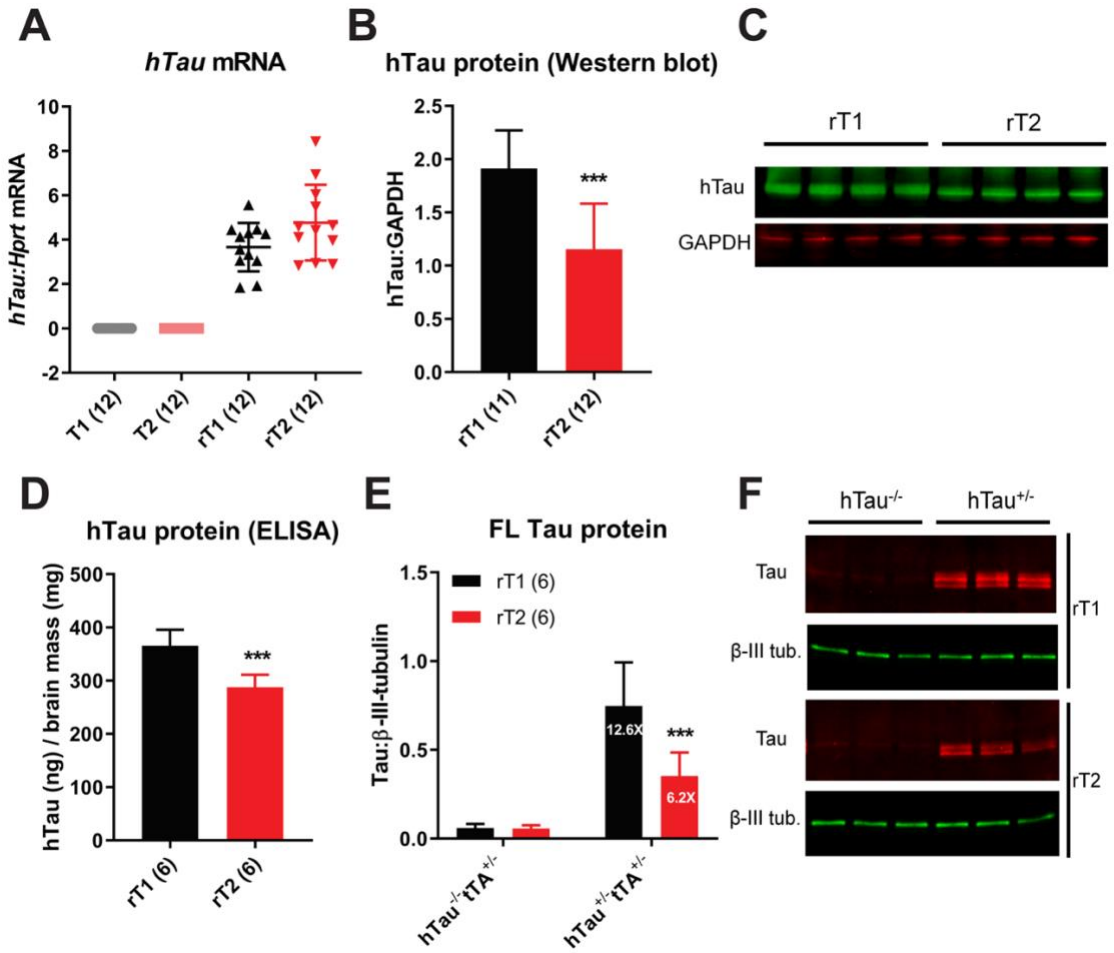

Figure 21. hTau expression in rT1 and rT2 mice. (A) Relative RT-qPCR shows similar *hTau* mRNA expression in 8-week old rT1 and rT2 forebrains. *hTau* mRNA was not detected in T1 or T2 responders, demonstrating a lack of leaky transgene expression in the absence of the activator transgene (data not shown). (B) Densitometric analysis of western blots shows higher steady-state levels of NM than P301L hTau in forebrains of 8-week old mice. (C) Representative immunoblots for hTau (Tau13 antibody) and GAPDH protein for data in *B*. Proteins were extracted in RIPA buffer and run on a 10-20% Tris-HCl gel. (D) Soluble tau extracted in TBS buffer and measured by human tau ELISA also shows higher steady-state levels of NM than P301L hTau in 8-week old forebrains. (E) Quantification of full-length (FL) human and mouse tau in phosphatase-treated samples from 8-week old forebrains, showing higher overexpression of hTau in rT1 (12.6-fold) than rT2 (6.2-fold) relative to $tTA^{+/-}$ mice. (F) Representative immunoblots for human and mouse tau (Tau46) and β-III tubulin for data in *E*. Proteins were extracted in RIPA buffer, treated with phosphatase, and run on a 10.5-14% Tris-HCl gel. *n*'s for each group in parentheses. Graphs display group means + SD. ***p<0.001

Longer half-life of 4R NM than P301L hTau

Because *hTau* mRNA levels are similar between rT1 and rT2, it is unlikely that hTau protein is higher in rT1 due to a higher rate of production. We therefore tested the hypothesis that the elevation in 4R NM hTau steady-state levels was due to a slower rate of degradation by measuring the half-life in 8-week old rT1 and rT2 mice in a manner similar to a previous study (401), taking advantage of doxycycline (DOX)-mediated suppression. Using ELISA measurements, we found that hTau levels declined with longer periods of transgene suppression ($F(3, 80) = 443.9$, $R^2 = 0.94$, $p < .000$), and that the clearance rate of soluble hTau was slower in 8-week old rT1 than rT2 forebrains (Figure 22A, Table 9).

To determine if clearance of 4R NM hTau was impaired in a specific subcellular compartment, forebrains were fractionated into GAPDH-enriched (G-E), synaptophysin-enriched (S-E), and PSD-95-enriched (P-E) fractions (Figure 22B). Again, hTau levels declined with longer periods of transgene suppression in the G-E ($F(3, 80) = 147.6$, $R^2 = 0.85$, $p < .000$), S-E ($F(3, 80) = 115.9$, $R^2 = 0.81$, $p < .000$), and P-E fractions ($F(3, 80) = 125.5$, $R^2 = 0.83$, $p < .000$) (Table 9). In addition, NM hTau degradation was significantly slower than P301L in the P-E fraction (Figure 22C, Table 9). The half-life of NM hTau was consistently longer than for P301L hTau in all fractions tested (Table 9). These results demonstrate that hTau steady-state levels are higher in rT1 than rT2 because of a slower clearance rate, and suggest that hTau degradation is impaired primarily in the postsynaptic compartment. Although only a small fraction of total hTau is localized to the postsynaptic compartment, reduced clearance may begin early and compound over time to cause elevated levels by 8 weeks of age.

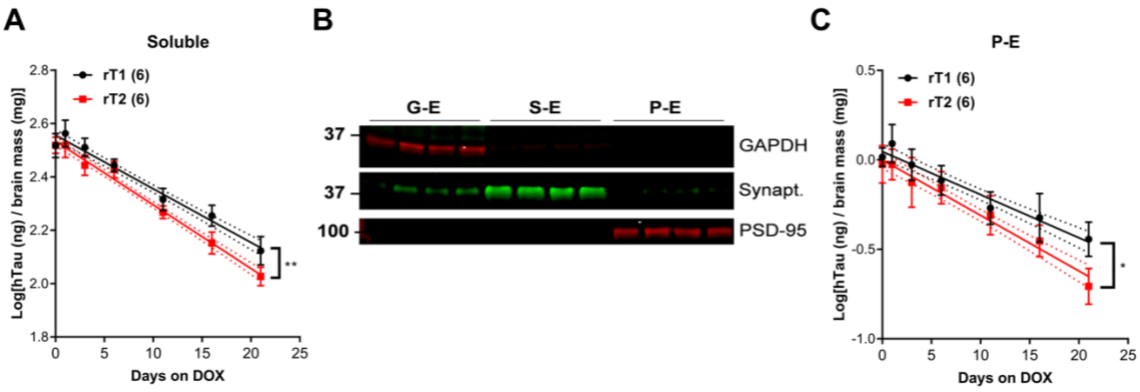

Figure 22. Slower clearance rate of 4R NM than P301L hTau. (A) The clearance rate of soluble NM hTau is slower than P301L hTau (see also Table 1). (B) Validation of biochemical fractionation method into GAPDH-enriched (G-E), Synaptophysin-enriched (S-E), and PSD-95-enriched (P-E) compartments. Proteins were run on a 10% Tris-HCl gel. (C) The clearance rate of NM hTau is slower than P301L hTau in the P-E fraction (see also Table 1). Symbols on graphs are group means ± error, solid lines represent linear regressions with standard error as dotted lines. *n*'s in parenthesis. *p<0.05, **p<0.01

Table 9. Summary of 4R NM and P301L hTau half-life and regression data. Half-lives of NM and P301L hTau as measured by the experiment shown in Figure 2 in rT1 and rT2 mice were calculated using the integrated rate law for first-order chemical reactions ($t_{1/2}$ = 0.693 / (2.303 x k') (401), where k' is the slope of the log-transformed values of tau plotted over time on DOX. Cofficients of determination (R^2) values, y-intercepts, and slopes from simple linear regressions (SLR) are listed. Multiple linear regressions (MLR) were used to test for differences between slopes, and p-values are shown.

Fraction	NM hTau half-life (days)	P301L hTau half-life (days)	SLR R^2 (NM, P301L)	SLR Y-intercept (NM, P301L)	SLR slope (NM, P301L)	MLR p-value
Soluble	15.0	12.5	0.92, 0.96	2.56, 2.53	-0.020, -0.024	0.00292
G-E	12.6	11.1	0.86, 0.83	2.14, 2.08	-0.024, -0.027	0.1762
S-E	18.5	15.6	0.78, 0.80	1.68, 1.61	-0.016, -0.019	0.14309
P-E	12.5	9.7	0.78, 0.84	0.047, 0.00014	-0.024, -0.031	0.0214

Hyperphosphorylation of 4R NM hTau compared to P301L hTau

We observed altered electrophoretic mobility of NM compared to P301L hTau, suggesting a difference in post-translational modifications (see Figure 21C). In addition, some studies indicate that NM tau has a higher propensity to become phosphorylated than P301L tau (313,381,385,386). Therefore, we next determined whether 4R NM hTau was hyperphosphorylated compared to P301L hTau in 8-week old rT1 and rT2 forebrains by immunoblotting with a series of antibodies that recognize well-known tau phosphoepitopes in human tauopathy post-mortem tissue.

While some antibodies showed no differences between rT1 and rT2, including AT8 (pSer202/pThr205) and PG5 (pSer409) (data not shown), CP13 (pSer202) and PHF-1 (pSer396/pSer404) revealed significantly higher phosphorylation levels of NM than P301L hTau (CP13: $t(10) = 11.47$, $p < .0001$, 95% CI [-.27 , -.18]; PHF-1: $t(10) = 6.18$, $p = .0001$, 95% CI [-.17 , -.08]) (Figure 23A, B). NM hTau was also hyperphosphorylated compared to P301L hTau in the biochemically isolated postsynaptic fraction (CP13: $t(10) = 3.32$, $p = .0078$, 95% CI [-.31 , -.062]; PHF-1: $t(10) = 6.35$, $p < .0001$, 95% CI [-.31 , -.15]) (Figure 23C, D). To determine how early this phosphorylation could be detected, we performed experiments in 3-, 5-, and 7- week old rT1 and rT2. First, we confirmed expression of hTau and tTA mRNA and hTau protein in postnatal mice (Figure 24, Table 10). We found that NM hTau hyperphosphorylation compared to P301L hTau could be detected as early as 5 weeks of age (CP13: $t(6) = 4.76$, $p = .0093$, 95% CI [-.402 , -.13]; PHF-1: $t(6) = 6.61$, $p = .0018$, 95% CI [-.33 , -.15]), and continued at 7 weeks (CP13: $t(5) = 7.38$, $p = .0021$, 95% CI [-.37 , -.18]; PHF-1: $t(5) = 4.11$, $p = .028$, 95% CI [-.44 , -.10]), suggesting that this could be a neurodevelopmental phenomenon (Figure 23E, F).

There is much overlap between the sites highly phosphorylated on tau during development and in aging-related neurodegenerative diseases, but normal developmental phosphorylation is insufficient to induce tau aggregation and insolubility (250). To determine whether phosphorylation of 4R NM hTau in young mice was associated with insolubility, protein from forebrains of 8-week old mice was extracted in sarkosyl. No high-molecular-weight hTau species above 55 kDa were observed (data not shown), indicating that the phosphorylation in rT1 brains does not induce the formation of insoluble aggregates.

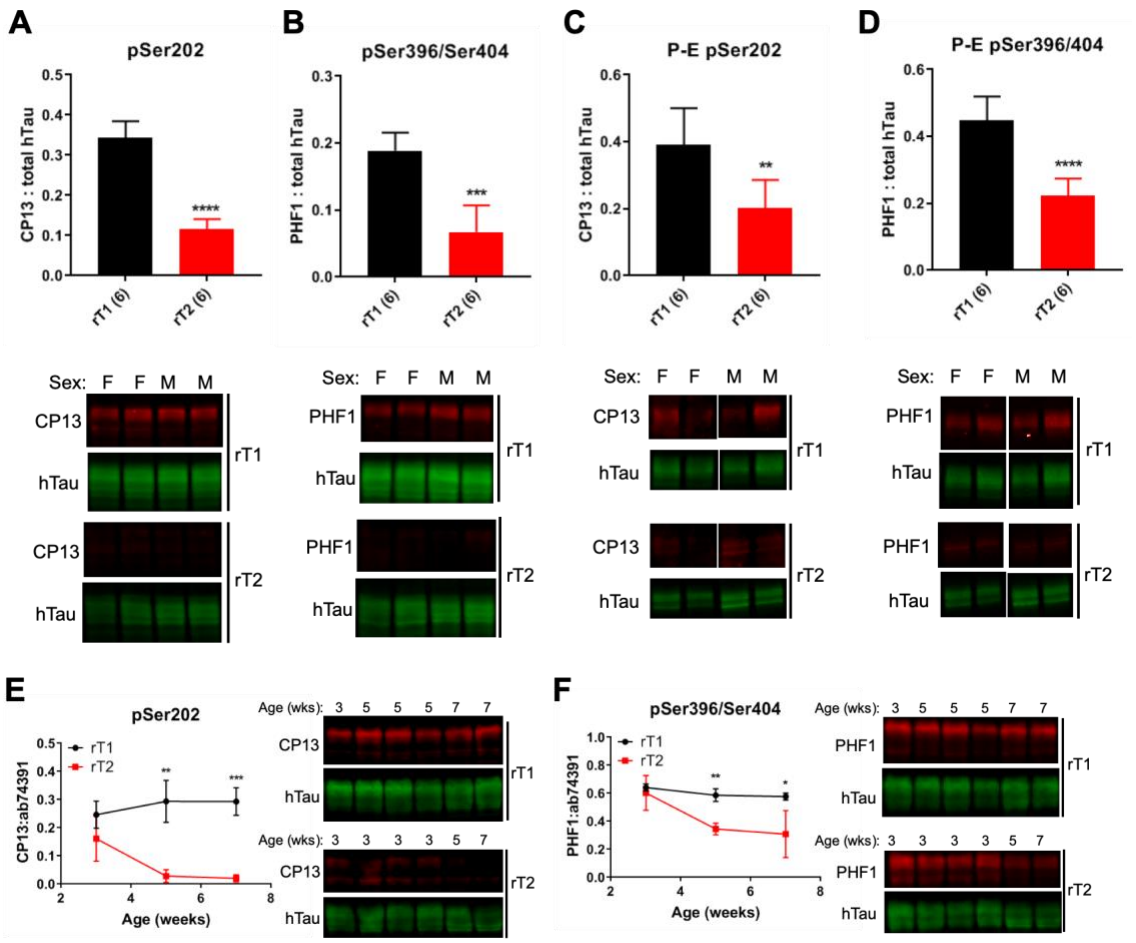

Figure 23. 4R NM hTau is hyperphosphorylated compared to P301L hTau by 5 weeks of age. Phosphorylation of hTau was greater in rT1 than in rT2 forebrains (A, B) and in the biochemically isolated PSD-95-enriched (P-E) fraction (C, D) at 8 weeks of age. Top panels: graphs summarizing densitometric analyses of western blots immunoblotted with CP13 (pSer202), PHF-1 (pSer396/Ser404), and ab74391 (hTau), with *n*'s for each group in parentheses. Bottom panels: representative western blots for data in top panels with sex of the animals indicated above. NM hTau becomes hyperphosphorylated as early as 5 weeks of age at both pSer202 (E) and pSer396/404 (F) (rT1: *n* = 4 3wk, 6 5wk, and 5 7wk; rT2: *n* = 6 3wk, 2 5wk, and 2 7wk). Densitometric quantification in E and F are in left panels with representative blots on the right, ages of animals indicated above. Proteins were extracted in RIPA buffer and run on 10% Tris-HCl gels. Graphs display group means ± SD. *p<0.05, **p<0.01, ***p<0.001, ****p<0.0001

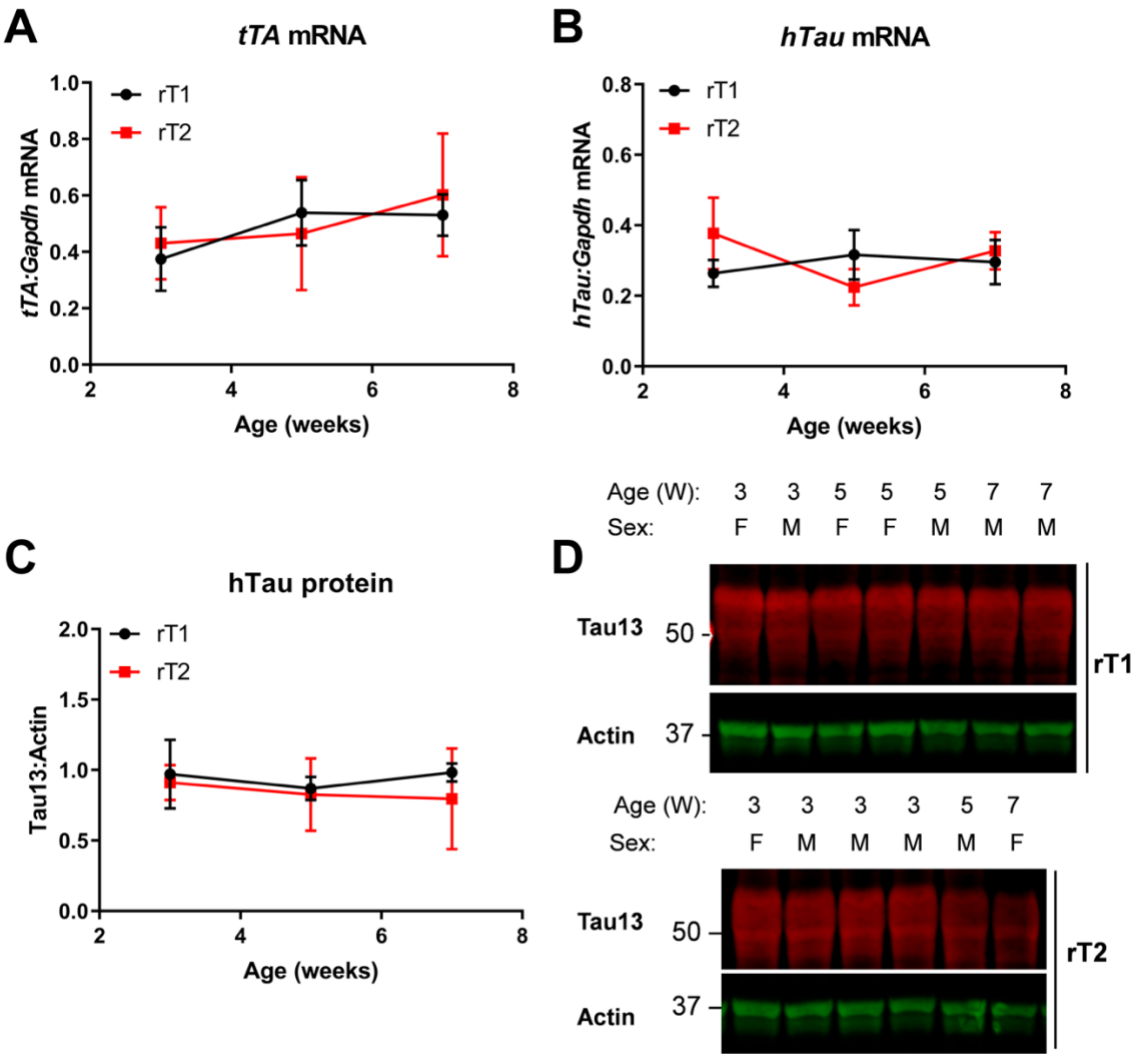

Figure 24. hTau and tTA expression in postnatal rT1 and rT2. Forebrain mRNA analysis in 3- , 5- , and 7- week old rT1 and rT2 (*n* = 2-6 per group) confirmed both tTA (A) and hTau (B) mRNA expression at these young ages and revealed no differences between the two lines. There was a trend indicating a steady rise in tTA mRNA as the mice get older (Two-way ANOVA: F (2, 18) = 3.24, p = 0.063). Forebrain protein analysis also confirmed hTau protein expression at these young ages (*n* = 2-6 per goup) and showed that by 7 weeks, there was still no difference hTau steady-state levels between the two lines or a change in levels over time (C). (D) Representative western blots for quantitative densitometry in panel *C.*

Developmental transgene suppression temporarily reduces NM hTau levels and phosphorylation

The predominance of 3R tau isoforms in the developing mouse brain (33) is essential for neurite polarity establishment (194) and neurite outgrowth (195,201). We therefore hypothesized that overexpression of 4R tau during a developmental period in which 3R normally predominates causes the abnormal molecular phenotype of NM hTau. We found that there was no effect of hTau expression on endogenous mouse tau (mTau) in postnatal mice at the mRNA level (Figure 25, Table 10). Still, overrepresentation of 4R hTau caused by overexpression could disrupt developmental processes, even in the presence of normal levels of 3R and 4R mTau isoforms. To determine whether the elevation in steady-state levels and hyperphosphorylation of NM compared to P301L hTau was due to overexpression during development, and whether pathogenicity of NM hTau is established during a specific developmental window, we suppressed hTau and tTA expression with DOX for either the first 4 or 12 weeks of life. Following suppression, mice were taken off of DOX chow for 4 or 8 weeks, and brain tissue was collected. Importantly, hTau expression and tTA toxicity in these models are intrinsically linked. Suppression of tTA during development prevents the observed reduction of dentate gyrus granule cells in that line (364), presumably by preventing off-target binding of the overexpressed tTA protein during this vulnerable period. However, we reiterate that this phenomenon is matched between rT1 and rT2.

Pilot experiments in rT2 mice showed that DOX suppresses hTau mRNA by 24 hours, and that hTau mRNA and protein return to normal levels following developmental suppression (Figure 26). Oddly, tTA mRNA expression following suppression surpassed normal levels, perhaps due to confounding effects of DOX on cell biology (408,409). Developmental suppression followed by 4 weeks of hTau and tTA expression lowered NM hTau levels ($F(2, 29) = 6.96$, $p = .0034$), pSer202 phosphorylation ($F(2,29) = 24.96$, $p < .0001$), and pSer396/404 phosphorylation ($F(2,29) = 9.45$, $p = .0007$), while suppression had no effect on P301L hTau biochemistry (Figure 27). There were also significantly higher levels of pSer202 phosphorylation of NM hTau than P301L hTau in non-suppressed control mice ($F(1, 29) = 46.96$, $p < .0001$) (Figure 27). After 8 weeks of post-suppression expression, there was no effect of suppression and no difference between rT1 and rT2 except for pSer202 phosphorylation, which remained reduced in suppressed mice ($F(2,29) = 8.88$, $p = .001$) and remained higher in rT1 than rT2 ($F(1,29)$

= 31.41, $p < .0001$). In conclusion, suppression of hTau and tTA for either 4 or 12 weeks reduced 4R NM hTau steady-state levels and phosphorylation to levels comparable to P301L hTau. However, these molecular phenotypes were partially or fully reversed after 8 weeks of expression, indicating that the effect of developmental transgene suppression on NM hTau regulation is only temporary.

Of note, we were not able to replicate differences in hTau steady-state levels (Figure 21) and pSer396/404 phosphorylation (Figure 23) in the 8-week old non-suppressed controls included in the DOX-suppression experiment (Figure 27). As these were different groups of mice, we attribute these observations to litter effects. However, the pSer202 observation remained quite robust in the suppression experiment (Figure 27), suggesting that this phosphorylation event occurs first and increases propensity for phosphorylation at pSer396 and pSer404 (253,254), leading to elevated stability (410,411). Our observations indicate that the timing of these events is highly variable in different litters of mice, and took longer in the mice included in the suppression experiment.

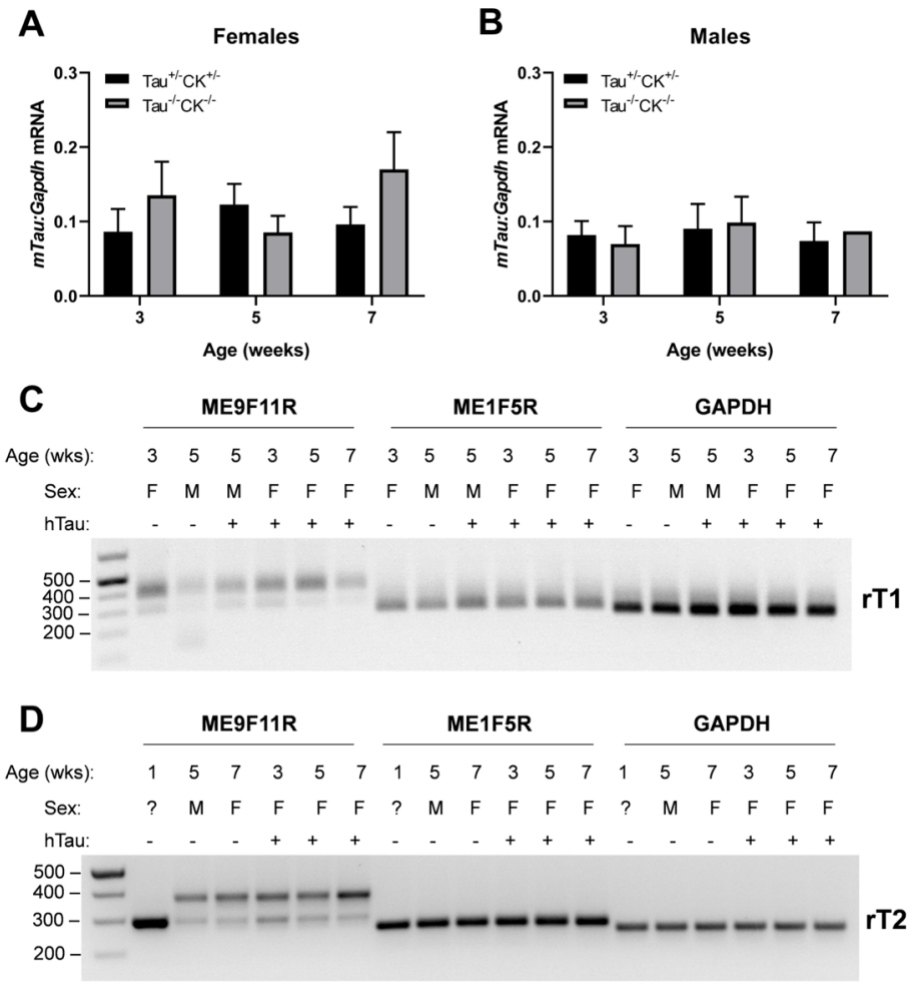

Figure 25. No effect of hTau expression on endogenous mTau mRNA. Forebrain mRNA analysis of endogenous mTau expression was performed in 3- , 5- , and 7- week old rT1 and rT2 mice (*n* = 2-6 per group). While, there was no difference between rT1 and rT2, we detected an effect of sex ($t(36) = 2.59$, $p = .014$) in that females expressed more mTau mRNA than males. Overall there was no effect of age or genotype for either females (A) or males (B) indicating that hTau expression does not affect mTau mRNA expression. To assess mTau splice variants individually in a qualitative manner, PCR was run on cDNA from rT1 and rT2 forebrains using forward (F) and reverse (R) primers flanking alternatively spliced mouse exon (ME) 10 (ME9F11R), flanking alternatively spliced exons 2, 3, and 4 (ME1F5R), or for total *Gapdh* as a control (412). This showed no obvious differences in relative levels of mTau splice variant mRNA expression in postnatal rT1 (C) or rT2 (D) whether or not hTau was being expressed. Note that for ME9F11R reactions, the 297 base-pair (bp) product is 3R (exon 10-) while the 390bp product is 4R (exon 10+) mTau. For ME1F5R reactions, the 260bp product is 1N mTau (exon 4+, exon 2- and exon 3-). PCR products were sequenced to confirm the correct splice variants.

Table 10. Primer sequences used for relative RT-qPCR and PCR experiments. Forward and reverse primers used to quantify *hTau* and *Hprt* mRNA in qPCR experiments are shown. Mouse exon (ME) forward (F) reverse (R)

Target	**Primers**	
	Forward	Reverse
hTau	5'- CTACACCATGCACCAAGACC -3'	5'- TGCTTTTACTGACCATGCGA -3'
tTA	5'- ACTACTGATAGTATGCCGCCATT -3'	5'- CAGGCCCTCGATGGTAGA -3'
Hprt	5'- GCTGGTGAAAAGGACCTCT -3'	5'- CCACAGGACTAGAACACCTGCTA -3'
Gapdh	5'- TGTCAGCAATGCATCCTGCA -3'	5'- CCGTTCAGCTCTGGGATGAC -3'
ME9F11R	5'- CACCAAAATCCGGAGAACGA -3'	5'- CTTTGCTCAGGTCCACCGGC -3'
ME1F5R	5'- TCCGCTGTCCTCTTCTGTC -3'	5'- TTCTCGTCATTTCCTGTCC -3'
XBP1	5'- GAACCAGGAGTTAAGAACACG -3'	5'- AGGCAACAGTGTCAGAGTCC -3'

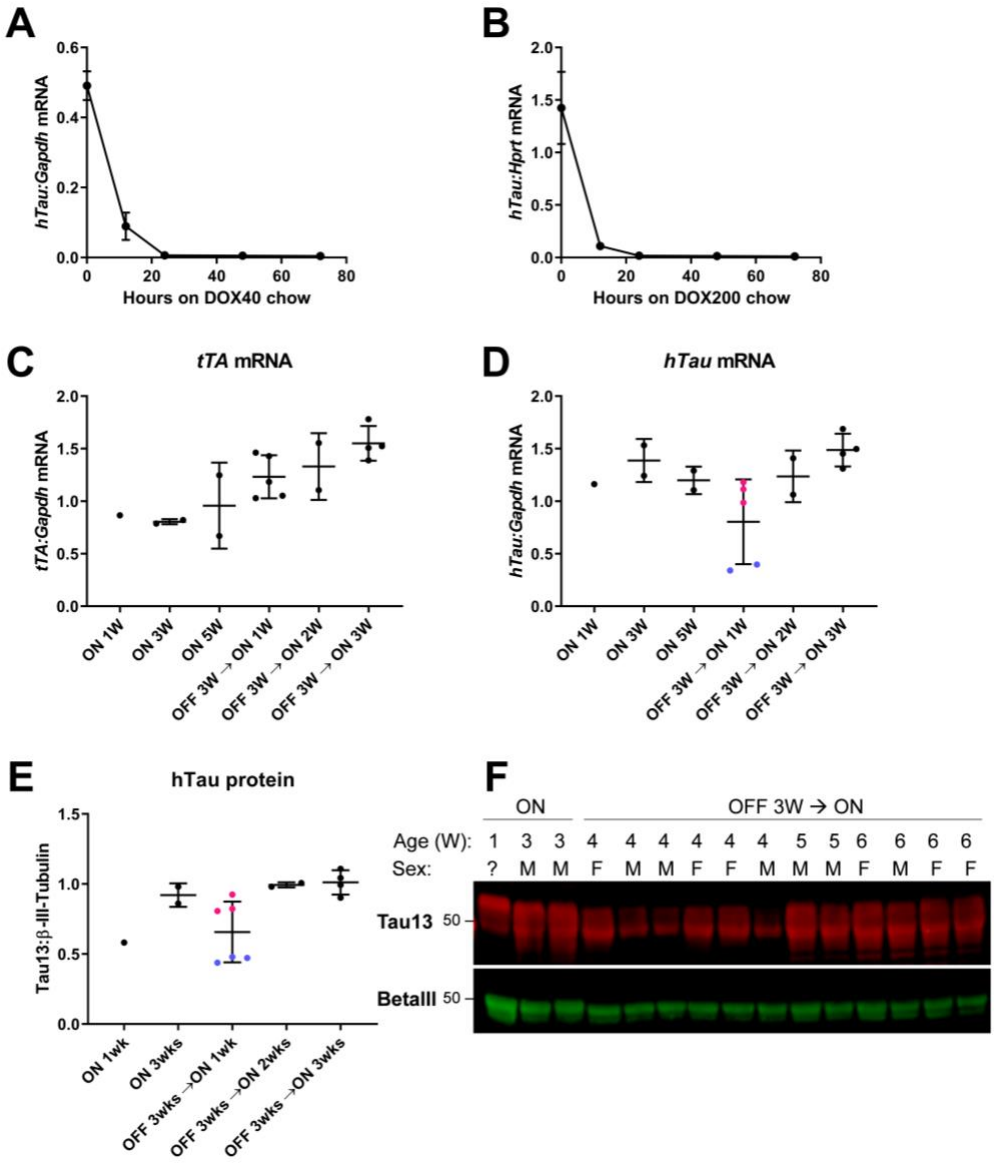

Figure 26. DOX pilot experiments in rT2 mice for hTau half-life and developmental suppression experiments. Forebrain mRNA analyses showed that DOX 40mg/kg (A) and DOX 200mg/kg (B) diets fully suppressed hTau expression by 24 hours after administration (*n* = 2-4 per group). Further forebrain mRNA analyses showed that with 3 weeks of developmental suppression using DOX40, tTA expression steadily rises and surpasses that of mice that have not been suppressed (C). After developmental suppression with DOX40, hTau mRNA in the forebrain returns to levels comparable to those of non-suppressed mice (D). Similarly, hTau protein returns to normal levels after developmental DOX40 treatment (E). (F) Representative western blot densitometrically quantified in panel *E.* Interestingly, after 1 week of post-suppression expression, hTau expression in females (pink dots) is higher than that of males (blue dots) in terms of both mRNA (D) and protein (E-F).

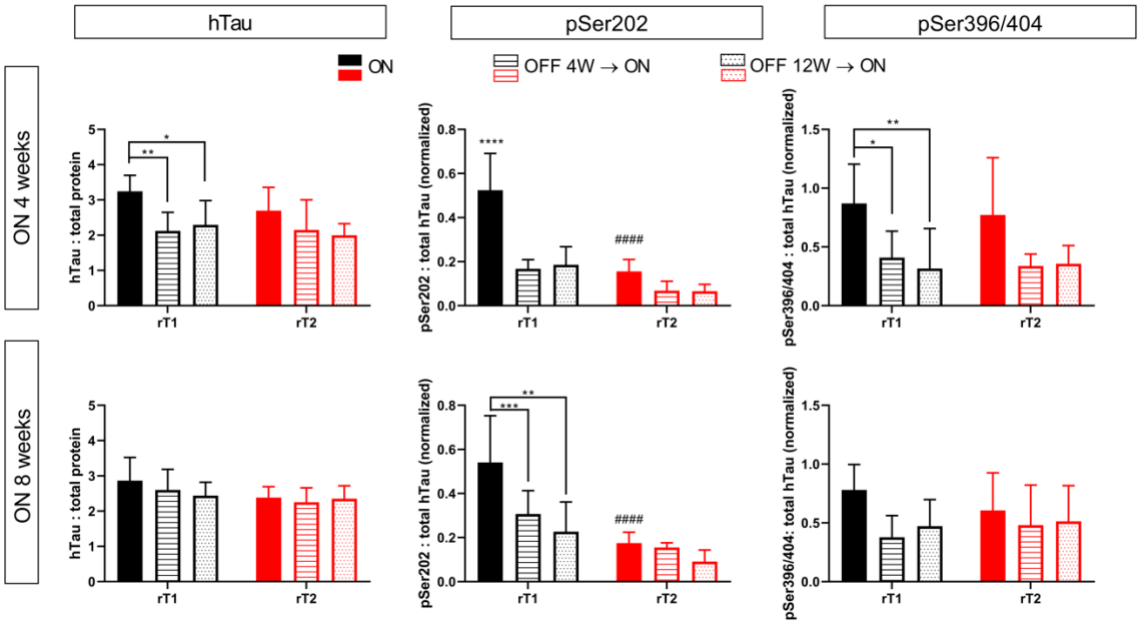

Figure 27. Developmental suppression temporarily reduces 4R NM hTau levels and phosphorylation in rT1 forebrains. Quantitative data from densitometry of western blots for human tau normalized to total protein, and phospho-hTau at pSer202 and pSer396/404 normalized to total protein, represented as ratios to normalized total hTau levels (phospho-hTau:total protein::hTau:total protein). hTau was suppressed for either the first 4 weeks (OFF 4W → ON) or 12 weeks (OFF 12W → ON) of life followed by expression for 4 (top row) or 8 (bottom row) weeks. Non-suppressed controls aged 4 or 8 weeks (ON) are included to match the expression period of suppressed mice. *n* = 5-6 per group. " * " symbols indicate effect of DOX treatment while " # " symbols indicate differences between rT1 and rT2. Graphs display group means + SD. *p<0.05, **p<0.01, ***p<0.001, **** or #### p<0.0001.

rT1 but not rT2 mice exhibit cognitive impairments

Behavioral studies to assess cognition in these lines were conducted before we were aware of the abnormal molecular phenotype of 4R NM hTau. Therefore, we originally predicted that the P301L mutation would be associated with spatial learning and memory deficits in the Morris Water Maze in 5-month old rT2 mice. Non-transgenic littermates were used as internal controls for 'batch effects' such as effects of season, times of day and week, and animal husbandry schedules in these experiments. However, cognitive phenotypes in rT1 and rT2 should be considered in relation to one another rather than to non-transgenic animals, which lack both hTau and tTA transgenes.

Both rT1 (main effect of Day: $F(4, 88) = 35.80$, $p<.0001$) and rT2 (main effect of Day: $F(4, 88) = 43.76$, $p<.0001$) path lengths to the visible platform were significantly reduced as training progressed, indicating sensorimotor acquisition of the task in both lines (Figure 28A). Path lengths to the hidden platform also decreased as training progressed for both rT1 (main effect of Day: $F(3, 66) = 7.521$, $p=.0002$) and rT2 (main effect of Day: $F(3, 66) = 9.752$, $p<.0001$), indicating improvements in spatial navigation (Figure 28B). However, when compared to non-transgenic littermates, we were surprised to find that 5-month old rT1 but not rT2 mice exhibited learning deficits during visible-platform training (main effect of Genotype: $F(1, 22) = 18.46$, $p = .0003$) and hidden-platform training (main effect of Genotype: $F(1, 22) = 23.76$, $p < .0001$) (Figure 28A, B).

rT1 mice also exhibited deficits in spatial reference memory during probe trials. Search bias was detected in $Tau^{-/-}tTA^{-/-}$ mice ($F(3,44) =15.79$, $p<.0001$) but not in $Tau^{+/-}tTA^{+/-}$ rT1 mice ($F(3,44) =3.72$, $p=.018$) (Figure 28C). In addition, $Tau^{+/-}tTA^{+/-}$ rT1 mice spent significantly less time in the target quadrant than non-transgenic littermates ($U = 8$, $p < .0001$) (Figure 28C). This indicates either a pure learning deficit or a combined learning and spatial memory deficit in rT1 mice, associated with the abnormal molecular phenotype of 4R NM hTau. In contrast, 5-month old rT2 mice exhibited no such deficits (Figure 28D, E, F), suggesting that the low levels of P301L hTau phosphorylation at this age are insufficient to cause cognitive deficits in rT2.

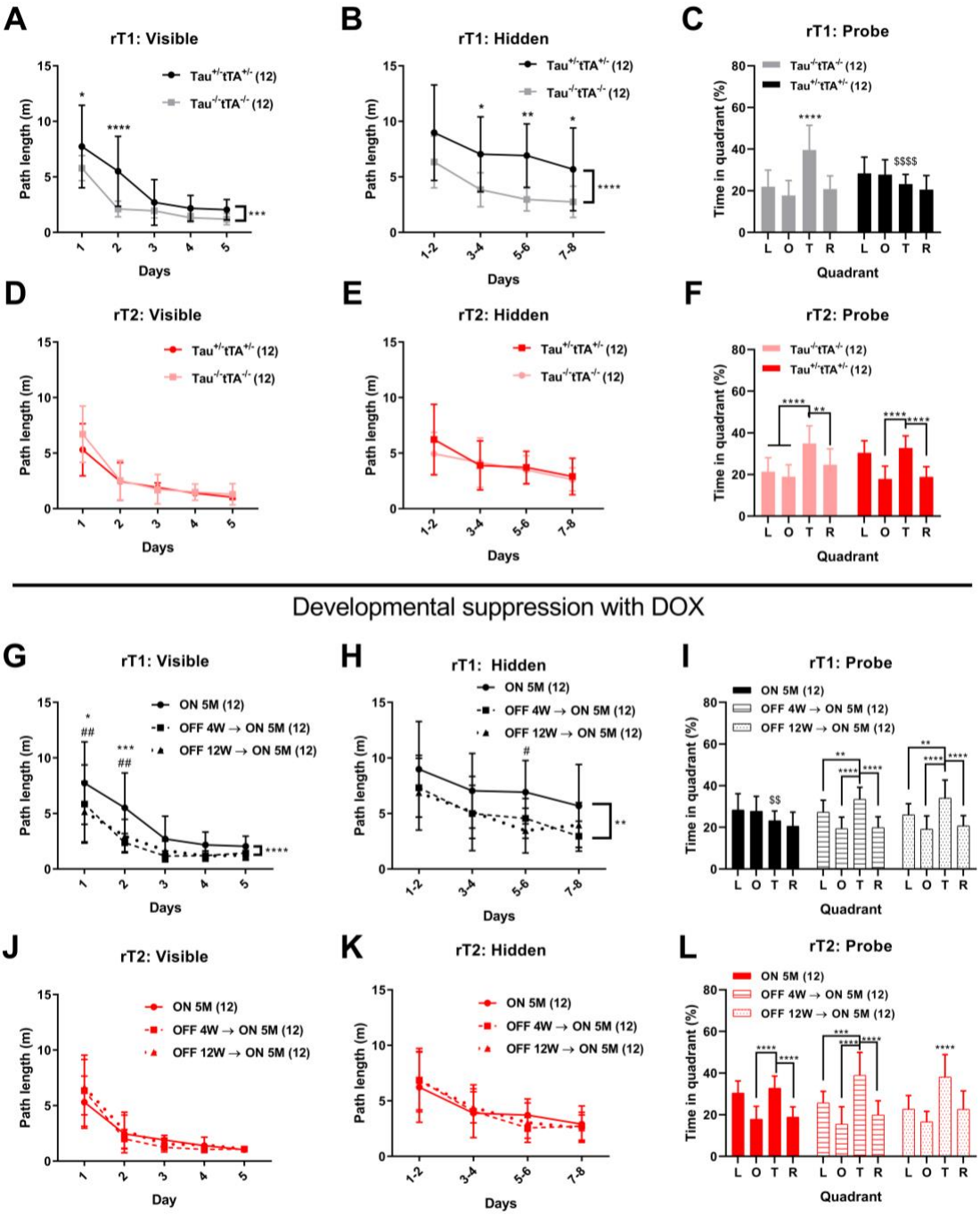
A
rT1: Visible
Tau+/-tTA+/- (12)
Tau-/-tTA-/- (12)
Path length (m)
Days
B
rT1: Hidden
C
rT1: Probe
Time in quadrant (%)
Quadrant
L O T R
D
rT2: Visible
E
rT2: Hidden
F
rT2: Probe
Developmental suppression with DOX
G
rT1: Visible
ON 5M (12)
OFF 4W → ON 5M (12)
OFF 12W → ON 5M (12)
H
rT1: Hidden
I
rT1: Probe
J
rT2: Visible
Day
K
rT2: Hidden
L
rT2: Probe

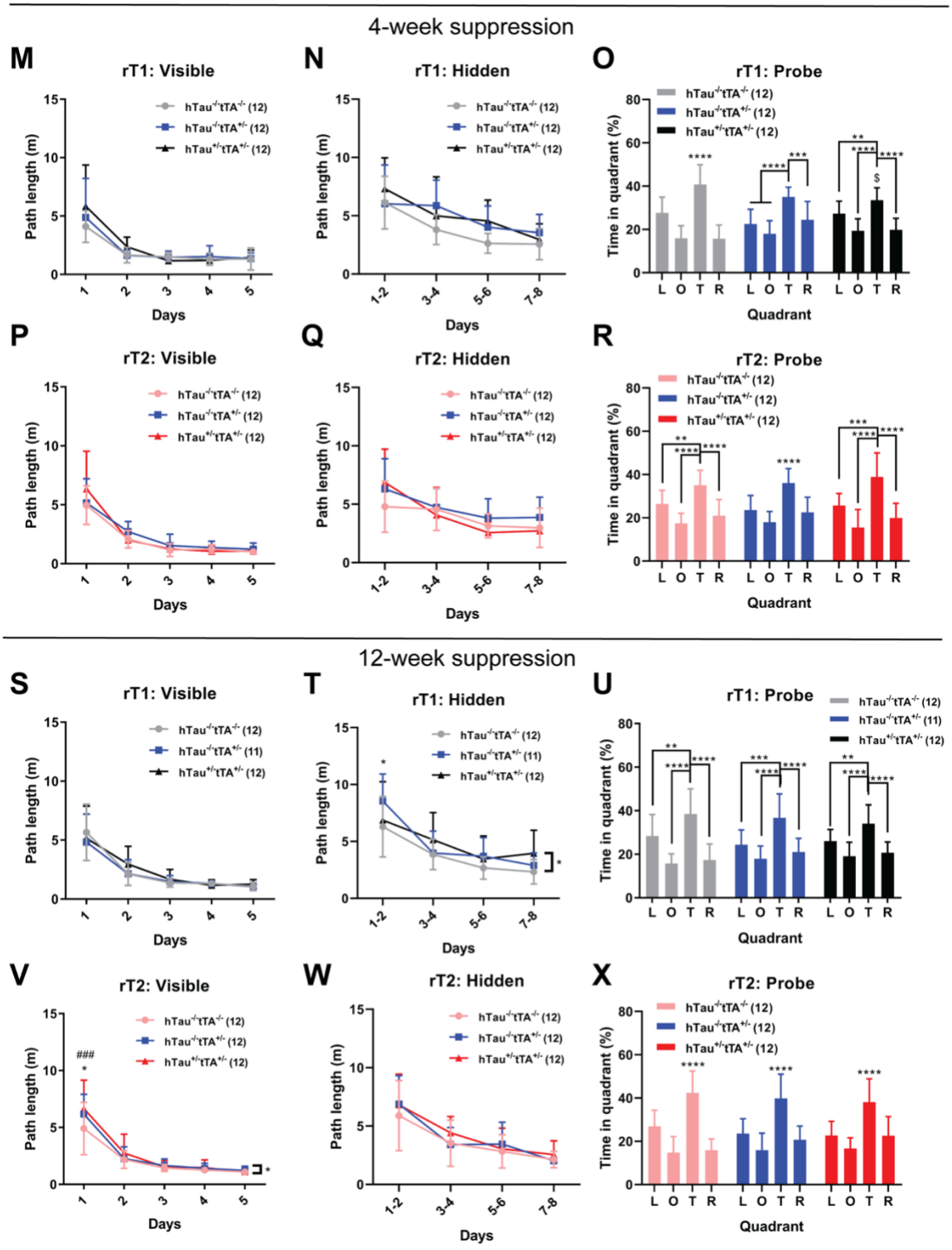

Figure 28. Cognitive deficits in rT1 are prevented with developmental suppression. The Morris water maze was used to measure cognitive function in rT1 and rT2 mice. 5-month old rT1 mice exhibit learning deficits in visible-platform training (A), in hidden-platform training (B), and in

spatial reference memory during probe trials (C). Probe trial data shows time spent in left (L), opposite (O), target (T), and right (R) quadrants to assess search bias. (D-F) Five-month old rT2 mice are indistinguishable from non-transgenic littermates in all trials. With doxycycline-mediated suppression of hTau during the first 4 weeks or 12 weeks of life, followed by hTau expression for 5 months, (OFF 4W → ON 5M and OFF 12W → ON 5M, respectively) rT1 performance improves in all aspects of the task when compared to 5-month old animals (ON 5M) (G-I). " * " indicates differences between ON 5M and OFF 4W groups while " # " indicates differences between ON 5M and OFF 12W groups (G, H). DOX treatment had no effect on rT2 cognition (J-L). rT1 and rT2 performance was comparable to $hTau^{-/-}tTA^{-/-}$ and $hTau^{-/-}tTA^{+/-}$ littermate controls with both 4 weeks (M-R) and 12 weeks (S-X) of suppression. " * " indicates differences between $hTau^{-/-}tTA^{-/-}$ and $hTau^{-/-}tTA^{+/-}$ while " # " indicates differences between $hTau^{-/-}tTA^{-/-}$ and $hTau^{+/-}tTA^{+/-}$ (T,V). For all probe data, " * " indicates tests for search bias while " $ " indicates differences in time spent in target quadrant (T) between groups. *n*'s for each group in parentheses. Graphs display group means ± SD. All probe data represent the average values for three probe trials. Symbols to right of Visible and Hidden graphs indicate main effect of Genotype (A-F, M-X) or DOX treatment (G-L). *, #, or $ $p<0.05$; ** or ## $p<0.01$; *** or ### $p<0.001$; $$$ or ****$p<0.0001$

Developmental transgene suppression prevents cognitive impairments in rT1

Developmental transgene suppression temporarily reduced 4R NM hTau steady-state levels and phosphorylation levels compared to P301L hTau (see Figure 27). To determine whether developmental suppression also prevents the cognitive deficits in rT1 mice, and whether pathogenicity is established during a specific developmental window, we again suppressed hTau and tTA expression with DOX for either the first 4 or 12 weeks of life. Following developmental suppression, hTau and tTA were expressed for 5 months so as to match the expression period of impaired rT1 mice. Data from non-suppressed mice are included for comparison, and therefore the same data from $hTau^{+/-}$ $tTA^{+/-}$ mice in Figure 28A-F are included in Figure 28G-L and 28M-X.

Both 4 weeks and 12 weeks of suppression prevented rT1 impairments in visible-platform training ($F(2, 33) = 12.9$, $p < .0001$) and hidden-platform training ($F(2, 33) = 6.89$, $p = .0032$) compared to non-suppressed rT1 mice (Figure 28G, H). Developmental suppression of hTau also improved spatial reference memory in probe trials. Search bias was detected in both the 4-week suppression ($F(3,44) = 18.45$, $p<.0001$) and 12-week suppression ($F(3,44)=15.33$, $p<.0001$) groups (Figure 28I). In addition, suppressed rT1 spent significantly more time in the target quadrant than non-suppressed mice ($F(2, 33) = 10.37$, $p = .0003$). In contrast, suppression of hTau and tTA had no effect on rT2 cognition (Figure 28J, K, L).

Suppressed rT1 and rT2 mice were also compared to $hTau^{-/-}tTA^{-/-}$ and $hTau^{-/-}$ $tTA^{+/-}$ littermates. In the 4-week suppression group, rT1 mice improved as visible training ($F(4, 132)=46.8$, $p<.0001$) and hidden training ($F(3, 99=21$, $p<.0001$) progressed, and no differences were detected between genotypes (Figure 28M, N). All rT1 genotypes exhibited search bias in probe trials: $hTau^{-/-}tTA^{-/-}$ ($F(3,44)=32.41$, $p<.0001$), $hTau^{-/-}tTA^{+/-}$ ($F(3,44)=14.43$, $p<.0001$), and $hTau^{+/-}tTA^{+/-}$ ($F(3,44)=17.6$, $p<.0001$) (Figure 28O). rT1 $hTau^{+/-}tTA^{+/-}$ spent less time in the target quadrant than $hTau^{-/-}tTA^{-/-}$ mice ($F(2,33)=3.89$, $p<.031$), but were comparable to $hTau^{-/-}tTA^{+/-}$ littermates (Figure 28O). With 4 weeks of suppression, all rT2 genotypes also improved during visible ($F(4,132)=87.15$, $p<.0001$) and hidden ($F(3,99)=18.28$, $p<.0001$) training with no differences between genotypes (Figure 28P, Q). All rT2 genotypes also exhibited search bias in probe trials: $hTau^{-/-}tTA^{-/-}$ ($F(3,44)=17.41$, $p<.0001$), $hTau^{-/-}tTA^{+/-}$ ($F(3,44)=17.45$, $p<.0001$), and $hTau^{+/-}tTA^{+/-}$ ($F(3,44)=18.45$, $p<.0001$) (Figure 28R). There was no difference in time spent in the target quadrant between rT2 genotypes (Figure 28R).

In the 12-week suppression group, rT1 performance was comparable to $hTau^{-/-}tTA^{-/-}$ and $hTau^{-/-}tTA^{+/-}$ littermates in visible ($F(4,128)=57.19$, $p<.0001$) and hidden ($F(3,96)=32.32$, $p<.0001$) training (Figure 28S, T). A main effect of genotype ($F(2,32)=3.66$, $p=0.037$) in hidden training arose due to slight differences on Day 1 (Figure 28T). All rT1 genotypes exhibited search bias in probe trials: $hTau^{-/-}tTA^{-/-}$ ($F(3,44)=17.71$, $p<.0001$), $hTau^{-/-}tTA^{+/-}$ ($F(3,44)=12.35$, $p<.0001$), and $hTau^{+/-}tTA^{+/-}$ ($F(3,44)=12.94$, $p<.0001$) (Figure 28W). No differences between rT1 genotypes were detected in terms of time spend in the target quadrant (Figure 28W). rT2 mice suppressed for 12 weeks also improved as visible ($F(4,132)=100.9$, $p<.0001$) and hidden ($F(3,99)=33.3$, $p<.0001$) training progressed (Figure 28V, W). A main effect of genotype ($F(2,33)=3.29$, $p=0.050$) arose due to slight differences between genotypes on Day 1 of visible training (Figure 28V). All rT2 genotypes also exhibited search bias in probe trials: $hTau^{-/-}tTA^{-/-}$ ($F(3,44)=33.1$, $p<.0001$), $hTau^{-/-}tTA^{+/-}$ ($F(3,44)=18.82$, $p<.0001$), and $hTau^{+/-}tTA^{+/-}$ ($F(3,44)=15.33$, $p<.0001$) (Figure 28X). There was no difference in time spent in the target quadrant between rT2 genotypes (Figure 28X). Taken together, these data show that developmental transgene suppression prevented the cognitive impairments in rT1 mice.

Higher ratios of microtubule-bound to –unbound 4R NM hTau than P301L hTau

If developmental overexpression of 4R tau is toxic, why are abnormal molecular phenotypes and cognitive dysfunction present only in rT1 mice and not also rT2? A major consequence of the P301L mutation, which lies in tau's second microtubule (MT) binding domain encoded by the alternatively spliced exon 10, is a reduction in the ability of tau to bind MTs (34). We hypothesized that this loss of function conferred by the pathogenic P301L mutation is protective against molecular and cognitive phenotypes associated with 4R NM hTau.

To quantify MT -bound vs. -unbound hTau in 8-week old rT1 and rT2, we isolated microtubules (MTs) and microtubule-associated proteins, MAPs, (290) from forebrains (Figure 29A). P301L hTau was found to be more abundant in the cytosol ($t(12) = 5.60$, $p = 0.0001$) while NM hTau was more abundant in the MT/MAP pellet ($t(12) = 5.21$, $p = 0.0002$) (Figure 29B, C). The mean ratios of MT -bound to -unbound hTau were 1.46 for NM and 0.70 for P301L hTau, demonstrating that 4R NM hTau binds MTs significantly

stronger than P301L hTau. This also suggests that reduced MT-binding of P301L hTau protects against abnormal molecular and cognitive phenotypes.

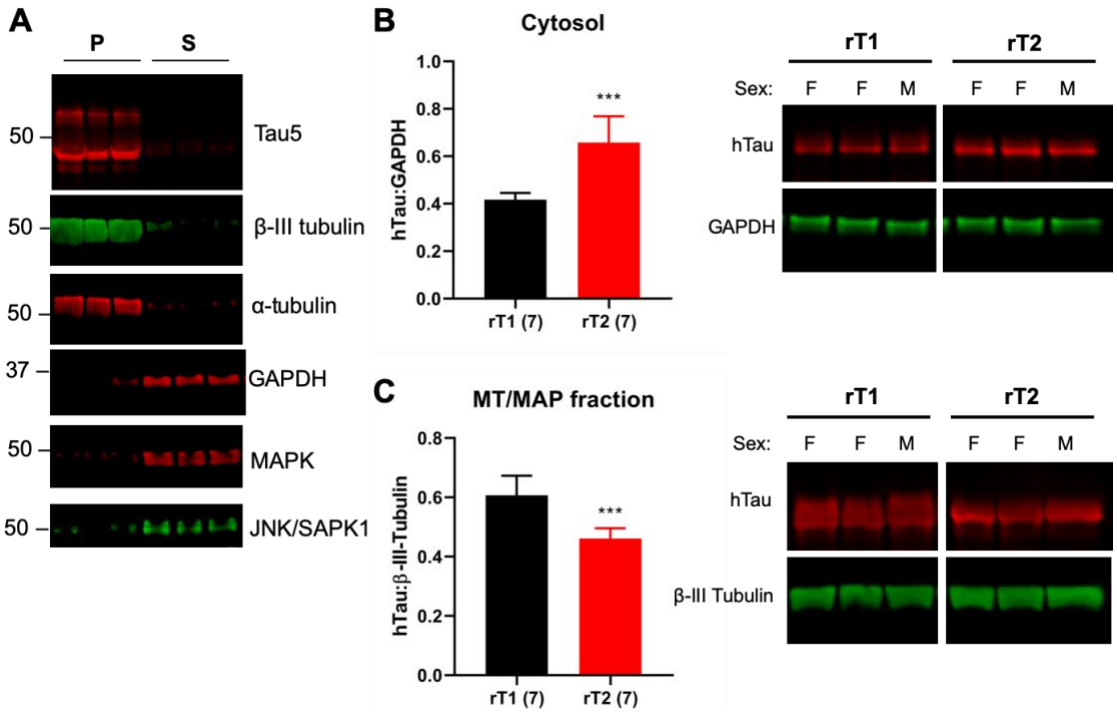

Figure 29. 4R NM hTau binds microtubules more strongly than P301L hTau. (A) Validation of protocol to isolate microtubules (MTs) and microtubule-associated proteins (290) in the pellet (P), leaving cytosolic elements in the supernatant (S). The cytosolic fractions (B) and MT/MAP fractions (C) were run through SDS-PAGE and immunolabled with hTau, GAPDH, and β-III tubulin antibodies (representative images in right panels). Proteins were run on 10.5-14% gels. Fluorescent signal from western blots was quantified by densitometry, and values represent averages of two separate experiments (left panels). Graphs show group means + SD with *n*'s indicated in parentheses. ***p<0.001

Mitochondrial abnormalities and oxidative stress in rT1

Overexpression of tau is known to cause a disruption of mitochondrial fission and fusion dynamics (413), which contributes to neurodevelopmental disorders (414). Therefore, we examined mitochondrial length in primary hippocampal neurons derived from P0 rT1 and rT2 mice. Active hTau expression was confirmed in our cultures (data not shown), which were transfected with an EGFP construct to identify axons and a mitochondria-specific RFP construct to visualize mitochondria within the axon, as done previously (404). We found that while there was no difference in mitochondria density (Figure 30B), mitochondria were longer in axons from rT1 ($hTau^{+/-}tTA^{+/-}$) than from control ($hTau^{+/-}tTA^{-/-}$) neurons (H = 10.9, p = 0.012) whereas there was no difference in mitochondrial length between rT2 and control neurons (Figure 30A, C). We also observed no differences in the percentages of moving mitochondria or the velocity of mobile mitochondria between groups (data not shown). Although we did not observe effects on mitochondrial transport, these findings are consistent with developmental pathogenicity of 4R NM hTau, and further suggest that impaired mitochondrial dynamics are part of that pathogenic pathway.

Disruptions in mitochondrial dynamics have been shown to be linked to oxidative stress (415). Therefore, we assessed oxidative damage to DNA and RNA using the marker 8-hydroxy-2'-deoxyguanosine (8OHdG) in 2-month old rT1, rT2, and littermate controls. We found that 8OHdG staining was more intense in rT1 than for other samples (Figure 31A). We also quantified the signal intensity and found that, indeed, oxidative stress was higher in rT1 than rT2 in the CA1 region of the hippocampus ($F(1,30) = 29.38$, $p<.0001$) and in cortex (Ctx) ($F(1,30) = 11.11$, $p=.0023$) (Figure 31B, C). Interestingly, oxidative stress in the dentate gyrus (DG) was highest in non-transgenic littermates ($F(2,30) = 16.93$, $p<.0001$) (Figure 31D), which may be explained by a requirement for high levels of reactive oxygen species in the regulation of adult neurogenesis (416,417). This suggests that tTA and hTau expression may contribute to redox imbalance in the DG, which could have consequences for adult neurogenesis and therefore cognition. We note that the 8OHdG signal may represent not only nuclear and mitochondrial DNA, but also RNA.

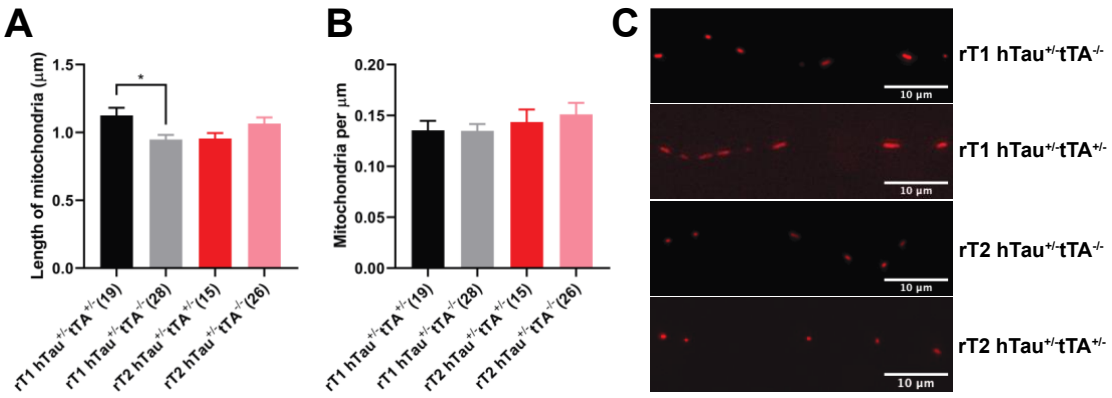

Figure 30. Elongated mitochondria with no change in density in rT1 hippocampal axons. The length of mitochondria (A) and density of mitochondria (B) were measured in primary hippocampal neurons derived from rT1 and rT2 postnatal day 0 pups. hTau-only ($hTau^{+/-}tTA^{-/-}$) controls were included for comparison. The number of axons in which mitochondria were counted and measured are shown in parenthesis for each group. Neurons were taken from a total of 10 rT1 $hTau^{+/-}tTA^{+/-}$, 7 rT1 $hTau^{+/-}tTA^{-/-}$, 7 rT2 $hTau^{+/-}tTA^{+/-}$, and 4 rT2 $hTau^{+/-}tTA^{-/-}$ mice. (C) Representative images of axonal mitochondria in hippocampal neurons. Graphs display group means + SEM. *p<0.05

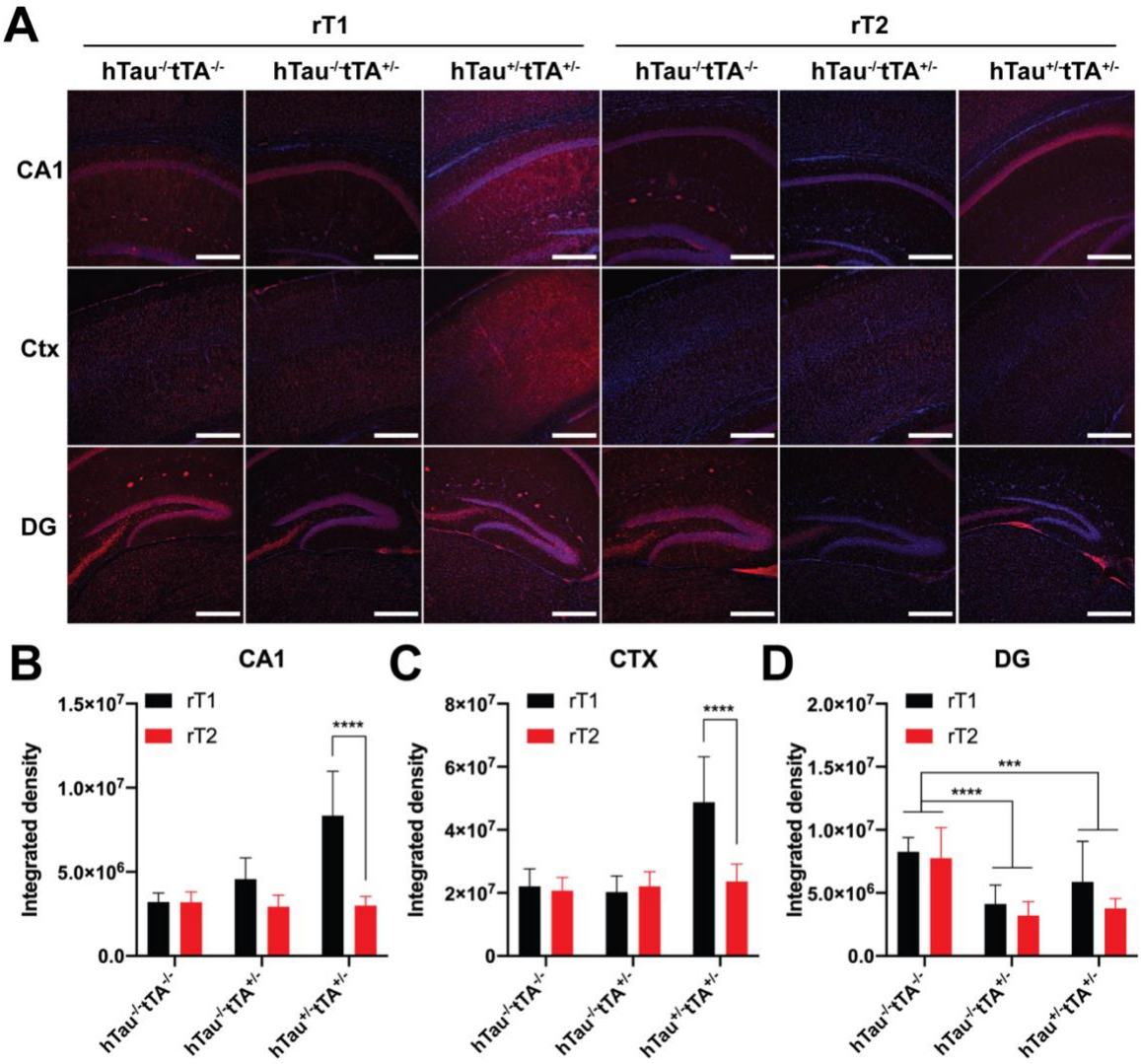

Figure 31. Elevated oxidative stress in 2-month rT1 brains. (A) Representative images showing 8-hydroxy-2'-deoxyguanosine (8OHdG, red), a marker for oxidative damage to DNA and RNA, in 2-month old rT1 and rT2 animals in addition to hTau$^{-/-}$tTA$^{-/-}$ and hTau$^{-/-}$tTA$^{+/-}$ littermate controls. Images are shown for the three areas assessed: hippocampal CA1, somatomotor areas of cortex (Ctx) and dentate gyrus (DG). DAPI is shown in blue. (B-D) Quantification of intensity of the red signal in terms of integrated density to account for differences in region of interest (ROI) areas. *n* = 3 males and 3 females per group. Graphs show group means + SD. Scale bars represent 500 μm. ***p<0.001, ****p<0.0001

Reduced brain mass in postnatal rT1 mice

Knowing that aberrantly elongated mitochondria in neurodevelopmental disorders are accompanied by microcephaly (414), and that an excess of tau interferes with cell division, leading to aneuploidy and neuronal apoptosis (418,419), we postulated that rT1 mice may have abnormal brain development. To test this, we simply weighed whole brains and compared brain mass of rT1, rT2, and littermates.

Our analysis of brain mass showed that rT1, rT2, and tTA mice had reduced brain mass compared to $hTau^{-/-}tTA^{-/-}$ and $hTau^{+/-}tTA^{-/-}$ controls ($F(3, 251) = 45.15$, $p < .0001$), and that rT1 mice had reduced brain mass compared to rT2 ($F(1, 251) = 19.27$, $p < .0001$; rT1 mean = .429g, SD = 0.018; rT2 mean = 0.443g, SD = 0.021) (Figure 32A). Despite the contribution of tTA-induced toxicity, 4R NM hTau was associated with reduced brain mass compared to P301L hTau. This suggests that tTA interferes with normal brain development and that P301L hTau is protective from tTA toxicity, while NM hTau is not. In addition, 4 weeks and, to a greater extent, 12 weeks of developmental suppression of hTau and tTA was associated with increases in brain mass in rT1 ($F(2, 46) = 17.67$, $p < .0001$), but had no effect on brain mass in rT2 mice (Figure 32B). Although we cannot exclude the possibility that the subtle difference in brain mass could be due to background strain variation in the breeding history of rT1 and rT2, the effect of developmental suppression was specific to rT1, suggesting that 4R NM hTau and tTA overexpression during postnatal development is associated with reduced brain size.

Finally, as forebrain neurons are overexpressing high levels of hTau, we hypothesized that endoplasmic reticulum (ER) stress may be occurring in rT1 and rT2 brains. We found no evidence of activation of the unfolded protein response (UPR), which occurs downstream of ER stress (Figure 33). This indicates that oxidative stress but not ER stress is ongoing in more so in rT1 than rT2 brains.

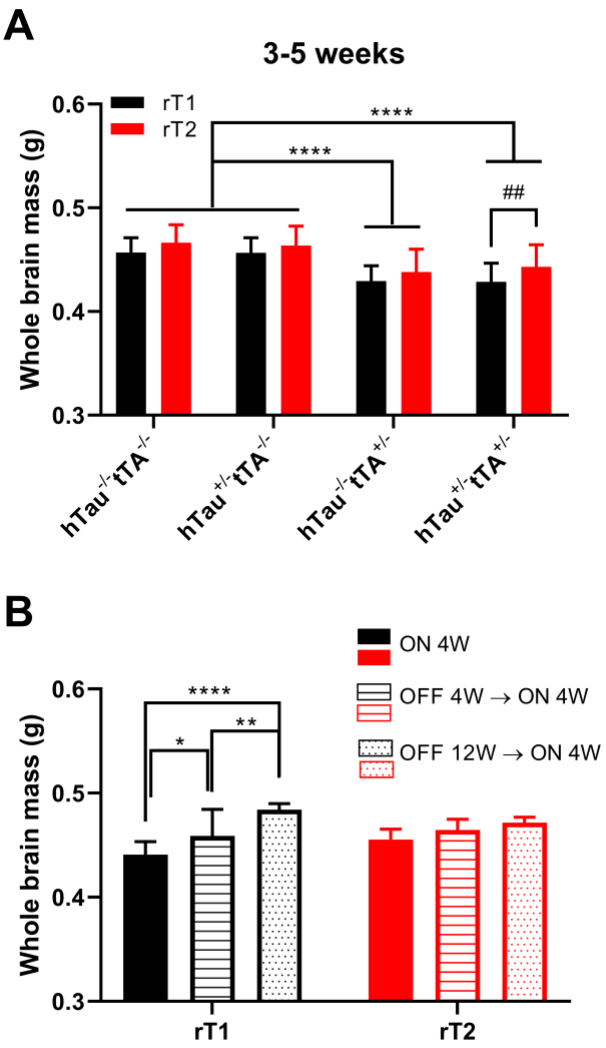

Figure 32. Reduced brain mass in postnatal rT1 mice. (A) Whole brains from rT1, rT2, and littermates between the ages of 3 and 5 weeks were weighed (rT1: *n* = 27 $hTau^{-/-}tTA^{-/-}$, 35 $hTau^{+/-}tTA^{-/-}$, 28 $hTau^{-/-}tTA^{+/-}$, and 33 $hTau^{+/-}tTA^{+/-}$; rT2: *n* = 33 $hTau^{-/-}tTA^{-/-}$, 33 $hTau^{+/-}tTA^{-/-}$, 36 $hTau^{-/-}tTA^{+/-}$, and 34 $hTau^{+/-}tTA^{+/-}$). " * " indicates differences between genotypes while " # " indicates differences between lines. (B) Brain mass was compared between 3 groups of $Tau^{+/-}tTA^{+/-}$ rT1 and rT2: 4 week-old animals (ON 4W, *n* = 12 rT1 and 7 rT2), hTau suppressed for 4 weeks followed by expression for 4 weeks (OFF 4W → ON 4W, *n* = 9 rT1 and 10 rT2), and 12 weeks of suppression followed by 4 weeks of expression (OFF 12W → ON 4W, *n* = 6 rT1 and 8 rT2). Graphs display group means + SD. *p<0.05, ** or ## p<0.01, ****p<0.0001.

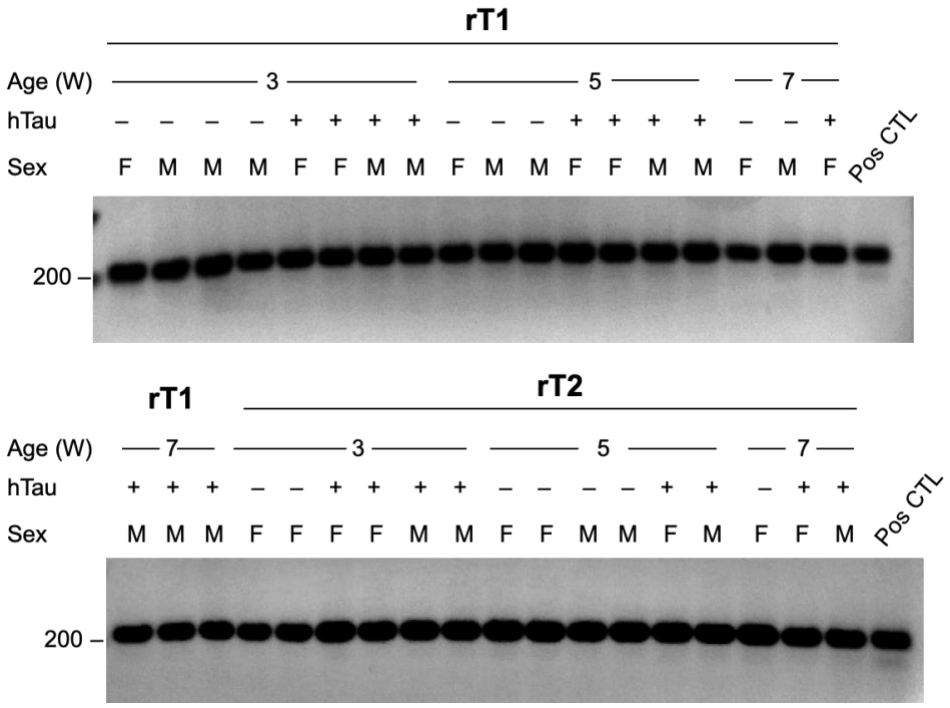

Figure 33. No evidence of ER stress in rT1 or rT2 brains. An *X-box binding protein 1* (*Xbp1*) splicing assay was run on cDNA from postnatal rT1 and rT2 forebrains. The presence of a faint lower band indicates mRNA processing of XBP1 by Inositol-requiring enzyme 1 (IRE1) to a shorter splice variant, which is indicates activation of the unfolded protein response (UPR). The short splice variant was detected in a positive control sample (medulloblastoma) but not in rT1 or rT2, regardless of hTau expression.

IV. Discussion

The 30 different tauopathy mouse models harboring *MAPT*-related modifications (https://www.alzforum.org/research-models) have extreme variability in their phenotypes, creating confusion in attempts to understand how the tau protein causes neurodegenerative diseases. Using novel genetically matched mouse lines, we sought to determine how the pathogenic P301L mutation affects tau biology *in vivo*. Surprisingly, we have identified a development-specific toxicity of 4R NM hTau, which undergoes abnormal regulation in very young animals and eventually causes cognitive impairments. Strikingly, both the molecular and behavioral phenotypes associated with 4R NM hTau were lost with the P301L mutation.

We found that clearance of hTau was impaired in rT1 mice, underlying an elevation of steady-state levels. The half-life of 4R NM hTau was significantly longer than P301L hTau (Figure 22, Table 9), and is comparable to a different tauopathy mouse model (401). The hyperphosphorylation of NM hTau (Figure 23) may explain its long half-life because phosphorylation of Ser396 and Ser404, elevated in rT1 mice, has been associated with impaired proteasome function (410,411). The robust pSer202 phosphorylation of NM hTau (Figures 23 and 27) may be particularly important for regulating tau dynamics because this event primes tau for Ser396/404 phosphorylation (253,254), which could ultimately lead to elevated stability due to proteasome inhibition.

Patterns of tau phosphorylation during normal rodent development suggest that NM hTau remains aberrantly hyperphosphorylated. Many sites on tau, including Ser202 and Ser404, are highly phosphorylated early on and slowly decline thereafter (250). P301L hTau in rT2 mice follows this normal developmental pattern, however, by 4-5 weeks of age 4R NM hTau remains hyperphosphorylated (Figures 23 and 27), strongly suggesting developmental dysregulation of hTau in rT1 brains. These findings parallel those of other transgenic lines in which developmental mislocalization (383) and hyperphosphorylation (385,393,394) of overexpressed NM hTau is observed. In particular, a non-progressive developmental phenotype associated with NM but not P301L hTau was previously published (173), suggesting a similar pathogenic process occurs in rT1 and rTg21221 (rTgWT) lines. We previously found that the level of hTau overexpression in P301L 0N4R transgenic lines positively correlates with the degree of hTau histopathology (hTau -hemizygous rT2 vs. -homozygous rT2/T2) (396). Similarly, our current results show elevated tau phosphorylation in rT1, which overexpress hTau

by about two-fold compared to rT2 (Figure 21E). Future studies on tau histopathology in young rT1 and rT2 will clarify whether the level of hTau overexpression, regardless of any disease-linked mutations, is the determining factor in the severity of histopathology.

The rise in 4R NM hTau levels in rT1 brains, in addition to the 12.6-fold overexpression of human relative to endogenous mouse tau, causes massive overrepresentation of 4R tau isoforms. Compounding this, although we detected normal levels of mTau mRNA (Figure 25), our collaborator has found severe downregulation of 3R mTau protein in rT1 and rT2 compared to tTA mice (M. Orr, personal communication). Most *MAPT* mutations that alter splicing in human tauopathies increase the 4R:3R ratio (14) (Table 1), leading 4R tau to be labeled as a toxic variant (420). Therefore, it is no surprise that 4R NM hTau exhibits an abnormal molecular phenotype, especially when considering the importance of splice variant regulation during development. In both rodent (33) and human (32) fetal brain, 3R tau is much more abundant than 4R tau. With a three-fold lower MT-binding capacity than 4R tau (196), 3R tau facilitates MT dynamics necessary for developmental processes such as neurite outgrowth (198,421). The dramatic imbalance of 3R and 4R tau in postnatal rT1, during which newborn neurons require dynamic rather than stable microtubules, likely contributes to the abnormal rT1 phenotype.

Counterintuitively, yet consistent with our other findings, rT1 and not rT2 mice were cognitively impaired in the Morris Water Maze at 5 months of age (Figure 28). Hyperphosphorylated tau, when mislocalized to dendritic spines, can cause deficits in postsynaptic transmission due to internalization of postsynaptic AMPA receptors (173). Phosphorylation at the sites we have reported here is required both for tau mislocalization to the postsynapse and for tau-induced reduction of AMPARs (422). Our observations of hyperphosphorylated 4R NM hTau within PSD-95-enriched fractions (Figure 23C, D) suggest that a reduction in postsynaptic signaling underlies rT1 cognitive deficits. Tau-induced deficits in presynaptic signaling (423,424) could also contribute to rT1 cognitive impairments.

Disruption of mitochondrial dynamics and oxidative stress (Figures 30-31) may be related to the subtle deficiencies in brain mass (Figure 32). Tau overexpression in other experimental models is associated with MT elongation (415) via increased expression of fusion proteins (413). Impaired fission is linked to neurodevelopmental abnormalities in humans (414) and rodents (425), as neural stem cell fate requires a

switch from elongated to fragmented mitochondria (426). Our findings suggest that 4R NM hTau is associated with a failure of mitochondria to switch to a fragmented phenotype, disrupting stem cell fate decisions. Although we do not show the relative timing of these events, previous studies suggest that oxidative stress associated with mitochondrial dysfunction occurs upstream of tau hyperphosphorylation via imbalanced activation of kinases and phosphatases (300,427). Taken together, our results are consistent with a neurodevelopmental failure, rather than a progressive neurodegenerative phenotype.

Developmental suppression temporarily reduced NM hTau levels and phosphorylation (Figure 27) and prevented cognitive deficits in rT1 (Figure 28G-I, M-O, S-U). 4 weeks had essentially the same effects as 12 weeks of suppression, suggesting that 4R NM hTau overexpression specifically interferes with developmental milestones during the first 4 weeks of life such as peaks in brain growth, synaptic density, and myelination rate (200). Importantly, DOX treatment did not lower hTau expression after 8 weeks (Figure 27), establishing that amelioration of the phenotype is not due to reduction of hTau per se. Furthermore, despite a moderate rise in NM hTau levels and phosphorylation after suppression (Figure 27), rT1 cognition remained intact, indicating that those molecular phenotypes are harmful during the first 4 weeks but not afterwards. Because hTau expression and tTA toxicity are intrinsically linked in our models, we cannot exclude the possibility that tTA-driven toxicity and suppression of tTA contribute to the abnormal rT1 phenotype and amelioration of that phenotype, respectively (364). Further examination of the tTA mouse phenotype in future studies may provide a mechanistic explanation for the specificity of these effects to rT1 mice.

We found that the MT-bound to -unbound ratio was significantly higher for 4R NM hTau than P301L hTau (Figure 29), suggesting that a function of the MT-binding domain encoded by exon 10 is part of a pathogenic pathway in developing rT1 brains. Because we made this observation in 8-week old mice, it is possible that stronger MT-binding of NM than P301L hTau is downstream of other events. However, because of natural physiological differences between 4R NM and P301L tau (34,196), we view strong MT-binding as a pathological trigger rather than a downstream effect. In this context, it appears that the P301L mutation is protective. Future studies on aged rT1 and rT2 will determine whether pathogenicity of P301L hTau requires the unique milieu of the aging brain.

The developmental pathogenicity of 4R NM hTau we have uncovered may be relevant to a range of neurological conditions. Infantile tauopathies, which include neurodevelopmental conditions such as hemimegalencephaly, ganglioglioma, and tuberous sclerosis, are characterized by upregulation and hyperphosphorylation of tau (428,429). Future experiments will determine if the pathway we have identified may be involved in the pathogenesis of these diseases. Although our results strongly suggest a development-specific mechanism, the massive overexpression of 4R tau may exaggerate and accelerate the phenotype. Therefore, our results may be indicative of an event that occurs early in human disease, yet slowly manifests over time, similar to what occurs in Huntington's disease (430).

In summary, genetic matching between transgenic mouse lines has allowed us to explore molecular and cognitive phenotypes associated with different forms of tau in a well-controlled manner, and to identify a pathogenic mechanism of 4R NM hTau distinct from classical aging-related tauopathy. Future studies using a tTA line without the transgene INDEL mutation (396) will clarify whether the phenotypes we observed here are due to hTau alone or in concert with other tTA-induced dysfunctions. It will also be useful to characterize phenotypes associated with other tau isoforms and expression patterns, and to use this system to test hypotheses concerning other disease-linked mutations, truncated forms of tau, etc.

We believe our findings also highlight the importance of assaying the effects of transgenic proteins at appropriate stages in life, as the milieu of the infantile brain consists of an entirely different proteome than the aged brain (431,432). This study is one example among others (364,365,433) demonstrating that the effects of transgenic proteins differ in mice at different times during their lifespan. Finally, now that advances in techniques allow more precise characterization and manipulation of genomes of transgenic mice, models of neurodegenerative diseases can be held to higher standards. We hope that this type of work will improve translatability of therapies from mice to humans in clinical trials, and bring the field closer to solving the complex puzzle of tauopathies like Alzheimer's disease.

Chapter Four:
Concluding Remarks

Mouse modeling is an invaluable research tool for studying human diseases for several reasons: 1) genetic variation can be minimized with inbreeding, 2) large numbers of mice can be obtained in a relatively short period of time, and 3) many aspects of biology are evolutionarily conserved between mice and humans (434,435). Using mice to study neurodegenerative diseases poses a unique challenge because mice do not naturally develop these diseases, perhaps due to their short lifespans. Therefore, transgenesis is frequently used to introduce human genes into the mouse genome in the hopes of mimicking human disease in a different species. Historically, technological limitations required the use of 'conventional' methods to generate transgenic mice by injecting artificial human mini-gene constructs into pronuclear mouse embryos, resulting in random integration of transgenes (436). Advances in genome engineering technology now allow more precise and sophisticated manipulation of transgenes such that longer sequences (including whole genes) can be inserted into predetermined genomic loci in a 'targeted' manner (437).

To date, 30 mouse models with *MAPT*-related modifications have been generated to study tauopathies (https://www.alzforum.org/research-models). Extreme variability in the phenotypes of these models, in part attributed to the choice of tau isoform, promoter, and expression level, has complicated our understanding of the role of tau in disease pathogenesis. In addition, over 300 therapeutics that have succeeded in such models have gone on to fail in human clinical trials (361). While this problem of translatability could be caused by a number of variables such as treating patients too late in disease progression, it is also strongly suggestive of shortcomings with the mouse models themselves (438). In what began as a project to determine the role of post-translational modifications in tau toxicity, we have found that genomic disruption is an additional variable contributing to phenotypic variability in mouse models, that the level of tau expression directly correlates with phenotype severity, and that developmental overexpression of transgenes can cause phenotypes irrelevant to aging-dependent neurodegenerative disease.

Ironically, efforts to accelerate drug discovery for tauopathies like Alzheimer's disease have in some ways slowed the progress of research. Researchers in the neurodegeneration field have been encouraged to prioritize phenotypes rather than genotypes of mouse models (361), and while following these guidelines has resulted in widespread use of models with robust tauopathy-like phenotypes, confounding genetic

variables have gone unnoticed or unpursued. As we have shown, unintended genomic disruption caused by random transgene insertion (conventional transgenesis) called into question the precise role of tau in the rTg4510 phenotype (396). The rTg4510 model was selected amongst other founder lines because of the dramatic loss of neurons (274,347), which other groups had achieved to a lesser degree with limited success in other P301L lines (348,380,382). However, the profound neurodegeneration in rTg4510 was interpreted as successful phenocopying of human disease rather than an indication of confounding variables. Because transgene suppression with doxycycline prevented neuron loss and cognitive deficits in rTg4510 (274), phenotypic improvements were assumed to be caused by reduction of hTau.

It has now come to light that the severity of the neurodegenerative phenotype in rTg4510 is due in part to disruption and dysregulation of *Fgf14*, a gene prominently expressed in the developing and adult mouse brain (368,371), with functions related to neurogenesis (374), learning and memory (372), and synaptic transmission (369). By comparing rTg4510 to a targeted-equivalent lacking the *Fgf14* Tg-INDEL mutation, rT2/T2, we were able to show that *Fgf14* disruption accelerates the progression of neurodegeneration and tau histopathology (396). However, the relative contribution of hTau and FGF14 to neurodegeneration is complicated by three factors: 1) hTau and FGF14 V1 overexpression are intrinsically linked, 2) rTg4510 is also haploinsufficient for FGF14 V2, X1, and X2, and 3) more than 100 other *Fgf14* transcripts may be involved (360). Furthermore, the $hTau_{P301L}$ Tg-INDEL mutation also affects chromatin architecture, modulating *Fgf14* expression in the absence of the activator transgene (396). To understand if this precise disruption of *Fgf14* can cause neurodegeneration in and of itself, all of these intricate details would need to be replicated in a mouse that does not express hTau – a daunting task that may introduce additional confounds. Importantly, a recent large-scale analysis revealed genomic disruptions in over 20 other conventionally made transgenic mice sold by The Jackson Laboratory (395), demonstrating that the rTg4510 story is not an isolated case.

An additional confounding variable in the rTg4510 line is the tTA TgINDEL that disrupts five annotated genes, four of which also have prominent forebrain expression patterns (396) (http://www.ncbi.nlm.nih.gov/gene/). Unfortunately, because tTA is intrinsically linked to hTau expression in all lines investigated in these studies, we cannot draw firm conclusions about the relative contributions of hTau, *Fgf14*, and tTA to mouse

phenotypes. Because this activator line exhibits a neurodegenerative phenotype (364), the tTA TgINDEL likely contributes to neuron loss and reduced brain mass in all mouse lines examined. Although the transgene itself is matched between rTg4510 and rT2/T2, the number of responder transgene copies may modulate the effect of tTA expression on neurons. Off-target DNA binding of tTA has phenotypic consequences (439), and the presence of a responder transgene could sequester excess tTA to reduce that binding. Therefore, the level of excess tTA is likely different between rT2/T2 and rTg4510 because of the large difference in responder transgene copies. Furthermore, the driver line itself can never serve as a perfect control due to the absence of a responder transgene to sequester tTA. Though there are many possible biological mechanisms to explain the progression of the rTg4510 phenotype, one model consistent with our findings is that a combination of tTA toxicity and *Fgf14* disruption makes forebrain neurons vulnerable to hTau overexpression, allowing for acceleration of hTau histopathology and neurodegeneration.

Fortunately, we avoid *Fgf14*-related confounding variables in our targeted lines, allowing us to conclude that the level of hTau expression positively correlates with severity of mouse phenotypes. rT2/T2 mice are homozygous for the hTau transgene and therefore express roughly twice the amount of hTau as hemizygous rT2 mice. Assessments of these lines revealed that in comparison to rT2, the progression of hTau histopathology, loss of brain mass, and behavioral deficits were accelerated and/or more severe in rT2/T2 (396). Acceleration of phenotypes in the field of neurodegeneration research has typically been viewed as a convenience because mice do not have to be aged as long, reducing costs and time needed for experiments. However, overexpression of transgenes is an artificial way of exaggerating phenotypes and may impact biology in ways that are not relevant to the disease of interest, for example, by introducing unnatural cellular stress. Extreme overexpression (or ‘hyperexpression’) of transgenes like that in rT2/T2 and rTg4510, which is 13-fold higher or more than the level of endogenous tau expression, may be even more problematic. Although a certain level of transgene overexpression may be needed to drive observable phenotypes, effects of overexpression on cell biology must be precisely defined in order to exclude it as an additional confounding variable in mouse models.

Genetic matching between rT1 and rT2 mice has advantageously provided a platform for probing molecular phenotypes of different forms of hTau, essentially using

the mammalian brain as an assay system. Importantly, these lines lack *Fgf14* disruption and have matched tTA-related confounds because both lines have a single copy of the responder transgene. The original intention was to use rT1 (NM hTau) as a control line to determine effects of the P301L mutation on hTau biology in rT2. Surprisingly, we found that rT1 mice had a neurodevelopmental phenotype characterized by slower turnover and hyperphosphorylation of NM hTau, underlying eventual cognitive deficits. We found that excessive MT-binding of NM hTau may trigger a pathogenic pathway in young rT1 mice that involves disruption of mitochondrial dynamics in neurons and interferes with normal brain development. Our developmental suppression experiments revealed that NM hTau overexpression during the first 4 weeks of life is necessary to drive hTau pathogenicity. We hypothesize that overrepresentation of 4R compared to 3R tau isoforms in this artificial system is pathogenic (14,420), and that the P301L mutation confers a beneficial loss of function in this context. In addition, we found that tTA contributes to reduced brain mass in postnatal rT1 and rT2, but NM hTau exacerbates this phenomenon. tTA toxicity is known to be development-specific (364), and may be a driving factor in NM hTau toxicity. Overall, these studies demonstrate the importance of expressing transgenes at relevant stages in life, as the milieu of the developing brain is different from the adult and aging brain (431,432). We have shown that the developing mouse brain is selectively vulnerable to NM hTau overexpression, and recommend delaying the start of hTau expression in these models to test hypotheses related to aging-dependent tauopathy.

This work represents a first step to understanding contributions of confounding variables to mouse model phenotypes, and has yielded three overarching themes: 1) random transgene insertion in conventional transgenesis can affect mouse phenotypes in surprising and complicated ways, 2) the level and timing of transgene expression needs to be taken into careful consideration when designing and using mouse models, and 3) genetic matching is an advantageous tool to probe phenotypes associated with different forms of a protein of interest. The observations made in this work are indicative of a much broader problem affecting the field of neurodegeneration research (395). Because mice do not naturally develop tauopathies, researchers have created increasingly artificial systems, deviating further away from normal mouse biology to generate robust phenotypes. In extreme cases, mice are generated to harbor multiple

transgenes and mutations that have never cooccurred in humans with tauopathies, such as in the 3xTg and 5xFAD models (440,441).

The work presented in this thesis advocates for elimination of confounding variables where possible, and for the use of proper controls to ensure phenotypes, whether molecular or behavioral, are relevant to the disease of interest. While models with robust phenotypes have a certain utility, prioritization of genotype over phenotype will hopefully be increasingly encouraged in light of these findings and those of similar studies. Avoiding genomic disruption will greatly improve the validity of mouse models, and the future of mouse modeling is heading in new directions due to continued technical advancements and widespread availability of sophisticated tools. For instance, inserting human orthologs into corresponding mouse genomic loci places genes in the correct regulatory context, an approach termed 'humanization' of mice (437). In theory, this would allow for expression of splice variants at appropriate times during development, in the appropriate cells, and at endogenous levels. A limited but growing number of validated humanized mouse models now exist, but investigating more complex disease loci may require humanization of multiple genes to fully replicate human biology (437).

Although less artificial models may exhibit mild phenotypes, more sensitive methods such as 'omics' approaches and detailed cellular and molecular analyses may bring the field closer to understanding human diseases (438). Even as genome engineering continues to improve, there will always be limitations with mouse models such as differences between mouse and human circuitry and biology and lack of genetic diversity in single-background strains. Therefore, further validation of findings in additional mouse models and other model systems like human-derived induced pluripotent stem cells (hIPSCs) (442), organoids (443), or in species more closely related to humans such as non-human primates (444) will always be beneficial to solidify findings and ultimately improve translatability of therapeutic approaches.

A plethora of complicated questions remain about tau biology: 1) which posttranslational modifications create toxic species of tau?, 2) is cellular dysfunction caused by soluble or insoluble tau?, 3) do glial cells play a role in tau toxicity?, etc. An important question raised from the current work is: does tau cause neuron loss? The failed attempts to generate *MAPT* mouse models with strong neurodegenerative phenotypes align with the idea that while tau is a pathogenic agent, it primarily functions

to reduce synaptic transmission without inducing neuron death (346). The rTg4510 model was initially lauded for its strong neurodegenerative phenotype, but we have now shown that confounding variables play a part. A final broad question is whether or not mutation-based models provide information relevant to sporadic diseases. Disease-linked mutations have traditionally been used as a modeling tool, but pathogenic mechanisms may nonetheless differ between familial and sporadic diseases. These types of questions can be answered with improvements in mouse modeling like the genetic matching approach we have employed, and with humanized models complemented by other methods like hIPSCs. Confounding variables in transgenic mouse models of tauopathy have complicated our understanding of the role of tau in neurodegenerative diseases, but if researchers take advantage of the new genome engineering tools available, we will move at a faster pace toward solving the complex tau puzzle, identifying new therapeutic avenues, and ultimately developing treatments for tauopathies like Alzheimer's disease.

Chapter Five:

Bibliography

1. Alzheimer, A. (1907) Über eine eigenartige Erkrankung der Hirnrinde. *Allg Z Psychiat* **64**, 146-148
2. Bielschowsky, M., and Brodman, K. (1905) Zur feineren Histologie und Histopathologie der Grosshirnrinde mit besonderer Berücksichtigung der Dementia paralytica, Dementia senilis und Idiotie. *J Psychol Neurol* **5**, 173-198
3. Fischer, O. (1907) Miliare Necrosen mit drusigen Wucherungen der Neurofibrillen, eine regelmässige Veränderung der Hirnrinde bei seniler Demenz. Monatsschrift für Psychi. *Neurol* **22**, 361-372
4. Pick, A. (1901) Senile Hirnatrophie als Grundlage von Herderscheinungen. *Wien Klin Wochenschr* **14**, 403-404
5. Pick, A. (1904) Zur Symptomatologie der linksseitigen Schläfenlappenatrophie. *Mschr Psychiat Neurol* **16**, 378-388
6. Alzheimer, A. (1911) Uber eigenartige Krankheitsfalle des spateren Alters. *Zeitschrift fur die gesamte Neurologie und Psychiatrie* **4**, 356-385
7. Weingarten, M. D., Lockwood, A. H., Hwo, S. Y., and Kirschner, M. W. (1975) A protein factor essential for microtubule assembly. *Proc Natl Acad Sci U S A* **72**, 1858-1862
8. Cleveland, D. W., Hwo, S. Y., and Kirschner, M. W. (1977) Physical and chemical properties of purified tau factor and the role of tau in microtubule assembly. *J Mol Biol* **116**, 227-247
9. Jameson, L., Frey, T., Zeeberg, B., Dalldorf, F., and Caplow, M. (1980) Inhibition of microtubule assembly by phosphorylation of microtubule-associated proteins. *Biochemistry* **19**, 2472-2479
10. Pollock, N. J., Mirra, S. S., Binder, L. I., Hansen, L. A., and Wood, J. G. (1986) Filamentous aggregates in Pick's disease, progressive supranuclear palsy, and Alzheimer's disease share antigenic determinants with microtubule-associated protein, tau. *Lancet* **2**, 1211
11. Brion, J. P., Passareiro, H., Nunez, J., and Flament-Durand, J. (1985) MISE EN EVIDENCE IMMUNOLOGIQUE DE LA PROTEINE TAU AU NIVEAU DES LESIONS DE DEGENERESCENCE NEUROFIBRILLAIRE DE LA MALADIE D'ALZHEIMER. *Arch Biol* **96**, 229-235
12. Kidd, M. (1963) Paired helical filaments in electron microscopy of Alzheimer's disease. *Nature* **197**, 192-193
13. Goedert, M., Wischik, C. M., Crowther, R. A., Walker, J. E., and Klug, A. (1988) Cloning and sequencing of the cDNA encoding a core protein of the paired helical filament of Alzheimer disease: identification as the microtubule-associated protein tau. *Proc Natl Acad Sci U S A* **85**, 4051-4055
14. Arendt, T., Stieler, J. T., and Holzer, M. (2016) Tau and tauopathies. *Brain Res Bull* **126**, 238-292
15. Arima, K., Hirai, S., Sunohara, N., Aoto, K., Izumiyama, Y., Ueda, K., Ikeda, K., and Kawai, M. (1999) Cellular co-localization of phosphorylated tau- and NACP/alpha-synuclein-epitopes in lewy bodies in sporadic Parkinson's disease and in dementia with Lewy bodies. *Brain Res* **843**, 53-61
16. Fernandez-Nogales, M., Cabrera, J. R., Santos-Galindo, M., Hoozemans, J. J., Ferrer, I., Rozemuller, A. J., Hernandez, F., Avila, J., and Lucas, J. J. (2014) Huntington's disease is a four-repeat tauopathy with tau nuclear rods. *Nat Med* **20**, 881-885
17. Nelson, P. T., Abner, E. L., Patel, E., Anderson, S., Wilcock, D. M., Kryscio, R. J., Van Eldik, L. J., Jicha, G. A., Gal, Z., Nelson, R. S., Nelson, B. G., Gal, J., Azam, M. T., Fardo, D. W., and Cykowski, M. D. (2018) The Amygdala as a Locus of Pathologic Misfolding in Neurodegenerative Diseases. *J Neuropathol Exp Neurol* **77**, 2-20

18. Mackenzie, I. R., and Neumann, M. (2016) Molecular neuropathology of frontotemporal dementia: insights into disease mechanisms from postmortem studies. *J Neurochem* **138 Suppl 1**, 54-70
19. Garre-Olmo, J., Genis Batlle, D., del Mar Fernandez, M., Marquez Daniel, F., de Eugenio Huelamo, R., Casadevall, T., Turbau Recio, J., Turon Estrada, A., Lopez-Pousa, S., and Registry of Dementia of Girona Study, G. (2010) Incidence and subtypes of early-onset dementia in a geographically defined general population. *Neurology* **75**, 1249-1255
20. Rohrer, J. D., Nicholas, J. M., Cash, D. M., van Swieten, J., Dopper, E., Jiskoot, L., van Minkelen, R., Rombouts, S. A., Cardoso, M. J., Clegg, S., Espak, M., Mead, S., Thomas, D. L., De Vita, E., Masellis, M., Black, S. E., Freedman, M., Keren, R., MacIntosh, B. J., Rogaeva, E., Tang-Wai, D., Tartaglia, M. C., Laforce, R., Jr., Tagliavini, F., Tiraboschi, P., Redaelli, V., Prioni, S., Grisoli, M., Borroni, B., Padovani, A., Galimberti, D., Scarpini, E., Arighi, A., Fumagalli, G., Rowe, J. B., Coyle-Gilchrist, I., Graff, C., Fallstrom, M., Jelic, V., Stahlbom, A. K., Andersson, C., Thonberg, H., Lilius, L., Frisoni, G. B., Pievani, M., Bocchetta, M., Benussi, L., Ghidoni, R., Finger, E., Sorbi, S., Nacmias, B., Lombardi, G., Polito, C., Warren, J. D., Ourselin, S., Fox, N. C., Rossor, M. N., and Binetti, G. (2015) Presymptomatic cognitive and neuroanatomical changes in genetic frontotemporal dementia in the Genetic Frontotemporal dementia Initiative (GENFI) study: a cross-sectional analysis. *Lancet Neurol* **14**, 253-262
21. Xia, C., and Dickerson, B. C. (2016) Tau PET: the next frontier in molecular imaging of dementia. *Int Psychogeriatr* **28**, 1403-1406
22. Association., A. s. (2018) Alzheimer's Disease Facts and Figures. *Alzheimers Dement* **14**, 367-429
23. Lane, C. A., Hardy, J., and Schott, J. M. (2018) Alzheimer's disease. *Eur J Neurol* **25**, 59-70
24. Cummings, J., Lee, G., Ritter, A., and Zhong, K. (2018) Alzheimer's disease drug development pipeline: 2018. *Alzheimers Dement (N Y)* **4**, 195-214
25. Sigurdsson, E. M. (2018) Tau Immunotherapies for Alzheimer's Disease and Related Tauopathies: Progress and Potential Pitfalls. *J Alzheimers Dis* **66**, 855-856
26. Coughlin, D., and Irwin, D. J. (2017) Emerging Diagnostic and Therapeutic Strategies for Tauopathies. *Curr Neurol Neurosci Rep* **17**, 72
27. Goedert, M., Spillantini, M. G., and Crowther, R. A. (1992) Cloning of a big tau microtubule-associated protein characteristic of the peripheral nervous system. *Proc Natl Acad Sci U S A* **89**, 1983-1987
28. Georgieff, I. S., Liem, R. K., Couchie, D., Mavilia, C., Nunez, J., and Shelanski, M. L. (1993) Expression of high molecular weight tau in the central and peripheral nervous systems. *J Cell Sci* **105 (Pt 3)**, 729-737
29. Gu, Y., Oyama, F., and Ihara, Y. (1996) Tau is widely expressed in rat tissues. *J Neurochem* **67**, 1235-1244
30. Wang, Y., Loomis, P. A., Zinkowski, R. P., and Binder, L. I. (1993) A novel tau transcript in cultured human neuroblastoma cells expressing nuclear tau. *J Cell Biol* **121**, 257-267
31. Takuma, H., Arawaka, S., and Mori, H. (2003) Isoforms changes of tau protein during development in various species. *Dev Brain Res* **142**, 121-127
32. Hefti, M. M., Farrell, K., Kim, S., Bowles, K. R., Fowkes, M. E., Raj, T., and Crary, J. F. (2018) High-resolution temporal and regional mapping of MAPT expression and splicing in human brain development. *PLoS One* **13**, e0195771
33. McMillan, P., Korvatska, E., Poorkaj, P., Evstafjeva, Z., Robinson, L., Greenup, L., Leverenz, J., Schellenberg, G. D., and D'Souza, I. (2008) Tau isoform regulation is region- and cell-specific in mouse brain. *J Comp Neurol* **511**, 788-803
34. Hong, M., Zhukareva, V., Vogelsberg-Ragaglia, V., Wszolek, Z., Reed, L., Miller, B. I., Geschwind, D. H., Bird, T. D., McKeel, D., Goate, A., Morris, J. C., Wilhelmsen, K. C., Schellenberg, G. D., Trojanowski, J. Q., and Lee, V. M. (1998) Mutation-specific functional impairments in distinct tau isoforms of hereditary FTDP-17. *Science* **282**, 1914-1917

35. Stefansson, H., Helgason, A., Thorleifsson, G., Steinthorsdottir, V., Masson, G., Barnard, J., Baker, A., Jonasdottir, A., Ingason, A., Gudnadottir, V. G., Desnica, N., Hicks, A., Gylfason, A., Gudbjartsson, D. F., Jonsdottir, G. M., Sainz, J., Agnarsson, K., Birgisdottir, B., Ghosh, S., Olafsdottir, A., Cazier, J. B., Kristjansson, K., Frigge, M. L., Thorgeirsson, T. E., Gulcher, J. R., Kong, A., and Stefansson, K. (2005) A common inversion under selection in Europeans. *Nat Genet* **37**, 129-137
36. Houlden, H., Baker, M., Morris, H. R., MacDonald, N., Pickering-Brown, S., Adamson, J., Lees, A. J., Rossor, M. N., Quinn, N. P., Kertesz, A., Khan, M. N., Hardy, J., Lantos, P. L., St George-Hyslop, P., Munoz, D. G., Mann, D., Lang, A. E., Bergeron, C., Bigio, E. H., Litvan, I., Bhatia, K. P., Dickson, D., Wood, N. W., and Hutton, M. (2001) Corticobasal degeneration and progressive supranuclear palsy share a common tau haplotype. *Neurology* **56**, 1702-1706
37. Kwok, J. B., Teber, E. T., Loy, C., Hallupp, M., Nicholson, G., Mellick, G. D., Buchanan, D. D., Silburn, P. A., and Schofield, P. R. (2004) Tau haplotypes regulate transcription and are associated with Parkinson's disease. *Ann Neurol* **55**, 329-334
38. Caffrey, T. M., Joachim, C., Paracchini, S., Esiri, M. M., and Wade-Martins, R. (2006) Haplotype-specific expression of exon 10 at the human MAPT locus. *Hum Mol Genet* **15**, 3529-3537
39. Baker, M., Litvan, I., Houlden, H., Adamson, J., Dickson, D., Perez-Tur, J., Hardy, J., Lynch, T., Bigio, E., and Hutton, M. (1999) Association of an extended haplotype in the tau gene with progressive supranuclear palsy. *Hum Mol Genet* **8**, 711-715
40. Caffrey, T. M., Joachim, C., and Wade-Martins, R. (2008) Haplotype-specific expression of the N-terminal exons 2 and 3 at the human MAPT locus. *Neurobiol Aging* **29**, 1923-1929
41. de Jong, S., Chepelev, I., Janson, E., Strengman, E., van den Berg, L. H., Veldink, J. H., and Ophoff, R. A. (2012) Common inversion polymorphism at 17q21.31 affects expression of multiple genes in tissue-specific manner. *BMC Genomics* **13**, 458
42. Pittman, A. M., Myers, A. J., Abou-Sleiman, P., Fung, H. C., Kaleem, M., Marlowe, L., Duckworth, J., Leung, D., Williams, D., Kilford, L., Thomas, N., Morris, C. M., Dickson, D., Wood, N. W., Hardy, J., Lees, A. J., and de Silva, R. (2005) Linkage disequilibrium fine mapping and haplotype association analysis of the tau gene in progressive supranuclear palsy and corticobasal degeneration. *J Med Genet* **42**, 837-846
43. Koolen, D. A., Sharp, A. J., Hurst, J. A., Firth, H. V., Knight, S. J., Goldenberg, A., Saugier-Veber, P., Pfundt, R., Vissers, L. E., Destree, A., Grisart, B., Rooms, L., Van der Aa, N., Field, M., Hackett, A., Bell, K., Nowaczyk, M. J., Mancini, G. M., Poddighe, P. J., Schwartz, C. E., Rossi, E., De Gregori, M., Antonacci-Fulton, L. L., McLellan, M. D., 2nd, Garrett, J. M., Wiechert, M. A., Miner, T. L., Crosby, S., Ciccone, R., Willatt, L., Rauch, A., Zenker, M., Aradhya, S., Manning, M. A., Strom, T. M., Wagenstaller, J., Krepischi-Santos, A. C., Vianna-Morgante, A. M., Rosenberg, C., Price, S. M., Stewart, H., Shaw-Smith, C., Brunner, H. G., Wilkie, A. O., Veltman, J. A., Zuffardi, O., Eichler, E. E., and de Vries, B. B. (2008) Clinical and molecular delineation of the 17q21.31 microdeletion syndrome. *J Med Genet* **45**, 710-720
44. Forrest, S. L., Kril, J. J., Stevens, C. H., Kwok, J. B., Hallupp, M., Kim, W. S., Huang, Y., McGinley, C. V., Werka, H., Kiernan, M. C., Gotz, J., Spillantini, M. G., Hodges, J. R., Ittner, L. M., and Halliday, G. M. (2018) Retiring the term FTDP-17 as MAPT mutations are genetic forms of sporadic frontotemporal tauopathies. *Brain* **141**, 521-534
45. Pottier, C., Ravenscroft, T. A., Sanchez-Contreras, M., and Rademakers, R. (2016) Genetics of FTLD: overview and what else we can expect from genetic studies. *J Neurochem* **138 Suppl 1**, 32-53
46. Forrest, S. L., Halliday, G. M., McCann, H., McGeachie, A. B., McGinley, C. V., Hodges, J. R., Piguet, O., Kwok, J. B., Spillantini, M. G., and Kril, J. J. (2019) Heritability in frontotemporal tauopathies. *Alzheimers Dement (Amst)* **11**, 115-124
47. Baker, M., Mackenzie, I. R., Pickering-Brown, S. M., Gass, J., Rademakers, R., Lindholm, C., Snowden, J., Adamson, J., Sadovnick, A. D., Rollinson, S., Cannon, A., Dwosh, E., Neary, D., Melquist, S., Richardson, A., Dickson, D., Berger, Z., Eriksen, J.,

Robinson, T., Zehr, C., Dickey, C. A., Crook, R., McGowan, E., Mann, D., Boeve, B., Feldman, H., and Hutton, M. (2006) Mutations in progranulin cause tau-negative frontotemporal dementia linked to chromosome 17. *Nature* **442**, 916-919

48. Cruts, M., Gijselinck, I., van der Zee, J., Engelborghs, S., Wils, H., Pirici, D., Rademakers, R., Vandenberghe, R., Dermaut, B., Martin, J. J., van Duijn, C., Peeters, K., Sciot, R., Santens, P., De Pooter, T., Mattheijssens, M., Van den Broeck, M., Cuijt, I., Vennekens, K., De Deyn, P. P., Kumar-Singh, S., and Van Broeckhoven, C. (2006) Null mutations in progranulin cause ubiquitin-positive frontotemporal dementia linked to chromosome 17q21. *Nature* **442**, 920-924
49. Murrell, J. R., Koller, D., Foroud, T., Goedert, M., Spillantini, M. G., Edenberg, H. J., Farlow, M. R., and Ghetti, B. (1997) Familial multiple-system tauopathy with presenile dementia is localized to chromosome 17. *Am J Hum Genet* **61**, 1131-1138
50. Poorkaj, P., Bird, T. D., Wijsman, E., Nemens, E., Garruto, R. M., Anderson, L., Andreadis, A., Wiederholt, W. C., Raskind, M., and Schellenberg, G. D. (1998) Tau is a candidate gene for chromosome 17 frontotemporal dementia. *Ann Neurol* **43**, 815-825
51. Spillantini, M. G., Murrell, J. R., Goedert, M., Farlow, M. R., Klug, A., and Ghetti, B. (1998) Mutation in the tau gene in familial multiple system tauopathy with presenile dementia. *Proc Natl Acad Sci U S A* **95**, 7737-7741
52. Wilhelmsen, K. C., Lynch, T., Pavlou, E., Higgins, M., and Nygaard, T. G. (1994) Localization of disinhibition-dementia-parkinsonism-amyotrophy complex to 17q21-22. *Am J Hum Genet* **55**, 1159-1165
53. Benussi, A., Padovani, A., and Borroni, B. (2015) Phenotypic Heterogeneity of Monogenic Frontotemporal Dementia. *Front Aging Neurosci* **7**, 171
54. Boeve, B. F., Tremont-Lukats, I. W., Waclawik, A. J., Murrell, J. R., Hermann, B., Jack, C. R., Jr., Shiung, M. M., Smith, G. E., Nair, A. R., Lindor, N., Koppikar, V., and Ghetti, B. (2005) Longitudinal characterization of two siblings with frontotemporal dementia and parkinsonism linked to chromosome 17 associated with the S305N tau mutation. *Brain* **128**, 752-772
55. Woollacott, I. O., and Rohrer, J. D. (2016) The clinical spectrum of sporadic and familial forms of frontotemporal dementia. *J Neurochem* **138 Suppl 1**, 6-31
56. Ghetti, B., Oblak, A. L., Boeve, B. F., Johnson, K. A., Dickerson, B. C., and Goedert, M. (2015) Invited review: Frontotemporal dementia caused by microtubule-associated protein tau gene (MAPT) mutations: a chameleon for neuropathology and neuroimaging. *Neuropathol Appl Neurobiol* **41**, 24-46
57. van Swieten, J., and Spillantini, M. G. (2007) Hereditary frontotemporal dementia caused by Tau gene mutations. *Brain Pathol* **17**, 63-73
58. Snowden, J. S., Adams, J., Harris, J., Thompson, J. C., Rollinson, S., Richardson, A., Jones, M., Neary, D., Mann, D. M., and Pickering-Brown, S. (2015) Distinct clinical and pathological phenotypes in frontotemporal dementia associated with MAPT, PGRN and C9orf72 mutations. *Amyotroph Lateral Scler Frontotemporal Degener* **16**, 497-505
59. Bonvicini, C., Scassellati, C., Benussi, L., Di Maria, E., Maj, C., Ciani, M., Fostinelli, S., Mega, A., Bocchetta, M., Lanzi, G., Giacopuzzi, E., Ferraboli, S., Pievani, M., Fedi, V., Defanti, C. A., Giliani, S., Alzheimer's Disease Neuroimaging, I., Frisoni, G. B., Ghidoni, R., and Gennarelli, M. (2019) Next Generation Sequencing Analysis in Early Onset Dementia Patients. *J Alzheimers Dis* **67**, 243-256
60. Tacik, P., Sanchez-Contreras, M., Rademakers, R., Dickson, D. W., and Wszolek, Z. K. (2016) Genetic Disorders with Tau Pathology: A Review of the Literature and Report of Two Patients with Tauopathy and Positive Family Histories. *Neurodegener Dis* **16**, 12-21
61. Sala Frigerio, C., Lau, P., Troakes, C., Deramecourt, V., Gele, P., Van Loo, P., Voet, T., and De Strooper, B. (2015) On the identification of low allele frequency mosaic mutations in the brains of Alzheimer's disease patients. *Alzheimers Dement* **11**, 1265-1276
62. Poorkaj, P., Muma, N. A., Zhukareva, V., Cochran, E. J., Shannon, K. M., Hurtig, H., Koller, W. C., Bird, T. D., Trojanowski, J. Q., Lee, V. M., and Schellenberg, G. D. (2002) An R5L tau mutation in a subject with a progressive supranuclear palsy phenotype. *Ann Neurol* **52**, 511-516

63. Chang, E., Kim, S., Yin, H., Nagaraja, H. N., and Kuret, J. (2008) Pathogenic missense MAPT mutations differentially modulate tau aggregation propensity at nucleation and extension steps. *J Neurochem* **107**, 1113-1123
64. Hayashi, S., Toyoshima, Y., Hasegawa, M., Umeda, Y., Wakabayashi, K., Tokiguchi, S., Iwatsubo, T., and Takahashi, H. (2002) Late-onset frontotemporal dementia with a novel exon 1 (Arg5His) tau gene mutation. *Ann Neurol* **51**, 525-530
65. Schulte, E. C., Fukumori, A., Mollenhauer, B., Hor, H., Arzberger, T., Perneczky, R., Kurz, A., Diehl-Schmid, J., Hull, M., Lichtner, P., Eckstein, G., Zimprich, A., Haubenberger, D., Pirker, W., Brucke, T., Bereznai, B., Molnar, M. J., Lorenzo-Betancor, O., Pastor, P., Peters, A., Gieger, C., Estivill, X., Meitinger, T., Kretzschmar, H. A., Trenkwalder, C., Haass, C., and Winkelmann, J. (2015) Rare variants in beta-Amyloid precursor protein (APP) and Parkinson's disease. *Eur J Hum Genet* **23**, 1328-1333
66. Shi, Z., Liu, S., Xiang, L., Wang, Y., Liu, M., Liu, S., Han, T., Zhou, Y., Wang, J., Cai, L., Gao, S., and Ji, Y. (2016) Frontotemporal dementia-related gene mutations in clinical dementia patients from a Chinese population. *J Hum Genet* **61**, 1003-1008
67. Iyer, A., Lapointe, N. E., Zielke, K., Berdynski, M., Guzman, E., Barczak, A., Chodakowska-Zebrowska, M., Barcikowska, M., Feinstein, S., and Zekanowski, C. (2013) A novel MAPT mutation, G55R, in a frontotemporal dementia patient leads to altered Tau function. *PLoS One* **8**, e76409
68. Gallo, M., Tomaino, C., Puccio, G., Frangipane, F., Curcio, S. A., Bernardi, L., Geracitano, S., Anfossi, M., Mirabelli, M., Colao, R., Vasso, F., Smirne, N., Maletta, R. G., and Bruni, A. C. (2010) Novel MAPT Val75Ala mutation and PSEN2 Arg62Hys in two siblings with frontotemporal dementia. *Neurol Sci* **31**, 65-70
69. Ling, H., Kara, E., Bandopadhyay, R., Hardy, J., Holton, J., Xiromerisiou, G., Lees, A., Houlden, H., and Revesz, T. (2013) TDP-43 pathology in a patient carrying G2019S LRRK2 mutation and a novel p.Q124E MAPT. *Neurobiol Aging* **34**, 2889 e2885-2889
70. Kim, E. J., Kwon, J. C., Park, K. H., Park, K. W., Lee, J. H., Choi, S. H., Jeong, J. H., Kim, B. C., Yoon, S. J., Yoon, Y. C., Kim, S., Park, K. C., Choi, B. O., Na, D. L., Ki, C. S., and Kim, S. H. (2014) Clinical and genetic analysis of MAPT, GRN, and C9orf72 genes in Korean patients with frontotemporal dementia. *Neurobiol Aging* **35**, 1213 e1213-1217
71. Tang, M., Gu, X., Wei, J., Jiao, B., Zhou, L., Zhou, Y., Weng, L., Yan, X., Tang, B., Xu, J., and Shen, L. (2016) Analyses MAPT, GRN, and C9orf72 mutations in Chinese patients with frontotemporal dementia. *Neurobiol Aging* **46**, 235 e211-235
72. Jin, S. C., Pastor, P., Cooper, B., Cervantes, S., Benitez, B. A., Razquin, C., Goate, A., Ibero-American Alzheimer Disease Genetics Group, R., and Cruchaga, C. (2012) Pooled-DNA sequencing identifies novel causative variants in PSEN1, GRN and MAPT in a clinical early-onset and familial Alzheimer's disease Ibero-American cohort. *Alzheimers Res Ther* **4**, 34
73. Sassi, C., Guerreiro, R., Gibbs, R., Ding, J., Lupton, M. K., Troakes, C., Al-Sarraj, S., Niblock, M., Gallo, J. M., Adnan, J., Killick, R., Brown, K. S., Medway, C., Lord, J., Turton, J., Bras, J., Alzheimer's Research, U. K. C., Morgan, K., Powell, J. F., Singleton, A., and Hardy, J. (2014) Investigating the role of rare coding variability in Mendelian dementia genes (APP, PSEN1, PSEN2, GRN, MAPT, and PRNP) in late-onset Alzheimer's disease. *Neurobiol Aging* **35**, 2881 e2881-2881 e2886
74. Piccoli, E., Rossi, G., Rossi, T., Pelliccioni, G., D'Amato, I., Tagliavini, F., and Di Fede, G. (2016) Novel PSEN1 mutations (H214N and R220P) associated with familial Alzheimer's disease identified by targeted exome sequencing. *Neurobiol Aging* **40**, 192 e197-192 e111
75. Maeda, S., Djukic, B., Taneja, P., Yu, G. Q., Lo, I., Davis, A., Craft, R., Guo, W., Wang, X., Kim, D., Ponnusamy, R., Gill, T. M., Masliah, E., and Mucke, L. (2016) Expression of A152T human tau causes age-dependent neuronal dysfunction and loss in transgenic mice. *EMBO Rep* **17**, 530-551
76. Houlden, H., Baker, M., Adamson, J., Grover, A., Waring, S., Dickson, D., Lynch, T., Boeve, B., Petersen, R. C., Pickering-Brown, S., Owen, F., Neary, D., Craufurd, D.,

Snowden, J., Mann, D., and Hutton, M. (1999) Frequency of tau mutations in three series of non-Alzheimer's degenerative dementia. *Ann Neurol* **46**, 243-248
77. Rademakers, R., Cruts, M., and van Broeckhoven, C. (2004) The role of tau (MAPT) in frontotemporal dementia and related tauopathies. *Hum Mutat* **24**, 277-295
78. Cruchaga, C., Haller, G., Chakraverty, S., Mayo, K., Vallania, F. L., Mitra, R. D., Faber, K., Williamson, J., Bird, T., Diaz-Arrastia, R., Foroud, T. M., Boeve, B. F., Graff-Radford, N. R., St Jean, P., Lawson, M., Ehm, M. G., Mayeux, R., Goate, A. M., and Consortium, N.-L. N. F. S. (2012) Rare variants in APP, PSEN1 and PSEN2 increase risk for AD in late-onset Alzheimer's disease families. *PLoS One* **7**, e31039
79. Meeus, B., Verstraeten, A., Crosiers, D., Engelborghs, S., Van den Broeck, M., Mattheijssens, M., Peeters, K., Corsmit, E., Elinck, E., Pickut, B., Vandenberghe, R., Cras, P., De Deyn, P. P., Van Broeckhoven, C., and Theuns, J. (2012) DLB and PDD: a role for mutations in dementia and Parkinson disease genes? *Neurobiol Aging* **33**, 629 e625-629 e618
80. Pickering-Brown, S. M., Richardson, A. M., Snowden, J. S., McDonagh, A. M., Burns, A., Braude, W., Baker, M., Liu, W. K., Yen, S. H., Hardy, J., Hutton, M., Davies, Y., Allsop, D., Craufurd, D., Neary, D., and Mann, D. M. (2002) Inherited frontotemporal dementia in nine British families associated with intronic mutations in the tau gene. *Brain* **125**, 732-751
81. King, A., Al-Sarraj, S., Troakes, C., Smith, B. N., Maekawa, S., Iovino, M., Spillantini, M. G., and Shaw, C. E. (2013) Mixed tau, TDP-43 and p62 pathology in FTLD associated with a C9ORF72 repeat expansion and p.Ala239Thr MAPT (tau) variant. *Acta Neuropathol* **125**, 303-310
82. Rizzini, C., Goedert, M., Hodges, J. R., Smith, M. J., Jakes, R., Hills, R., Xuereb, J. H., Crowther, R. A., and Spillantini, M. G. (2000) Tau gene mutation K257T causes a tauopathy similar to Pick's disease. *J Neuropathol Exp Neurol* **59**, 990-1001
83. Grover, A., England, E., Baker, M., Sahara, N., Adamson, J., Granger, B., Houlden, H., Passant, U., Yen, S. H., DeTure, M., and Hutton, M. (2003) A novel tau mutation in exon 9 (1260V) causes a four-repeat tauopathy. *Exp Neurol* **184**, 131-140
84. Benitez, B. A., Karch, C. M., Cai, Y., Jin, S. C., Cooper, B., Carrell, D., Bertelsen, S., Chibnik, L., Schneider, J. A., Bennett, D. A., Alzheimer's Disease Neuroimaging, I., Genetic, Environmental Risk for Alzheimer's Disease Consortium, G., Fagan, A. M., Holtzman, D., Morris, J. C., Goate, A. M., and Cruchaga, C. (2013) The PSEN1, p.E318G variant increases the risk of Alzheimer's disease in APOE-epsilon4 carriers. *PLoS Genet* **9**, e1003685
85. Hogg, M., Grujic, Z. M., Baker, M., Demirci, S., Guillozet, A. L., Sweet, A. P., Herzog, L. L., Weintraub, S., Mesulam, M. M., LaPointe, N. E., Gamblin, T. C., Berry, R. W., Binder, L. I., de Silva, R., Lees, A., Espinoza, M., Davies, P., Grover, A., Sahara, N., Ishizawa, T., Dickson, D., Yen, S. H., Hutton, M., and Bigio, E. H. (2003) The L266V tau mutation is associated with frontotemporal dementia and Pick-like 3R and 4R tauopathy. *Acta Neuropathol* **106**, 323-336
86. Kobayashi, T., Ota, S., Tanaka, K., Ito, Y., Hasegawa, M., Umeda, Y., Motoi, Y., Takanashi, M., Yasuhara, M., Anno, M., Mizuno, Y., and Mori, H. (2003) A novel L266V mutation of the tau gene causes frontotemporal dementia with a unique tau pathology. *Ann Neurol* **53**, 133-137
87. Bronner, I. F., ter Meulen, B. C., Azmani, A., Severijnen, L. A., Willemsen, R., Kamphorst, W., Ravid, R., Heutink, P., and van Swieten, J. C. (2005) Hereditary Pick's disease with the G272V tau mutation shows predominant three-repeat tau pathology. *Brain* **128**, 2645-2653
88. van der Zee, J., Rademakers, R., Engelborghs, S., Gijselinck, I., Bogaerts, V., Vandenberghe, R., Santens, P., Caekebeke, J., De Pooter, T., Peeters, K., Lubke, U., Van den Broeck, M., Martin, J. J., Cruts, M., De Deyn, P. P., Van Broeckhoven, C., and Dermaut, B. (2006) A Belgian ancestral haplotype harbours a highly prevalent mutation for 17q21-linked tau-negative FTLD. *Brain* **129**, 841-852

89. Clark, L. N., Poorkaj, P., Wszolek, Z., Geschwind, D. H., Nasreddine, Z. S., Miller, B., Li, D., Payami, H., Awert, F., Markopoulou, K., Andreadis, A., D'Souza, I., Lee, V. M., Reed, L., Trojanowski, J. Q., Zhukareva, V., Bird, T., Schellenberg, G., and Wilhelmsen, K. C. (1998) Pathogenic implications of mutations in the tau gene in pallido-ponto-nigral degeneration and related neurodegenerative disorders linked to chromosome 17. *Proc Natl Acad Sci U S A* **95**, 13103-13107
90. Wren, M. C., Zhao, J., Liu, C. C., Murray, M. E., Atagi, Y., Davis, M. D., Fu, Y., Okano, H. J., Ogaki, K., Strongosky, A. J., Tacik, P., Rademakers, R., Ross, O. A., Dickson, D. W., Wszolek, Z. K., Kanekiyo, T., and Bu, G. (2015) Frontotemporal dementia-associated N279K tau mutant disrupts subcellular vesicle trafficking and induces cellular stress in iPSC-derived neural stem cells. *Mol Neurodegener* **10**, 46
91. Rohrer, J. D., Paviour, D., Vandrovcova, J., Hodges, J., de Silva, R., and Rossor, M. N. (2011) Novel L284R MAPT mutation in a family with an autosomal dominant progressive supranuclear palsy syndrome. *Neurodegener Dis* **8**, 149-152
92. Ogaki, K., Li, Y., Takanashi, M., Ishikawa, K., Kobayashi, T., Nonaka, T., Hasegawa, M., Kishi, M., Yoshino, H., Funayama, M., Tsukamoto, T., Shioya, K., Yokochi, M., Imai, H., Sasaki, R., Kokubo, Y., Kuzuhara, S., Motoi, Y., Tomiyama, H., and Hattori, N. (2013) Analyses of the MAPT, PGRN, and C9orf72 mutations in Japanese patients with FTLD, PSP, and CBS. *Parkinsonism Relat Disord* **19**, 15-20
93. Marshall, C. R., Guerreiro, R., Thust, S., Fletcher, P., Rohrer, J. D., and Fox, N. C. (2015) A Novel MAPT Mutation Causing Corticobasal Syndrome Led by Progressive Apraxia of Speech. *J Alzheimers Dis* **48**, 923-926
94. Cohn-Hokke, P. E., Wong, T. H., Rizzu, P., Breedveld, G., van der Flier, W. M., Scheltens, P., Baas, F., Heutink, P., Meijers-Heijboer, E. J., van Swieten, J. C., and Pijnenburg, Y. A. (2014) Mutation frequency of PRKAR1B and the major familial dementia genes in a Dutch early onset dementia cohort. *J Neurol* **261**, 2085-2092
95. de Silva, R., Lashley, T., Strand, C., Shiarli, A. M., Shi, J., Tian, J., Bailey, K. L., Davies, P., Bigio, E. H., Arima, K., Iseki, E., Murayama, S., Kretzschmar, H., Neumann, M., Lippa, C., Halliday, G., MacKenzie, J., Ravid, R., Dickson, D., Wszolek, Z., Iwatsubo, T., Pickering-Brown, S. M., Holton, J., Lees, A., Revesz, T., and Mann, D. M. (2006) An immunohistochemical study of cases of sporadic and inherited frontotemporal lobar degeneration using 3R- and 4R-specific tau monoclonal antibodies. *Acta Neuropathol* **111**, 329-340
96. Grover, A., DeTure, M., Yen, S. H., and Hutton, M. (2002) Effects on splicing and protein function of three mutations in codon N296 of tau in vitro. *Neurosci Lett* **323**, 33-36
97. Iseki, E., Matsumura, T., Marui, W., Hino, H., Odawara, T., Sugiyama, N., Suzuki, K., Sawada, H., Arai, T., and Kosaka, K. (2001) Familial frontotemporal dementia and parkinsonism with a novel N296H mutation in exon 10 of the tau gene and a widespread tau accumulation in the glial cells. *Acta Neuropathol* **102**, 285-292
98. Iovino, M., Pfisterer, U., Holton, J. L., Lashley, T., Swingler, R. J., Calo, L., Treacy, R., Revesz, T., Parmar, M., Goedert, M., Muqit, M. M., and Spillantini, M. G. (2014) The novel MAPT mutation K298E: mechanisms of mutant tau toxicity, brain pathology and tau expression in induced fibroblast-derived neurons. *Acta Neuropathol* **127**, 283-295
99. Che, X. Q., Zhao, Q. H., Huang, Y., Li, X., Ren, R. J., Chen, S. D., Wang, G., and Guo, Q. H. (2017) Genetic Features of MAPT, GRN, C9orf72 and CHCHD10 Gene Mutations in Chinese Patients with Frontotemporal Dementia. *Curr Alzheimer Res* **14**, 1102-1108
100. Llado, A., Ezquerra, M., Sanchez-Valle, R., Rami, L., Tolosa, E., and Molinuevo, J. L. (2007) A novel MAPT mutation (P301T) associated with familial frontotemporal dementia. *Eur J Neurol* **14**, e9-10
101. Strang, K. H., Croft, C. L., Sorrentino, Z. A., Chakrabarty, P., Golde, T. E., and Giasson, B. I. (2018) Distinct differences in prion-like seeding and aggregation between Tau protein variants provide mechanistic insights into tauopathies. *J Biol Chem* **293**, 4579
102. Bull, N. D., Guidi, A., Goedert, M., Martin, K. R., and Spillantini, M. G. (2012) Reduced axonal transport and increased excitotoxic retinal ganglion cell degeneration in mice transgenic for human mutant P301S tau. *PLoS One* **7**, e34724

103. Gasparini, L., Crowther, R. A., Martin, K. R., Berg, N., Coleman, M., Goedert, M., and Spillantini, M. G. (2011) Tau inclusions in retinal ganglion cells of human P301S tau transgenic mice: effects on axonal viability. *Neurobiol Aging* **32**, 419-433
104. Lossos, A., Reches, A., Gal, A., Newman, J. P., Soffer, D., Gomori, J. M., Boher, M., Ekstein, D., Biran, I., Meiner, Z., Abramsky, O., and Rosenmann, H. (2003) Frontotemporal dementia and parkinsonism with the P301S tau gene mutation in a Jewish family. *J Neurol* **250**, 733-740
105. Hutton, M., Lendon, C. L., Rizzu, P., Baker, M., Froelich, S., Houlden, H., Pickering-Brown, S., Chakraverty, S., Isaacs, A., Grover, A., Hackett, J., Adamson, J., Lincoln, S., Dickson, D., Davies, P., Petersen, R. C., Stevens, M., de Graaff, E., Wauters, E., van Baren, J., Hillebrand, M., Joosse, M., Kwon, J. M., Nowotny, P., Che, L. K., Norton, J., Morris, J. C., Reed, L. A., Trojanowski, J., Basun, H., Lannfelt, L., Neystat, M., Fahn, S., Dark, F., Tannenberg, T., Dodd, P. R., Hayward, N., Kwok, J. B., Schofield, P. R., Andreadis, A., Snowden, J., Craufurd, D., Neary, D., Owen, F., Oostra, B. A., Hardy, J., Goate, A., van Swieten, J., Mann, D., Lynch, T., and Heutink, P. (1998) Association of missense and 5'-splice-site mutations in tau with the inherited dementia FTDP-17. *Nature* **393**, 702-705
106. Rizzu, P., Van Swieten, J. C., Joosse, M., Hasegawa, M., Stevens, M., Tibben, A., Niermeijer, M. F., Hillebrand, M., Ravid, R., Oostra, B. A., Goedert, M., van Duijn, C. M., and Heutink, P. (1999) High prevalence of mutations in the microtubule-associated protein tau in a population study of frontotemporal dementia in the Netherlands. *Am J Hum Genet* **64**, 414-421
107. Ros, R., Thobois, S., Streichenberger, N., Kopp, N., Sanchez, M. P., Perez, M., Hoenicka, J., Avila, J., Honnorat, J., and de Yebenes, J. G. (2005) A new mutation of the tau gene, G303V, in early-onset familial progressive supranuclear palsy. *Arch Neurol* **62**, 1444-1450
108. Villa, C., Ghezzi, L., Pietroboni, A. M., Fenoglio, C., Cortini, F., Serpente, M., Cantoni, C., Ridolfi, E., Marcone, A., Benussi, L., Ghidoni, R., Jacini, F., Arighi, A., Fumagalli, G. G., Mandelli, A., Binetti, G., Cappa, S., Bresolin, N., Scarpini, E., and Galimberti, D. (2011) A novel MAPT mutation associated with the clinical phenotype of progressive nonfluent aphasia. *J Alzheimers Dis* **26**, 19-26
109. Iijima, M., Tabira, T., Poorkaj, P., Schellenberg, G. D., Trojanowski, J. Q., Lee, V. M., Schmidt, M. L., Takahashi, K., Nabika, T., Matsumoto, T., Yamashita, Y., Yoshioka, S., and Ishino, H. (1999) A distinct familial presenile dementia with a novel missense mutation in the tau gene. *Neuroreport* **10**, 497-501
110. Kobayashi, K., Hayashi, M., Kidani, T., Nakano, H., Miyazu, K., Ujike, H., Kuroda, S., and Koshino, Y. (2002) Pick's disease in 2 brothers with S305N mutation: note in supplement to an earlier communication. *Clin Neuropathol* **21**, 191-193
111. Kovacs, G. G., Pittman, A., Revesz, T., Luk, C., Lees, A., Kiss, E., Tariska, P., Laszlo, L., Molnar, K., Molnar, M. J., Tolnay, M., and de Silva, R. (2008) MAPT S305I mutation: implications for argyrophilic grain disease. *Acta Neuropathol* **116**, 103-118
112. van Herpen, E., Rosso, S. M., Serverijnen, L. A., Yoshida, H., Breedveld, G., van de Graaf, R., Kamphorst, W., Ravid, R., Willemsen, R., Dooijes, D., Majoor-Krakauer, D., Kros, J. M., Crowther, R. A., Goedert, M., Heutink, P., and van Swieten, J. C. (2003) Variable phenotypic expression and extensive tau pathology in two families with the novel tau mutation L315R. *Ann Neurol* **54**, 573-581
113. Zarranz, J. J., Ferrer, I., Lezcano, E., Forcadas, M. I., Eizaguirre, B., Atares, B., Puig, B., Gomez-Esteban, J. C., Fernandez-Maiztegui, C., Rouco, I., Perez-Concha, T., Fernandez, M., Rodriguez, O., Rodriguez-Martinez, A. B., de Pancorbo, M. M., Pastor, P., and Perez-Tur, J. (2005) A novel mutation (K317M) in the MAPT gene causes FTDP and motor neuron disease. *Neurology* **64**, 1578-1585
114. Tacik, P., DeTure, M., Lin, W. L., Sanchez Contreras, M., Wojtas, A., Hinkle, K. M., Fujioka, S., Baker, M. C., Walton, R. L., Carlomagno, Y., Brown, P. H., Strongosky, A. J., Kouri, N., Murray, M. E., Petrucelli, L., Josephs, K. A., Rademakers, R., Ross, O. A.,

Wszolek, Z. K., and Dickson, D. W. (2015) A novel tau mutation, p.K317N, causes globular glial tauopathy. *Acta Neuropathol* **130**, 199-214
115. Rosso, S. M., van Herpen, E., Deelen, W., Kamphorst, W., Severijnen, L. A., Willemsen, R., Ravid, R., Niermeijer, M. F., Dooijes, D., Smith, M. J., Goedert, M., Heutink, P., and van Swieten, J. C. (2002) A novel tau mutation, S320F, causes a tauopathy with inclusions similar to those in Pick's disease. *Ann Neurol* **51**, 373-376
116. Deramecourt, V., Lebert, F., Maurage, C. A., Fernandez-Gomez, F. J., Dujardin, S., Colin, M., Sergeant, N., Buee-Scherrer, V., Clot, F., Ber, I. L., Brice, A., Pasquier, F., and Buee, L. (2012) Clinical, neuropathological, and biochemical characterization of the novel tau mutation P332S. *J Alzheimers Dis* **31**, 741-749
117. Spina, S., Murrell, J. R., Yoshida, H., Ghetti, B., Bermingham, N., Sweeney, B., Dlouhy, S. R., Crowther, R. A., Goedert, M., and Keohane, C. (2007) The novel Tau mutation G335S: clinical, neuropathological and molecular characterization. *Acta Neuropathol* **113**, 461-470
118. Neumann, M., Diekmann, S., Bertsch, U., Vanmassenhove, B., Bogerts, B., and Kretzschmar, H. A. (2005) Novel G335V mutation in the tau gene associated with early onset familial frontotemporal dementia. *Neurogenetics* **6**, 91-95
119. Pickering-Brown, S. M., Baker, M., Nonaka, T., Ikeda, K., Sharma, S., Mackenzie, J., Simpson, S. A., Moore, J. W., Snowden, J. S., de Silva, R., Revesz, T., Hasegawa, M., Hutton, M., and Mann, D. M. (2004) Frontotemporal dementia with Pick-type histology associated with Q336R mutation in the tau gene. *Brain* **127**, 1415-1426
120. Tacik, P., DeTure, M., Hinkle, K. M., Lin, W. L., Sanchez-Contreras, M., Carlomagno, Y., Pedraza, O., Rademakers, R., Ross, O. A., Wszolek, Z. K., and Dickson, D. W. (2015) A Novel Tau Mutation in Exon 12, p.Q336H, Causes Hereditary Pick Disease. *J Neuropathol Exp Neurol* **74**, 1042-1052
121. Han, D., Qureshi, H. Y., Lu, Y., and Paudel, H. K. (2009) Familial FTDP-17 missense mutations inhibit microtubule assembly-promoting activity of tau by increasing phosphorylation at Ser202 in vitro. *J Biol Chem* **284**, 13422-13433
122. Lippa, C. F., Zhukareva, V., Kawarai, T., Uryu, K., Shafiq, M., Nee, L. E., Grafman, J., Liang, Y., St George-Hyslop, P. H., Trojanowski, J. Q., and Lee, V. M. (2000) Frontotemporal dementia with novel tau pathology and a Glu342Val tau mutation. *Ann Neurol* **48**, 850-858
123. Combs, B., and Gamblin, T. C. (2012) FTDP-17 tau mutations induce distinct effects on aggregation and microtubule interactions. *Biochemistry* **51**, 8597-8607
124. Nicholl, D. J., Greenstone, M. A., Clarke, C. E., Rizzu, P., Crooks, D., Crowe, A., Trojanowski, J. Q., Lee, V. M., and Heutink, P. (2003) An English kindred with a novel recessive tauopathy and respiratory failure. *Ann Neurol* **54**, 682-686
125. Momeni, P., Wickremaratchi, M. M., Bell, J., Arnold, R., Beer, R., Hardy, J., Revesz, T., Neal, J. W., and Morris, H. R. (2010) Familial early onset frontotemporal dementia caused by a novel S356T MAPT mutation, initially diagnosed as schizophrenia. *Clin Neurol Neurosurg* **112**, 917-920
126. Anfossi, M., Bernardi, L., Gallo, M., Geracitano, S., Colao, R., Puccio, G., Curcio, S. A., Frangipane, F., Mirabelli, M., Tomaino, C., Smirne, N., Maletta, R., and Bruni, A. C. (2011) MAPT V363I variation in a sporadic case of frontotemporal dementia: variable penetrant mutation or rare polymorphism? *Alzheimer Dis Assoc Disord* **25**, 96-99
127. Rossi, G., Bastone, A., Piccoli, E., Morbin, M., Mazzoleni, G., Fugnanesi, V., Beeg, M., Del Favero, E., Cantu, L., Motta, S., Salsano, E., Pareyson, D., Erbetta, A., Elia, A. E., Del Sorbo, F., Silani, V., Morelli, C., Salmona, M., and Tagliavini, F. (2014) Different mutations at V363 MAPT codon are associated with atypical clinical phenotypes and show unusual structural and functional features. *Neurobiol Aging* **35**, 408-417
128. Rossi, G., Bastone, A., Piccoli, E., Mazzoleni, G., Morbin, M., Uggetti, A., Giaccone, G., Sperber, S., Beeg, M., Salmona, M., and Tagliavini, F. (2012) New mutations in MAPT gene causing frontotemporal lobar degeneration: biochemical and structural characterization. *Neurobiol Aging* **33**, 834 e831-836

129. Rossi, G., Conconi, D., Panzeri, E., Redaelli, S., Piccoli, E., Paoletta, L., Dalpra, L., and Tagliavini, F. (2013) Mutations in MAPT gene cause chromosome instability and introduce copy number variations widely in the genome. *J Alzheimers Dis* **33**, 969-982
130. Neumann, M., Schulz-Schaeffer, W., Crowther, R. A., Smith, M. J., Spillantini, M. G., Goedert, M., and Kretzschmar, H. A. (2001) Pick's disease associated with the novel Tau gene mutation K369I. *Ann Neurol* **50**, 503-513
131. Tacik, P., DeTure, M. A., Carlomagno, Y., Lin, W. L., Murray, M. E., Baker, M. C., Josephs, K. A., Boeve, B. F., Wszolek, Z. K., Graff-Radford, N. R., Parisi, J. E., Petrucelli, L., Rademakers, R., Isaacson, R. S., Heilman, K. M., Petersen, R. C., Dickson, D. W., and Kouri, N. (2017) FTDP-17 with Pick body-like inclusions associated with a novel tau mutation, p.E372G. *Brain Pathol* **27**, 612-626
132. Chaunu, M. P., Deramecourt, V., Buee-Scherrer, V., Le Ber, I., Brice, A., Ehrle, N., El Hachimi, K., Pluot, M., Maurage, C. A., Bakchine, S., and Buee, L. (2013) Juvenile frontotemporal dementia with parkinsonism associated with tau mutation G389R. *J Alzheimers Dis* **37**, 769-776
133. Ghetti, B., Murrell, J. R., Zolo, P., Spillantini, M. G., and Goedert, M. (2000) Progress in hereditary tauopathies: a mutation in the Tau gene (G389R) causes a Pick disease-like syndrome. *Ann N Y Acad Sci* **920**, 52-62
134. Rossi, G., Marelli, C., Farina, L., Laura, M., Maria Basile, A., Ciano, C., Tagliavini, F., and Pareyson, D. (2008) The G389R mutation in the MAPT gene presenting as sporadic corticobasal syndrome. *Mov Disord* **23**, 892-895
135. Pickering-Brown, S., Baker, M., Yen, S. H., Liu, W. K., Hasegawa, M., Cairns, N., Lantos, P. L., Rossor, M., Iwatsubo, T., Davies, Y., Allsop, D., Furlong, R., Owen, F., Hardy, J., Mann, D., and Hutton, M. (2000) Pick's disease is associated with mutations in the tau gene. *Ann Neurol* **48**, 859-867
136. Murrell, J. R., Spillantini, M. G., Zolo, P., Guazzelli, M., Smith, M. J., Hasegawa, M., Redi, F., Crowther, R. A., Pietrini, P., Ghetti, B., and Goedert, M. (1999) Tau gene mutation G389R causes a tauopathy with abundant pick body-like inclusions and axonal deposits. *J Neuropathol Exp Neurol* **58**, 1207-1226
137. Lindquist, S. G., Holm, I. E., Schwartz, M., Law, I., Stokholm, J., Batbayli, M., Waldemar, G., and Nielsen, J. E. (2008) Alzheimer disease-like clinical phenotype in a family with FTDP-17 caused by a MAPT R406W mutation. *Eur J Neurol* **15**, 377-385
138. Kouri, N., Carlomagno, Y., Baker, M., Liesinger, A. M., Caselli, R. J., Wszolek, Z. K., Petrucelli, L., Boeve, B. F., Parisi, J. E., Josephs, K. A., Uitti, R. J., Ross, O. A., Graff-Radford, N. R., DeTure, M. A., Dickson, D. W., and Rademakers, R. (2014) Novel mutation in MAPT exon 13 (p.N410H) causes corticobasal degeneration. *Acta Neuropathol* **127**, 271-282
139. Giaccone, G., Rossi, G., Farina, L., Marcon, G., Di Fede, G., Catania, M., Morbin, M., Sacco, L., Bugiani, O., and Tagliavini, F. (2005) Familial frontotemporal dementia associated with the novel MAPT mutation T427M. *J Neurol* **252**, 1543-1545
140. Anfossi, M., Vuono, R., Maletta, R., Virdee, K., Mirabelli, M., Colao, R., Puccio, G., Bernardi, L., Frangipane, F., Gallo, M., Geracitano, S., Tomaino, C., Curcio, S. A., Zannino, G., Lamenza, F., Duyckaerts, C., Spillantini, M. G., Losso, M. A., and Bruni, A. C. (2011) Compound heterozygosity of 2 novel MAPT mutations in frontotemporal dementia. *Neurobiol Aging* **32**, 757 e751-757 e711
141. Malkani, R., D'Souza, I., Gwinn-Hardy, K., Schellenberg, G. D., Hardy, J., and Momeni, P. (2006) A MAPT mutation in a regulatory element upstream of exon 10 causes frontotemporal dementia. *Neurobiol Dis* **22**, 401-403
142. D'Souza, I., Poorkaj, P., Hong, M., Nochlin, D., Lee, V. M., Bird, T. D., and Schellenberg, G. D. (1999) Missense and silent tau gene mutations cause frontotemporal dementia with parkinsonism-chromosome 17 type, by affecting multiple alternative RNA splicing regulatory elements. *Proc Natl Acad Sci U S A* **96**, 5598-5603
143. Poorkaj, P., Grossman, M., Steinbart, E., Payami, H., Sadovnick, A., Nochlin, D., Tabira, T., Trojanowski, J. Q., Borson, S., Galasko, D., Reich, S., Quinn, B., Schellenberg, G.,

and Bird, T. D. (2001) Frequency of tau gene mutations in familial and sporadic cases of non-Alzheimer dementia. *Arch Neurol* **58**, 383-387
144. Rohrer, J. D., Guerreiro, R., Vandrovcova, J., Uphill, J., Reiman, D., Beck, J., Isaacs, A. M., Authier, A., Ferrari, R., Fox, N. C., Mackenzie, I. R., Warren, J. D., de Silva, R., Holton, J., Revesz, T., Hardy, J., Mead, S., and Rossor, M. N. (2009) The heritability and genetics of frontotemporal lobar degeneration. *Neurology* **73**, 1451-1456
145. Spillantini, M. G., Yoshida, H., Rizzini, C., Lantos, P. L., Khan, N., Rossor, M. N., Goedert, M., and Brown, J. (2000) A novel tau mutation (N296N) in familial dementia with swollen achromatic neurons and corticobasal inclusion bodies. *Ann Neurol* **48**, 939-943
146. Miyamoto, K., Kowalska, A., Hasegawa, M., Tabira, T., Takahashi, K., Araki, W., Akiguchi, I., and Ikemoto, A. (2001) Familial frontotemporal dementia and parkinsonism with a novel mutation at an intron 10+11-splice site in the tau gene. *Ann Neurol* **50**, 117-120
147. Ronnback, A., Nennesmo, I., Tuominen, H., Grueninger, F., Viitanen, M., and Graff, C. (2014) Neuropathological characterization of two siblings carrying the MAPT S305S mutation demonstrates features resembling argyrophilic grain disease. *Acta Neuropathol* **127**, 297-298
148. Skoglund, L., Viitanen, M., Kalimo, H., Lannfelt, L., Jonhagen, M. E., Ingelsson, M., Glaser, A., and Herva, R. (2008) The tau S305S mutation causes frontotemporal dementia with parkinsonism. *Eur J Neurol* **15**, 156-161
149. Stanford, P. M., Halliday, G. M., Brooks, W. S., Kwok, J. B., Storey, C. E., Creasey, H., Morris, J. G., Fulham, M. J., and Schofield, P. R. (2000) Progressive supranuclear palsy pathology caused by a novel silent mutation in exon 10 of the tau gene: expansion of the disease phenotype caused by tau gene mutations. *Brain* **123 (Pt 5)**, 880-893
150. Deters, K. D., Risacher, S. L., Farlow, M. R., Unverzagt, F. W., Kareken, D. A., Hutchins, G. D., Yoder, K. K., Murrell, J. R., Spina, S., Epperson, F., Gao, S., Saykin, A. J., and Ghetti, B. (2014) Cerebral hypometabolism and grey matter density in MAPT intron 10 +3 mutation carriers. *Am J Neurodegener Dis* **3**, 103-114
151. Spina, S., Farlow, M. R., Unverzagt, F. W., Kareken, D. A., Murrell, J. R., Fraser, G., Epperson, F., Crowther, R. A., Spillantini, M. G., Goedert, M., and Ghetti, B. (2008) The tauopathy associated with mutation +3 in intron 10 of Tau: characterization of the MSTD family. *Brain* **131**, 72-89
152. Kowalska, A., Hasegawa, M., Miyamoto, K., Akiguchi, I., Ikemoto, A., Takahashi, K., Araki, W., and Tabira, T. (2002) A novel mutation at position +11 in the intron following exon 10 of the tau gene in FTDP-17. *J Appl Genet* **43**, 535-543
153. Yasuda, M., Takamatsu, J., D'Souza, I., Crowther, R. A., Kawamata, T., Hasegawa, M., Hasegawa, H., Spillantini, M. G., Tanimukai, S., Poorkaj, P., Varani, L., Varani, G., Iwatsubo, T., Goedert, M., Schellenberg, D. G., and Tanaka, C. (2000) A novel mutation at position +12 in the intron following exon 10 of the tau gene in familial frontotemporal dementia (FTD-Kumamoto). *Ann Neurol* **47**, 422-429
154. Morris, H. R., Khan, M. N., Janssen, J. C., Brown, J. M., Perez-Tur, J., Baker, M., Ozansoy, M., Hardy, J., Hutton, M., Wood, N. W., Lees, A. J., Revesz, T., Lantos, P., and Rossor, M. N. (2001) The genetic and pathological classification of familial frontotemporal dementia. *Arch Neurol* **58**, 1813-1816
155. Rodriguez-Martin, T., Anthony, K., Garcia-Blanco, M. A., Mansfield, S. G., Anderton, B. H., and Gallo, J. M. (2009) Correction of tau mis-splicing caused by FTDP-17 MAPT mutations by spliceosome-mediated RNA trans-splicing. *Hum Mol Genet* **18**, 3266-3273
156. Varani, L., Hasegawa, M., Spillantini, M. G., Smith, M. J., Murrell, J. R., Ghetti, B., Klug, A., Goedert, M., and Varani, G. (1999) Structure of tau exon 10 splicing regulatory element RNA and destabilization by mutations of frontotemporal dementia and parkinsonism linked to chromosome 17. *Proc Natl Acad Sci U S A* **96**, 8229-8234
157. McCarthy, A., Lonergan, R., Olszewska, D. A., O'Dowd, S., Cummins, G., Magennis, B., Fallon, E. M., Pender, N., Huey, E. D., Cosentino, S., O'Rourke, K., Kelly, B. D., O'Connell, M., Delon, I., Farrell, M., Spillantini, M. G., Rowland, L. P., Fahn, S., Craig, P.,

Hutton, M., and Lynch, T. (2015) Closing the tau loop: the missing tau mutation. *Brain* **138**, 3100-3109
158. Larner, A. J. (2009) Intrafamilial clinical phenotypic heterogeneity with MAPT gene splice site IVS10+16C>T mutation. *J Neurol Sci* **287**, 253-256
159. Stanford, P. M., Shepherd, C. E., Halliday, G. M., Brooks, W. S., Schofield, P. W., Brodaty, H., Martins, R. N., Kwok, J. B., and Schofield, P. R. (2003) Mutations in the tau gene that cause an increase in three repeat tau and frontotemporal dementia. *Brain* **126**, 814-826
160. Roks, G., Dermaut, B., Heutink, P., Julliams, A., Backhovens, H., Van de Broeck, M., Serneels, S., Hofman, A., Van Broeckhoven, C., van Duijn, C. M., and Cruts, M. (1999) Mutation screening of the tau gene in patients with early-onset Alzheimer's disease. *Neurosci Lett* **277**, 137-139
161. Bullido, M. J., Aldudo, J., Frank, A., Coria, F., Avila, J., and Valdivieso, F. (2000) A polymorphism in the tau gene associated with risk for Alzheimer's disease. *Neurosci Lett* **278**, 49-52
162. Momeni, P., Pittman, A., Lashley, T., Vandrovcova, J., Malzer, E., Luk, C., Hulette, C., Lees, A., Revesz, T., Hardy, J., and de Silva, R. (2009) Clinical and pathological features of an Alzheimer's disease patient with the MAPT Delta K280 mutation. *Neurobiol Aging* **30**, 388-393
163. D'Souza, I., and Schellenberg, G. D. (2002) tau Exon 10 expression involves a bipartite intron 10 regulatory sequence and weak 5' and 3' splice sites. *J Biol Chem* **277**, 26587-26599
164. Larini, L., Gessel, M. M., LaPointe, N. E., Do, T. D., Bowers, M. T., Feinstein, S. C., and Shea, J. E. (2013) Initiation of assembly of tau(273-284) and its DeltaK280 mutant: an experimental and computational study. *Phys Chem Chem Phys* **15**, 8916-8928
165. Pastor, P., Pastor, E., Carnero, C., Vela, R., Garcia, T., Amer, G., Tolosa, E., and Oliva, R. (2001) Familial atypical progressive supranuclear palsy associated with homozigosity for the delN296 mutation in the tau gene. *Ann Neurol* **49**, 263-267
166. Magnani, E., Fan, J., Gasparini, L., Golding, M., Williams, M., Schiavo, G., Goedert, M., Amos, L. A., and Spillantini, M. G. (2007) Interaction of tau protein with the dynactin complex. *EMBO J* **26**, 4546-4554
167. Rossi, G., and Tagliavini, F. (2015) Frontotemporal lobar degeneration: old knowledge and new insight into the pathogenetic mechanisms of tau mutations. *Front Aging Neurosci* **7**, 192
168. Czech, A., Fedyunin, I., Zhang, G., and Ignatova, Z. (2010) Silent mutations in sight: co-variations in tRNA abundance as a key to unravel consequences of silent mutations. *Mol Biosyst* **6**, 1767-1772
169. Cruts, M., Theuns, J., and Van Broeckhoven, C. (2012) Locus-specific mutation databases for neurodegenerative brain diseases. *Hum Mutat* **33**, 1340-1344
170. Alonso Adel, C., Mederlyova, A., Novak, M., Grundke-Iqbal, I., and Iqbal, K. (2004) Promotion of hyperphosphorylation by frontotemporal dementia tau mutations. *J Biol Chem* **279**, 34873-34881
171. von Bergen, M., Barghorn, S., Li, L., Marx, A., Biernat, J., Mandelkow, E. M., and Mandelkow, E. (2001) Mutations of tau protein in frontotemporal dementia promote aggregation of paired helical filaments by enhancing local beta-structure. *J Biol Chem* **276**, 48165-48174
172. Barghorn, S., Zheng-Fischhofer, Q., Ackmann, M., Biernat, J., von Bergen, M., Mandelkow, E. M., and Mandelkow, E. (2000) Structure, microtubule interactions, and paired helical filament aggregation by tau mutants of frontotemporal dementias. *Biochemistry* **39**, 11714-11721
173. Hoover, B. R., Reed, M. N., Su, J., Penrod, R. D., Kotilinek, L. A., Grant, M. K., Pitstick, R., Carlson, G. A., Lanier, L. M., Yuan, L. L., Ashe, K. H., and Liao, D. (2010) Tau mislocalization to dendritic spines mediates synaptic dysfunction independently of neurodegeneration. *Neuron* **68**, 1067-1081

174. Drechsel, D. N., Hyman, A. A., Cobb, M. H., and Kirschner, M. W. (1992) Modulation of the dynamic instability of tubulin assembly by the microtubule-associated protein tau. *Mol Biol Cell* **3**, 1141-1154
175. Butner, K. A., and Kirschner, M. W. (1991) Tau protein binds to microtubules through a flexible array of distributed weak sites. *J Cell Biol* **115**, 717-730
176. Brandt, R., and Lee, G. (1993) Functional organization of microtubule-associated protein tau. Identification of regions which affect microtubule growth, nucleation, and bundle formation in vitro. *J Biol Chem* **268**, 3414-3419
177. Goode, B. L., Denis, P. E., Panda, D., Radeke, M. J., Miller, H. P., Wilson, L., and Feinstein, S. C. (1997) Functional interactions between the proline-rich and repeat regions of tau enhance microtubule binding and assembly. *Mol Biol Cell* **8**, 353-365
178. Mukhopadhyay, R., and Hoh, J. H. (2001) AFM force measurements on microtubule-associated proteins: the projection domain exerts a long-range repulsive force. *FEBS Lett* **505**, 374-378
179. Chen, J., Kanai, Y., Cowan, N. J., and Hirokawa, N. (1992) Projection domains of MAP2 and tau determine spacings between microtubules in dendrites and axons. *Nature* **360**, 674-677
180. Amos, L. A. (2004) Microtubule structure and its stabilisation. *Org Biomol Chem* **2**, 2153-2160
181. Al-Bassam, J., Ozer, R. S., Safer, D., Halpain, S., and Milligan, R. A. (2002) MAP2 and tau bind longitudinally along the outer ridges of microtubule protofilaments. *J Cell Biol* **157**, 1187-1196
182. Igaev, M., Janning, D., Sundermann, F., Niewidok, B., Brandt, R., and Junge, W. (2014) A refined reaction-diffusion model of tau-microtubule dynamics and its application in FDAP analysis. *Biophys J* **107**, 2567-2578
183. Janning, D., Igaev, M., Sundermann, F., Bruhmann, J., Beutel, O., Heinisch, J. J., Bakota, L., Piehler, J., Junge, W., and Brandt, R. (2014) Single-molecule tracking of tau reveals fast kiss-and-hop interaction with microtubules in living neurons. *Mol Biol Cell* **25**, 3541-3551
184. Dixit, R., Ross, J. L., Goldman, Y. E., and Holzbaur, E. L. (2008) Differential regulation of dynein and kinesin motor proteins by tau. *Science* **319**, 1086-1089
185. Black, M. M., Slaughter, T., Moshiach, S., Obrocka, M., and Fischer, I. (1996) Tau is enriched on dynamic microtubules in the distal region of growing axons. *J Neurosci* **16**, 3601-3619
186. McVicker, D. P., Chrin, L. R., and Berger, C. L. (2011) The nucleotide-binding state of microtubules modulates kinesin processivity and the ability of Tau to inhibit kinesin-mediated transport. *J Biol Chem* **286**, 42873-42880
187. Hirokawa, N., Funakoshi, T., Sato-Harada, R., and Kanai, Y. (1996) Selective stabilization of tau in axons and microtubule-associated protein 2C in cell bodies and dendrites contributes to polarized localization of cytoskeletal proteins in mature neurons. *J Cell Biol* **132**, 667-679
188. Aronov, S., Aranda, G., Behar, L., and Ginzburg, I. (2001) Axonal tau mRNA localization coincides with tau protein in living neuronal cells and depends on axonal targeting signal. *J Neurosci* **21**, 6577-6587
189. Larcher, J. C., Gasmi, L., Viranaicken, W., Edde, B., Bernard, R., Ginzburg, I., and Denoulet, P. (2004) Ilf3 and NF90 associate with the axonal targeting element of Tau mRNA. *FASEB J* **18**, 1761-1763
190. Gauthier-Kemper, A., Weissmann, C., Golovyashkina, N., Sebo-Lemke, Z., Drewes, G., Gerke, V., Heinisch, J. J., and Brandt, R. (2011) The frontotemporal dementia mutation R406W blocks tau's interaction with the membrane in an annexin A2-dependent manner. *J Cell Biol* **192**, 647-661
191. Li, X., Kumar, Y., Zempel, H., Mandelkow, E. M., Biernat, J., and Mandelkow, E. (2011) Novel diffusion barrier for axonal retention of Tau in neurons and its failure in neurodegeneration. *EMBO J* **30**, 4825-4837

192. Paglini, G., Peris, L., Mascotti, F., Quiroga, S., and Caceres, A. (2000) Tau protein function in axonal formation. *Neurochem Res* **25**, 37-42
193. Dawson, H. N., Ferreira, A., Eyster, M. V., Ghoshal, N., Binder, L. I., and Vitek, M. P. (2001) Inhibition of neuronal maturation in primary hippocampal neurons from tau deficient mice. *J Cell Sci* **114**, 1179-1187
194. Caceres, A., and Kosik, K. S. (1990) Inhibition of neurite polarity by tau antisense oligonucleotides in primary cerebellar neurons. *Nature* **343**, 461-463
195. Sayas, C. L., Tortosa, E., Bollati, F., Ramirez-Rios, S., Arnal, I., and Avila, J. (2015) Tau regulates the localization and function of End-binding proteins 1 and 3 in developing neuronal cells. *J Neurochem* **133**, 653-667
196. Goode, B. L., Chau, M., Denis, P. E., and Feinstein, S. C. (2000) Structural and functional differences between 3-repeat and 4-repeat tau isoforms - Implications for normal tau function and the onset of neurodegenerative disease. *Journal of Biological Chemistry* **275**, 38182-38189
197. Gustke, N., Trinczek, B., Biernat, J., Mandelkow, E. M., and Mandelkow, E. (1994) Domains of Tau-Protein and Interactions with Microtubules. *Biochemistry* **33**, 9511-9522
198. Bunker, J. M., Wilson, L., Jordan, M. A., and Feinstein, S. C. (2004) Modulation of microtubule dynamics by tau in living cells: Implications for development and neurodegeneration. *Molecular Biology of the Cell* **15**, 2720-2728
199. Panda, D., Samuel, J. C., Massie, M., Feinstein, S. C., and Wilson, L. (2003) Differential regulation of microtubule dynamics by three- and four-repeat tau: Implications for the onset of neurodegenerative disease. *P Natl Acad Sci USA* **100**, 9548-9553
200. Semple, B. D., Blomgren, K., Gimlin, K., Ferriero, D. M., and Noble-Haeusslein, L. J. (2013) Brain development in rodents and humans: Identifying benchmarks of maturation and vulnerability to injury across species. *Prog Neurobiol* **106-107**, 1-16
201. Hanemaaijer, R., and Ginzburg, I. (1991) Involvement of mature tau isoforms in the stabilization of neurites in PC12 cells. *J Neurosci Res* **30**, 163-171
202. Liu, C., and Gotz, J. (2013) Profiling murine tau with 0N, 1N and 2N isoform-specific antibodies in brain and peripheral organs reveals distinct subcellular localization, with the 1N isoform being enriched in the nucleus. *PLoS One* **8**, e84849
203. Zempel, H., Dennissen, F. J. A., Kumar, Y., Luedtke, J., Biernat, J., Mandelkow, E. M., and Mandelkow, E. (2017) Axodendritic sorting and pathological missorting of Tau are isoform-specific and determined by axon initial segment architecture. *J Biol Chem* **292**, 12192-12207
204. Cingolani, L. A., and Goda, Y. (2008) Actin in action: the interplay between the actin cytoskeleton and synaptic efficacy. *Nat Rev Neurosci* **9**, 344-356
205. Moraga, D. M., Nunez, P., Garrido, J., and Maccioni, R. B. (1993) A tau fragment containing a repetitive sequence induces bundling of actin filaments. *J Neurochem* **61**, 979-986
206. Frandemiche, M. L., De Seranno, S., Rush, T., Borel, E., Elie, A., Arnal, I., Lante, F., and Buisson, A. (2014) Activity-dependent tau protein translocation to excitatory synapse is disrupted by exposure to amyloid-beta oligomers. *J Neurosci* **34**, 6084-6097
207. Kobayashi, S., Tanaka, T., Soeda, Y., Almeida, O. F. X., and Takashima, A. (2017) Local Somatodendritic Translation and Hyperphosphorylation of Tau Protein Triggered by AMPA and NMDA Receptor Stimulation. *EBioMedicine* **20**, 120-126
208. Mondragon-Rodriguez, S., Trillaud-Doppia, E., Dudilot, A., Bourgeois, C., Lauzon, M., Leclerc, N., and Boehm, J. (2012) Interaction of endogenous tau protein with synaptic proteins is regulated by N-methyl-D-aspartate receptor-dependent tau phosphorylation. *J Biol Chem* **287**, 32040-32053
209. Lee, G., Newman, S. T., Gard, D. L., Band, H., and Panchamoorthy, G. (1998) Tau interacts with src-family non-receptor tyrosine kinases. *J Cell Sci* **111 (Pt 21)**, 3167-3177
210. Tezuka, T., Umemori, H., Akiyama, T., Nakanishi, S., and Yamamoto, T. (1999) PSD-95 promotes Fyn-mediated tyrosine phosphorylation of the N-methyl-D-aspartate receptor subunit NR2A. *Proc Natl Acad Sci U S A* **96**, 435-440

211. Ittner, L. M., Ke, Y. D., Delerue, F., Bi, M., Gladbach, A., van Eersel, J., Wolfing, H., Chieng, B. C., Christie, M. J., Napier, I. A., Eckert, A., Staufenbiel, M., Hardeman, E., and Gotz, J. (2010) Dendritic function of tau mediates amyloid-beta toxicity in Alzheimer's disease mouse models. *Cell* **142**, 387-397
212. Regan, P., Piers, T., Yi, J. H., Kim, D. H., Huh, S., Park, S. J., Ryu, J. H., Whitcomb, D. J., and Cho, K. (2015) Tau phosphorylation at serine 396 residue is required for hippocampal LTD. *J Neurosci* **35**, 4804-4812
213. Biundo, F., Del Prete, D., Zhang, H., Arancio, O., and D'Adamio, L. (2018) A role for tau in learning, memory and synaptic plasticity. *Sci Rep* **8**, 3184
214. Pallas-Bazarra, N., Jurado-Arjona, J., Navarrete, M., Esteban, J. A., Hernandez, F., Avila, J., and Llorens-Martin, M. (2016) Novel function of Tau in regulating the effects of external stimuli on adult hippocampal neurogenesis. *EMBO J* **35**, 1417-1436
215. Lu, J., Li, T., He, R., Bartlett, P. F., and Gotz, J. (2014) Visualizing the microtubule-associated protein tau in the nucleus. *Sci China Life Sci* **57**, 422-431
216. Qi, H., Cantrelle, F. X., Benhelli-Mokrani, H., Smet-Nocca, C., Buee, L., Lippens, G., Bonnefoy, E., Galas, M. C., and Landrieu, I. (2015) Nuclear magnetic resonance spectroscopy characterization of interaction of Tau with DNA and its regulation by phosphorylation. *Biochemistry* **54**, 1525-1533
217. Violet, M., Delattre, L., Tardivel, M., Sultan, A., Chauderlier, A., Caillierez, R., Talahari, S., Nesslany, F., Lefebvre, B., Bonnefoy, E., Buee, L., and Galas, M. C. (2014) A major role for Tau in neuronal DNA and RNA protection in vivo under physiological and hyperthermic conditions. *Front Cell Neurosci* **8**, 84
218. Benhelli-Mokrani, H., Mansuroglu, Z., Chauderlier, A., Albaud, B., Gentien, D., Sommer, S., Schirmer, C., Laqueuvre, L., Josse, T., Buee, L., Lefebvre, B., Galas, M. C., Soues, S., and Bonnefoy, E. (2018) Genome-wide identification of genic and intergenic neuronal DNA regions bound by Tau protein under physiological and stress conditions. *Nucleic Acids Res* **46**, 11405-11422
219. Sultan, A., Nesslany, F., Violet, M., Begard, S., Loyens, A., Talahari, S., Mansuroglu, Z., Marzin, D., Sergeant, N., Humez, S., Colin, M., Bonnefoy, E., Buee, L., and Galas, M. C. (2011) Nuclear tau, a key player in neuronal DNA protection. *J Biol Chem* **286**, 4566-4575
220. Camero, S., Benitez, M. J., Cuadros, R., Hernandez, F., Avila, J., and Jimenez, J. S. (2014) Thermodynamics of the interaction between Alzheimer's disease related tau protein and DNA. *PLoS One* **9**, e104690
221. Mansuroglu, Z., Benhelli-Mokrani, H., Marcato, V., Sultan, A., Violet, M., Chauderlier, A., Delattre, L., Loyens, A., Talahari, S., Begard, S., Nesslany, F., Colin, M., Soues, S., Lefebvre, B., Buee, L., Galas, M. C., and Bonnefoy, E. (2016) Loss of Tau protein affects the structure, transcription and repair of neuronal pericentromeric heterochromatin. *Sci Rep* **6**, 33047
222. Rossi, G., Dalpra, L., Crosti, F., Lissoni, S., Sciacca, F. L., Catania, M., Di Fede, G., Mangieri, M., Giaccone, G., Croci, D., and Tagliavini, F. (2008) A new function of microtubule-associated protein tau: involvement in chromosome stability. *Cell Cycle* **7**, 1788-1794
223. Papasozomenos, S. C., and Binder, L. I. (1987) Phosphorylation determines two distinct species of Tau in the central nervous system. *Cell Motil Cytoskeleton* **8**, 210-226
224. Lopresti, P., Szuchet, S., Papasozomenos, S. C., Zinkowski, R. P., and Binder, L. I. (1995) Functional Implications for the Microtubule-Associated Protein-Tau - Localization in Oligodendrocytes. *P Natl Acad Sci USA* **92**, 10369-10373
225. Muller, R., Heinrich, M., Heck, S., Blohm, D., and Richter-Landsberg, C. (1997) Expression of microtubule-associated proteins MAP2 and tau in cultured rat brain oligodendrocytes. *Cell Tissue Res* **288**, 239-249
226. Ferrer, I. (2017) Diversity of astroglial responses across human neurodegenerative disorders and brain aging. *Brain Pathology* **27**, 645-674
227. Seiberlich, V., Bauer, N. G., Schwarz, L., Ffrench-Constant, C., Goldbaum, O., and Richter-Landsberg, C. (2015) Downregulation of the microtubule associated protein Tau

impairs process outgrowth and myelin basic protein mRNA transport in oligodendrocytes. *Glia* **63**, 1621-1635
228. LoPresti, P. (2015) Inducible Expression of a Truncated Form of Tau in Oligodendrocytes Elicits Gait Abnormalities and a Decrease in Myelin: Implications for Selective CNS Degenerative Diseases. *Neurochem Res* **40**, 2188-2199
229. Richter-Landsberg, C., and Gorath, M. (1999) Developmental regulation of alternatively spliced isoforms of mRNA encoding MAP2 and tau in rat brain oligodendrocytes during culture maturation. *J Neurosci Res* **56**, 259-270
230. Gorath, M., Stahnke, T., Mronga, T., Goldbaum, O., and Richter-Landsberg, C. (2001) Developmental changes of tau protein and mRNA in cultured rat brain oligodendrocytes. *Glia* **36**, 89-101
231. LoPresti, P. (2018) Tau in Oligodendrocytes Takes Neurons in Sickness and in Health. *Int J Mol Sci* **19**
232. Leugers, C. J., and Lee, G. (2010) Tau potentiates nerve growth factor-induced mitogen-activated protein kinase signaling and neurite initiation without a requirement for microtubule binding. *J Biol Chem* **285**, 19125-19134
233. Pooler, A. M., Usardi, A., Evans, C. J., Philpott, K. L., Noble, W., and Hanger, D. P. (2012) Dynamic association of tau with neuronal membranes is regulated by phosphorylation. *Neurobiol Aging* **33**, 431 e427-438
234. Abisambra, J. F., Jinwal, U. K., Blair, L. J., O'Leary, J. C., 3rd, Li, Q., Brady, S., Wang, L., Guidi, C. E., Zhang, B., Nordhues, B. A., Cockman, M., Suntharalingham, A., Li, P., Jin, Y., Atkins, C. A., and Dickey, C. A. (2013) Tau accumulation activates the unfolded protein response by impairing endoplasmic reticulum-associated degradation. *J Neurosci* **33**, 9498-9507
235. Farah, C. A., Perreault, S., Liazoghli, D., Desjardins, M., Anton, A., Lauzon, M., Paiement, J., and Leclerc, N. (2006) Tau interacts with Golgi membranes and mediates their association with microtubules. *Cell Motil Cytoskeleton* **63**, 710-724
236. Tang, Z., Ioja, E., Bereczki, E., Hultenby, K., Li, C., Guan, Z., Winblad, B., and Pei, J. J. (2015) mTor mediates tau localization and secretion: Implication for Alzheimer's disease. *Biochim Biophys Acta* **1853**, 1646-1657
237. Mietelska-Porowska, A., Wasik, U., Goras, M., Filipek, A., and Niewiadomska, G. (2014) Tau protein modifications and interactions: their role in function and dysfunction. *Int J Mol Sci* **15**, 4671-4713
238. Mandelkow, E. M., Drewes, G., Biernat, J., Gustke, N., Van Lint, J., Vandenheede, J. R., and Mandelkow, E. (1992) Glycogen synthase kinase-3 and the Alzheimer-like state of microtubule-associated protein tau. *FEBS Lett* **314**, 315-321
239. Kobayashi, S., Ishiguro, K., Omori, A., Takamatsu, M., Arioka, M., Imahori, K., and Uchida, T. (1993) A cdc2-related kinase PSSALRE/cdk5 is homologous with the 30 kDa subunit of tau protein kinase II, a proline-directed protein kinase associated with microtubule. *FEBS Lett* **335**, 171-175
240. Yoshida, H., and Goedert, M. (2006) Sequential phosphorylation of tau protein by cAMP-dependent protein kinase and SAPK4/p38delta or JNK2 in the presence of heparin generates the AT100 epitope. *J Neurochem* **99**, 154-164
241. Baudier, J., and Cole, R. D. (1987) Phosphorylation of tau proteins to a state like that in Alzheimer's brain is catalyzed by a calcium/calmodulin-dependent kinase and modulated by phospholipids. *J Biol Chem* **262**, 17577-17583
242. Park, S., Lee, J. H., Jeon, J. H., and Lee, M. J. (2018) Degradation or aggregation: the ramifications of post-translational modifications on tau. *BMB Rep* **51**, 265-273
243. Ramirez-Rios, S., Denarier, E., Prezel, E., Vinit, A., Stoppin-Mellet, V., Devred, F., Barbier, P., Peyrot, V., Sayas, C. L., Avila, J., Peris, L., Andrieux, A., Serre, L., Fourest-Lieuvin, A., and Arnal, I. (2016) Tau antagonizes end-binding protein tracking at microtubule ends through a phosphorylation-dependent mechanism. *Mol Biol Cell* **27**, 2924-2934

244. Maas, T., Eidenmuller, J., and Brandt, R. (2000) Interaction of tau with the neural membrane cortex is regulated by phosphorylation at sites that are modified in paired helical filaments. *J Biol Chem* **275**, 15733-15740
245. Mandell, J. W., and Banker, G. A. (1996) A spatial gradient of tau protein phosphorylation in nascent axons. *J Neurosci* **16**, 5727-5740
246. Arendt, T., Stieler, J., Strijkstra, A. M., Hut, R. A., Rudiger, J., Van der Zee, E. A., Harkany, T., Holzer, M., and Hartig, W. (2003) Reversible paired helical filament-like phosphorylation of tau is an adaptive process associated with neuronal plasticity in hibernating animals. *J Neurosci* **23**, 6972-6981
247. Stieler, J. T., Bullmann, T., Kohl, F., Toien, O., Bruckner, M. K., Hartig, W., Barnes, B. M., and Arendt, T. (2011) The physiological link between metabolic rate depression and tau phosphorylation in mammalian hibernation. *PLoS One* **6**, e14530
248. Arendt, T., and Bullmann, T. (2013) Neuronal plasticity in hibernation and the proposed role of the microtubule-associated protein tau as a "master switch" regulating synaptic gain in neuronal networks. *Am J Physiol Regul Integr Comp Physiol* **305**, R478-489
249. Kelleher, I., Garwood, C., Hanger, D. P., Anderton, B. H., and Noble, W. (2007) Kinase activities increase during the development of tauopathy in htau mice. *J Neurochem* **103**, 2256-2267
250. Yu, Y., Run, X., Liang, Z., Li, Y., Liu, F., Liu, Y., Iqbal, K., Grundke-Iqbal, I., and Gong, C. X. (2009) Developmental regulation of tau phosphorylation, tau kinases, and tau phosphatases. *J Neurochem* **108**, 1480-1494
251. Stefanoska, K., Volkerling, A., Bertz, J., Poljak, A., Ke, Y. D., Ittner, L. M., and Ittner, A. (2018) An N-terminal motif unique to primate tau enables differential protein-protein interactions. *J Biol Chem* **293**, 3710-3719
252. Grundke-Iqbal, I., Iqbal, K., Tung, Y. C., Quinlan, M., Wisniewski, H. M., and Binder, L. I. (1986) Abnormal phosphorylation of the microtubule-associated protein tau (tau) in Alzheimer cytoskeletal pathology. *Proc Natl Acad Sci U S A* **83**, 4913-4917
253. Li, T., Hawkes, C., Qureshi, H. Y., Kar, S., and Paudel, H. K. (2006) Cyclin-dependent protein kinase 5 primes microtubule-associated protein tau site-specifically for glycogen synthase kinase 3beta. *Biochemistry* **45**, 3134-3145
254. Li, T., and Paudel, H. K. (2006) Glycogen synthase kinase 3beta phosphorylates Alzheimer's disease-specific Ser396 of microtubule-associated protein tau by a sequential mechanism. *Biochemistry* **45**, 3125-3133
255. Jho, Y. S., Zhulina, E. B., Kim, M. W., and Pincus, P. A. (2010) Monte carlo simulations of tau proteins: effect of phosphorylation. *Biophys J* **99**, 2387-2397
256. Fischer, D., Mukrasch, M. D., Biernat, J., Bibow, S., Blackledge, M., Griesinger, C., Mandelkow, E., and Zweckstetter, M. (2009) Conformational changes specific for pseudophosphorylation at serine 262 selectively impair binding of tau to microtubules. *Biochemistry* **48**, 10047-10055
257. Jeganathan, S., von Bergen, M., Brutlach, H., Steinhoff, H. J., and Mandelkow, E. (2006) Global hairpin folding of tau in solution. *Biochemistry* **45**, 2283-2293
258. von Bergen, M., Friedhoff, P., Biernat, J., Heberle, J., Mandelkow, E. M., and Mandelkow, E. (2000) Assembly of tau protein into Alzheimer paired helical filaments depends on a local sequence motif ((306)VQIVYK(311)) forming beta structure. *Proc Natl Acad Sci U S A* **97**, 5129-5134
259. Lathuilière, A., Valdés, P., Papin, S., Cacquevel, M., Maclachlan, C., Knott, G. W., Muhs, A., Paganetti, P., and Schneider, B. L. (2017) Motifs in the tau protein that control binding to microtubules and aggregation determine pathological effects. *Sci Rep* **7**, 13556
260. Alonso, A. C., Grundke-Iqbal, I., and Iqbal, K. (1996) Alzheimer's disease hyperphosphorylated tau sequesters normal tau into tangles of filaments and disassembles microtubules. *Nat Med* **2**, 783-787
261. Kanaan, N. M., Morfini, G. A., LaPointe, N. E., Pigino, G. F., Patterson, K. R., Song, Y., Andreadis, A., Fu, Y., Brady, S. T., and Binder, L. I. (2011) Pathogenic forms of tau inhibit kinesin-dependent axonal transport through a mechanism involving activation of axonal phosphotransferases. *J Neurosci* **31**, 9858-9868

262. Cowan, C. M., and Mudher, A. (2013) Are tau aggregates toxic or protective in tauopathies? *Front Neurol* **4**, 114
263. Chirita, C. N., Congdon, E. E., Yin, H., and Kuret, J. (2005) Triggers of full-length tau aggregation: a role for partially folded intermediates. *Biochemistry* **44**, 5862-5872
264. Wille, H., Drewes, G., Biernat, J., Mandelkow, E. M., and Mandelkow, E. (1992) Alzheimer-like paired helical filaments and antiparallel dimers formed from microtubule-associated protein tau in vitro. *J Cell Biol* **118**, 573-584
265. Maeda, S., Sahara, N., Saito, Y., Murayama, M., Yoshiike, Y., Kim, H., Miyasaka, T., Murayama, S., Ikai, A., and Takashima, A. (2007) Granular tau oligomers as intermediates of tau filaments. *Biochemistry* **46**, 3856-3861
266. von Bergen, M., Barghorn, S., Biernat, J., Mandelkow, E. M., and Mandelkow, E. (2005) Tau aggregation is driven by a transition from random coil to beta sheet structure. *Biochim Biophys Acta* **1739**, 158-166
267. Crowther, R. A., and Goedert, M. (2000) Abnormal tau-containing filaments in neurodegenerative diseases. *J Struct Biol* **130**, 271-279
268. Crowther, R. A., and Wischik, C. M. (1985) Image reconstruction of the Alzheimer paired helical filament. *EMBO J* **4**, 3661-3665
269. Rankin, C. A., Sun, Q., and Gamblin, T. C. (2008) Pre-assembled tau filaments phosphorylated by GSK-3b form large tangle-like structures. *Neurobiol Dis* **31**, 368-377
270. Arriagada, P. V., Growdon, J. H., Hedley-Whyte, E. T., and Hyman, B. T. (1992) Neurofibrillary tangles but not senile plaques parallel duration and severity of Alzheimer's disease. *Neurology* **42**, 631-639
271. Giannakopoulos, P., Herrmann, F. R., Bussiere, T., Bouras, C., Kovari, E., Perl, D. P., Morrison, J. H., Gold, G., and Hof, P. R. (2003) Tangle and neuron numbers, but not amyloid load, predict cognitive status in Alzheimer's disease. *Neurology* **60**, 1495-1500
272. van Rossum, I. A., Visser, P. J., Knol, D. L., van der Flier, W. M., Teunissen, C. E., Barkhof, F., Blankenstein, M. A., and Scheltens, P. (2012) Injury markers but not amyloid markers are associated with rapid progression from mild cognitive impairment to dementia in Alzheimer's disease. *J Alzheimers Dis* **29**, 319-327
273. Jack, C. R., Jr., Wiste, H. J., Weigand, S. D., Therneau, T. M., Knopman, D. S., Lowe, V., Vemuri, P., Mielke, M. M., Roberts, R. O., Machulda, M. M., Senjem, M. L., Gunter, J. L., Rocca, W. A., and Petersen, R. C. (2017) Age-specific and sex-specific prevalence of cerebral beta-amyloidosis, tauopathy, and neurodegeneration in cognitively unimpaired individuals aged 50-95 years: a cross-sectional study. *Lancet Neurol* **16**, 435-444
274. Santacruz, K., Lewis, J., Spires, T., Paulson, J., Kotilinek, L., Ingelsson, M., Guimaraes, A., DeTure, M., Ramsden, M., McGowan, E., Forster, C., Yue, M., Orne, J., Janus, C., Mariash, A., Kuskowski, M., Hyman, B., Hutton, M., and Ashe, K. H. (2005) Tau suppression in a neurodegenerative mouse model improves memory function. *Science* **309**, 476-481
275. Morsch, R., Simon, W., and Coleman, P. D. (1999) Neurons may live for decades with neurofibrillary tangles. *J Neuropathol Exp Neurol* **58**, 188-197
276. Kumar, S., Tepper, K., Kaniyappan, S., Biernat, J., Wegmann, S., Mandelkow, E. M., Muller, D. J., and Mandelkow, E. (2014) Stages and conformations of the Tau repeat domain during aggregation and its effect on neuronal toxicity. *J Biol Chem* **289**, 20318-20332
277. Kimura, T., Fukuda, T., Sahara, N., Yamashita, S., Murayama, M., Mizoroki, T., Yoshiike, Y., Lee, B., Sotiropoulos, I., Maeda, S., and Takashima, A. (2010) Aggregation of detergent-insoluble tau is involved in neuronal loss but not in synaptic loss. *J Biol Chem* **285**, 38692-38699
278. de Calignon, A., Fox, L. M., Pitstick, R., Carlson, G. A., Bacskai, B. J., Spires-Jones, T. L., and Hyman, B. T. (2010) Caspase activation precedes and leads to tangles. *Nature* **464**, 1201-1204
279. Jarero-Basulto, J. J., Luna-Munoz, J., Mena, R., Kristofikova, Z., Ripova, D., Perry, G., Binder, L. I., and Garcia-Sierra, F. (2013) Proteolytic cleavage of polymeric tau protein by caspase-3: implications for Alzheimer disease. *J Neuropathol Exp Neurol* **72**, 1145-1161

280. Zhao, X., Kotilinek, L. A., Smith, B., Hlynialuk, C., Zahs, K., Ramsden, M., Cleary, J., and Ashe, K. H. (2016) Caspase-2 cleavage of tau reversibly impairs memory. *Nat Med* **22**, 1268-1276
281. Saito, Y., Ruberu, N. N., Sawabe, M., Arai, T., Tanaka, N., Kakuta, Y., Yamanouchi, H., and Murayama, S. (2004) Staging of argyrophilic grains: an age-associated tauopathy. *J Neuropathol Exp Neurol* **63**, 911-918
282. Williams, D. R., Holton, J. L., Strand, C., Pittman, A., de Silva, R., Lees, A. J., and Revesz, T. (2007) Pathological tau burden and distribution distinguishes progressive supranuclear palsy-parkinsonism from Richardson's syndrome. *Brain* **130**, 1566-1576
283. Braak, H., and Del Tredici, K. (2011) Alzheimer's pathogenesis: is there neuron-to-neuron propagation? *Acta Neuropathol* **121**, 589-595
284. Clavaguera, F., Akatsu, H., Fraser, G., Crowther, R. A., Frank, S., Hench, J., Probst, A., Winkler, D. T., Reichwald, J., Staufenbiel, M., Ghetti, B., Goedert, M., and Tolnay, M. (2013) Brain homogenates from human tauopathies induce tau inclusions in mouse brain. *Proc Natl Acad Sci U S A* **110**, 9535-9540
285. Yamada, K., Cirrito, J. R., Stewart, F. R., Jiang, H., Finn, M. B., Holmes, B. B., Binder, L. I., Mandelkow, E. M., Diamond, M. I., Lee, V. M., and Holtzman, D. M. (2011) In vivo microdialysis reveals age-dependent decrease of brain interstitial fluid tau levels in P301S human tau transgenic mice. *J Neurosci* **31**, 13110-13117
286. Goedert, M., Eisenberg, D. S., and Crowther, R. A. (2017) Propagation of Tau Aggregates and Neurodegeneration. *Annu Rev Neurosci* **40**, 189-210
287. Holmes, B. B., DeVos, S. L., Kfoury, N., Li, M., Jacks, R., Yanamandra, K., Ouidja, M. O., Brodsky, F. M., Marasa, J., Bagchi, D. P., Kotzbauer, P. T., Miller, T. M., Papy-Garcia, D., and Diamond, M. I. (2013) Heparan sulfate proteoglycans mediate internalization and propagation of specific proteopathic seeds. *Proc Natl Acad Sci U S A* **110**, E3138-3147
288. Wu, J. W., Hussaini, S. A., Bastille, I. M., Rodriguez, G. A., Mrejeru, A., Rilett, K., Sanders, D. W., Cook, C., Fu, H., Boonen, R. A., Herman, M., Nahmani, E., Emrani, S., Figueroa, Y. H., Diamond, M. I., Clelland, C. L., Wray, S., and Duff, K. E. (2016) Neuronal activity enhances tau propagation and tau pathology in vivo. *Nat Neurosci* **19**, 1085-1092
289. Asai, H., Ikezu, S., Tsunoda, S., Medalla, M., Luebke, J., Haydar, T., Wolozin, B., Butovsky, O., Kugler, S., and Ikezu, T. (2015) Depletion of microglia and inhibition of exosome synthesis halt tau propagation. *Nat Neurosci* **18**, 1584-1593
290. Fiandaca, M. S., Kapogiannis, D., Mapstone, M., Boxer, A., Eitan, E., Schwartz, J. B., Abner, E. L., Petersen, R. C., Federoff, H. J., Miller, B. L., and Goetzl, E. J. (2015) Identification of preclinical Alzheimer's disease by a profile of pathogenic proteins in neurally derived blood exosomes: A case-control study. *Alzheimers Dement* **11**, 600-607 e601
291. Sohn, P. D., Tracy, T. E., Son, H. I., Zhou, Y., Leite, R. E., Miller, B. L., Seeley, W. W., Grinberg, L. T., and Gan, L. (2016) Acetylated tau destabilizes the cytoskeleton in the axon initial segment and is mislocalized to the somatodendritic compartment. *Mol Neurodegener* **11**, 47
292. Miller, E. C., Teravskis, P. J., Dummer, B. W., Zhao, X., Huganir, R. L., and Liao, D. (2014) Tau phosphorylation and tau mislocalization mediate soluble Abeta oligomer-induced AMPA glutamate receptor signaling deficits. *Eur J Neurosci* **39**, 1214-1224
293. Tracy, T. E., and Gan, L. (2017) Acetylated tau in Alzheimer's disease: An instigator of synaptic dysfunction underlying memory loss: Increased levels of acetylated tau blocks the postsynaptic signaling required for plasticity and promotes memory deficits associated with tauopathy. *Bioessays* **39**
294. Miyamoto, T., Stein, L., Thomas, R., Djukic, B., Taneja, P., Knox, J., Vossel, K., and Mucke, L. (2017) Phosphorylation of tau at Y18, but not tau-fyn binding, is required for tau to modulate NMDA receptor-dependent excitotoxicity in primary neuronal culture. *Mol Neurodegener* **12**, 41
295. Zempel, H., Thies, E., Mandelkow, E., and Mandelkow, E. M. (2010) Abeta oligomers cause localized Ca(2+) elevation, missorting of endogenous Tau into dendrites, Tau

phosphorylation, and destruction of microtubules and spines. *J Neurosci* **30**, 11938-11950
296. Kim, T. S., Pae, C. U., Yoon, S. J., Jang, W. Y., Lee, N. J., Kim, J. J., Lee, S. J., Lee, C., Paik, I. H., and Lee, C. U. (2006) Decreased plasma antioxidants in patients with Alzheimer's disease. *Int J Geriatr Psychiatry* **21**, 344-348
297. Good, P. F., Werner, P., Hsu, A., Olanow, C. W., and Perl, D. P. (1996) Evidence of neuronal oxidative damage in Alzheimer's disease. *Am J Pathol* **149**, 21-28
298. Keller, J. N., Schmitt, F. A., Scheff, S. W., Ding, Q., Chen, Q., Butterfield, D. A., and Markesbery, W. R. (2005) Evidence of increased oxidative damage in subjects with mild cognitive impairment. *Neurology* **64**, 1152-1156
299. Rinaldi, P., Polidori, M. C., Metastasio, A., Mariani, E., Mattioli, P., Cherubini, A., Catani, M., Cecchetti, R., Senin, U., and Mecocci, P. (2003) Plasma antioxidants are similarly depleted in mild cognitive impairment and in Alzheimer's disease. *Neurobiol Aging* **24**, 915-919
300. Su, B., Wang, X., Lee, H. G., Tabaton, M., Perry, G., Smith, M. A., and Zhu, X. (2010) Chronic oxidative stress causes increased tau phosphorylation in M17 neuroblastoma cells. *Neurosci Lett* **468**, 267-271
301. Lovell, M. A., Xiong, S., Xie, C., Davies, P., and Markesbery, W. R. (2004) Induction of hyperphosphorylated tau in primary rat cortical neuron cultures mediated by oxidative stress and glycogen synthase kinase-3. *J Alzheimers Dis* **6**, 659-671; discussion 673-681
302. Cho, M. H., Kim, D. H., Choi, J. E., Chang, E. J., and Seung, Y. (2012) Increased phosphorylation of dynamin-related protein 1 and mitochondrial fission in okadaic acid-treated neurons. *Brain Res* **1454**, 100-110
303. Shahpasand, K., Uemura, I., Saito, T., Asano, T., Hata, K., Shibata, K., Toyoshima, Y., Hasegawa, M., and Hisanaga, S. (2012) Regulation of mitochondrial transport and inter-microtubule spacing by tau phosphorylation at the sites hyperphosphorylated in Alzheimer's disease. *J Neurosci* **32**, 2430-2441
304. Schulz, K. L., Eckert, A., Rhein, V., Mai, S., Haase, W., Reichert, A. S., Jendrach, M., Muller, W. E., and Leuner, K. (2012) A new link to mitochondrial impairment in tauopathies. *Mol Neurobiol* **46**, 205-216
305. Wang, X., Su, B., Lee, H. G., Li, X., Perry, G., Smith, M. A., and Zhu, X. (2009) Impaired balance of mitochondrial fission and fusion in Alzheimer's disease. *J Neurosci* **29**, 9090-9103
306. Hirai, K., Aliev, G., Nunomura, A., Fujioka, H., Russell, R. L., Atwood, C. S., Johnson, A. B., Kress, Y., Vinters, H. V., Tabaton, M., Shimohama, S., Cash, A. D., Siedlak, S. L., Harris, P. L., Jones, P. K., Petersen, R. B., Perry, G., and Smith, M. A. (2001) Mitochondrial abnormalities in Alzheimer's disease. *J Neurosci* **21**, 3017-3023
307. Wang, X., Su, B., Fujioka, H., and Zhu, X. (2008) Dynamin-like protein 1 reduction underlies mitochondrial morphology and distribution abnormalities in fibroblasts from sporadic Alzheimer's disease patients. *Am J Pathol* **173**, 470-482
308. Manczak, M., and Reddy, P. H. (2012) Abnormal interaction between the mitochondrial fission protein Drp1 and hyperphosphorylated tau in Alzheimer's disease neurons: implications for mitochondrial dysfunction and neuronal damage. *Hum Mol Genet* **21**, 2538-2547
309. Gibson, G. E., Sheu, K. F., and Blass, J. P. (1998) Abnormalities of mitochondrial enzymes in Alzheimer disease. *J Neural Transm (Vienna)* **105**, 855-870
310. Quintanilla, R. A., Dolan, P. J., Jin, Y. N., and Johnson, G. V. (2012) Truncated tau and Abeta cooperatively impair mitochondria in primary neurons. *Neurobiol Aging* **33**, 619 e625-635
311. David, D. C., Hauptmann, S., Scherping, I., Schuessel, K., Keil, U., Rizzu, P., Ravid, R., Drose, S., Brandt, U., Muller, W. E., Eckert, A., and Gotz, J. (2005) Proteomic and functional analyses reveal a mitochondrial dysfunction in P301L tau transgenic mice. *J Biol Chem* **280**, 23802-23814

312. Esteras, N., Rohrer, J. D., Hardy, J., Wray, S., and Abramov, A. Y. (2017) Mitochondrial hyperpolarization in iPSC-derived neurons from patients of FTDP-17 with 10+16 MAPT mutation leads to oxidative stress and neurodegeneration. *Redox Biol* **12**, 410-422
313. Rodriguez-Martin, T., Pooler, A. M., Lau, D. H. W., Morotz, G. M., De Vos, K. J., Gilley, J., Coleman, M. P., and Hanger, D. P. (2016) Reduced number of axonal mitochondria and tau hypophosphorylation in mouse P301L tau knockin neurons. *Neurobiol Dis* **85**, 1-10
314. Liu, Z., Li, T., Li, P., Wei, N., Zhao, Z., Liang, H., Ji, X., Chen, W., Xue, M., and Wei, J. (2015) The Ambiguous Relationship of Oxidative Stress, Tau Hyperphosphorylation, and Autophagy Dysfunction in Alzheimer's Disease. *Oxid Med Cell Longev* **2015**, 352723
315. Delobel, P., Lavenir, I., Ghetti, B., Holzer, M., and Goedert, M. (2006) Cell-cycle markers in a transgenic mouse model of human tauopathy: increased levels of cyclin-dependent kinase inhibitors p21Cip1 and p27Kip1. *Am J Pathol* **168**, 878-887
316. Frost, B., Hemberg, M., Lewis, J., and Feany, M. B. (2014) Tau promotes neurodegeneration through global chromatin relaxation. *Nat Neurosci* **17**, 357-366
317. Ke, Y. D., Dramiga, J., Schutz, U., Kril, J. J., Ittner, L. M., Schroder, H., and Gotz, J. (2012) Tau-mediated nuclear depletion and cytoplasmic accumulation of SFPQ in Alzheimer's and Pick's disease. *PLoS One* **7**, e35678
318. Khurana, V., Lu, Y., Steinhilb, M. L., Oldham, S., Shulman, J. M., and Feany, M. B. (2006) TOR-mediated cell-cycle activation causes neurodegeneration in a Drosophila tauopathy model. *Curr Biol* **16**, 230-241
319. Andorfer, C., Acker, C. M., Kress, Y., Hof, P. R., Duff, K., and Davies, P. (2005) Cell-cycle reentry and cell death in transgenic mice expressing nonmutant human tau isoforms. *J Neurosci* **25**, 5446-5454
320. Busser, J., Geldmacher, D. S., and Herrup, K. (1998) Ectopic cell cycle proteins predict the sites of neuronal cell death in Alzheimer's disease brain. *J Neurosci* **18**, 2801-2807
321. Arendt, T., Holzer, M., Stobe, A., Gartner, U., Luth, H. J., Bruckner, M. K., and Ueberham, U. (2000) Activated mitogenic signaling induces a process of dedifferentiation in Alzheimer's disease that eventually results in cell death. *Ann N Y Acad Sci* **920**, 249-255
322. Fischer, H. G., Morawski, M., Bruckner, M. K., Mittag, A., Tarnok, A., and Arendt, T. (2012) Changes in neuronal DNA content variation in the human brain during aging. *Aging Cell* **11**, 628-633
323. Mosch, B., Morawski, M., Mittag, A., Lenz, D., Tarnok, A., and Arendt, T. (2007) Aneuploidy and DNA replication in the normal human brain and Alzheimer's disease. *J Neurosci* **27**, 6859-6867
324. Arendt, T., Bruckner, M. K., Mosch, B., and Losche, A. (2010) Selective cell death of hyperploid neurons in Alzheimer's disease. *Am J Pathol* **177**, 15-20
325. Kahlson, M. A., and Colodner, K. J. (2015) Glial Tau Pathology in Tauopathies: Functional Consequences. *J Exp Neurosci* **9**, 43-50
326. Morales, I., Jimenez, J. M., Mancilla, M., and Maccioni, R. B. (2013) Tau oligomers and fibrils induce activation of microglial cells. *J Alzheimers Dis* **37**, 849-856
327. Liddelow, S. A., Guttenplan, K. A., Clarke, L. E., Bennett, F. C., Bohlen, C. J., Schirmer, L., Bennett, M. L., Munch, A. E., Chung, W. S., Peterson, T. C., Wilton, D. K., Frouin, A., Napier, B. A., Panicker, N., Kumar, M., Buckwalter, M. S., Rowitch, D. H., Dawson, V. L., Dawson, T. M., Stevens, B., and Barres, B. A. (2017) Neurotoxic reactive astrocytes are induced by activated microglia. *Nature* **541**, 481-487
328. Bhaskar, K., Konerth, M., Kokiko-Cochran, O. N., Cardona, A., Ransohoff, R. M., and Lamb, B. T. (2010) Regulation of tau pathology by the microglial fractalkine receptor. *Neuron* **68**, 19-31
329. Li, Y., Liu, L., Barger, S. W., and Griffin, W. S. (2003) Interleukin-1 mediates pathological effects of microglia on tau phosphorylation and on synaptophysin synthesis in cortical neurons through a p38-MAPK pathway. *J Neurosci* **23**, 1605-1611
330. von Bernhardi, R., Eugenin-von Bernhardi, L., and Eugenin, J. (2015) Microglial cell dysregulation in brain aging and neurodegeneration. *Front Aging Neurosci* **7**, 124

331. Zhang, J., Malik, A., Choi, H. B., Ko, R. W., Dissing-Olesen, L., and MacVicar, B. A. (2014) Microglial CR3 activation triggers long-term synaptic depression in the hippocampus via NADPH oxidase. *Neuron* **82**, 195-207
332. Guerreiro, R., Wojtas, A., Bras, J., Carrasquillo, M., Rogaeva, E., Majounie, E., Cruchaga, C., Sassi, C., Kauwe, J. S., Younkin, S., Hazrati, L., Collinge, J., Pocock, J., Lashley, T., Williams, J., Lambert, J. C., Amouyel, P., Goate, A., Rademakers, R., Morgan, K., Powell, J., St George-Hyslop, P., Singleton, A., Hardy, J., and Alzheimer Genetic Analysis, G. (2013) TREM2 variants in Alzheimer's disease. *N Engl J Med* **368**, 117-127
333. Corder, E. H., Saunders, A. M., Strittmatter, W. J., Schmechel, D. E., Gaskell, P. C., Small, G. W., Roses, A. D., Haines, J. L., and Pericak-Vance, M. A. (1993) Gene dose of apolipoprotein E type 4 allele and the risk of Alzheimer's disease in late onset families. *Science* **261**, 921-923
334. Sapir, T., Frotscher, M., Levy, T., Mandelkow, E. M., and Reiner, O. (2012) Tau's role in the developing brain: implications for intellectual disability. *Hum Mol Genet* **21**, 1681-1692
335. Min, S. W., Chen, X., Tracy, T. E., Li, Y., Zhou, Y., Wang, C., Shirakawa, K., Minami, S. S., Defensor, E., Mok, S. A., Sohn, P. D., Schilling, B., Cong, X., Ellerby, L., Gibson, B. W., Johnson, J., Krogan, N., Shamloo, M., Gestwicki, J., Masliah, E., Verdin, E., and Gan, L. (2015) Critical role of acetylation in tau-mediated neurodegeneration and cognitive deficits. *Nat Med* **21**, 1154-1162
336. Apicco, D. J., Ash, P. E. A., Maziuk, B., LeBlang, C., Medalla, M., Al Abdullatif, A., Ferragud, A., Botelho, E., Ballance, H. I., Dhawan, U., Boudeau, S., Cruz, A. L., Kashy, D., Wong, A., Goldberg, L. R., Yazdani, N., Zhang, C., Ung, C. Y., Tripodis, Y., Kanaan, N. M., Ikezu, T., Cottone, P., Leszyk, J., Li, H., Luebke, J., Bryant, C. D., and Wolozin, B. (2018) Reducing the RNA binding protein TIA1 protects against tau-mediated neurodegeneration in vivo. *Nat Neurosci* **21**, 72-80
337. Maziuk, B. F., Apicco, D. J., Cruz, A. L., Jiang, L., Ash, P. E. A., da Rocha, E. L., Zhang, C., Yu, W. H., Leszyk, J., Abisambra, J. F., Li, H., and Wolozin, B. (2018) RNA binding proteins co-localize with small tau inclusions in tauopathy. *Acta Neuropathol Commun* **6**, 71
338. Vanderweyde, T., Apicco, D. J., Youmans-Kidder, K., Ash, P. E. A., Cook, C., Lummertz da Rocha, E., Jansen-West, K., Frame, A. A., Citro, A., Leszyk, J. D., Ivanov, P., Abisambra, J. F., Steffen, M., Li, H., Petrucelli, L., and Wolozin, B. (2016) Interaction of tau with the RNA-Binding Protein TIA1 Regulates tau Pathophysiology and Toxicity. *Cell Rep* **15**, 1455-1466
339. Gratuze, M., Joly-Amado, A., Vieau, D., Buee, L., and Blum, D. (2018) Mutual Relationship between Tau and Central Insulin Signalling: Consequences for AD and Tauopathies? *Neuroendocrinology* **107**, 181-195
340. Steen, E., Terry, B. M., Rivera, E. J., Cannon, J. L., Neely, T. R., Tavares, R., Xu, X. J., Wands, J. R., and de la Monte, S. M. (2005) Impaired insulin and insulin-like growth factor expression and signaling mechanisms in Alzheimer's disease--is this type 3 diabetes? *J Alzheimers Dis* **7**, 63-80
341. Rodriguez-Rodriguez, P., Sandebring-Matton, A., Merino-Serrais, P., Parrado-Fernandez, C., Rabano, A., Winblad, B., Avila, J., Ferrer, I., and Cedazo-Minguez, A. (2017) Tau hyperphosphorylation induces oligomeric insulin accumulation and insulin resistance in neurons. *Brain* **140**, 3269-3285
342. Komuro, Y., Xu, G., Bhaskar, K., and Lamb, B. T. (2015) Human tau expression reduces adult neurogenesis in a mouse model of tauopathy. *Neurobiol Aging* **36**, 2034-2042
343. Thompson, A., Boekhoorn, K., Van Dam, A. M., and Lucassen, P. J. (2008) Changes in adult neurogenesis in neurodegenerative diseases: cause or consequence? *Genes Brain Behav* **7 Suppl 1**, 28-42
344. Bennett, R. E., Robbins, A. B., Hu, M., Cao, X., Betensky, R. A., Clark, T., Das, S., and Hyman, B. T. (2018) Tau induces blood vessel abnormalities and angiogenesis-related

gene expression in P301L transgenic mice and human Alzheimer's disease. *Proc Natl Acad Sci U S A* **115**, E1289-E1298
345. Kametani, F., and Hasegawa, M. (2018) Reconsideration of Amyloid Hypothesis and Tau Hypothesis in Alzheimer's Disease. *Front Neurosci* **12**, 25
346. Liao, D., Miller, E. C., and Teravskis, P. J. (2014) Tau acts as a mediator for Alzheimer's disease-related synaptic deficits. *Eur J Neurosci* **39**, 1202-1213
347. Ramsden, M., Kotilinek, L., Forster, C., Paulson, J., McGowan, E., SantaCruz, K., Guimaraes, A., Yue, M., Lewis, J., Carlson, G., Hutton, M., and Ashe, K. H. (2005) Age-dependent neurofibrillary tangle formation, neuron loss, and memory impairment in a mouse model of human tauopathy (P301L). *J Neurosci* **25**, 10637-10647
348. Lewis, J., McGowan, E., Rockwood, J., Melrose, H., Nacharaju, P., Van Slegtenhorst, M., Gwinn-Hardy, K., Paul Murphy, M., Baker, M., Yu, X., Duff, K., Hardy, J., Corral, A., Lin, W. L., Yen, S. H., Dickson, D. W., Davies, P., and Hutton, M. (2000) Neurofibrillary tangles, amyotrophy and progressive motor disturbance in mice expressing mutant (P301L) tau protein. *Nat Genet* **25**, 402-405
349. Gotz, J., Chen, F., Barmettler, R., and Nitsch, R. M. (2001) Tau filament formation in transgenic mice expressing P301L tau. *J Biol Chem* **276**, 529-534
350. Mayford, M., Bach, M. E., Huang, Y. Y., Wang, L., Hawkins, R. D., and Kandel, E. R. (1996) Control of memory formation through regulated expression of a CaMKII transgene. *Science* **274**, 1678-1683
351. Planel, E., Bretteville, A., Liu, L., Virag, L., Du, A. L., Yu, W. H., Dickson, D. W., Whittington, R. A., and Duff, K. E. (2009) Acceleration and persistence of neurofibrillary pathology in a mouse model of tauopathy following anesthesia. *FASEB J* **23**, 2595-2604
352. Aldridge, G. M., Podrebarac, D. M., Greenough, W. T., and Weiler, I. J. (2008) The use of total protein stains as loading controls: an alternative to high-abundance single-protein controls in semi-quantitative immunoblotting. *J Neurosci Methods* **172**, 250-254
353. Afgan, E., Baker, D., van den Beek, M., Blankenberg, D., Bouvier, D., Cech, M., Chilton, J., Clements, D., Coraor, N., Eberhard, C., Gruning, B., Guerler, A., Hillman-Jackson, J., Von Kuster, G., Rasche, E., Soranzo, N., Turaga, N., Taylor, J., Nekrutenko, A., and Goecks, J. (2016) The Galaxy platform for accessible, reproducible and collaborative biomedical analyses: 2016 update. *Nucleic Acids Res* **44**, W3-W10
354. Kent, W. J. (2002) BLAT--the BLAST-like alignment tool. *Genome Res* **12**, 656-664
355. Langmead, B., and Salzberg, S. L. (2012) Fast gapped-read alignment with Bowtie 2. *Nat Methods* **9**, 357-359
356. Thorvaldsdottir, H., Robinson, J. T., and Mesirov, J. P. (2013) Integrative Genomics Viewer (IGV): high-performance genomics data visualization and exploration. *Brief Bioinform* **14**, 178-192
357. Westaway, D., Cooper, C., Turner, S., Da Costa, M., Carlson, G. A., and Prusiner, S. B. (1994) Structure and polymorphism of the mouse prion protein gene. *Proc Natl Acad Sci U S A* **91**, 6418-6422
358. Bankevich, A., Nurk, S., Antipov, D., Gurevich, A. A., Dvorkin, M., Kulikov, A. S., Lesin, V. M., Nikolenko, S. I., Pham, S., Prjibelski, A. D., Pyshkin, A. V., Sirotkin, A. V., Vyahhi, N., Tesler, G., Alekseyev, M. A., and Pevzner, P. A. (2012) SPAdes: a new genome assembly algorithm and its applications to single-cell sequencing. *J Comput Biol* **19**, 455-477
359. Beard, C., Hochedlinger, K., Plath, K., Wutz, A., and Jaenisch, R. (2006) Efficient method to generate single-copy transgenic mice by site-specific integration in embryonic stem cells. *Genesis* **44**, 23-28
360. Pardo, L. M., Rizzu, P., Francescatto, M., Vitezic, M., Leday, G. G., Sanchez, J. S., Khamis, A., Takahashi, H., van de Berg, W. D., Medvedeva, Y. A., van de Wiel, M. A., Daub, C. O., Carninci, P., and Heutink, P. (2013) Regional differences in gene expression and promoter usage in aged human brains. *Neurobiol Aging* **34**, 1825-1836
361. Shineman, D. W., Basi, G. S., Bizon, J. L., Colton, C. A., Greenberg, B. D., Hollister, B. A., Lincecum, J., Leblanc, G. G., Lee, L. B., Luo, F., Morgan, D., Morse, I., Refolo, L. M., Riddell, D. R., Scearce-Levie, K., Sweeney, P., Yrjanheikki, J., and Fillit, H. M. (2011)

Accelerating drug discovery for Alzheimer's disease: best practices for preclinical animal studies. *Alzheimers Res Ther* **3**, 28

362. Yue, F., Cheng, Y., Breschi, A., Vierstra, J., Wu, W., Ryba, T., Sandstrom, R., Ma, Z., Davis, C., Pope, B. D., Shen, Y., Pervouchine, D. D., Djebali, S., Thurman, R. E., Kaul, R., Rynes, E., Kirilusha, A., Marinov, G. K., Williams, B. A., Trout, D., Amrhein, H., Fisher-Aylor, K., Antoshechkin, I., DeSalvo, G., See, L. H., Fastuca, M., Drenkow, J., Zaleski, C., Dobin, A., Prieto, P., Lagarde, J., Bussotti, G., Tanzer, A., Denas, O., Li, K., Bender, M. A., Zhang, M., Byron, R., Groudine, M. T., McCleary, D., Pham, L., Ye, Z., Kuan, S., Edsall, L., Wu, Y. C., Rasmussen, M. D., Bansal, M. S., Kellis, M., Keller, C. A., Morrissey, C. S., Mishra, T., Jain, D., Dogan, N., Harris, R. S., Cayting, P., Kawli, T., Boyle, A. P., Euskirchen, G., Kundaje, A., Lin, S., Lin, Y., Jansen, C., Malladi, V. S., Cline, M. S., Erickson, D. T., Kirkup, V. M., Learned, K., Sloan, C. A., Rosenbloom, K. R., Lacerda de Sousa, B., Beal, K., Pignatelli, M., Flicek, P., Lian, J., Kahveci, T., Lee, D., Kent, W. J., Ramalho Santos, M., Herrero, J., Notredame, C., Johnson, A., Vong, S., Lee, K., Bates, D., Neri, F., Diegel, M., Canfield, T., Sabo, P. J., Wilken, M. S., Reh, T. A., Giste, E., Shafer, A., Kutyavin, T., Haugen, E., Dunn, D., Reynolds, A. P., Neph, S., Humbert, R., Hansen, R. S., De Bruijn, M., Selleri, L., Rudensky, A., Josefowicz, S., Samstein, R., Eichler, E. E., Orkin, S. H., Levasseur, D., Papayannopoulou, T., Chang, K. H., Skoultchi, A., Gosh, S., Disteche, C., Treuting, P., Wang, Y., Weiss, M. J., Blobel, G. A., Cao, X., Zhong, S., Wang, T., Good, P. J., Lowdon, R. F., Adams, L. B., Zhou, X. Q., Pazin, M. J., Feingold, E. A., Wold, B., Taylor, J., Mortazavi, A., Weissman, S. M., Stamatoyannopoulos, J. A., Snyder, M. P., Guigo, R., Gingeras, T. R., Gilbert, D. M., Hardison, R. C., Beer, M. A., Ren, B., and Mouse, E. C. (2014) A comparative encyclopedia of DNA elements in the mouse genome. *Nature* **515**, 355-364
363. Smith, E. D., Xu, Y., Tomson, B. N., Leung, C. G., Fujiwara, Y., Orkin, S. H., and Crispino, J. D. (2004) More than blood, a novel gene required for mammalian postimplantation development. *Mol Cell Biol* **24**, 1168-1173
364. Han, H. J., Allen, C. C., Buchovecky, C. M., Yetman, M. J., Born, H. A., Marin, M. A., Rodgers, S. P., Song, B. J., Lu, H. C., Justice, M. J., Probst, F. J., and Jankowsky, J. L. (2012) Strain background influences neurotoxicity and behavioral abnormalities in mice expressing the tetracycline transactivator. *J Neurosci* **32**, 10574-10586
365. Helboe, L., Egebjerg, J., Barkholt, P., and Volbracht, C. (2017) Early depletion of CA1 neurons and late neurodegeneration in a mouse tauopathy model. *Brain Res* **1665**, 22-35
366. Bejar, R., Yasuda, R., Krugers, H., Hood, K., and Mayford, M. (2002) Transgenic calmodulin-dependent protein kinase II activation: dose-dependent effects on synaptic plasticity, learning, and memory. *J Neurosci* **22**, 5719-5726
367. Di Re, J., Wadsworth, P. A., and Laezza, F. (2017) Intracellular Fibroblast Growth Factor 14: Emerging Risk Factor for Brain Disorders. *Front Cell Neurosci* **11**, 103
368. Wang, Q., McEwen, D. G., and Ornitz, D. M. (2000) Subcellular and developmental expression of alternatively spliced forms of fibroblast growth factor 14. *Mech Dev* **90**, 283-287
369. Laezza, F., Lampert, A., Kozel, M. A., Gerber, B. R., Rush, A. M., Nerbonne, J. M., Waxman, S. G., Dib-Hajj, S. D., and Ornitz, D. M. (2009) FGF14 N-terminal splice variants differentially modulate Nav1.2 and Nav1.6-encoded sodium channels. *Mol Cell Neurosci* **42**, 90-101
370. Pablo, J. L., Wang, C., Presby, M. M., and Pitt, G. S. (2016) Polarized localization of voltage-gated Na+ channels is regulated by concerted FGF13 and FGF14 action. *Proc Natl Acad Sci U S A* **113**, E2665-2674
371. Smallwood, P. M., Munoz-Sanjuan, I., Tong, P., Macke, J. P., Hendry, S. H., Gilbert, D. J., Copeland, N. G., Jenkins, N. A., and Nathans, J. (1996) Fibroblast growth factor (FGF) homologous factors: new members of the FGF family implicated in nervous system development. *Proc Natl Acad Sci U S A* **93**, 9850-9857
372. Xiao, M., Xu, L., Laezza, F., Yamada, K., Feng, S., and Ornitz, D. M. (2007) Impaired hippocampal synaptic transmission and plasticity in mice lacking fibroblast growth factor 14. *Mol Cell Neurosci* **34**, 366-377

373. Alshammari, T. K., Alshammari, M. A., Nenov, M. N., Hoxha, E., Cambiaghi, M., Marcinno, A., James, T. F., Singh, P., Labate, D., Li, J., Meltzer, H. Y., Sacchetti, B., Tempia, F., and Laezza, F. (2016) Genetic deletion of fibroblast growth factor 14 recapitulates phenotypic alterations underlying cognitive impairment associated with schizophrenia. *Transl Psychiatry* **6**, e806
374. Alshammari, M. A., Alshammari, T. K., Nenov, M. N., Scala, F., and Laezza, F. (2016) Fibroblast Growth Factor 14 Modulates the Neurogenesis of Granule Neurons in the Adult Dentate Gyrus. *Mol Neurobiol* **53**, 7254-7270
375. Lou, J. Y., Laezza, F., Gerber, B. R., Xiao, M., Yamada, K. A., Hartmann, H., Craig, A. M., Nerbonne, J. M., and Ornitz, D. M. (2005) Fibroblast growth factor 14 is an intracellular modulator of voltage-gated sodium channels. *J Physiol* **569**, 179-193
376. Misceo, D., Fannemel, M., Baroy, T., Roberto, R., Tvedt, B., Jaeger, T., Bryn, V., Stromme, P., and Frengen, E. (2009) SCA27 caused by a chromosome translocation: further delineation of the phenotype. *Neurogenetics* **10**, 371-374
377. Cook, C., Kang, S. S., Carlomagno, Y., Lin, W. L., Yue, M., Kurti, A., Shinohara, M., Jansen-West, K., Perkerson, E., Castanedes-Casey, M., Rousseau, L., Phillips, V., Bu, G., Dickson, D. W., Petrucelli, L., and Fryer, J. D. (2015) Tau deposition drives neuropathological, inflammatory and behavioral abnormalities independently of neuronal loss in a novel mouse model. *Hum Mol Genet* **24**, 6198-6212
378. Saito, T., Matsuba, Y., Mihira, N., Takano, J., Nilsson, P., Itohara, S., Iwata, N., and Saido, T. C. (2014) Single App knock-in mouse models of Alzheimer's disease. *Nat Neurosci* **17**, 661-663
379. Sasaguri, H., Nilsson, P., Hashimoto, S., Nagata, K., Saito, T., De Strooper, B., Hardy, J., Vassar, R., Winblad, B., and Saido, T. C. (2017) APP mouse models for Alzheimer's disease preclinical studies. *EMBO J* **36**, 2473-2487
380. de Calignon, A., Polydoro, M., Suarez-Calvet, M., William, C., Adamowicz, D. H., Kopeikina, K. J., Pitstick, R., Sahara, N., Ashe, K. H., Carlson, G. A., Spires-Jones, T. L., and Hyman, B. T. (2012) Propagation of tau pathology in a model of early Alzheimer's disease. *Neuron* **73**, 685-697
381. Gilley, J., Seereeram, A., Ando, K., Mosely, S., Andrews, S., Kerschensteiner, M., Misgeld, T., Brion, J. P., Anderton, B., Hanger, D. P., and Coleman, M. P. (2012) Age-dependent axonal transport and locomotor changes and tau hypophosphorylation in a "P301L" tau knockin mouse. *Neurobiol Aging* **33**, 621 e621-621 e615
382. Boekhoorn, K., Terwel, D., Biemans, B., Borghgraef, P., Wiegert, O., Ramakers, G. J., de Vos, K., Krugers, H., Tomiyama, T., Mori, H., Joels, M., van Leuven, F., and Lucassen, P. J. (2006) Improved long-term potentiation and memory in young tau-P301L transgenic mice before onset of hyperphosphorylation and tauopathy. *J Neurosci* **26**, 3514-3523
383. Brion, J. P., Tremp, G., and Octave, J. N. (1999) Transgenic expression of the shortest human tau affects its compartmentalization and its phosphorylation as in the pretangle stage of Alzheimer's disease. *Am J Pathol* **154**, 255-270
384. Gotz, J., Probst, A., Spillantini, M. G., Schafer, T., Jakes, R., Burki, K., and Goedert, M. (1995) Somatodendritic localization and hyperphosphorylation of tau protein in transgenic mice expressing the longest human brain tau isoform. *EMBO J* **14**, 1304-1313
385. Terwel, D., Lasrado, R., Snauwaert, J., Vandeweert, E., Van Haesendonck, C., Borghgraef, P., and Van Leuven, F. (2005) Changed conformation of mutant Tau-P301L underlies the moribund tauopathy, absent in progressive, nonlethal axonopathy of Tau-4R/2N transgenic mice. *J Biol Chem* **280**, 3963-3973
386. Orr, M. E., Pitstick, R., Canine, B., Ashe, K. H., and Carlson, G. A. (2012) Genotype-specific differences between mouse CNS stem cell lines expressing frontotemporal dementia mutant or wild type human tau. *PLoS One* **7**, e39328
387. Polydoro, M., Acker, C. M., Duff, K., Castillo, P. E., and Davies, P. (2009) Age-dependent impairment of cognitive and synaptic function in the htau mouse model of tau pathology. *J Neurosci* **29**, 10741-10749
388. Adams, S. J., Crook, R. J., Deture, M., Randle, S. J., Innes, A. E., Yu, X. Z., Lin, W. L., Dugger, B. N., McBride, M., Hutton, M., Dickson, D. W., and McGowan, E. (2009)

Overexpression of wild-type murine tau results in progressive tauopathy and neurodegeneration. *Am J Pathol* **175**, 1598-1609
389. Ishihara, T., Hong, M., Zhang, B., Nakagawa, Y., Lee, M. K., Trojanowski, J. Q., and Lee, V. M. (1999) Age-dependent emergence and progression of a tauopathy in transgenic mice overexpressing the shortest human tau isoform. *Neuron* **24**, 751-762
390. Ishihara, T., Zhang, B., Higuchi, M., Yoshiyama, Y., Trojanowski, J. Q., and Lee, V. M. (2001) Age-dependent induction of congophilic neurofibrillary tau inclusions in tau transgenic mice. *Am J Pathol* **158**, 555-562
391. Forman, M. S., Lal, D., Zhang, B., Dabir, D. V., Swanson, E., Lee, V. M., and Trojanowski, J. Q. (2005) Transgenic mouse model of tau pathology in astrocytes leading to nervous system degeneration. *J Neurosci* **25**, 3539-3550
392. Higuchi, M., Ishihara, T., Zhang, B., Hong, M., Andreadis, A., Trojanowski, J., and Lee, V. M. (2002) Transgenic mouse model of tauopathies with glial pathology and nervous system degeneration. *Neuron* **35**, 433-446
393. Probst, A., Gotz, J., Wiederhold, K. H., Tolnay, M., Mistl, C., Jaton, A. L., Hong, M., Ishihara, T., Lee, V. M., Trojanowski, J. Q., Jakes, R., Crowther, R. A., Spillantini, M. G., Burki, K., and Goedert, M. (2000) Axonopathy and amyotrophy in mice transgenic for human four-repeat tau protein. *Acta Neuropathol* **99**, 469-481
394. Spittaels, K., Van den Haute, C., Van Dorpe, J., Bruynseels, K., Vandezande, K., Laenen, I., Geerts, H., Mercken, M., Sciot, R., Van Lommel, A., Loos, R., and Van Leuven, F. (1999) Prominent axonopathy in the brain and spinal cord of transgenic mice overexpressing four-repeat human tau protein. *Am J Pathol* **155**, 2153-2165
395. Goodwin, L. O., Splinter, E., Davis, T. L., Urban, R., He, H., Braun, R. E., Chesler, E. J., Kumar, V., van Min, M., Ndukum, J., Philip, V. M., Reinholdt, L. G., Svenson, K., White, J. K., Sasner, M., Lutz, C., and Murray, S. A. (2019) Large-scale discovery of mouse transgenic integration sites reveals frequent structural variation and insertional mutagenesis. *Genome Res*
396. Gamache, J., Benzow, K., Forster, C., Kemper, L., Hlynialuk, C., Furrow, E., Ashe, K. H., and Koob, M. D. (2019) Factors other than hTau overexpression that contribute to tauopathy-like phenotype in rTg4510 mice. *Nature Communications* **10**, 2479
397. Wang, X., Zhao, Y., Zhang, X., Badie, H., Zhou, Y., Mu, Y., Loo, L. S., Cai, L., Thompson, R. C., Yang, B., Chen, Y., Johnson, P. F., Wu, C., Bu, G., Mobley, W. C., Zhang, D., Gage, F. H., Ranscht, B., Zhang, Y. W., Lipton, S. A., Hong, W., and Xu, H. (2013) Loss of sorting nexin 27 contributes to excitatory synaptic dysfunction by modulating glutamate receptor recycling in Down's syndrome. *Nat Med* **19**, 473-480
398. Miller, L. M., Xiao, H., Burd, B., Horwitz, S. B., Angeletti, R. H., and Verdier-Pinard, P. (2010) Methods in tubulin proteomics. *Methods Cell Biol* **95**, 105-126
399. Kuznetsov, S. A., Rodionov, V. I., Gelfand, V. I., and Rosenblat, V. A. (1981) Purification of high-Mr microtubule proteins MAP1 and MAP2. *FEBS Lett* **135**, 237-240
400. Vallee, R. B. (1982) A taxol-dependent procedure for the isolation of microtubules and microtubule-associated proteins (MAPs). *J Cell Biol* **92**, 435-442
401. Yamada, K., Patel, T. K., Hochgrafe, K., Mahan, T. E., Jiang, H., Stewart, F. R., Mandelkow, E. M., and Holtzman, D. M. (2015) Analysis of in vivo turnover of tau in a mouse model of tauopathy. *Mol Neurodegener* **10**, 55
402. Weitzner, D. S., Engler-Chiurazzi, E. B., Kotilinek, L. A., Ashe, K. H., and Reed, M. N. (2015) Morris Water Maze Test: Optimization for Mouse Strain and Testing Environment. *J Vis Exp*, e52706
403. Moutier, R., Tchang, F., Caucheteux, S. M., and Kanellopoulos-Langevin, C. (2003) Placental anomalies and fetal loss in mice, after administration of doxycycline in food for tet-system activation. *Transgenic Res* **12**, 369-373
404. Vossel, K. A., Xu, J. C., Fomenko, V., Miyamoto, T., Suberbielle, E., Knox, J. A., Ho, K., Kim, D. H., Yu, G. Q., and Mucke, L. (2015) Tau reduction prevents Abeta-induced axonal transport deficits by blocking activation of GSK3beta. *J Cell Biol* **209**, 419-433

405. Lois, C., Hong, E. J., Pease, S., Brown, E. J., and Baltimore, D. (2002) Germline transmission and tissue-specific expression of transgenes delivered by lentiviral vectors. *Science* **295**, 868-872
406. Yoon, Y., Krueger, E. W., Oswald, B. J., and McNiven, M. A. (2003) The mitochondrial protein hFis1 regulates mitochondrial fission in mammalian cells through an interaction with the dynamin-like protein DLP1. *Mol Cell Biol* **23**, 5409-5420
407. Sakimura, K., Kutsuwada, T., Ito, I., Manabe, T., Takayama, C., Kushiya, E., Yagi, T., Aizawa, S., Inoue, Y., Sugiyama, H., and et al. (1995) Reduced hippocampal LTP and spatial learning in mice lacking NMDA receptor epsilon 1 subunit. *Nature* **373**, 151-155
408. Moullan, N., Mouchiroud, L., Wang, X., Ryu, D., Williams, E. G., Mottis, A., Jovaisaite, V., Frochaux, M. V., Quiros, P. M., Deplancke, B., Houtkooper, R. H., and Auwerx, J. (2015) Tetracyclines Disturb Mitochondrial Function across Eukaryotic Models: A Call for Caution in Biomedical Research. *Cell Rep* **10**, 1681-1691
409. Sultan, S., Gebara, E., and Toni, N. (2013) Doxycycline increases neurogenesis and reduces microglia in the adult hippocampus. *Front Neurosci* **7**, 131
410. Poppek, D., Keck, S., Ermak, G., Jung, T., Stolzing, A., Ullrich, O., Davies, K. J., and Grune, T. (2006) Phosphorylation inhibits turnover of the tau protein by the proteasome: influence of RCAN1 and oxidative stress. *Biochem J* **400**, 511-520
411. Ren, Q. G., Liao, X. M., Chen, X. Q., Liu, G. P., and Wang, J. Z. (2007) Effects of tau phosphorylation on proteasome activity. *FEBS Lett* **581**, 1521-1528
412. Duff, K., Knight, H., Refolo, L. M., Sanders, S., Yu, X., Picciano, M., Malester, B., Hutton, M., Adamson, J., Goedert, M., Burki, K., and Davies, P. (2000) Characterization of pathology in transgenic mice over-expressing human genomic and cDNA tau transgenes. *Neurobiol Dis* **7**, 87-98
413. Li, X. C., Hu, Y., Wang, Z. H., Luo, Y., Zhang, Y., Liu, X. P., Feng, Q., Wang, Q., Ye, K., Liu, G. P., and Wang, J. Z. (2016) Human wild-type full-length tau accumulation disrupts mitochondrial dynamics and the functions via increasing mitofusins. *Sci Rep* **6**, 24756
414. Waterham, H. R., Koster, J., van Roermund, C. W., Mooyer, P. A., Wanders, R. J., and Leonard, J. V. (2007) A lethal defect of mitochondrial and peroxisomal fission. *N Engl J Med* **356**, 1736-1741
415. DuBoff, B., Gotz, J., and Feany, M. B. (2012) Tau promotes neurodegeneration via DRP1 mislocalization in vivo. *Neuron* **75**, 618-632
416. Wilson, C., Munoz-Palma, E., and Gonzalez-Billault, C. (2018) From birth to death: A role for reactive oxygen species in neuronal development. *Semin Cell Dev Biol* **80**, 43-49
417. Le Belle, J. E., Orozco, N. M., Paucar, A. A., Saxe, J. P., Mottahedeh, J., Pyle, A. D., Wu, H., and Kornblum, H. I. (2011) Proliferative neural stem cells have high endogenous ROS levels that regulate self-renewal and neurogenesis in a PI3K/Akt-dependant manner. *Cell Stem Cell* **8**, 59-71
418. Bouge, A. L., and Parmentier, M. L. (2016) Tau excess impairs mitosis and kinesin-5 function, leading to aneuploidy and cell death. *Dis Model Mech* **9**, 307-319
419. Malmanche, N., Dourlen, P., Gistelinck, M., Demiautte, F., Link, N., Dupont, C., Vanden Broeck, L., Werkmeister, E., Amouyel, P., Bongiovanni, A., Bauderlique, H., Moechars, D., Royou, A., Bellen, H. J., Lafont, F., Callaerts, P., Lambert, J. C., and Dermaut, B. (2017) Developmental Expression of 4-Repeat-Tau Induces Neuronal Aneuploidy in Drosophila Tauopathy Models. *Sci Rep* **7**, 40764
420. Schoch, K. M., DeVos, S. L., Miller, R. L., Chun, S. J., Norrbom, M., Wozniak, D. F., Dawson, H. N., Bennett, C. F., Rigo, F., and Miller, T. M. (2016) Increased 4R-Tau Induces Pathological Changes in a Human-Tau Mouse Model. *Neuron* **90**, 941-947
421. Shea, T. B., and Beermann, M. L. (1994) Respective roles of neurofilaments, microtubules, MAP1B, and tau in neurite outgrowth and stabilization. *Mol Biol Cell* **5**, 863-875
422. Teravskis, P. J., Oxnard, B. R., Miller, E. C., Kemper, L., Ashe, K. H., and Liao, D. (2019) Phosphorylation in two discrete tau domains regulates a stepwise process leading to postsynaptic dysfunction. *J Physiol*

423. McInnes, J., Wierda, K., Snellinx, A., Bounti, L., Wang, Y. C., Stancu, I. C., Apostolo, N., Gevaert, K., Dewachter, I., Spires-Jones, T. L., De Strooper, B., De Wit, J., Zhou, L., and Verstreken, P. (2018) Synaptogyrin-3 Mediates Presynaptic Dysfunction Induced by Tau. *Neuron* **97**, 823-835 e828
424. Zhou, L., McInnes, J., Wierda, K., Holt, M., Herrmann, A. G., Jackson, R. J., Wang, Y. C., Swerts, J., Beyens, J., Miskiewicz, K., Vilain, S., Dewachter, I., Moechars, D., De Strooper, B., Spires-Jones, T. L., De Wit, J., and Verstreken, P. (2017) Tau association with synaptic vesicles causes presynaptic dysfunction. *Nat Commun* **8**, 15295
425. Ishihara, N., Nomura, M., Jofuku, A., Kato, H., Suzuki, S. O., Masuda, K., Otera, H., Nakanishi, Y., Nonaka, I., Goto, Y., Taguchi, N., Morinaga, H., Maeda, M., Takayanagi, R., Yokota, S., and Mihara, K. (2009) Mitochondrial fission factor Drp1 is essential for embryonic development and synapse formation in mice. *Nat Cell Biol* **11**, 958-966
426. Khacho, M., Clark, A., Svoboda, D. S., Azzi, J., MacLaurin, J. G., Meghaizel, C., Sesaki, H., Lagace, D. C., Germain, M., Harper, M. E., Park, D. S., and Slack, R. S. (2016) Mitochondrial Dynamics Impacts Stem Cell Identity and Fate Decisions by Regulating a Nuclear Transcriptional Program. *Cell Stem Cell* **19**, 232-247
427. Melov, S., Adlard, P. A., Morten, K., Johnson, F., Golden, T. R., Hinerfeld, D., Schilling, B., Mavros, C., Masters, C. L., Volitakis, I., Li, Q. X., Laughton, K., Hubbard, A., Cherny, R. A., Gibson, B., and Bush, A. I. (2007) Mitochondrial oxidative stress causes hyperphosphorylation of tau. *PLoS One* **2**, e536
428. Ohmi, K., Kudo, L. C., Ryazantsev, S., Zhao, H. Z., Karsten, S. L., and Neufeld, E. F. (2009) Sanfilippo syndrome type B, a lysosomal storage disease, is also a tauopathy. *Proc Natl Acad Sci U S A* **106**, 8332-8337
429. Sarnat, H. B., and Flores-Sarnat, L. (2015) Infantile tauopathies: Hemimegalencephaly; tuberous sclerosis complex; focal cortical dysplasia 2; ganglioglioma. *Brain Dev* **37**, 553-562
430. Wiatr, K., Szlachcic, W. J., Trzeciak, M., Figlerowicz, M., and Figiel, M. (2018) Huntington Disease as a Neurodevelopmental Disorder and Early Signs of the Disease in Stem Cells. *Mol Neurobiol* **55**, 3351-3371
431. Emilsson, V., Ilkov, M., Lamb, J. R., Finkel, N., Gudmundsson, E. F., Pitts, R., Hoover, H., Gudmundsdottir, V., Horman, S. R., Aspelund, T., Shu, L., Trifonov, V., Sigurdsson, S., Manolescu, A., Zhu, J., Olafsson, O., Jakobsdottir, J., Lesley, S. A., To, J., Zhang, J., Harris, T. B., Launer, L. J., Zhang, B., Eiriksdottir, G., Yang, X., Orth, A. P., Jennings, L. L., and Gudnason, V. (2018) Co-regulatory networks of human serum proteins link genetics to disease. *Science* **361**, 769-773
432. Yousefzadeh, M. J., Schafer, M. J., Noren Hooten, N., Atkinson, E. J., Evans, M. K., Baker, D. J., Quarles, E. K., Robbins, P. D., Ladiges, W. C., LeBrasseur, N. K., and Niedernhofer, L. J. (2018) Circulating levels of monocyte chemoattractant protein-1 as a potential measure of biological age in mice and frailty in humans. *Aging Cell* **17**
433. Serra, H. G., Duvick, L., Zu, T., Carlson, K., Stevens, S., Jorgensen, N., Lysholm, A., Burright, E., Zoghbi, H. Y., Clark, H. B., Andresen, J. M., and Orr, H. T. (2006) RORalpha-mediated Purkinje cell development determines disease severity in adult SCA1 mice. *Cell* **127**, 697-708
434. Merlo, G., Altruda, F., and Poli, V. (2012) Mice as experimental organisms. *In eLS, (Ed.)*
435. Justice, M. J., and Dhillon, P. (2016) Using the mouse to model human disease: increasing validity and reproducibility. *Dis Model Mech* **9**, 101-103
436. Gordon, J. W., and Ruddle, F. H. (1981) Integration and stable germ line transmission of genes injected into mouse pronuclei. *Science* **214**, 1244-1246
437. Zhu, F., Nair, R. R., Fisher, E. M. C., and Cunningham, T. J. (2019) Humanising the mouse genome piece by piece. *Nat Commun* **10**, 1845
438. Dawson, T. M., Golde, T. E., and Lagier-Tourenne, C. (2018) Animal models of neurodegenerative diseases. *Nat Neurosci* **21**, 1370-1379
439. Ottina, E., Peperzak, V., Schoeler, K., Carrington, E., Sgonc, R., Pellegrini, M., Preston, S., Herold, M. J., Strasser, A., and Villunger, A. (2017) DNA-binding of the Tet-

transactivator curtails antigen-induced lymphocyte activation in mice. *Nat Commun* **8**, 1028

440. Oakley, H., Cole, S. L., Logan, S., Maus, E., Shao, P., Craft, J., Guillozet-Bongaarts, A., Ohno, M., Disterhoft, J., Van Eldik, L., Berry, R., and Vassar, R. (2006) Intraneuronal beta-amyloid aggregates, neurodegeneration, and neuron loss in transgenic mice with five familial Alzheimer's disease mutations: potential factors in amyloid plaque formation. *J Neurosci* **26**, 10129-10140
441. Oddo, S., Caccamo, A., Shepherd, J. D., Murphy, M. P., Golde, T. E., Kayed, R., Metherate, R., Mattson, M. P., Akbari, Y., and LaFerla, F. M. (2003) Triple-transgenic model of Alzheimer's disease with plaques and tangles: intracellular Abeta and synaptic dysfunction. *Neuron* **39**, 409-421
442. Han, S. S., Williams, L. A., and Eggan, K. C. (2011) Constructing and deconstructing stem cell models of neurological disease. *Neuron* **70**, 626-644
443. Jo, J., Xiao, Y., Sun, A. X., Cukuroglu, E., Tran, H. D., Goke, J., Tan, Z. Y., Saw, T. Y., Tan, C. P., Lokman, H., Lee, Y., Kim, D., Ko, H. S., Kim, S. O., Park, J. H., Cho, N. J., Hyde, T. M., Kleinman, J. E., Shin, J. H., Weinberger, D. R., Tan, E. K., Je, H. S., and Ng, H. H. (2016) Midbrain-like Organoids from Human Pluripotent Stem Cells Contain Functional Dopaminergic and Neuromelanin-Producing Neurons. *Cell Stem Cell* **19**, 248-257
444. Heuer, E., Rosen, R. F., Cintron, A., and Walker, L. C. (2012) Nonhuman primate models of Alzheimer-like cerebral proteopathy. *Curr Pharm Des* **18**, 1159-1169